STUDIES OF THE AUTOCORRELATION MATRIX AND FOURIER TRANSFORM ANALYSES OF SEISMIC DATA

a thesis submitted by

BRIAN LUCIAN ANGEL HAINS, B.Sc., A.R.C.S.,

for the degree of

Doctor of Philosophy,

in the Faculty of Science of the University of London.

June, 1973

Department of Geophysics,
Imperial College,
London S.W.7

ABSTRACT

A very brief introduction is given to the principles underlying seismic data processing. A model for the generation of synthetic seismograms is presented and discussed.

The multichannel Wiener filter is presented and discussed as a data processing tool for the detection of moveout. A number of such filters are computed to pass/reject correlated events of both linear and quadratic moveout. Experiments are performed on a variety of synthetic data, in order to ascertain how such filters will perform in a given situation. It is shown that very low levels of signal can be successfully recovered by multichannel filtering, and that a very close match must exist between the moveouts present in the data and those specified for the particular filter design. Application of these filters to real data records give results in good agreement to that expected from a study of the synthetic case.

The analytical methods of (i) the autocorrelation matrix, and (ii) the Fourier Transform, are presented and discussed. The "average" or second order autocorrelation matrix is developed, and a multichannel filter scan of a column from this matrix is incorporated in the former method. A variety of experiments are performed on syhthetic data, of both linear and quadratic moveout, for different noise conditions in order to ascertain the ability of these methods to detect low power correlated events. It is shown that such detection can be successful, provided that the random noise is not too severe. The benefits of removing the obvious moveouts, by a multichannel filter, from the input data before commencing analysis, is also demonstrated. Results from the analyses of real data records are generally consistent with those of the synthetic case.

CONTENTS

page

ABSTRACT 1

CONTENTS 2

CHAPTER 1 - INTRODUCTION 5

1.0 Introduction 5

1.1 Background discussion 7

1.1.1 linearity and the convolution theorem 7

1.1.2 statistical assumptions 7

1.1.3 Wold Decomposition Theorem 8

1.1.4 sampling theorem 8

1.2 Synthetic data seismic, model 9

1.2.1 moveout functions 10

1.2.2 discussion of model 11

1.3 Real data 11

CHAPTER 2 - MULTICHANNEL WIENER MOVEOUT FILTERS IN SEISMIC DATA PROCESSING 22

2.0 Introduction 22

2.1 Filter theory and design 23

2.2 Filter applications to synthetic data 31

2.2.1 effects of different noise levels 34

2.2.2 matching of moveout between filter and data 49

2.2.3 number of traces in filter design 51

2.2.4 quadratic filtering 53

2.3 Filter applications to real data 58

2.4 Conclusions 73

CHAPTER 3 - THE AUTOCORRELATION MATRIX AND ITS APPLICATION TO THE ANALYSIS OF MOVEOUT 75

3.0 Introduction 75

3.1 Autocorrelation theory 75

3.1.1 definition of autocorrelation matrix 75

3.1.2 detection of moveout 77

3.1.3 second order autocorrelation matrix 81

3.1.4 statistical considerations of the autocorrelation matrix technique 83

3.2 Applications to synthetic data 85

3.2.1 development of analytical approach 85

3.2.2 importance of record length 95

3.2.3 effects of different noise levels 100

3.2.4 pre-filtering experiments with correlation analyses 111

3.3 Applications to real data 116

3.4 Conclusions 134

CHAPTER 4 - THE TWO-DIMENSIONAL FOURIER TRANSFORM AND ITS APPLICATION TO THE ANALYSIS OF MOVEOUT 137

4.0 Introduction 137

4.1 Fourier Transform theory 137

4.1.1 definition of the discrete two-dimensional Fourier Transform 138

4.1.2 interpretation of the f-k plane 139

4.1.3 statistical considerations of the Fourier Transform 141

4.2 Applications to synthetic data 146

4.2.1 development of analytical approach 146

4.2.2 effects of different noise levels 162

4.3 Pre-filtering experiments in Fourier analyses 175

4.4 Applications to real data 184

4.5 Conclusions 201

CHAPTER 5 - CONCLUSIONS AND SUGGESTIONS FOR FURTHER RESEARCH 204

ACKNOWLEDGEMENTS 207

REFERENCES 208

APPENDIX 211

CHAPTER 1

INTRODUCTION

1.0 Introduction

One subject that has received a great deal of attention in recent years, within the field of applied geophysics, has been that of multichannel seismic data processing. By means of multichannel filtering techniques it was hoped to improve the quality of seismic records by using information from several data channels, that could not be obtained from the use of one channel alone. For example, it is known that the wanted reflections on a seismic record (the "signals") have a lower trace-to-trace "moveout" than the unwanted reflections (the "correlated noise"). In principle, a multichannel filter could be designed that would "pass" the low-moveout signals and "reject" the high-moveout correlated noise.

The results from multichannel filtering processes have, however, been rather disappointing when applied to real data. The reasons for this are many and varied. Lindsey (1970), for example, states that the channel to channel perturbations in a multichannel recording system set a 15 decibel fidelity limit to the whole system. In particular, the unit-impulse response for each channel is not, in general, identical. The problems of stationarity (e.g. Wadsworth et al., 1953), preclude the taking of a large record length for processing. Schneider in fact, (1971), refers to multichannel filtering as a "processing curiosity". None the less, it is the purpose of this thesis to investigate the analytical methods of correlation and Fourier analysis, and to assess to what extent these methods may be successfully applied to multichannel moveout filters.

The filter used in this thesis is the multichannel Wiener moveout filter. The reason for this choice is that this thesis forms part of a continuing research programme at Imperial College into the

theory, design and application of multichannel filters. The previous thesis to this (Hubral, 1970), showed that the Wiener filter was a very good moveout filter. The choice is vindicated by the quality of results shown in this thesis. In the context of this thesis it should be noted that a "multichannel filter" will be taken to mean a "multichannel moveout filter of the Wiener type".

Chapter two deals with the application of a number of multichannel Wiener filters to a variety of synthetic data, in order to gain some insight into the performance of such filters. It is shown that these filters form a useful processing tool, in their own right. Chapter three investigates various aspects of the correlation analysis of seismic traces, and shows how multichannel filters may be used to good effect in this analysis. Chapter four describes a similar investigation on the two-dimensional Fourier analysis of a seismic section, though with a rather more restricted use of multichannel filters. The methods were tried on such examples of real data as were available, and discussion of these results, together with comparisons between the different methods, are presented where appropriate.

All computing work was effected through the use of the seismic moveout data processing package "Geodat". This package was designed and implemented by the author and makes use of a number of subroutines obtained from various sources. A descriptive flow chart for this package, together with the colour code for the contour maps of the Fourier Transform (Chapter four), are presented in the Appendix.

It should be noted that the intention of the treatment in this thesis was that it should be sufficiently clear to enable the reader to identify and pursue the relevant themes being discussed, while at the same time being sufficiently concise so that the essential features of the study are not clouded by a wealth of mathematical

detail. It is hoped that any further information that may be required on a particular topic may be obtained through one of the references quoted in the text.

1.1 Background discussion

Although no truly comprehensive text-book of seismic data processing is currently available, of which the author is aware, none the less a great many papers and books have been published that deal with particular aspects of the subject, to some degree (Finetti et al, 1971, gives a long list of suitable references). It is the purpose of this section only to bring together the salient points necessary for an understanding of the context in which this work was set. These points are listed below, together with a few sentences on each :

1.1.1 linearity and the convolution theorem

The earth is assumed to behave as a linear system. Any linear system may be characterised by its "unit-impulse response function", i.e. the response of the system to a unit-impulse (!). The output function, $y(t)$, of a linear system of unit-impulse response function $a(t)$, to an input function, $x(t)$, is given by the convolution (denoted by the symbol *) of the input function with the unit-impulse response function. Hence, $y(t) = x(t) * a(t)$. In the frequency domain this result becomes $Y(f) = X(f).A(f)$, i.e. convolution in the time domain is equivalent to multiplication in the frequency domain (convolution theorem). The functions $Y(f)$, $X(f)$ and $A(f)$ are the Fourier transforms of $y(t)$, $x(t)$ and $a(t)$ respectively.

1.1.2 statistical assumptions

The seismogram that is observed is regarded as being only one out of a large number of possible seismograms that could have been observed. This vast collection of seismograms is termed an "ensemble", $X(t)$, and the observed seismogram is a particular "realisation" of it, $x_i(t)$, i.e. $x_i(t) \in \{X(t)\}$.

It is assumed that a seismic trace constitutes a "stationary" time series, i.e. that measurements of autocorrelation functions, power spectral estimates and so on, do not depend upon the time origin chosen for their measurement. Such an assumption is generally only true, in real data, for short record lengths (Wadsworth et al., 1953). It is further assumed (ergodic hypothesis) that the time average and the ensemble average are the same, i.e. that the average value of some quantity, obtained by averaging any one trace over all time, is equal to that obtained by averaging over all the traces at one time, hence $\overline{x_i(t)} = \overline{\{X(t_i)\}}$. These notions of average behaviour form the cornerstone of statistical communication theory, from which much of current data processing is derived. Further discussion may be found in Lee (1960).

1.1.3 Wold Decomposition Theorem

This theorem states that a stationary time series, of absolutely continuous spectral distribution function, may be regarded as the convolution of a minimum-delay wavelet with a random spike series (Robinson, 1967a). The application of this theorem to seismic data processing has been amply dealt with by Robinson (1957), and is used as the basis for the synthetic data model of this thesis. Briefly, a minimum-delay wavelet is that wavelet which has the most rapid build up of energy for a given power spectrum. It is assumed (for convenience) that the response function of the earth is minimum-delay, and that the random spike series represents the random reflection coefficients of the different seismic reflectors. The random position of these reflectors lead to a randomness in the spacing of the random spikes.

1.1.4 Sampling theorem

The Shannon sampling theorem states that a continuous function may only be recovered from its samples if the continuous function contains no components of greater frequency than half the sampling frequency. The violation of this theorem gives rise to what

is termed "aliasing", a concept that is readily understood in the frequency domain :

Let the bandwidth of a continuous function x(t) be given by 2B, then, if this function is sampled every T units of time, the spectrum of the continuous series will be repeated every 1/T cycles per time unit in the frequency domain. The Shannon theorem requires that $T \leq 1/2B$. If $T > 1/2B$, then the repeated spectra will overlap to give "Nyquist foldover" or "aliasing". The limiting frequency is termed the "Nyquist frequency" and is equal to 0.5 cycles per time unit.

Whenever continuous data is sampled, or discrete data resampled, an appropriate anti-alias filter should always be incorporated. Further discussion on sampling may be found in Bendat and Piersol (1966).

1.2 Synthetic data seismic model

The seismic model chosen for the computation of synthetic data in this thesis is defined by the following relation :

$$x_i(t) = s(t-\alpha_i) + \frac{1}{\sqrt{\rho}}.r(t-\beta_i) + \frac{1}{\sqrt{\nu}}.n_i(t) \qquad (i=1,\ldots,N)$$

where i = trace number (or channel number)

N = total number of traces

t = discrete time index, at unit sampling interval

$x_i(t)$ = output trace on channel i

$s(t)$ = signal trace component

$r(t)$ = correlated noise trace component

$n_i(t)$ = uncorrelated noise trace component for channel i

α_i = signal moveout on channel i

β_i = correlated noise moveout on channel i

ρ = signal to correlated noise power ratio

ν = signal to uncorrelated noise power ratio

After the fashion of Wold and Robinson (1.1.3), the three consituent traces s(t), r(t) and n(t) were constructed from minimum-delay wavelets and random spike series according to

$$s(t) = b_1(t) * \Psi(t)$$

$$r(t) = b_2(t) * \zeta(t)$$

$$n_i(t) = b_3(t) * \xi_i(t)$$

The functions $b_1(t)$, $b_2(t)$ and $b_3(t)$ were the minimum-delay wavelets, and were each taken to be the impulse response of an appropriate Butterworth filter. Defining such a filter by $(f_1/m_1 - f_2/m_2)$, where f_1 and f_2 are the half-power frequencies (in cycles per second) and m_1 and m_2 are the slopes through those frequencies (in decibels per octave), the wavelets used in the model were taken to be as follows :

$b_1(t) = 20/24 - 80/18$, (signal wavelet)

$b_2(t) = 10/12 - 50/18$, (correlated noise wavelet)

$b_3(t) = 15/24 - 80/18$, (uncorrelated noise wavelet)

The functions $\Psi(t)$, $\zeta(t)$ and $\xi_i(t)$ were all different sets of random numbers, each set having a rectangular probability distribution function and giving random amplitudes, within the interval $(-\sqrt{3}, \sqrt{3})$, at unit sampling interval. It should be noted that it was not considered necessary to have a random distribution for the arrival times of these random amplitudes, particularly since the position of a large reflection in the synthetic record would be random, in any case, due to the random amplitudes.

The sampling rate of all synthetic data in this thesis was taken to be 2 msec, thereby giving a Nyquist frequency of 250 c.p.s.

1.2.1 moveout functions

It is pointed out in Chapter two that the filtering of non-linear moveouts require many more filters than that for linear moveouts. Accordingly, it was felt sufficient for the present content to deal largely with linear moveouts. The moveout function for the

signal was taken to be zero samples per trace, $\alpha_i = 0$, and that for the correlated noise was taken to be 1, 2, 3 or 4 samples per trace as the particular example demanded.

For a few examples a quadratic moveout function was taken for the correlated noise, $\beta_i = i^2/24$. Strictly speaking, a hyperbolic function should have been chosen, but due to difficulties with the filter design in the present filter-producing program (written by P. Hubral and based on Robinson, 1967a), a quadratic function was taken. This distinction is unlikely to be of importance for the present work. Further discussion on moveout may be found in Robinson (1970b) and in Robinson (1972).

1.2.2 discussion of model

In addition to what has already been said, it should be noted that the gain level and signal to noise ratios are constant for each trace in the synthetic record. This is unlikely to be the case for real data. Also, of course, the impulse response functions for the signal and noise are identical across the record and the whole record is statistically stationary. None the less, it is envisaged that the model used will suffice for the particular problems studied in this thesis. Further development, however, may well require the introduction of other features into it.

1.3 Real data

The real data used for this thesis was a "noise spread" provided by British Petroleum (Sunbury), to whom the author is greatly indebted. The records contained many linear or quasi-linear moveout events, and gave several different examples of signal to noise conditions. The sampling rate of this digitised data was 2 msec. The records are uncorrected and correspond to a unique field experiment in geophone group research, in which continuous offset cover is simulated for a single shot-point. In point of fact, of course,

several shots were used and the geophone array was appropriately displaced for each shot.

For ease of later comparison in the thesis, the different sections taken from the spread are presented as Fig 1.1 - Fig 1.6. The table below lists the relevant information for these records :

Figure number	shot-point number	number of traces	length of trace (in samples)	offset of trace (in samples)
1.1	3001	24	250	275
1.2	3002	24	250	75
1.3	3003	24	250	485
1.4	3005	24	250	375
1.5	3006	24	250	375
1.6	3007	24	250	210

Table 1.1 Index of real data

It should be noted that each 24-trace record consists of two 12-trace records, the last and first traces of which overlap (i.e. traces 12 and 13 are the same). This leads, of course, to a "kink" in any moveout straddling the middle traces. In order to overcome this effect a 23-trace record was used for processing, consisting of traces 1 - 11 and traces 13 - 24, renumbered as traces 1 - 23.

Comparison of these results clearly show the presence of ground roll on Fig. 1.2, Fig. 1.4 and Fig. 1.5. Some of the work in this thesis necessitated the removal of this ground roll, a task that was effected by the application of a simple band pass filter, designed to pass frequencies in the range 30 c.p.s. to 250 c.p.s. (the Nyquist frequency) and to reject those frequencies below 30 c.p.s., to these records. The results are referred to as the "band pass filtered version

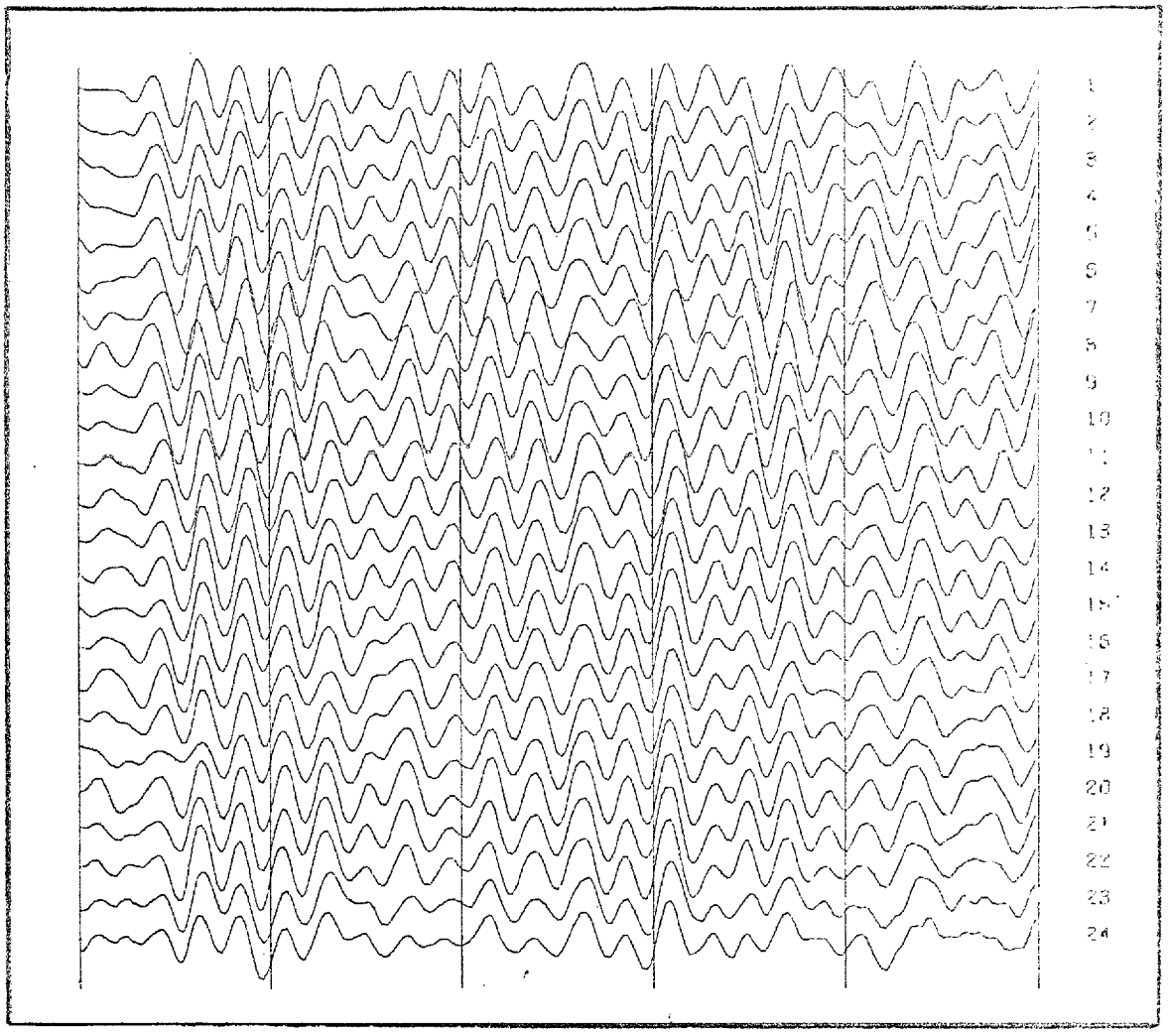
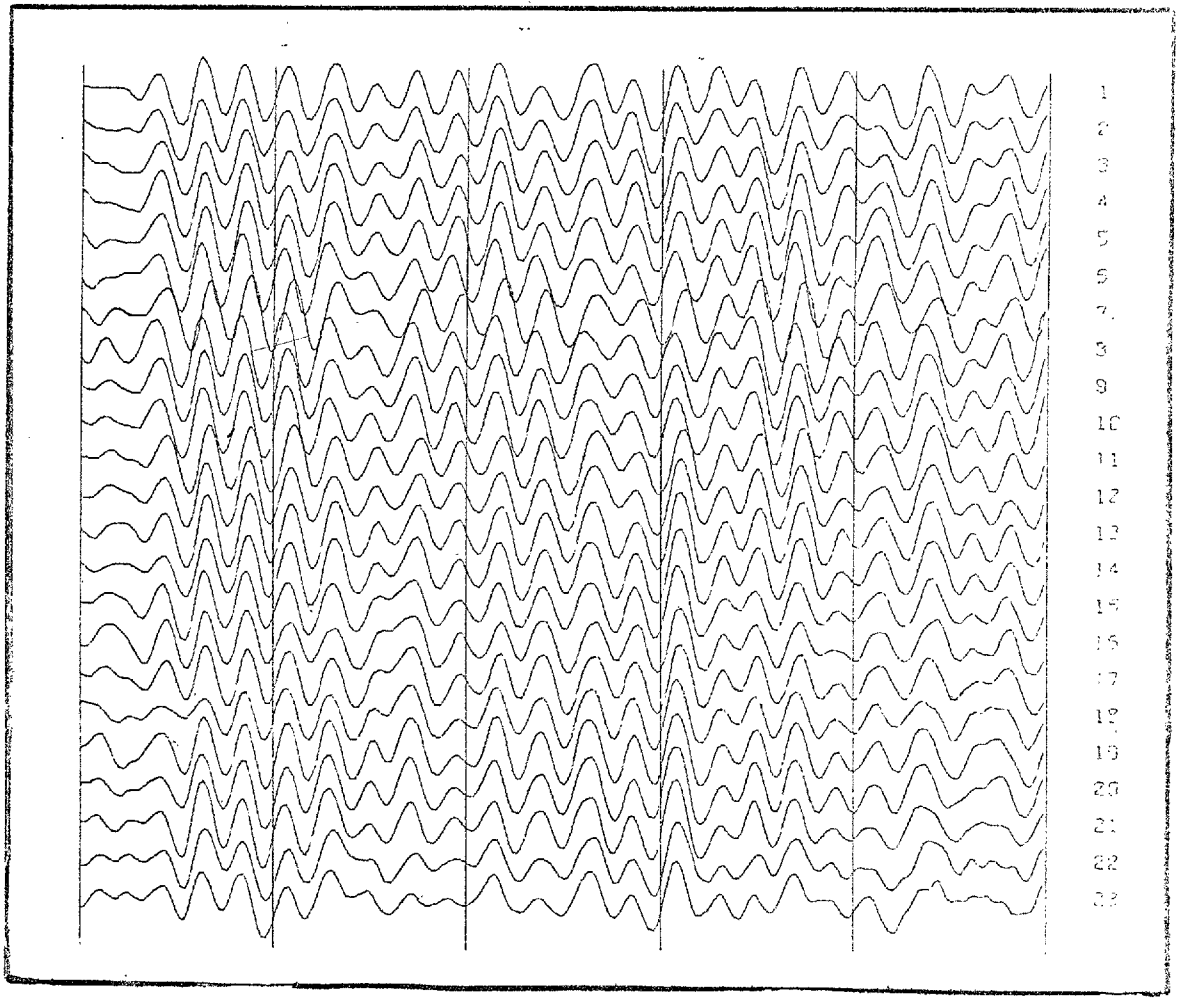


Fig. 1.1 shotpoint 3001, 24 traces (upper), 23 traces (lower)



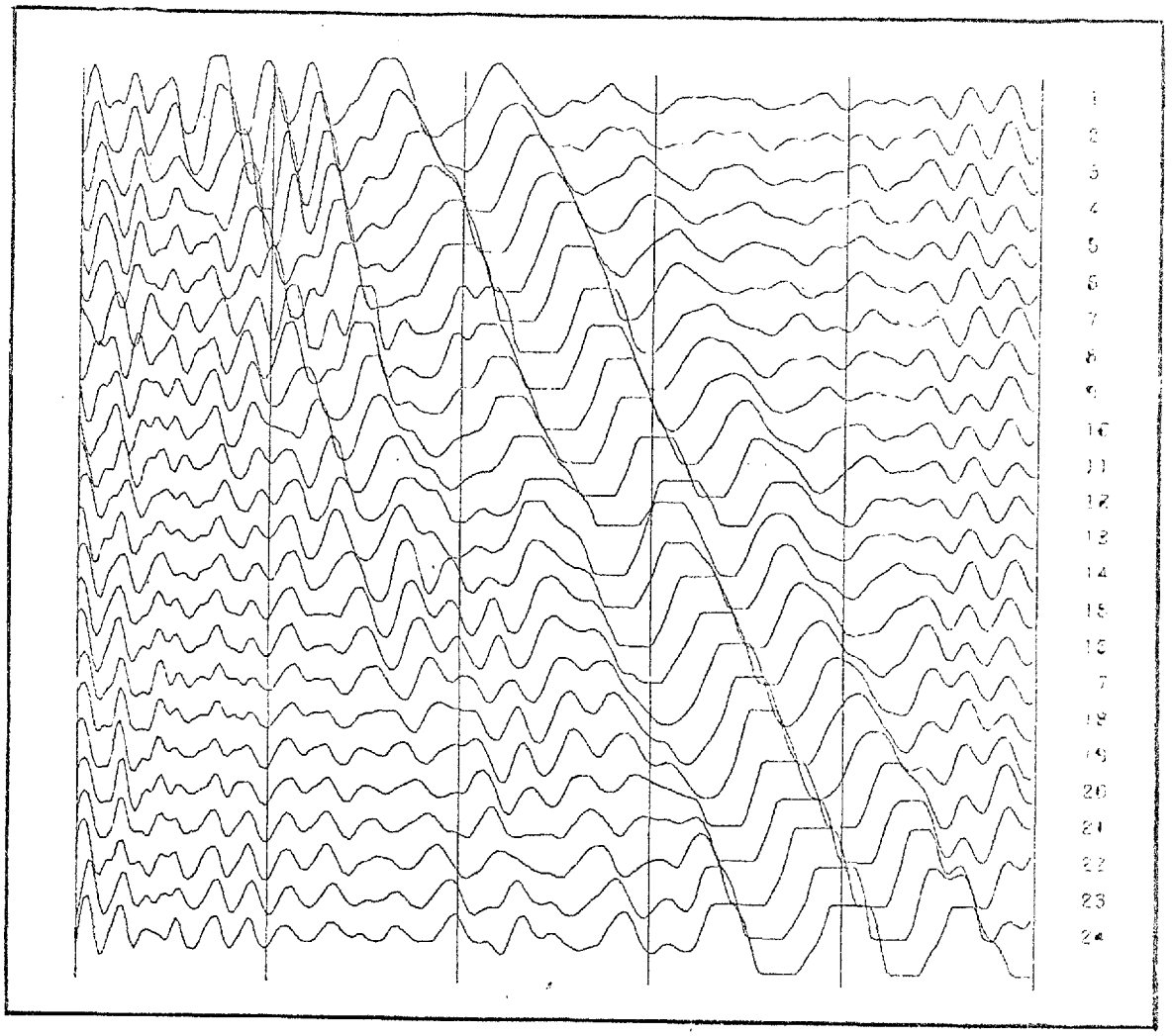
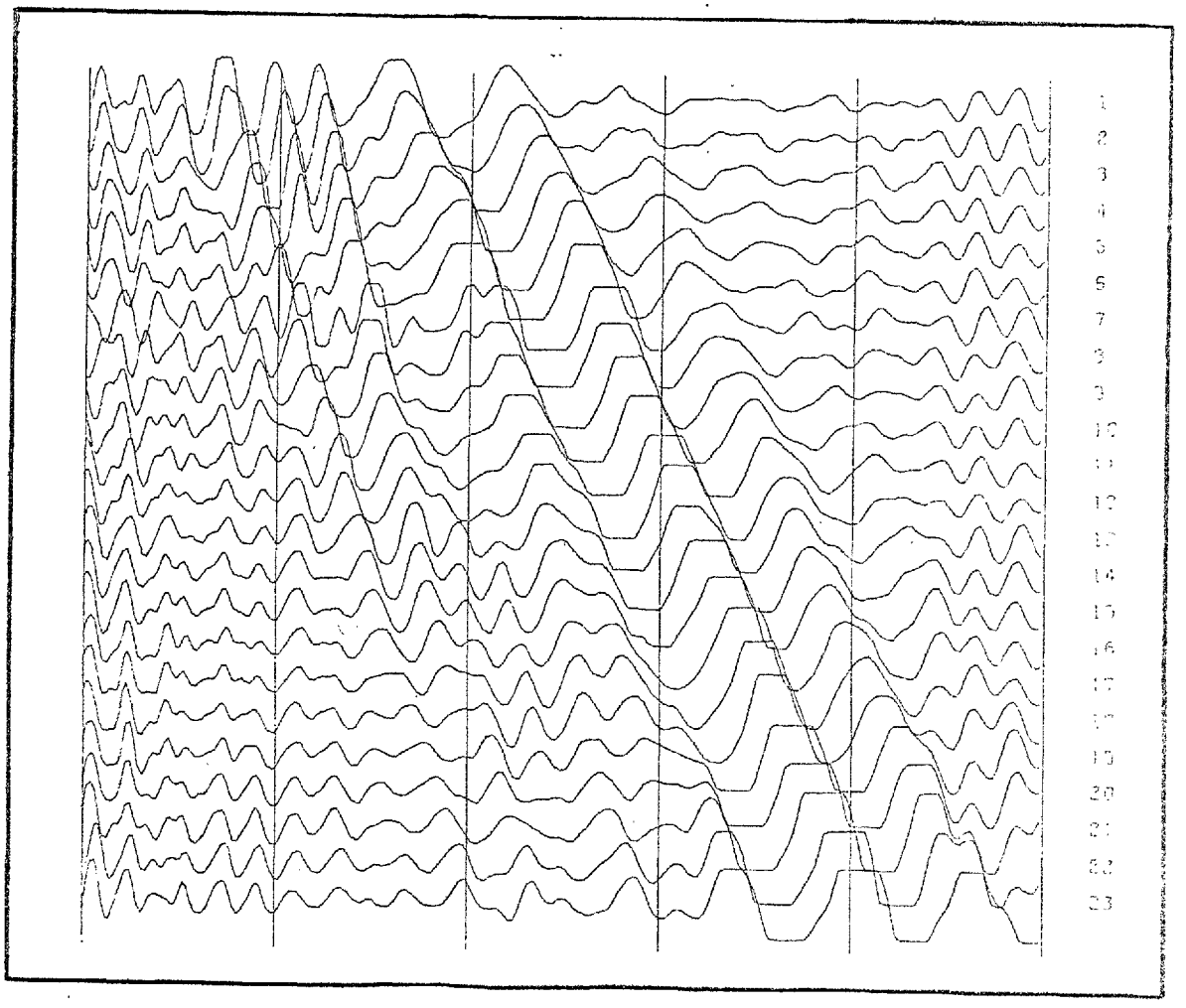


Fig. 1.2 shotpoint 3002, 24 traces (upper), 23 traces (lower)



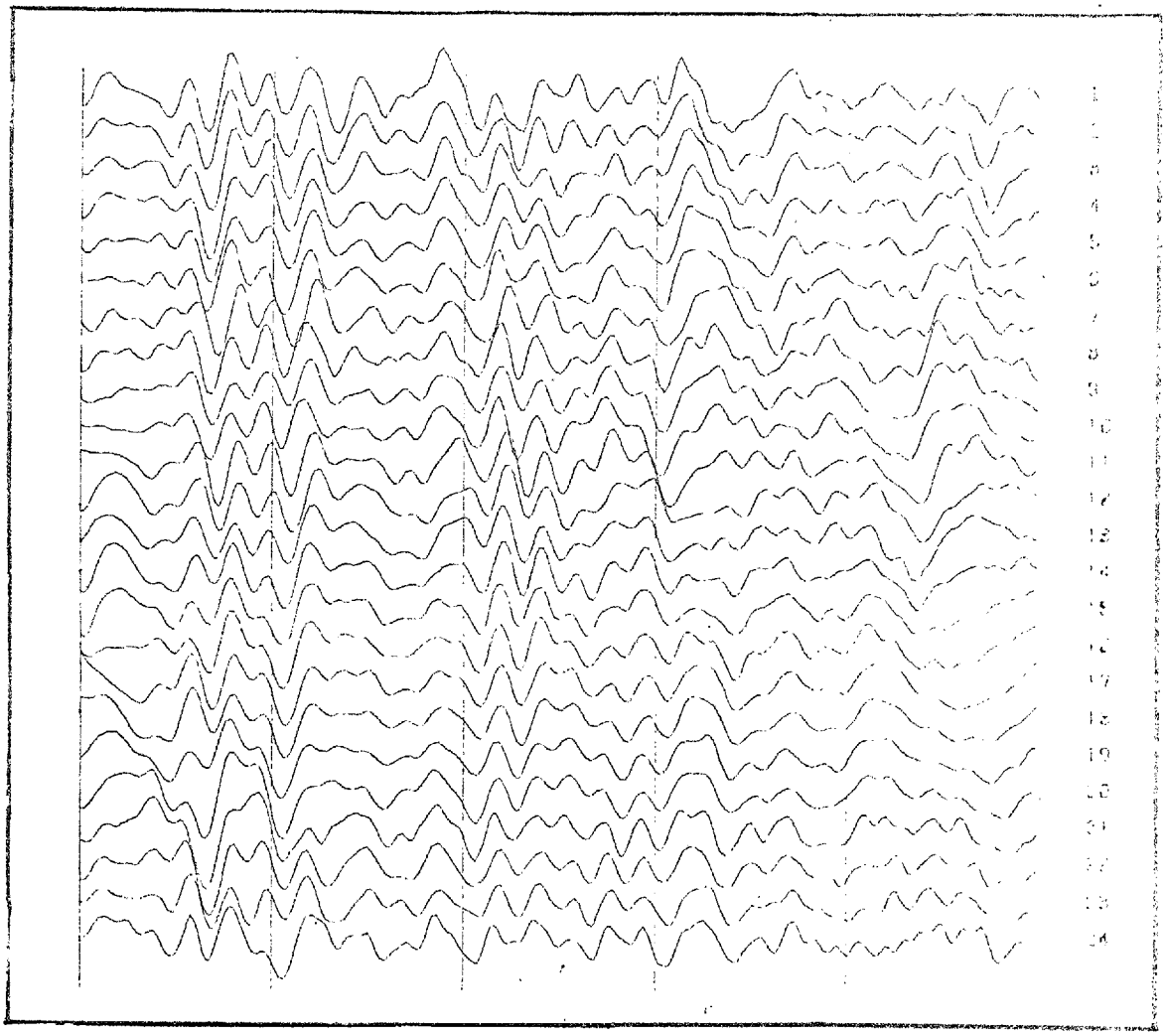
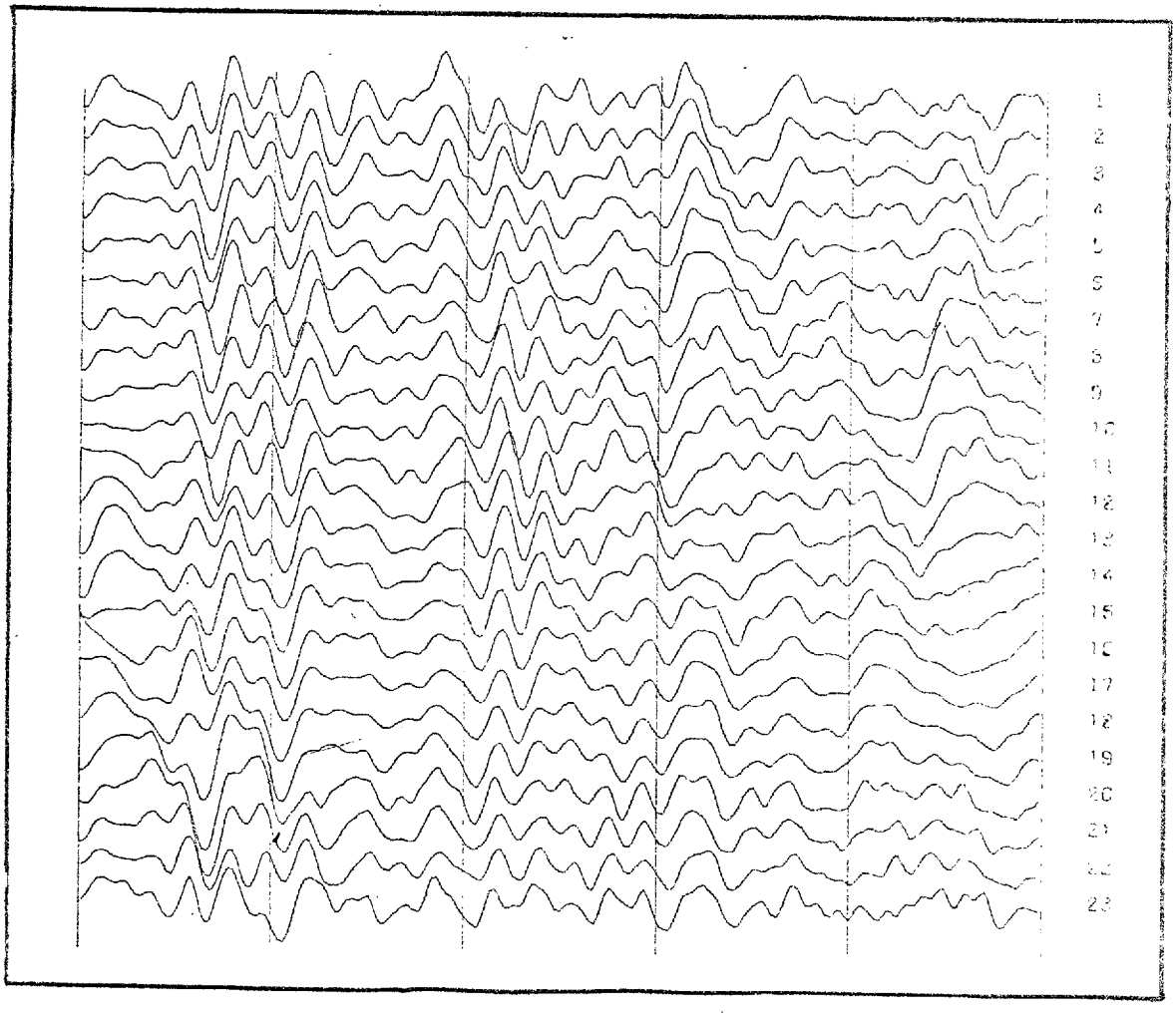


Fig. 1.3 shotpoint 3003, 24 traces (upper), 23 traces (lower)



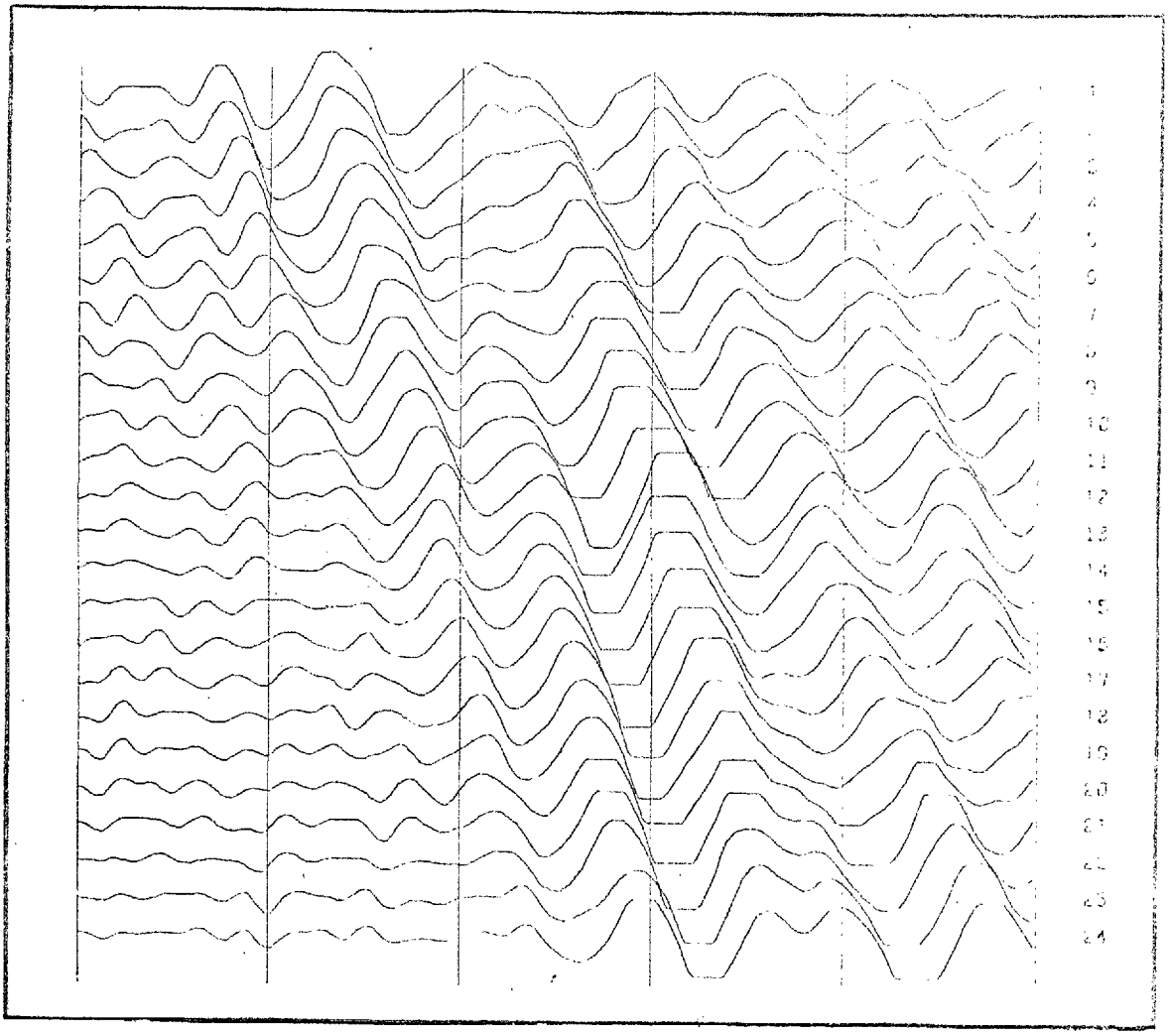
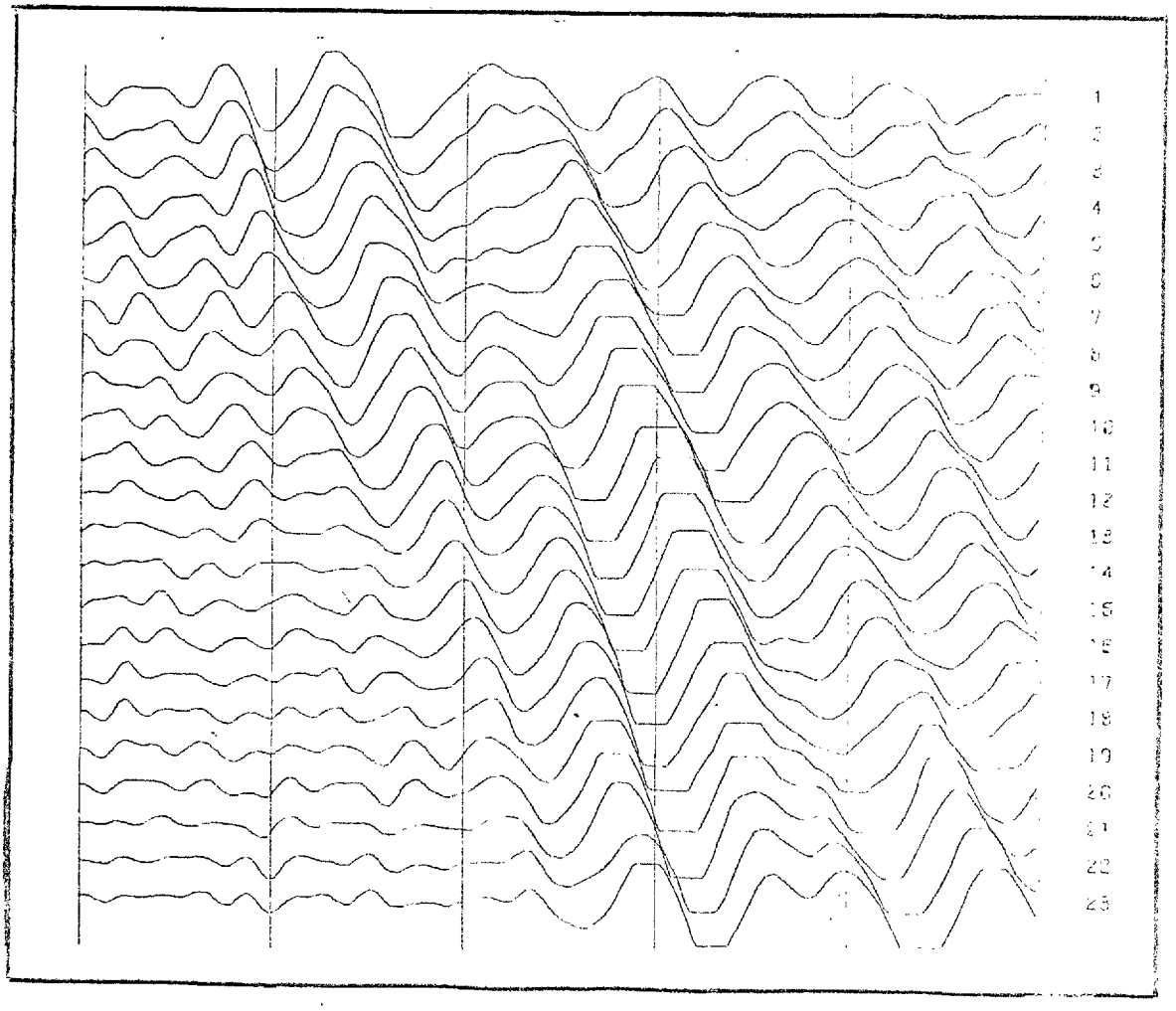


Fig. 1.4 shotpoint 3005, 24 traces (upper), 23 traces (lower)



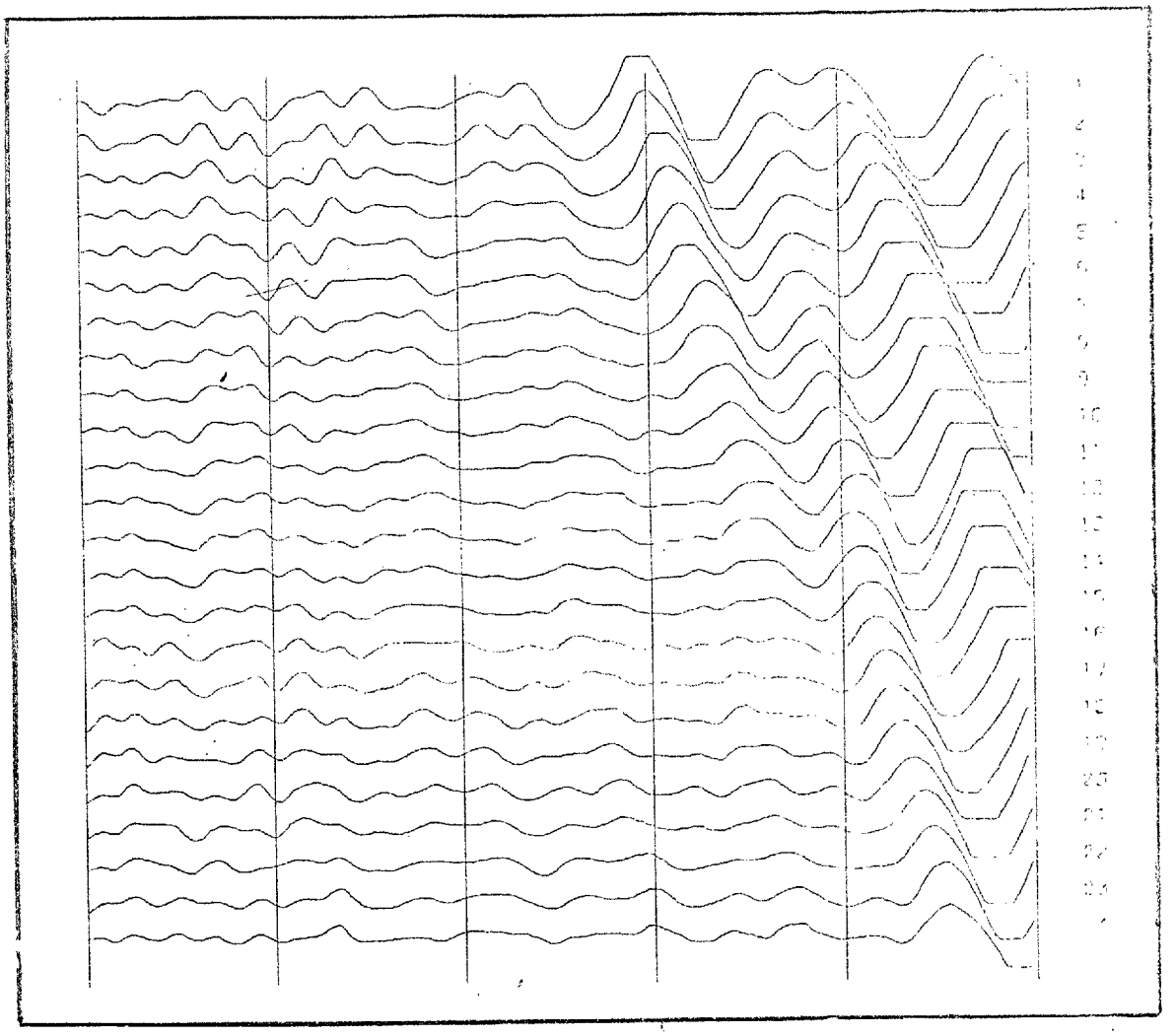
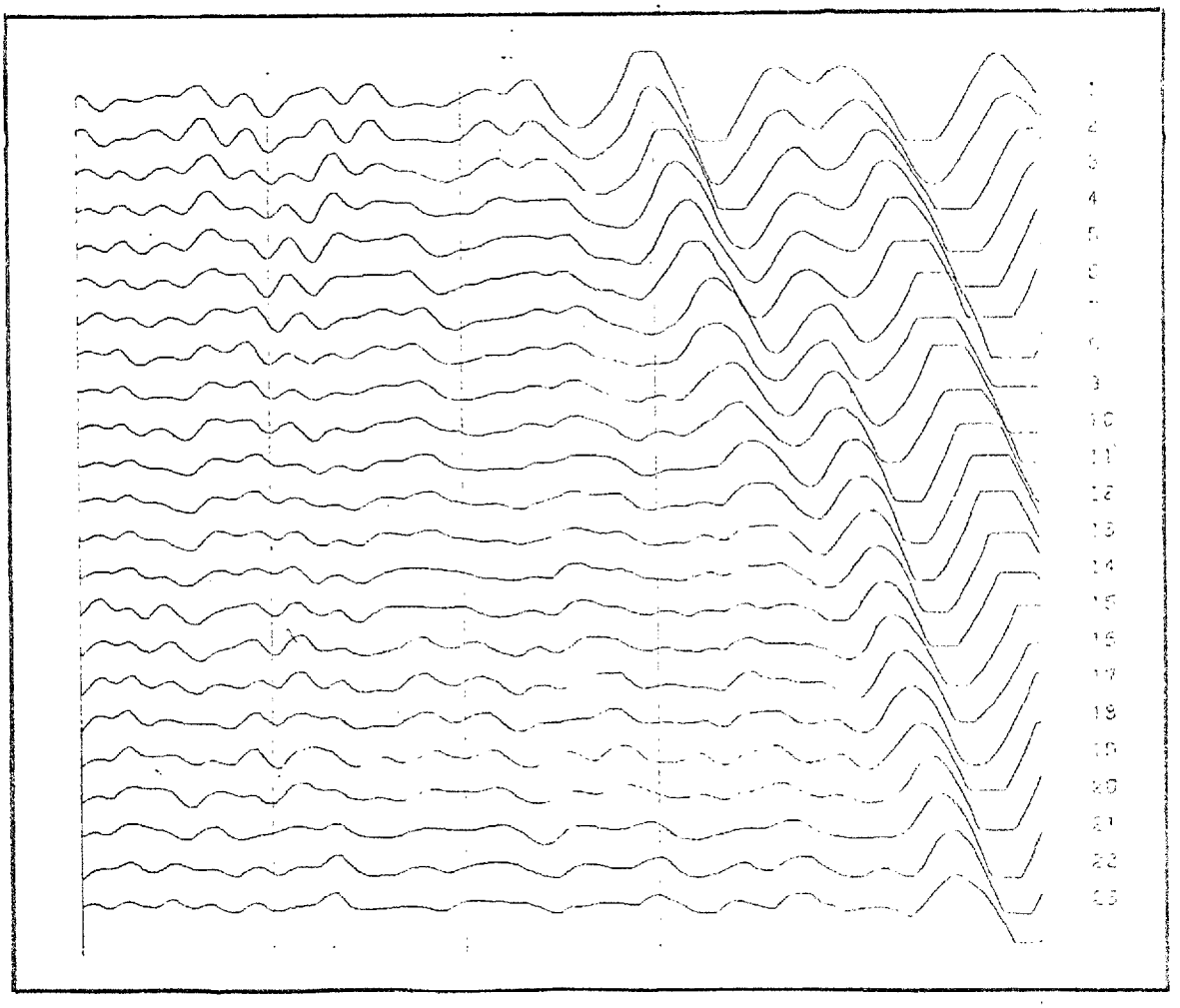


Fig. 1.5 shotpoint 3006, 24 traces (upper), 23 traces (lower)



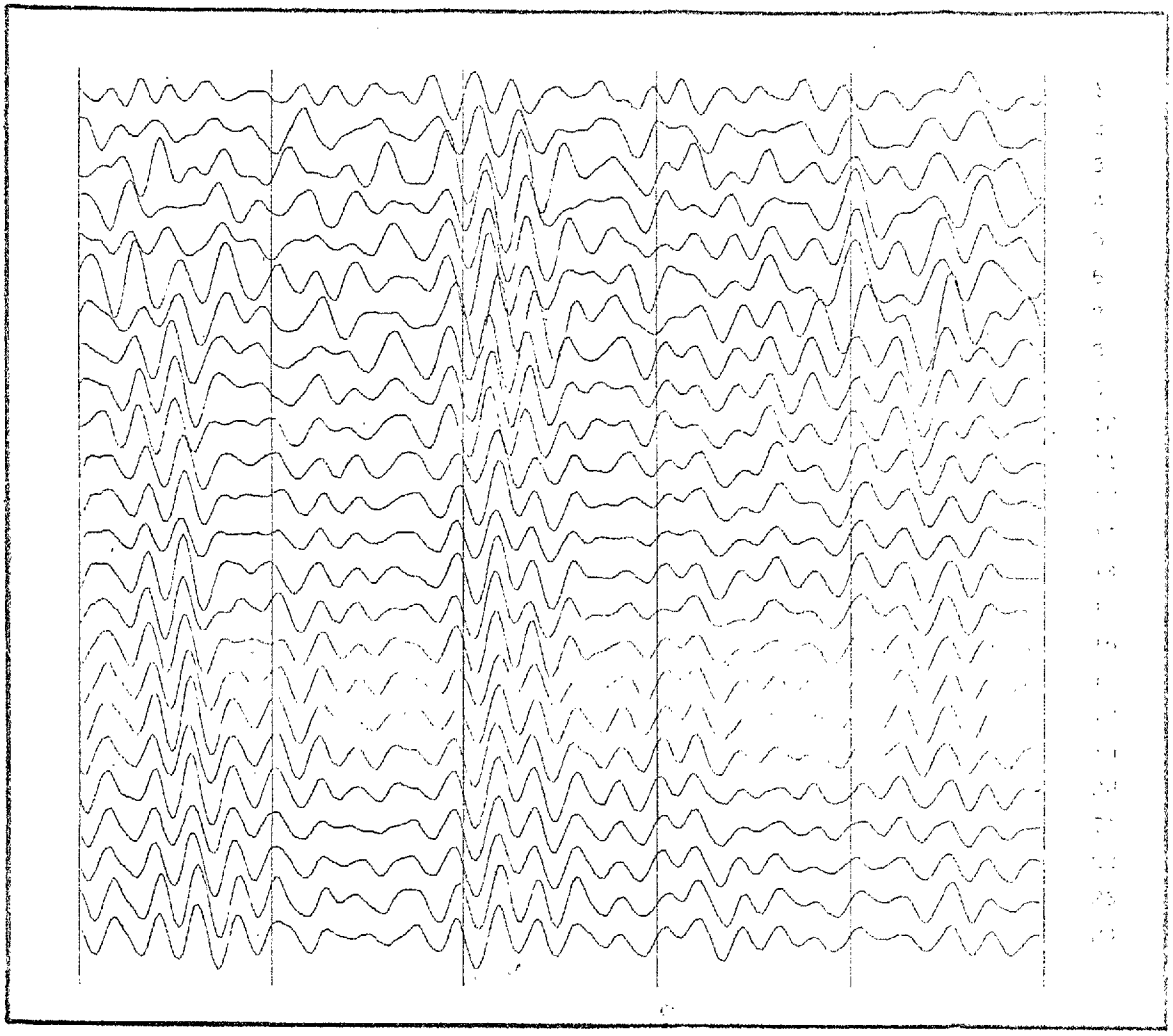
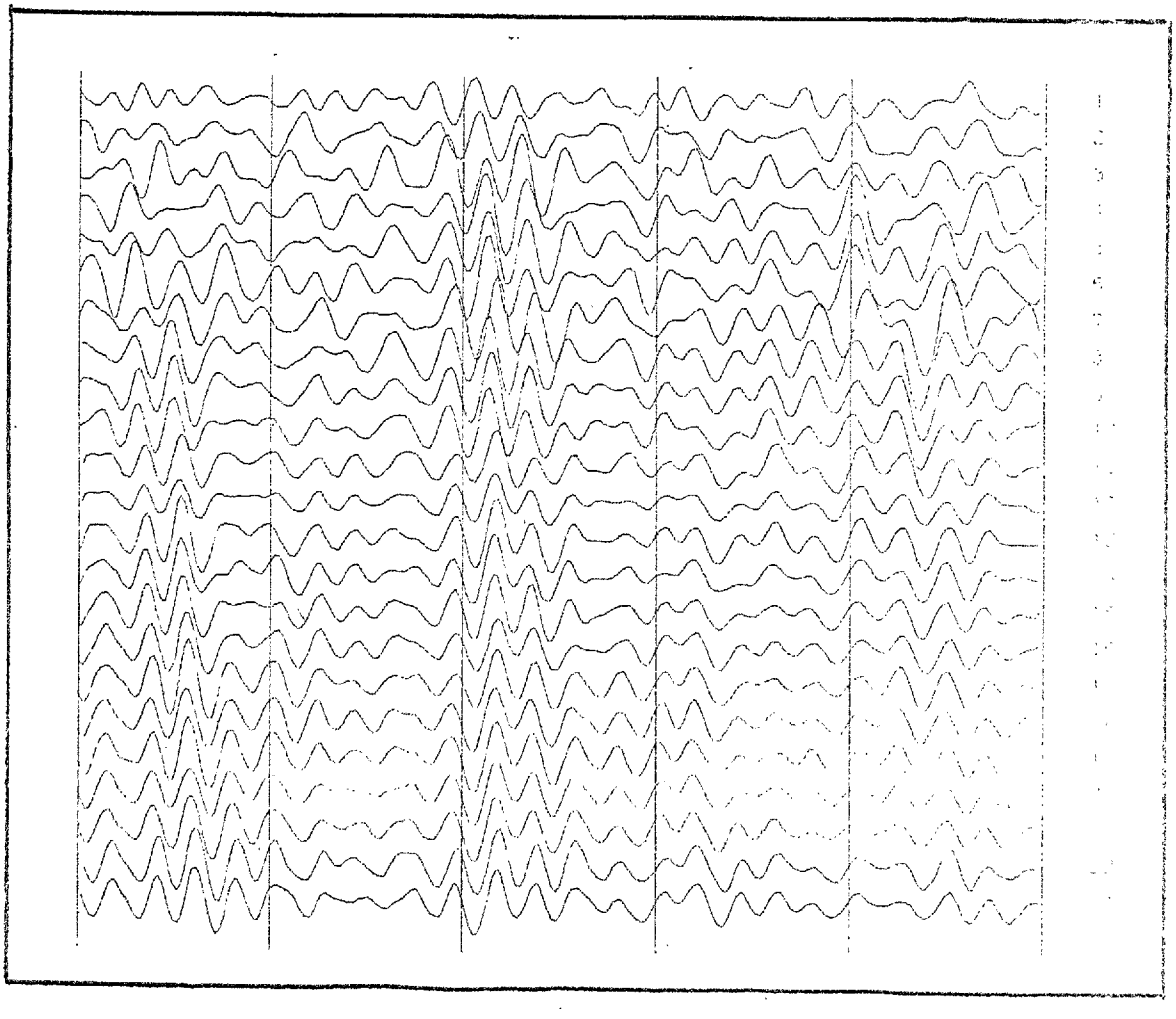


Fig. 1.6 shotpoint 3007, 24 traces (upper), 23 traces (lower)



of the record", and are presented as Fig. 1.7 (shotpoint 3002), Fig. 1.8 (shotpoint 3005) and Fig. 1.9 (shotpoint 3006). This information is summarised in Table 1.2.

Figure number	shot-point number	number of traces	length of trace (in samples)
1.7	3002	23	298
1.8	3005	23	298
1.9	3006	23	298

Table 1.2 Index of band pass filtered real data records

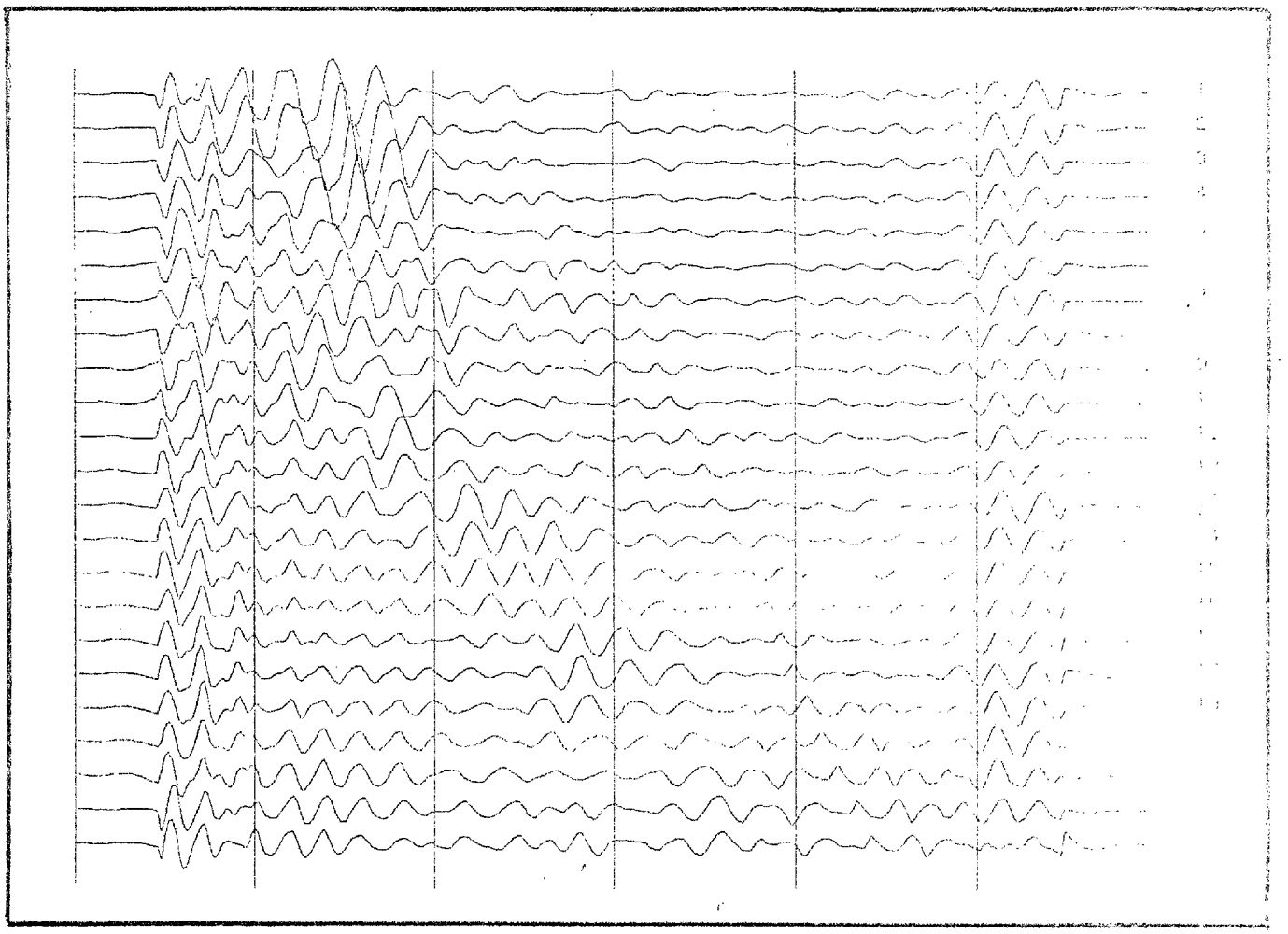
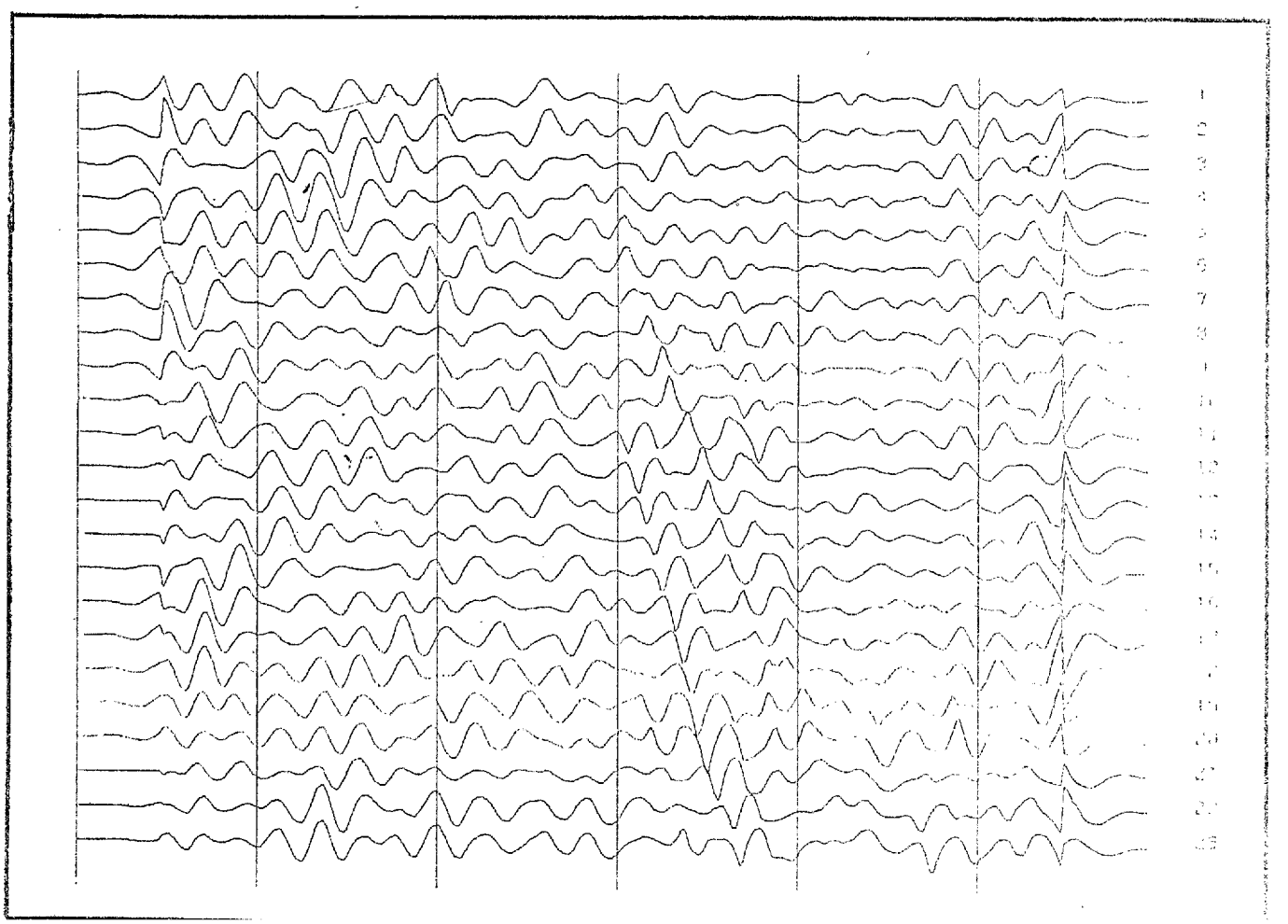


Fig. 1.7 (upper) band-pass filtered shotpoint 3002

Fig. 1.8 (lower) band-pass filtered shotpoint 3005



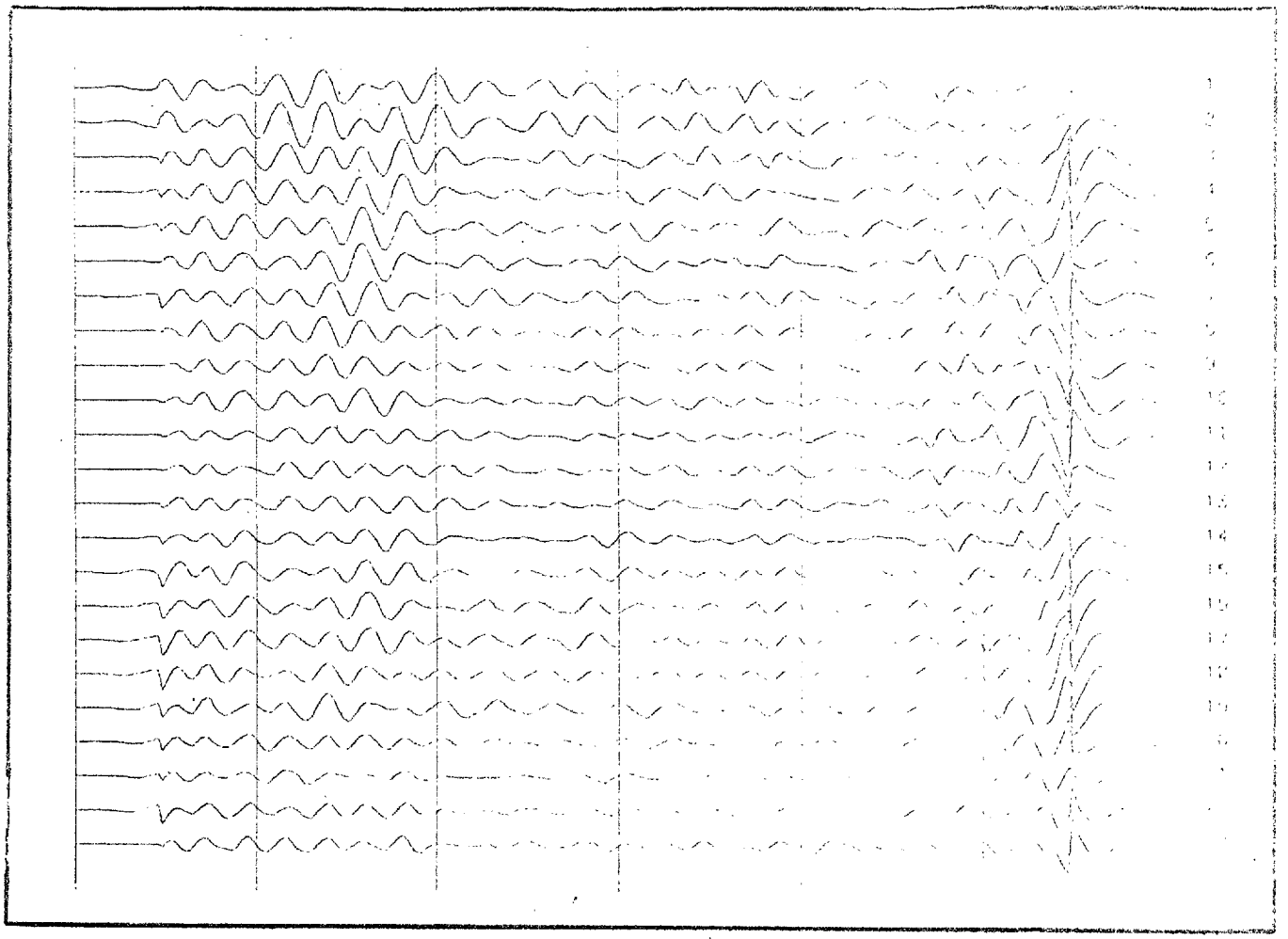


Fig. 1.9 band-pass filtered shotpoint 3006

CHAPTER 2

MULTICHANNEL WIENER MOVEOUT FILTERS IN SEISMIC DATA PROCESSING

2.0 Introduction

The purpose of this chapter is to develop a certain "feel" for multichannel Wiener moveout filters, so that one may educe, for a given situation, just what it is that these filters may be expected to achieve. The filter used, in fact, is the optimum multichannel stacking filter of P. Hubral (1970), which is a development of the Wiener filter (1949). However, the term "multichannel filter" will still suffice.

In the comparison between results produced by different filters it should be noted that the design characteristics of each filter were generally different. Although it would have been desirable for all filters to have the same design characteristics, such as the same weightings on the reject regions, same noise stabilising power and so on, this was just not possible. For example, the same noise stabilising power on two reject/pass filters would produce a mean-square-error of 5% for one and 60% for the other. The compromise solution that was reached was to ensure that each filter had a mean-square-error at maximum lag that was less than 10% that of zero lag. Hence, some difference in the filtered results would be expected on this basis alone. However, it is felt that these differences will not greatly affect the validity of comparing the results of different filters. In any case, one is rather more interested in observing the filtered records than the filters themselves.

The purpose of a multichannel moveout filter is to pass those events of one moveout range, and to reject those events of another moveout range. For this thesis the phrase "moveout of the

filter" will be taken to mean "that moveout for which the filter was designed to pass/reject".

The two basic questions to be investigated in this chapter, by the application of multichannel filters to a variety of real and synthetic data, are (i) to what extent is the performance of a multichannel filter dependent upon different signal to noise ratios?, and (ii) to what accuracy must the moveout of the filter be matched to the moveout of the data?

2.1 Filter theory and design

The optimum multichannel stacking filter, designed to pass one set of moveouts and to reject another set of moveouts, requires that the error between the desired and actual output traces shall be a minimum, in a least squares sense (Treitel, 1970; Finetti et al. 1971). This criterion leads to the following set of normal equations :

$$\sum_{i=1}^{N} A_i(f)\, R_{ij}(f) = G_j(f), \qquad (j=1,\ldots,N)$$

where $A_i(f)$ = required filter components

$R_{ij}(f) = E\left\{\Phi_{ij}(f)\right\}_s + \sigma E\left\{\Phi_{ij}(f)\right\}_r + \mu\, \mathrm{box}(f).\delta_{ij}$

$G_j(f) = E\left\{\Phi_j(f)\right\}$

N = number of traces

and $\Phi_{ij}(f)$ = cross-power soectrum of input traces i,j

$\Phi_j(f)$ = cross-power spectrum of output trace j with the signal on input trace j

$E\{\ \}$ = the expected value of the quantity in brackets

σ = weighting factor for correlated noise

μ = weighting factor for uncorrelated noise

box (f) = 1, for $|f| < \frac{1}{2}$, box (f) = $\frac{1}{2}$, for $|f| = \frac{1}{2}$,

and box (f) = 0, for $|f| > \frac{1}{2}$.

$\delta_{ij} = 1$, for $i = j$; $\delta_{ij} = 0$, for $i \neq j$.

Quite clearly, the terms for $R_{ij}(f)$ refer to contributions from signal, correlated noise and uncorrelated noise. Note that it has been assumed that the input signals are broad-band, i.e.

$$E\{\Phi_{ii}(f)\} = \text{box}(f).$$

The arrival time of the signal, α_j, is regarded as a random variable and is confined to arrive within a time window specified by t_j and $t_j + \Delta t_j$. A reference trace r is chosen so that

$$\alpha_j = t_j + \frac{\Delta t_j}{2} + \eta \frac{\Delta t_j}{\Delta t_r} + \gamma_j$$

The parameters η and γ_j are both random variables, of probability distribution functions given by

$$p(\eta) = \frac{1}{\Delta t_r} \text{box}(\eta / \Delta t_r), \qquad p(\gamma_j) = \frac{1}{t_c} \text{box}(\gamma_j / t_c)$$

From these relations it can be seen that the random variable η forces the arrival times of the signals to fall on non-overlapping curves, dividing the window for each trace in the same ratio. The random variable γ_j allows for some random deviation from any curve determined by η on each trace. The parameter t_c is termed the "chatter parameter" (cf. Galbraith and Wiggins, 1968).

All these considerations are included in the filter-producing program of Hubral, which uses many of the subroutines presented by Robinson (1967a). For this present work it is sufficient to merely consider those features that are directly relevant to the computation of a multichannel moveout filter.

Figure 2.1 shows a typical time window used for the computation of linear moveout Wiener filters. Such a time window would pass (reject) moveouts in the range $|\tau| \leq \tau_c$, and reject (pass) moveouts in the range $\alpha.\tau_c \leq |\tau| \leq \gamma.\tau_c$. It is possible, of course, to introduce more regions into the time window so as to reject more

than one range of moveouts. However, it has been shown (Hubral) that the performance of a filter is generally better for fewer design regions. A number of filters were computed for different moveouts, and the specifications are presented in Table 2.1. The length chosen for a filter was generally taken to be twice that of the maximum moveout displacement encompassed by the number of filter components, e.g. a 12-trace filter designed to reject a moveout of 1 sample per trace would have each component of length 24 samples. Such a choice gives phase-free filters.

A list of all the terms used in Table 2.1 appear as follows :

filter name = name by which the filter will be referred.

ID, NUMB = filter code for use with the "Geodat" package.

τ_c = critical moveout it is desired to accept/reject for the central region, in samples per trace.

τ_b = principal moveout it is desired to accept/reject for the outer regions, in samples per trace.

$\Delta\tau_b$ = tolerated difference about τ_b, in samples per trace.

α, γ = parameters determining the boundaries of the outer regions.

NF = number of filter components.

LF = length of each filter component, in samples.

e = mean square error at maximum lag, as a % of that at zero lag.

σ = weighting factor for correlated noise

μ = weighting factor for uncorrelated noise, i.e. the noise stabilising power.

From Figure 2.1 it can be seen that $\Delta\tau_b = (\gamma - \alpha).\tau_c / 2$.

Filter *RP10, for example, is a reject-pass filter that is designed to reject moveouts in the range $|\tau| \leq 0.5$, and to pass moveouts in the range $1.5 \leq |\tau| \leq 2.5$.

The differences between the desired and actual characteristics of a multichannel filter, and the effects of varying the design parameters on these characteristics, have been discussed by Hubral, (1970).

The chatter parameter for all filters was taken to be 0.01, and the output trace was taken to be where the window cross-over took place.

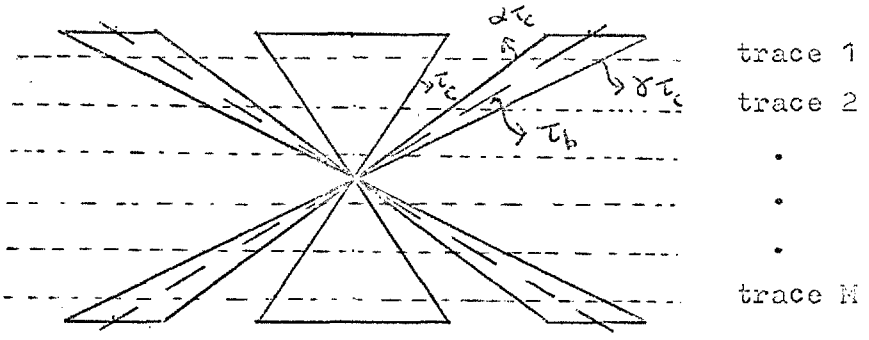


Fig. 2.1 time window for a moveout filter

The application of a multichannel filter was effected through the use of the "Geodat" package. The input traces, $(x_i(t),\ i=1,,,N)$, were convolved with the appropriate filter components, $(f_j(t),\ j=1,,,M)$, to give the filtered output traces, $(y_k(t),\ k=1,,,N-M+1)$, according to

$$y_k(t) = \sum_{j=1}^{M} f_j(t) * x_{k+j-1}(t)$$

The relation for the number of output traces may be derived as follows :

Let max(q) denote the maximum value of the parameter q.

Hence, max(k+j-1) = N

$$\therefore \max(k) + \max(j) - 1 = N$$

But max(j) = M,

$$\therefore \max(k) = N - M + 1$$

It should be noted that each filtered output trace has undergone an M-fold stacking process. Hence it can be expected that each output trace would have an M-fold reduction in the signal to uncorrelated noise power ratio (Robinson, 1970a).

If it is desired to filter a given record more than once, then it is clearly necessary to choose the number of filter components in each filter very carefully. If both filters have a large number of components, then the number of output traces will be very few; conversely, fewer filter components will lead to more output traces, but these traces will probably be of a poorer quality than those of the former case. Each individual filtering problem has to be considered on its own merits, but one should aim to have at least six traces in the final record in order to ascertain the presence of any residual moveouts.

The analysis so far is only valid for linear moveout. Because linear moveout is linear (sic) the same filter $\{f_j(t)\}$ may be applied (N-M+1) times in succession to the N sets of input traces. However, for hyperbolic moveout, each of the (N-M+1) applications require a different filter - hence $\{f_j(t)\}$ becomes $\{f_j^k(t)\}$. Hyperbolic moveout filters have the problem that the random variable η does not divide the window for each trace in the same ratio. This problem does not exist, however, for quadratic moveout filters. Accordingly, therefore, a quadratic filter will be taken in order to effect a more suitable comparison between the results of linear and non-linear filtering.

It was decided to compute a "quadratic analogue" of filter *PR1, that would pass low moveout linear events, and reject high moveout quadratic events. Consequently, the time window of Figure 2.1 was taken, with the boundaries of the outer regions now being quadratic rather than linear. The widths of the upper and lower extremities of these regions are, of course, now different. In order

to filter out a moveout of the form $\beta_i = q^2/24$, where q is the trace number, the set of filters presented in Table 2.2 were computed. The filters were designed to pass linear moveouts $|\tau| \leq 0.25$, and to reject quadratic moveouts $q^2/24 - \Delta q \leq |\tau| \leq q^2/24 + \Delta q$, where

$$\Delta_q = \frac{1}{2}\left(\frac{q^2 - q_{ref}^2}{q_{max}^2 - q_{ref}^2}\right)$$

and q_{ref} = reference trace number

q_{max} = maximum trace number

The total set of quadratic filters needed to filter out a given moveout will often be referred to as a "quadratic filter". The equations for the inner (b_{in}) and outer (b_{out}) boundaries of the quadratic regions were given by

$$b_{in} = \frac{1}{24} - \frac{z}{q_{ref}^2}, \quad b_{out} = \frac{1}{24} + \frac{z}{q_{ref}^2}$$

where $z = \dfrac{q_{ref}^2 \cdot d}{2\left(q_{max}^2 - q_{ref}^2\right)}$, and $d = 1.0$ (window width at lower extremity)

The set of filters Q1 - Q13 will often be referred to by the filter name "Q".

REJECT-PASS FILTERS

filter name	filter code ID	filter code NUMB	τ_c	τ_b	$\Delta\tau_b$	α	γ	NF	LF	ϵ	σ	μ
*RP1	2	1	0.5	1.0	0.5	1	3	12	25	8	20	3.0
*RP2	2	2	0.5	2.0	0.5	3	5	6	25	5	20	1.0
*RP3	2	3	0.5	4.0	0.5	7	9	6	50	4	20	1.0
*RP4	2	4	0.5	3.0	0.5	5	7	6	38	1	20	0.5
*RP5	2	5	0.5	1.0	0.5	1	3	6	13	3	20	0.5
*RP7	2	7	0.5	3.0	0.5	5	7	9	54	6	25	4.0
*RP10	2	10	0.5	2.0	0.5	3	5	10	40	4	20	2.0

PASS-REJECT FILTERS

filter name	filter code ID	filter code NUMB	τ_c	τ_b	$\Delta\tau_b$	α	γ	NF	LF	ϵ	σ	μ
*PR1	1	1	0.25	1.0	0.5	2	6	12	25	7	1.0	0.05
*PR2	1	2	0.25	2.0	0.25	7	9	10	41	4	0.9	0.05
*PR3	1	3	0.25	0.6	0.4	1	4	12	25	8	0.9	0.05
*PR4	1	4	0.25	1.0	0.5	2	6	6	25	8	0.3	0.05
*PR6	1	6	0.25	0.5	0.25	1	3	12	25	0	0.8	0.05
*PR7	1	7	0.25	1.5	0.25	5	7	12	32	6	1.0	0.05
*PR8	1	8	0.25	3.0	0.5	10	14	9	54	8	0.9	0.05
*PR9	1	9	0.25	3.0	1.0	8	16	9	54	2	0.6	0.05
*PR10	1	10	0.25	3.0	2.0	4	20	9	54	3	0.6	0.05

Table 2.1 specifications for linear moveout filters

PASS-REJECT FILTERS

filter name	filter code ID	filter code NUMB	τ_L	NF	LF	ℓ	σ	μ
Q1	5	1	0.25	12	25	5	0.8	0.8
Q2	5	2	0.25	12	25	3	0.8	0.8
Q3	5	3	0.25	12	25	6	0.9	0.5
Q4	5	4	0.25	12	25	5	0.9	0.5
Q5	5	5	0.25	12	25	3	0.8	1.0
Q6	5	6	0.25	12	25	3	0.8	1.0
Q7	5	7	0.25	12	25	2	0.8	1.0
Q8	5	8	0.25	12	25	8	0.9	0.8
Q9	5	9	0.25	12	25	9	0.9	0.9
Q10	5	10	0.25	12	25	7	0.9	0.8
Q11	5	11	0.25	12	25	7	0.9	0.8
Q12	5	12	0.25	12	25	6	1.0	0.2
Q13	5	13	0.25	12	25	6	1.0	0.2

Table 2.2 specifications for quadratic moveout filters

2.2 Filter applications to synthetic data

The specifications for all the synthetic data computed in this chapter, together with the appropriate filtering information, is presented in Table 2.3. In order to facilitate the comparison of results between real and synthetic data, a record length of 250 samples was chosen in each case. Each plot was normalised by the maximum trace amplitude present in that plot, and was also assigned a unique figure number. All the synthetic records consist of 24 traces, corresponding to the common "end-on" shooting arrangement, with trace 1 nearest the shot. A little further discussion on the synthetic data is now appropriate.

The analyses of noise theory (e.g. Bracewell, 1965), require that the average amplitude of the noise component shall be zero. Quite clearly it is impossible to guarantee this condition for real data, so consequently no attempt was made to satisfy this requirement for synthetic data. The taking of large record lengths, of course, improves the statistical independence of the random noise and also causes the average amplitude of this noise to tend towards zero. However, as was indicated in the previous chapter, very large record lengths of real data have to be excluded due to problems of stationarity. Furthermore, it was not considered necessary to remove the average amplitude of each trace from each trace, since no noticeable vertical translation of the autocorrelation functions could be observed (see Chapter 3). It is assumed, therefore, that the average amplitude of each trace is either zero or very nearly zero, with a similar assumption for the random noise component. These two assumptions apply to both real and synthetic data.

In comparing the results from real and synthetic data it must be remembered that real data will generally contain fewer reflections "per unit record length" than will synthetic data. Hence, a given signal to noise ratio for real data will result in a more

"readable" record than that for synthetic data. On this basis of signal to noise ratio, then, one would expect better results from real data than from synthetic data. Other considerations, however, such as those mentioned in the previous chapter, will degrade the real data results.

N.B. In all the plots of input traces and filtered records, the vertical scale corresponds to the trace numbering system and the horizontal scale to time (in milliseconds). A "timing line" is drawn across each record at 100 msec. intervals (i.e. every 50 samples). The origin is always taken to be 0 msec., and the traces are played out in the direction left to right.

SYNTHETIC DATA

UNFILTERED RECORDS					FILTERED RESULTS		
Figure number	ρ (db)	ν (db)	α_i	β_i	unfiltered Fig. No.	filtered Fig. No	filter name
2.2	-6.0	6.0	0	i	2.2	2.3	*PR1
2.4	-15.0	6.0	0	i	2.4	2.5	*PR1
2.6	-20.0	6.0	0	i	2.6	2.7	*PR1
2.8	-30.0	6.0	0	i	2.8	2.9	*PR1
2.10	0.0	0.0	0	i	2.10	2.11	*PR1
2.12	0.0	-6.0	0	i	2.12	2.13	*PR1
2.14	0.0	-12.0	0	i	2.14	2.15	*PR1
2.16	-15.0	-6.0	0	i	2.16	2.17	*PR1
2.18	0.0	-9.0	0	3i	2.18	2.19	*PR8
					2.18	2.20	*PR9
					2.18	2.21	*PR10
					2.4	2.22	*PR7
					2.4	2.23	*PR2
					2.4	2.24	*PR4
					2.4	2.25	*PR4 (twice)
2.26	-15.0	6.0	0	$i^2/24$	2.26	2.27	Q
2.28	0.0	0.0	0	$i^2/24$	2.28	2.29	Q
2.30	0.0	-6.0	0	$i^2/24$	2.30	2.31	Q
					2.26	2.32	*PR1

Table 2.3 specifications for synthetic data

2.2.1 effects of different noise levels

This section is concerned with the effect of different signal to noise ratios, for both correlated and uncorrelated noise, on the performance of a multichannel filter. All moveout and filtering information may be found in Table 2.3.

Fig. 2.2 shows an input record for a correlated noise level of ρ = -6.0 db, and an uncorrelated noise level of ν = 6.0 db. Applying pass/reject filter *PR1 gives the result of Fig. 2.3, where it is seen that the correlated noise has been completely removed and that the signal has been successfully recovered. Similarity of signal shape across the record is very good.

Increasing the correlated noise level in successive stages, whilst keeping the random noise level constant at 6.0 db, gives the input records of Fig. 2.4 (ρ = -15.0 db), Fig. 2.6 (ρ = -20.0 db) and Fig. 2.8 (ρ = -30.0 db). The results of applying filter *PR1 are given as Fig. 2.5, Fig. 2.7 and Fig. 2.9, respectively. Fig. 2.5 shows that the very strong correlated noise of Fig. 2.4 has been almost completely removed, and that signal recovery compares quite favourably with Fig. 2.3. Comparing the input data of Fig. 2.2 and Fig. 2.4, together with their respective filtered results, show that the multichannel filter has certainly achieved a quite remarkable result. Increasing the correlated noise level (Fig. 2.6) leads to a deterioration in the rejection of correlated noise (Fig. 2.7), though the detection of signal is still apparent. Increasing the correlated noise still further (Fig.2.8) leads to a complete breakdown in the filtering (Fig. 2.9). No signal can be seen and rejection of correlated noise is very poor. (A better presentation of Fig. 2.9 is given in Fig. 2.9(b) - the former picture has a "suppressed" appearance due to the presence of very large amplitudes at the end of the record, accordingly, the latter picture consists of the first 500 msec. of the former picture).

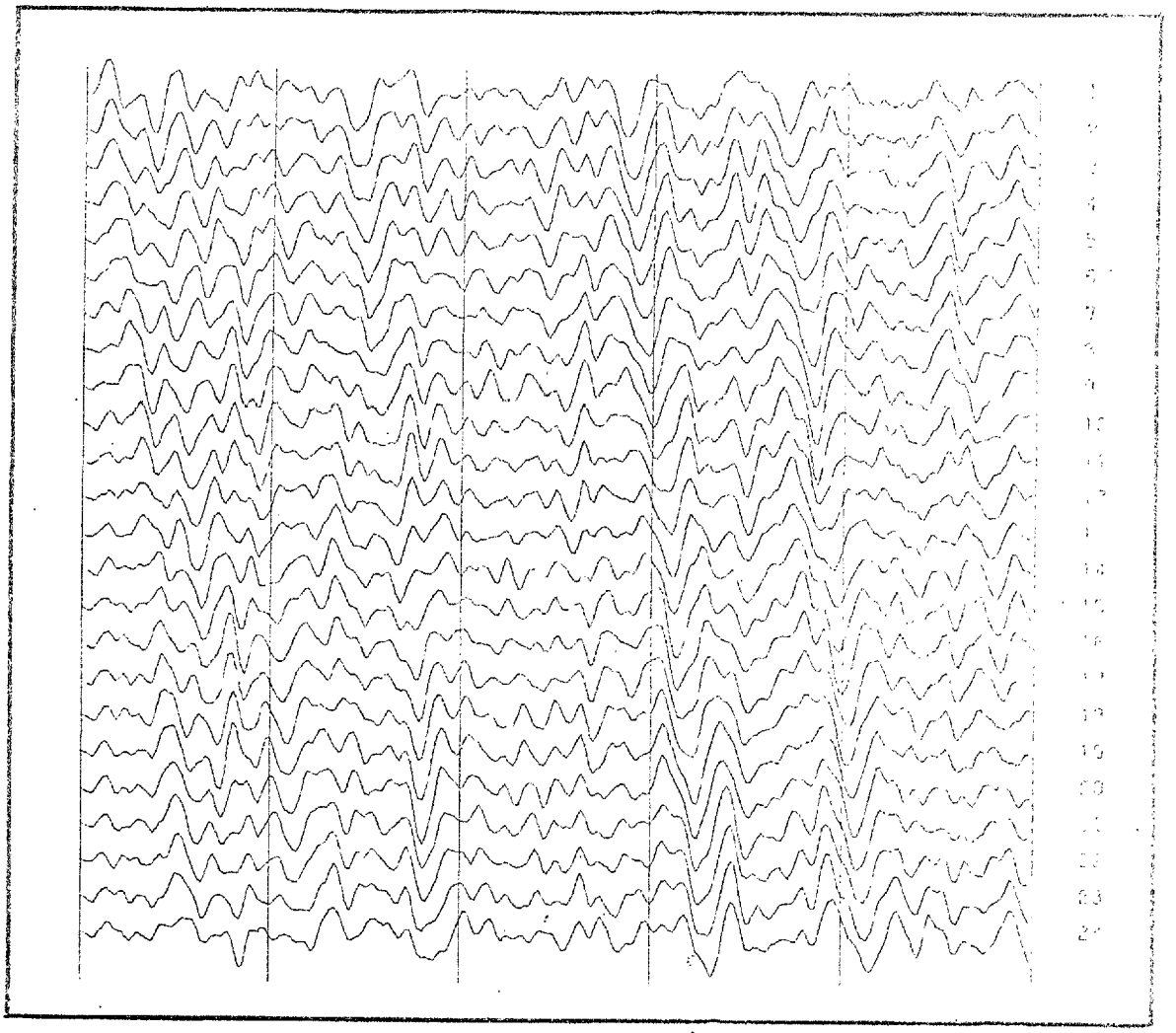


Fig. 2.2 input record, ρ = -6.0, ν = 6.0

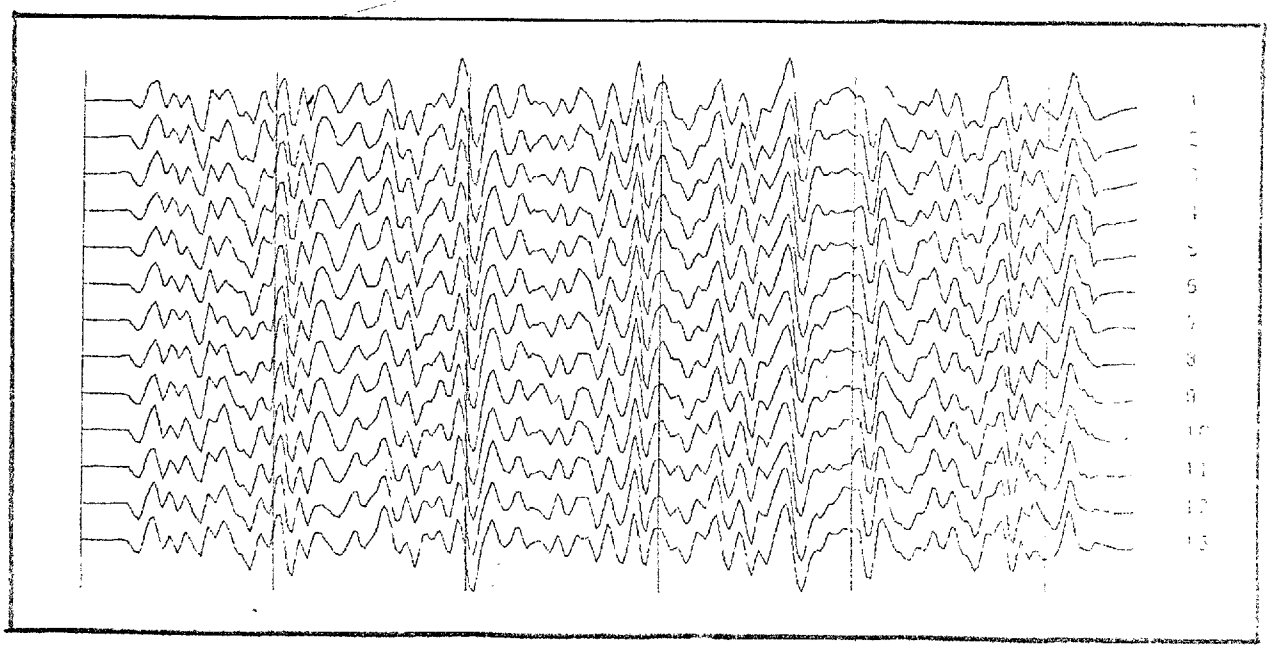


Fig. 2.3 result of filtering Fig. 2.2 with *PR1

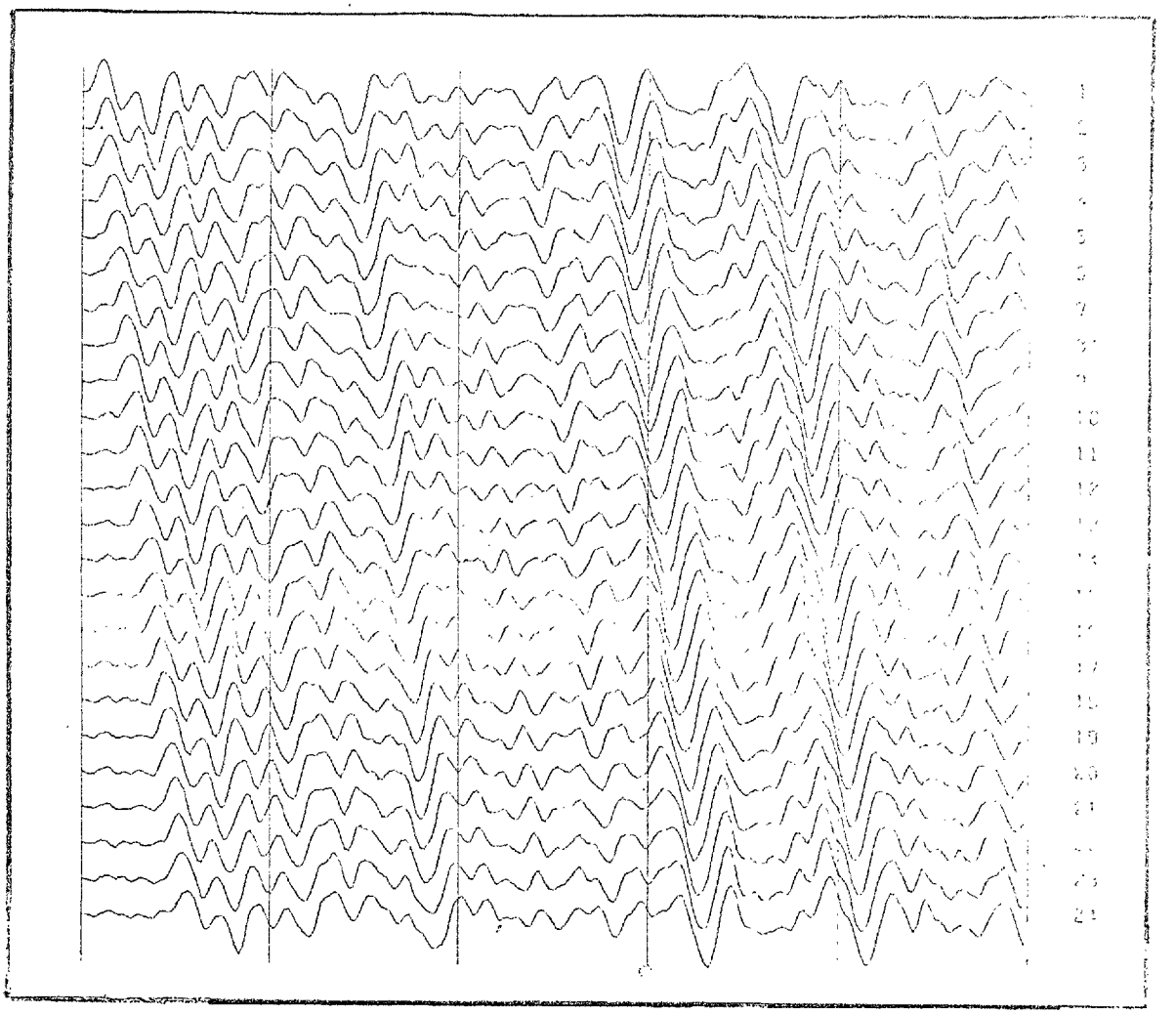


Fig. 2.4 input record, $P = -15.0$, $\nu = 6.0$

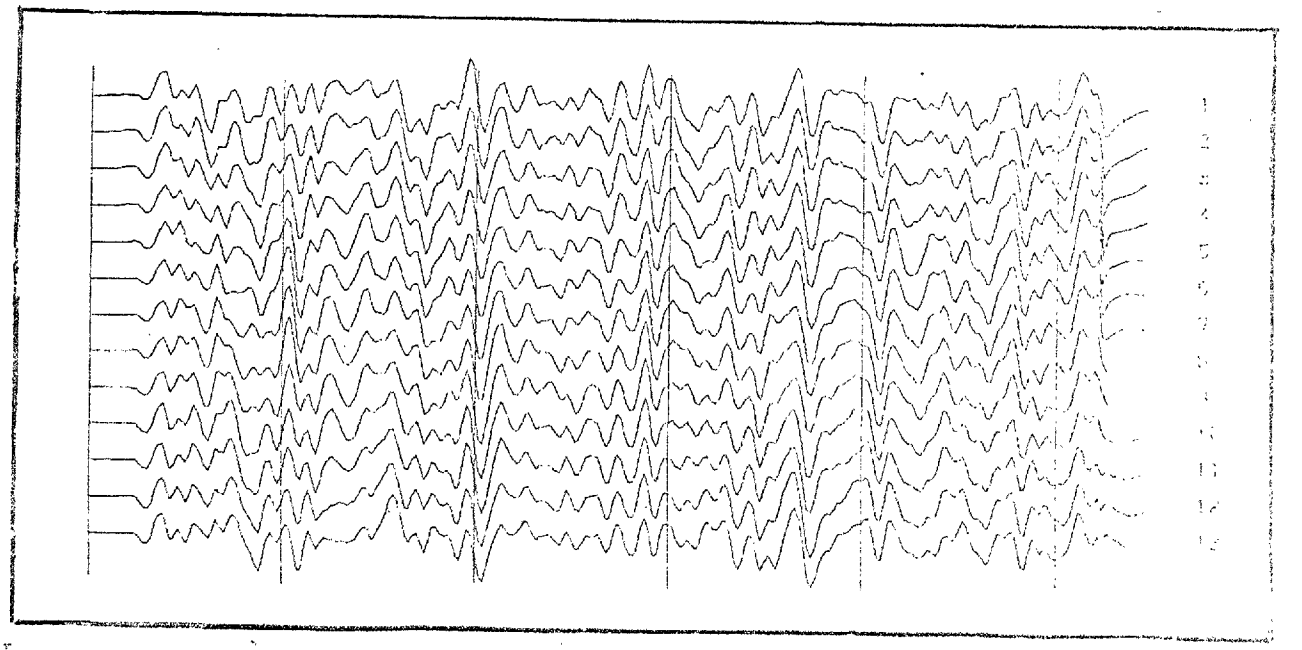


Fig. 2.5 result of filtering Fig. 2.4 with F_{KM}

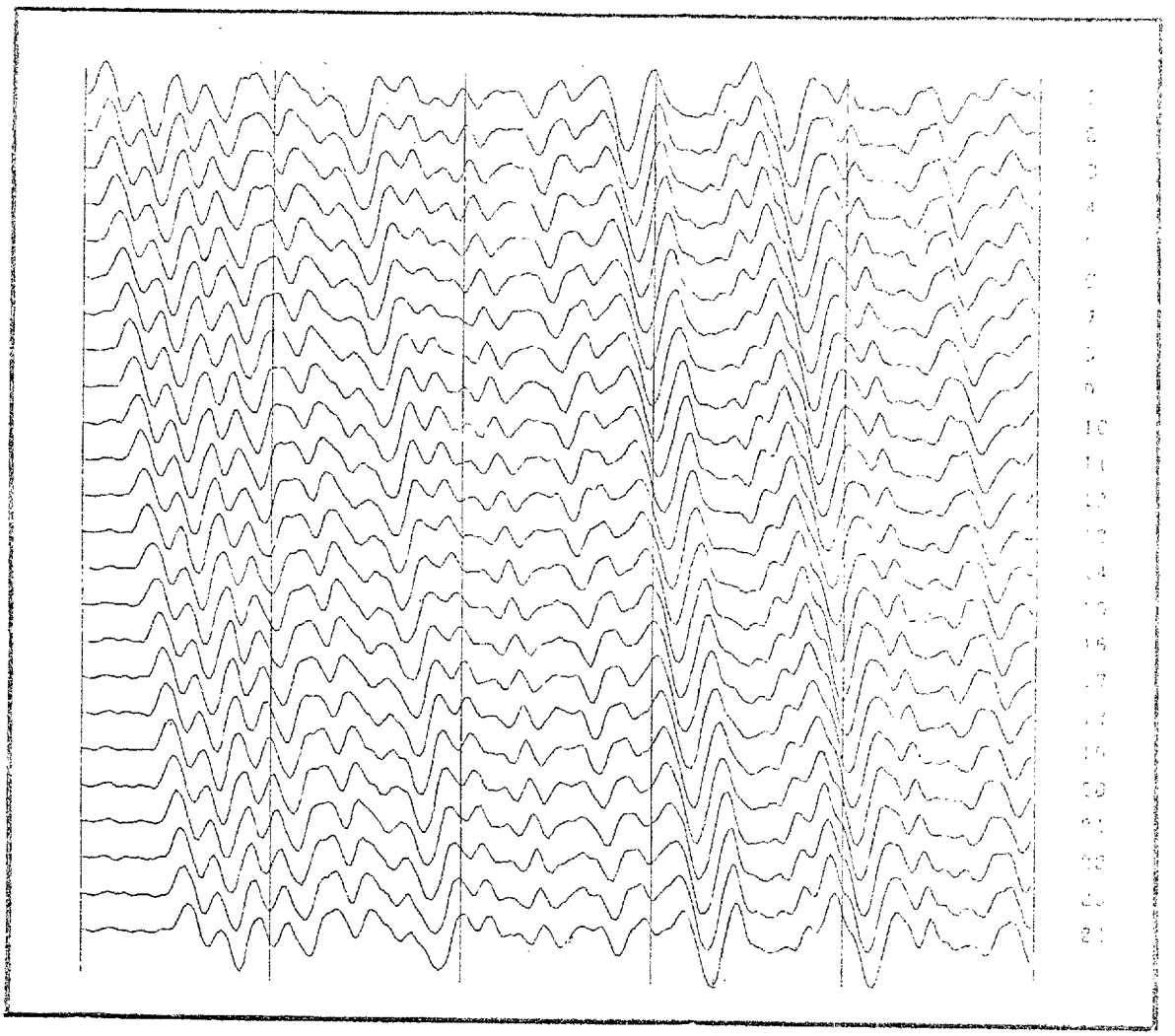


Fig. 2.6 input record, $p = -20.0$, $\nu = 6.0$

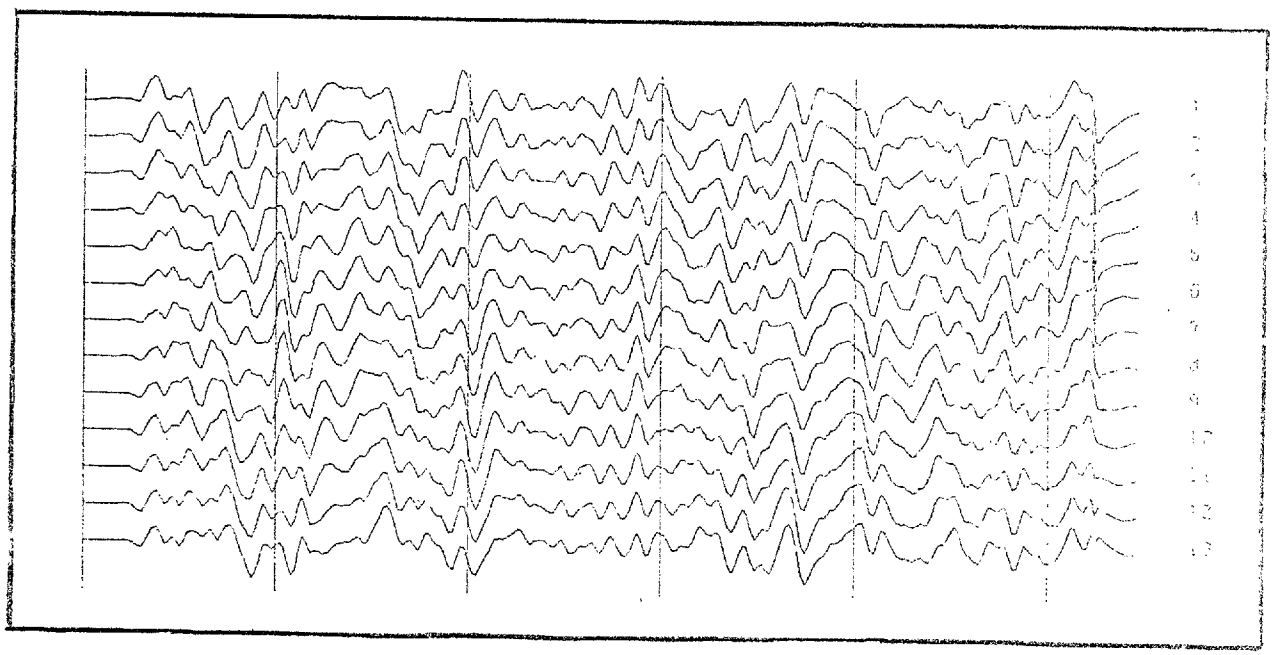


Fig. 2.7 result of filtering Fig. 2.6 with *PR1

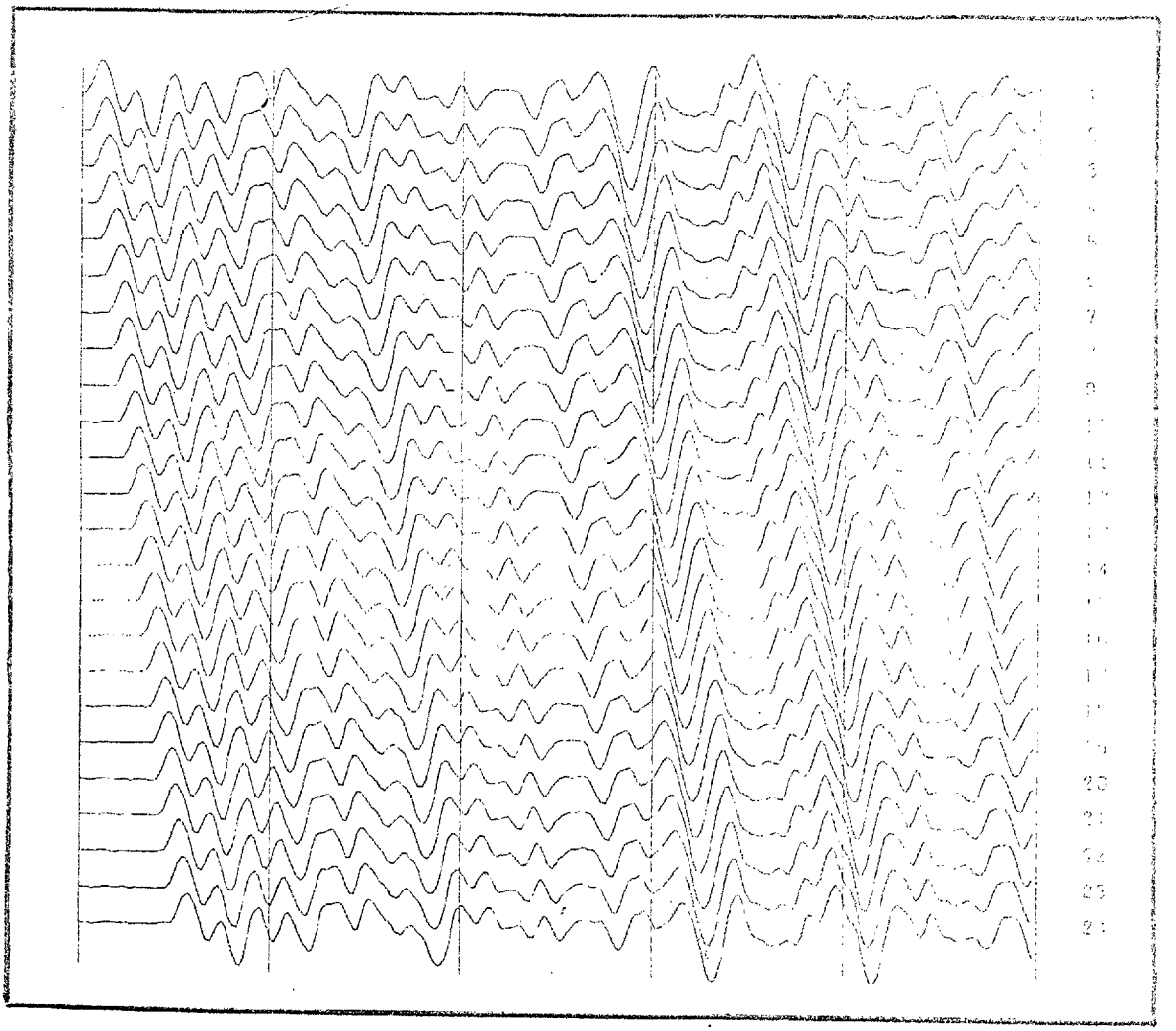


Fig. 2.8 input record, $P = -30.0$, $\nu = 6.0$

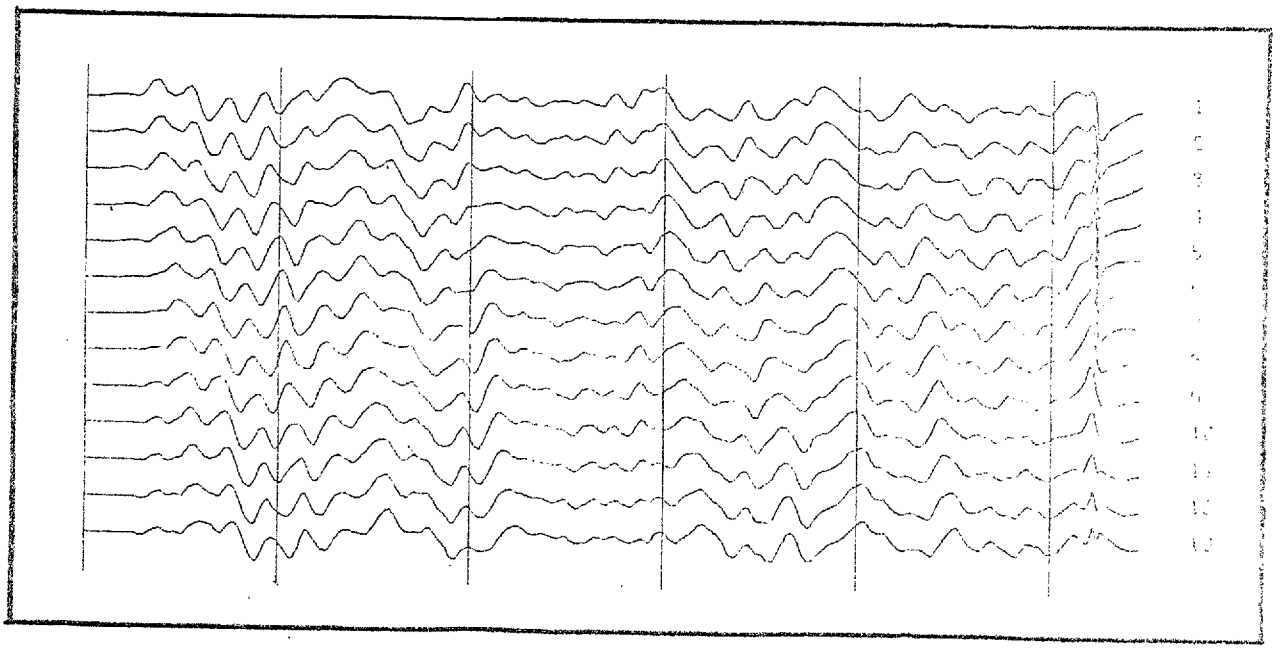


Fig. 2.9 result of filtering Fig. 2.8 with *1R1

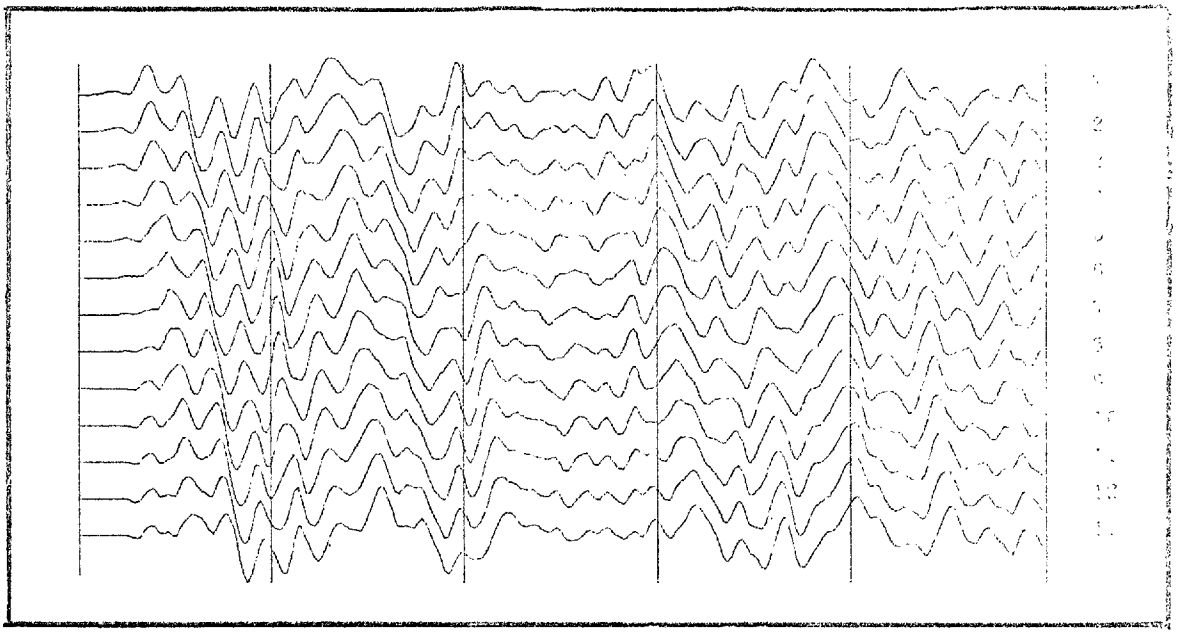


Fig. 2.9(b) the first 500msec of Fig. 2.9

The next records show the effect of increasing the random noise level, whilst keeping the level of correlated noise constant at ρ = 0.0 db. Since a multichannel filter is designed with the specific intention of passing one range of moveouts and rejecting another range of moveouts, it may be suspected "a priori" that the filter will fare less well when presented with an infinite number of large moveouts, i.e. when presented with a large content of random noise. The results confirm that this in fact the case.

Fig. 2.10 shows an input record of uncorrelated noise level ν = 0.0 db. The filtered result (Fig. 2.11) is quite good, signal detection being very much in evidence. Increasing the random noise by -6.0 db (Fig. 2.12) leads to a poorer filtered result (Fig. 2.13), but some signal detection is still good. Increasing this noise by a further -6.0 db (Fig. 2.14), however, completely destroys the filtered result (Fig. 2.15).

An example of high correlated noise (ρ = -15.0 db) and appreciable uncorrelated noise (ν = -6.0 db) is presented in Fig. 2.16, with the filtered result as Fig. 2.17. Signal recovery and rejection of correlated noise are both good.

Cancellation of random noise is primarily due to the stacking process by which each filtered output trace is derived from a set of single channel filtered traces. Some "rejection" of random noise occurs, of course, due to the number of random moveouts that are encompassed by the reject region of the filter. One would expect, therefore, that wide angle reject regions would be more successful in the cancellation of random noise than would narrow angle regions. An illustration of this is given by Fig. 2.18 - Fig. 2.21. Fig. 2.18 shows an input record for a correlated noise level of ρ = 0.0 db, and an uncorrelated noise level of ν = -9.0 db. The result of filtering this record by a narrow angle filter (*FR8), a medium angle filter (*FR9) and a wide angle filter (*FR10), are presented as Fig. 2.19,

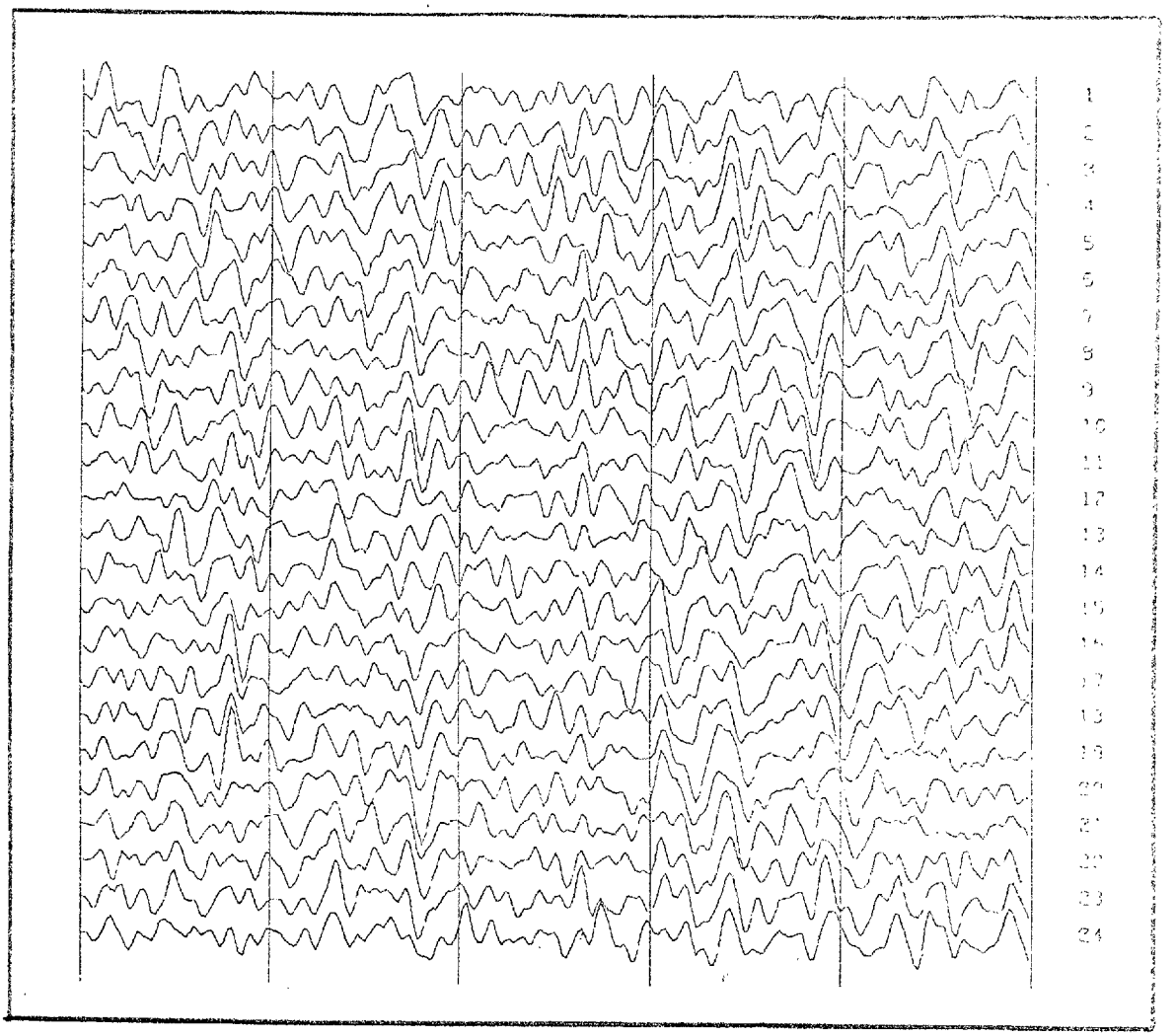


Fig. 2.10 input record, $P = 0.0$, $\nu = 0.0$

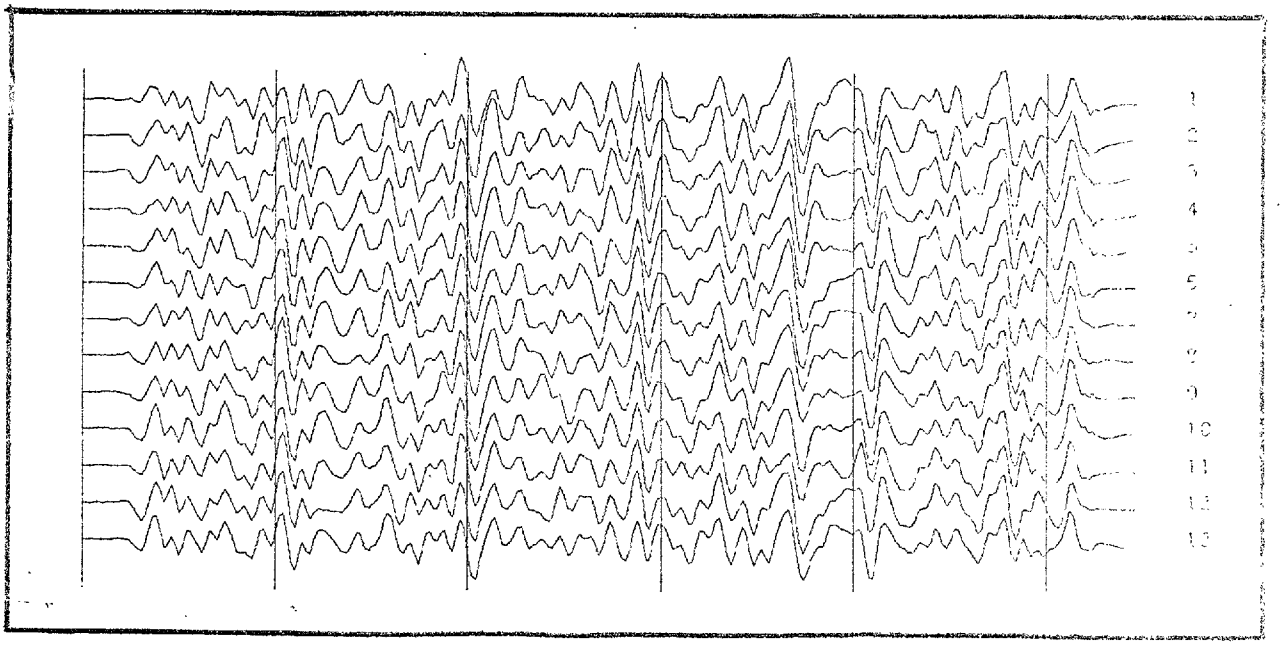


Fig. 2.11 result of filtering Fig. 2.10 with *FR1

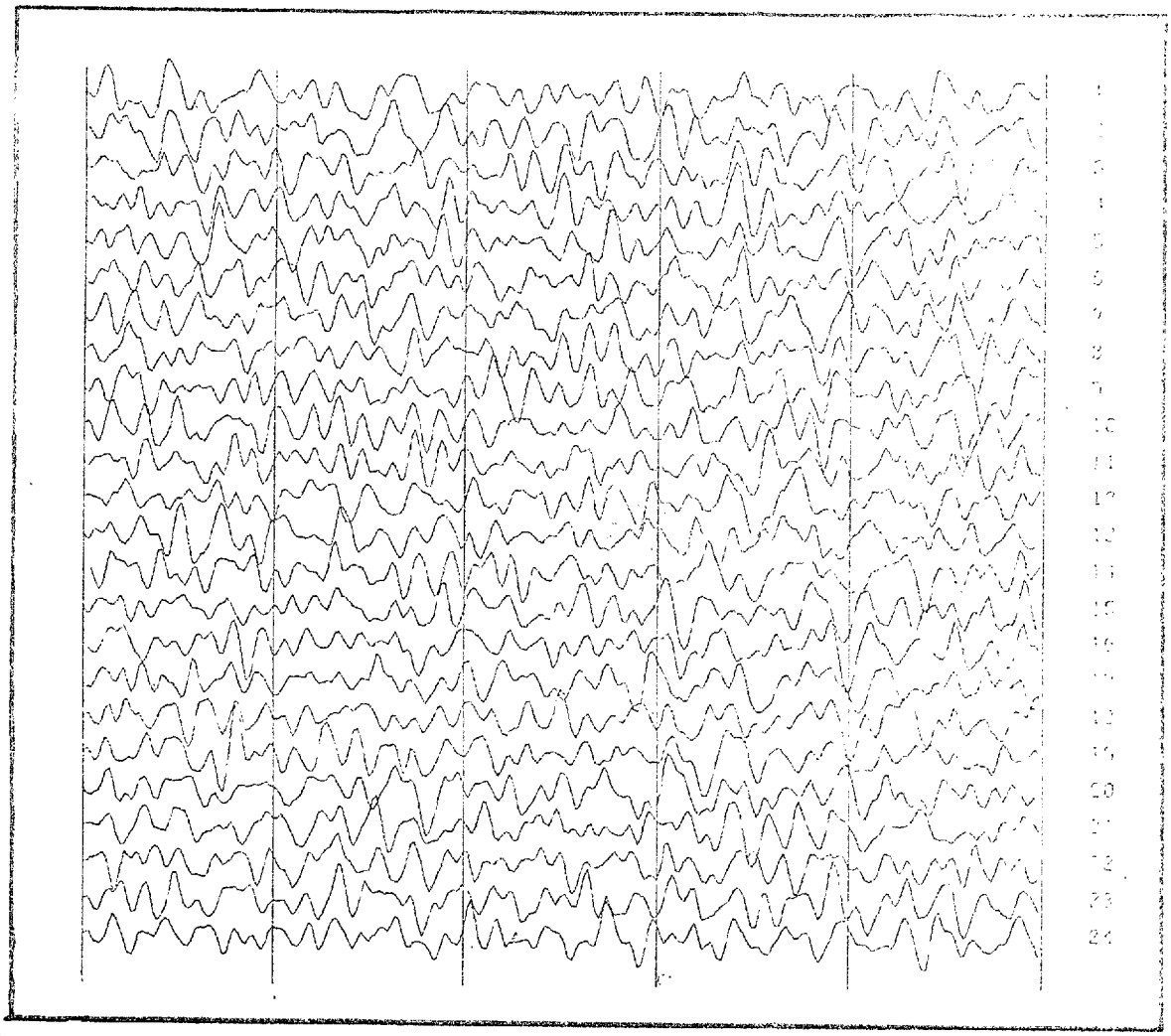


Fig. 2.12 input record, $P = 0.0$, $\nu = -6.0$

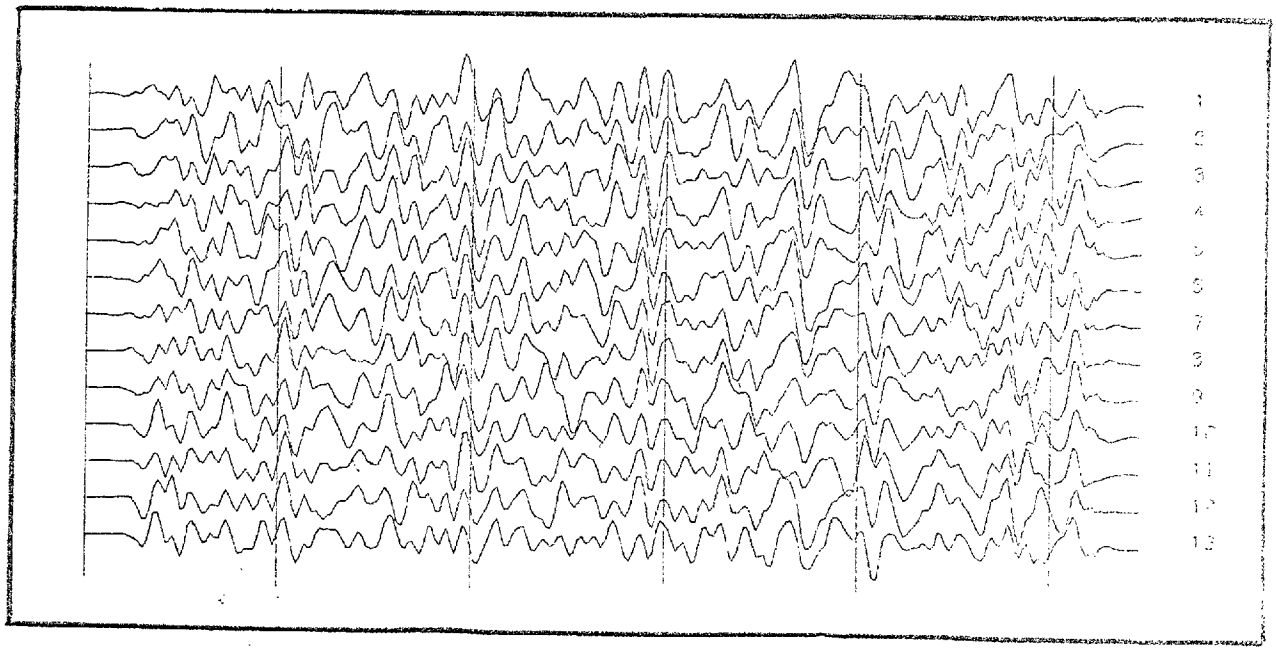


Fig. 2.13 result of filtering Fig. 2.12 with *FR1

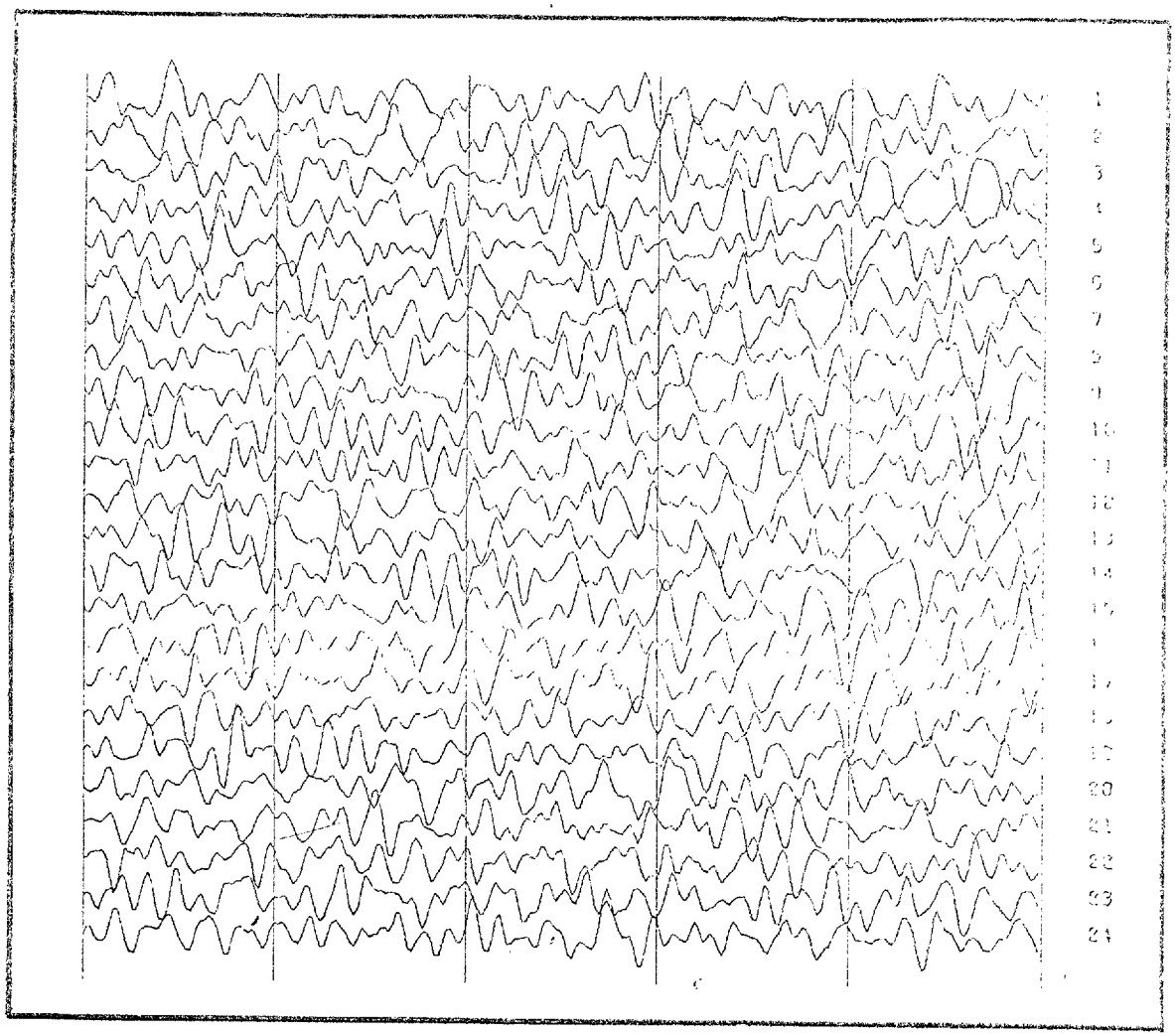


Fig. 2.14 input record, $\rho = 0.0$, $\nu = -12.0$

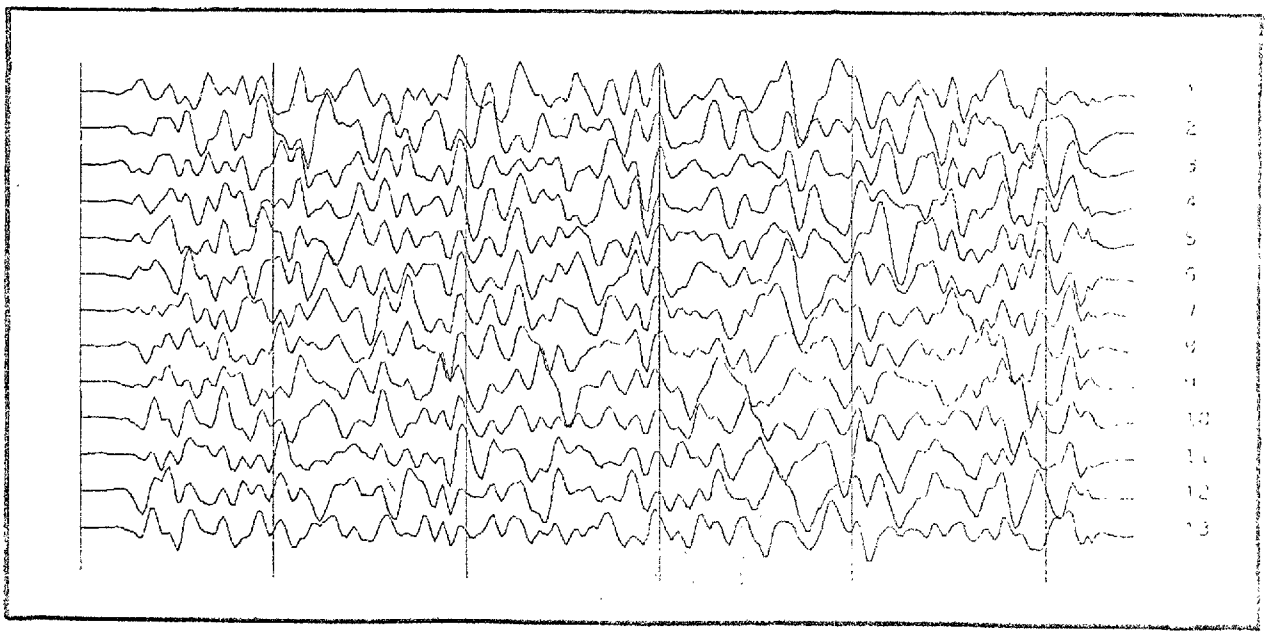


Fig. 2.15 result of filtering Fig. 2.14 with *PR1

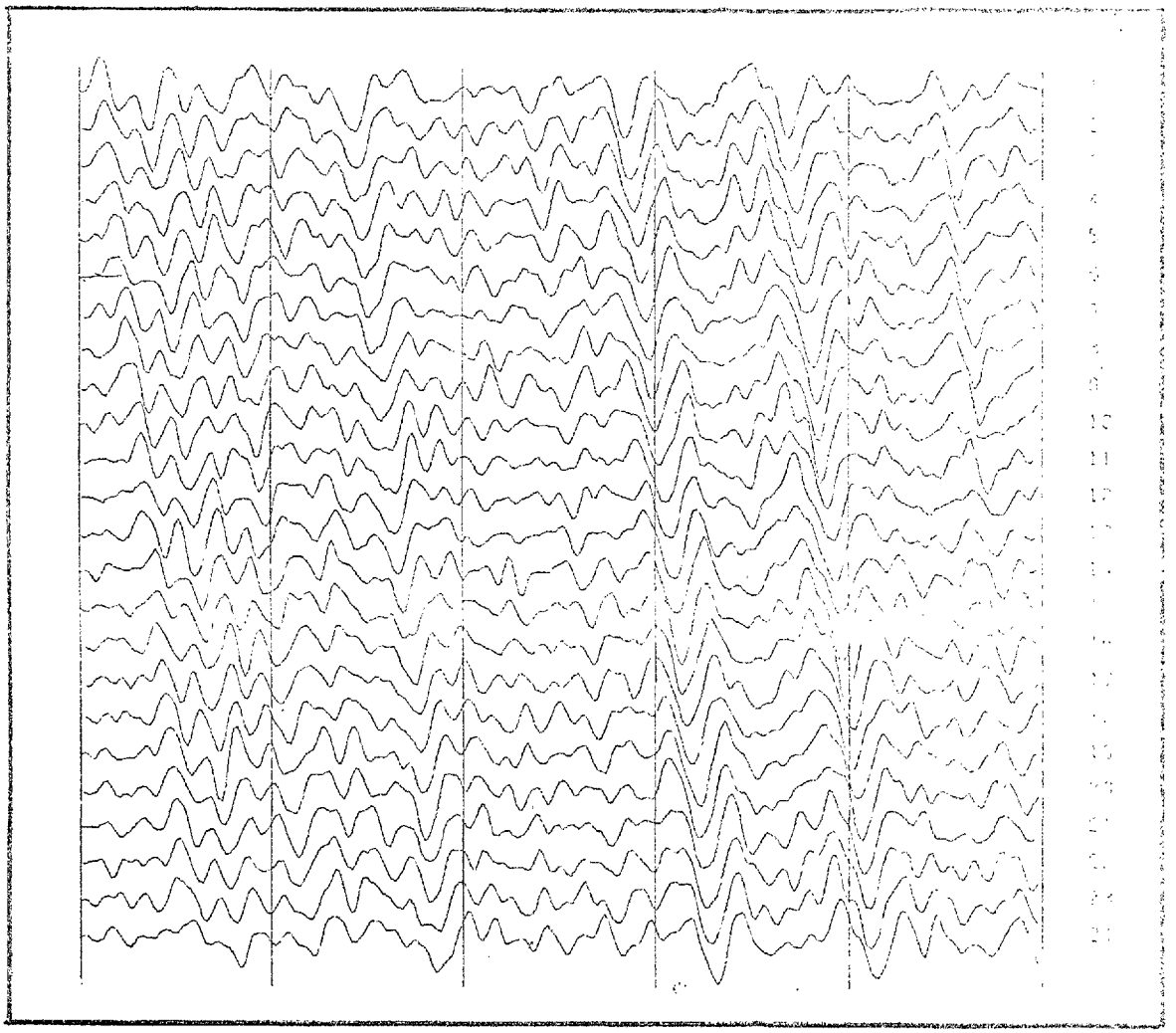


Fig. 2.16 input record, ρ = -15.0, ν = -6.0

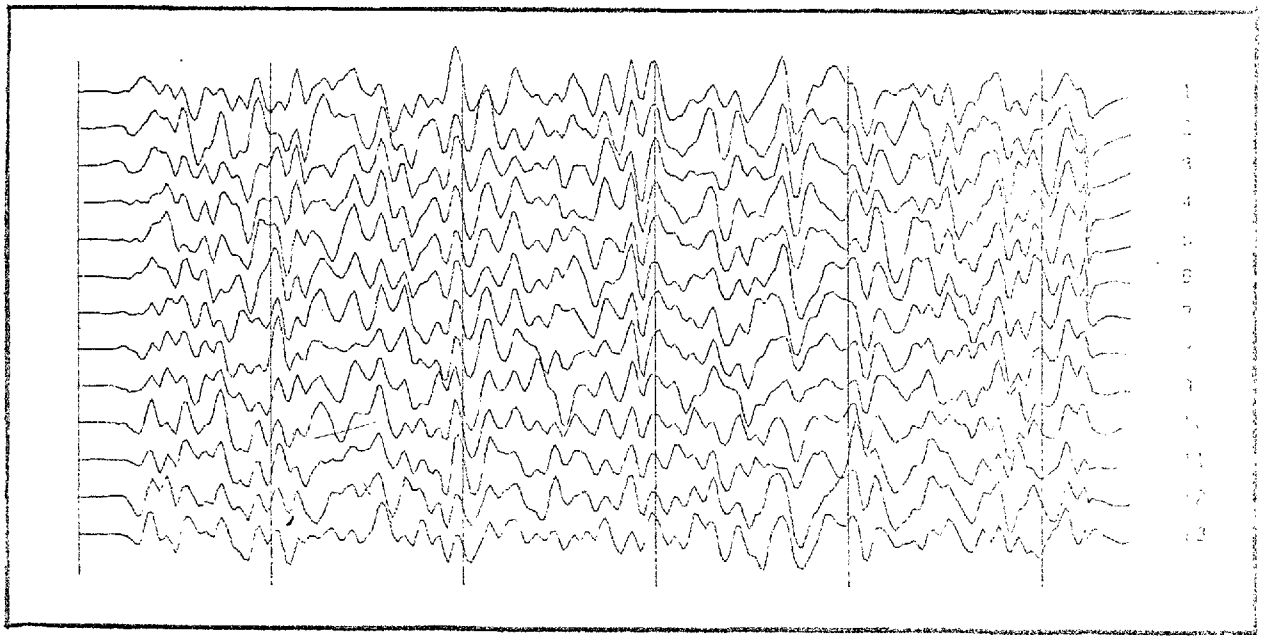


Fig. 2.17 result of filtering Fig. 2.16 with *1R1

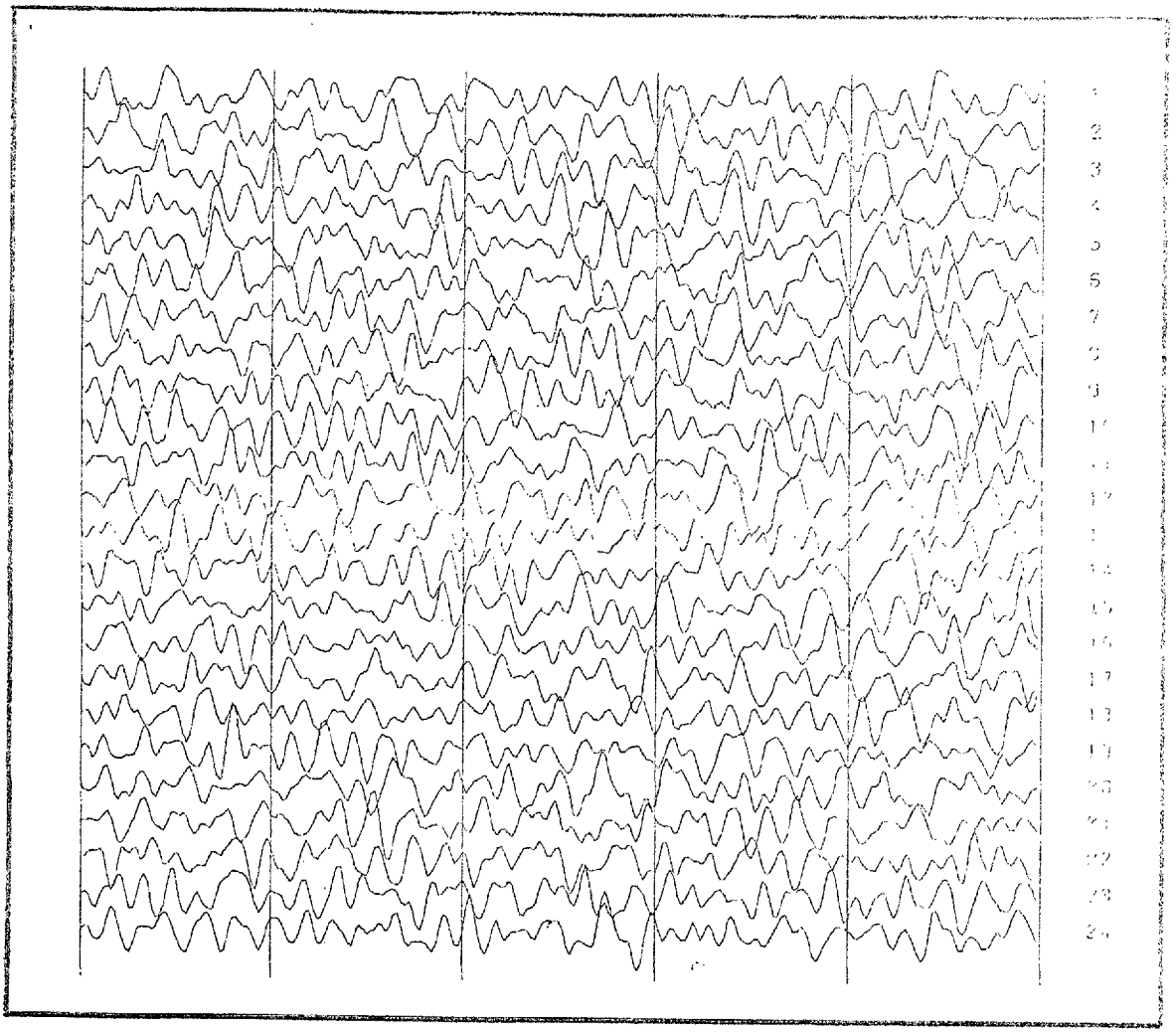


Fig. 2.18 input record, $\rho = 0.0$, $\nu = -9.0$

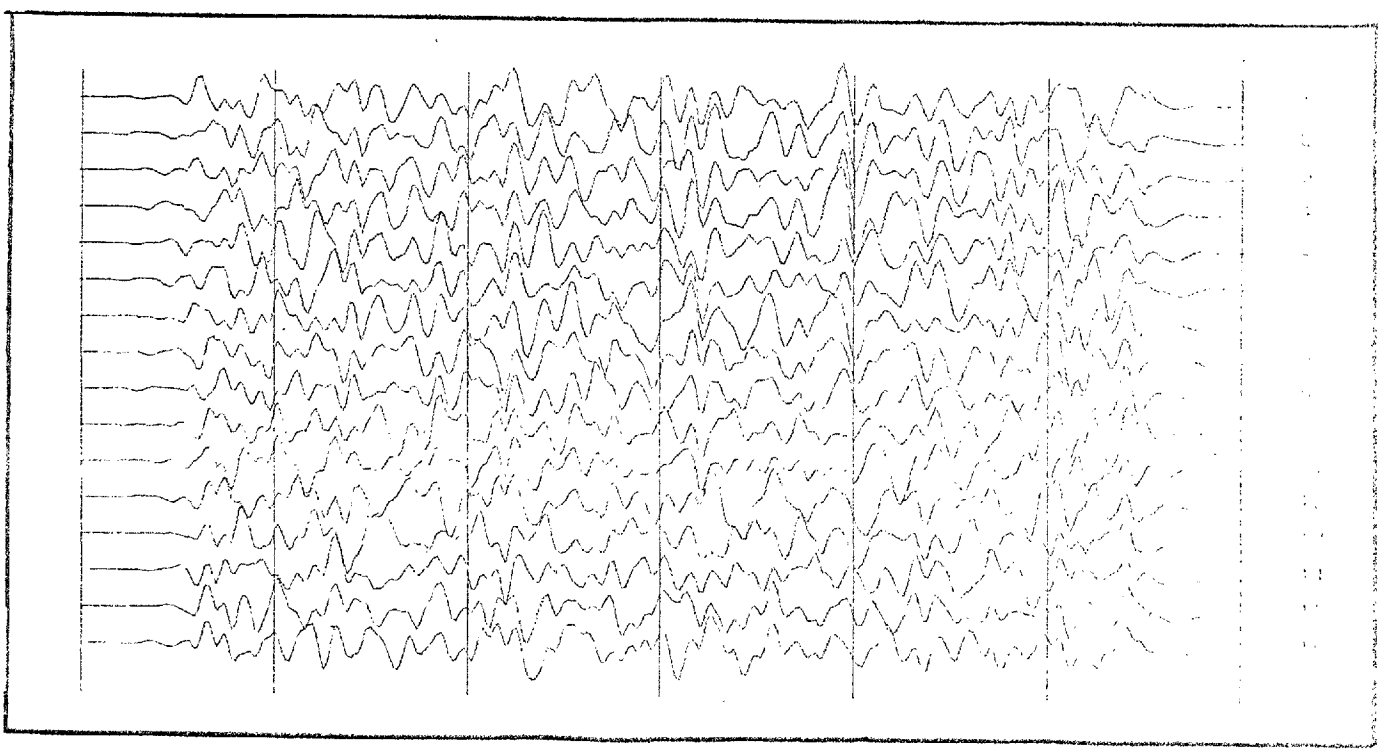


Fig. 2.19 result of filtering Fig. 2.18 with *FR8



Fig. 2.20 result of filtering Fig. 2.18 with *1R9



Fig. 2.21 result of filtering Fig. 2.18 with *1R10

Fig. 2.20 and Fig. 2.21, respectively. It is immediately apparent from these results that a wide angle reject region filter can be quite efficacious in the cancellation of uncorrelated noise.

The results of this section have shown, therefore, that multichannel filtering is a very powerful tool for the detection of low power events, even in the presence of appreciable uncorrelated noise. Considerable levels of correlated noise can be successfully rejected, with wide angle filters having particular application for high random noise. As might be expected, the filtering process is far more sensitive to the level of uncorrelated noise than it is to correlated noise. The method was "broken" by a level of -30.0 db of correlated noise, whereas a level of only -12.0 db of uncorrelated noise was necessary to achieve a similar result.

An interesting comparison is made between Fig. 2.5 and Fig. 2.11. Both these filtered records have the same general appearance, though the unfiltered records, Fig. 2.4 and Fig. 2.10, are markedly different. Similarly, Fig. 2.4 and Fig. 2.16 share some common characteristics, though a greater difference is revealed in the filtered records Fig. 2.5 and Fig. 2.17. This would suggest the following "two-tier" interpretation of the filtering process. The first stage is where the filter itself tries to (i) pass the signal and (ii) reject the correlated noise, as specified by the filter design. The uncorrelated noise is not greatly affected by the filter, unless the reject region is particularly wide. The second stage is the stacking process, where the amplitude of the signal is enhanced relative to that of any residual correlated noise, together with a concomitant reduction of the random noise. The quality of the final result may largely depend upon the residual level of random noise, i.e. the filtering could have been quite successful, with good signal recovery and rejection of correlated noise, but whether or not such

a result would be in evidence could be determined by the efficacy of the stack in cancelling the uncorrelated noise.

Multichannel filtering may then have application, not only as an "optional extra" to be included in the common-depth-point stacking process, but also in the removal of residual moveouts from conventional common-depth-point stacks.

2.2.2 matching of moveout between filter and data

The coefficients of a multichannel filter may be obtained by performing a correlation analysis on the input traces themselves (Davies and Mercado, 1968). An alternative approach, namely specifying the desired filter output (a unit spike) and the time window configuration, is used in this thesis. Applying one filter from a set of pre-calculated filters involves, of course, the possibility of selecting the wrong filter. The purpose of this section is to investigate the sensitivity of multichannel filter performance to the agreement between a moveout in the data it is desired to reject, and the reject moveout actually specified for the filter.

Fig. 2.5 showed the result of filtering Fig. 2.4 with pass/reject filter *PR1. The correlated noise moveout in the data was 1 sample per trace, and the filter was designed to reject a moveout of 1.0 ± 0.5 samples per trace. This same record, Fig. 2.4, was then filtered by pass/reject filter *PR7, a filter designed to reject moveouts in the range 1.5 ± 0.25, and also by pass/reject filter *PR2, a filter designed to reject moveouts in the range 2.0 ± 0.25, samples per trace. These filtered results are given as Fig. 2.22 and Fig. 2.23, respectively. The degradation of quality in the filtered records from Fig. 2.5, through Fig. 2.22 to Fig. 2.23, is immediately apparent.

Hence it may be concluded that multichannel filtering is a very sensitive method that largely depends upon an accurate "match" between the moveouts of filter and data for its success.

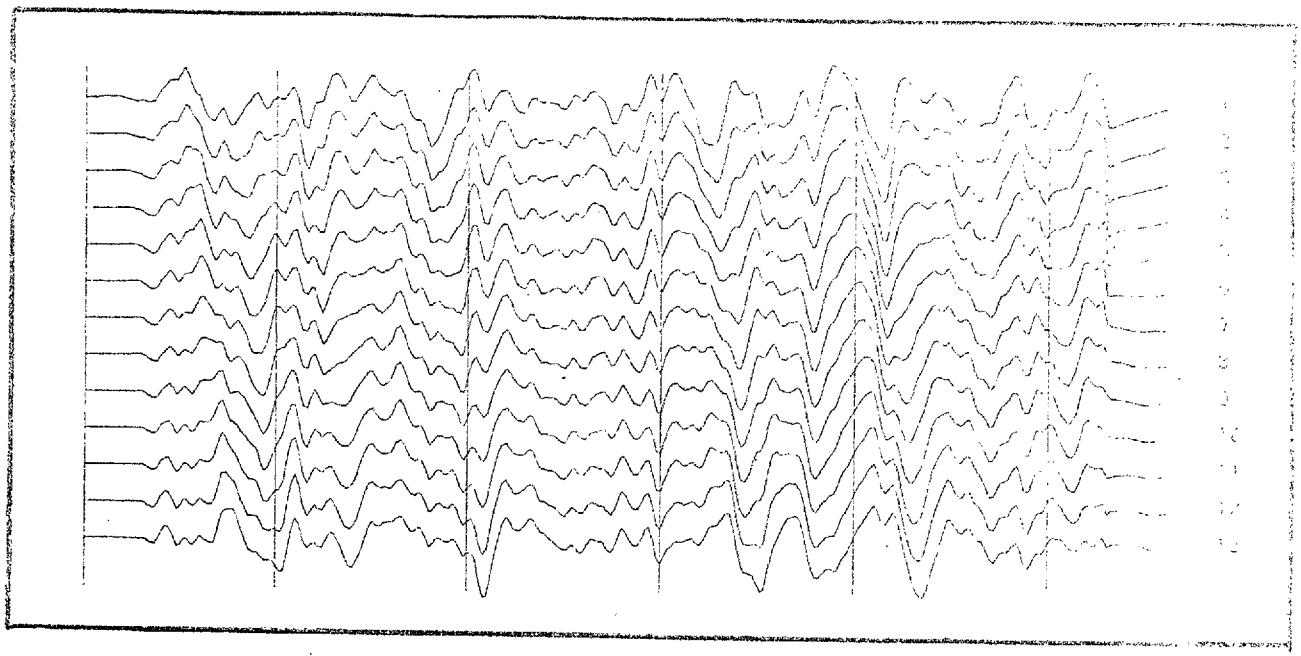


Fig. 2.22 result of filtering Fig. 2.4 with *PR7

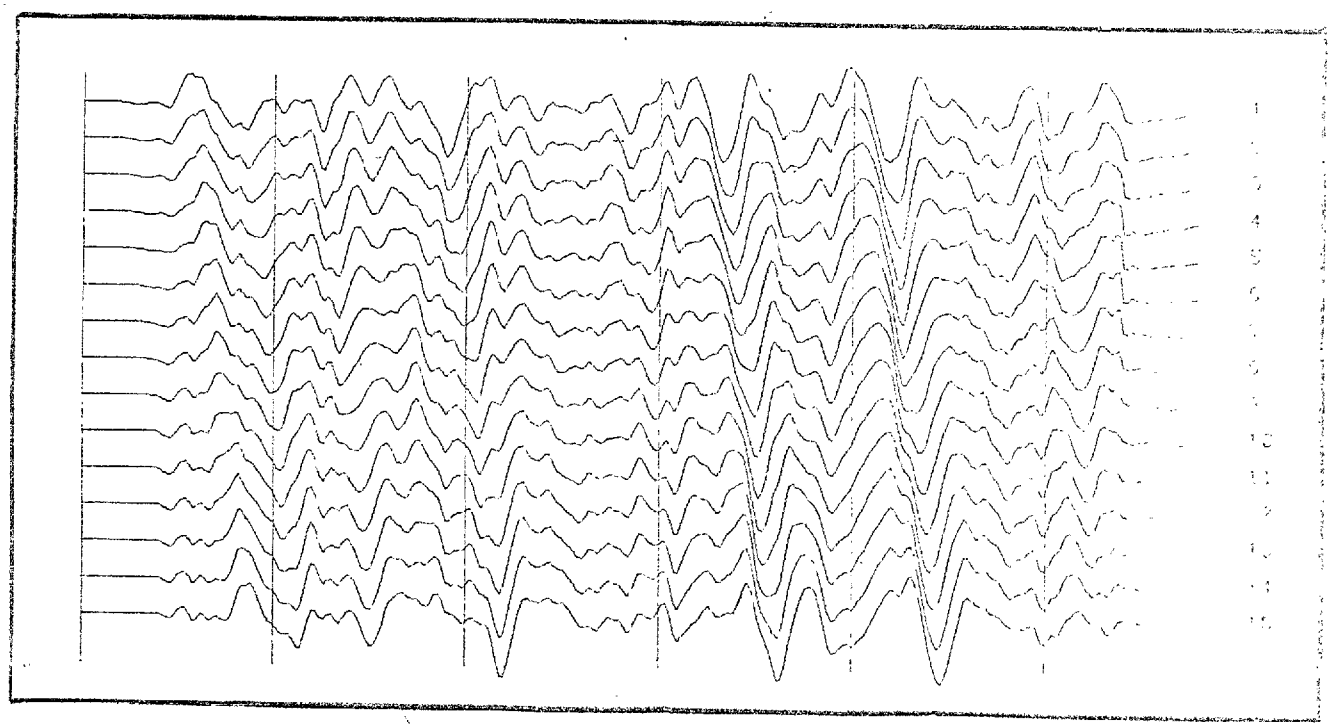


Fig. 2.23 result of filtering Fig. 2.4 with *PR2

2.2.3 number of traces in filter design

It is felt that the number of traces used in the design of a multichannel filter can be of considerable importance. Unfortunately, for reasons mentioned earlier, it was not possible to compare the performance of two filters for which all design characteristics were exactly the same, save for that of the number of traces. Accordingly, therefore, in comparing the performance of the two filters used in this section, the 12 trace filter *PR1 and the 6 trace filter *PR4, the difference in the weighting factor "σ" must be taken into consideration (Ref. Table 2.1). Both these filters were designed for the same time window configuration, random noise weighting and similar mean square error.

The result of applying filter *PR4 to the input record of Fig. 2.4 is presented as Fig. 2.24. Comparison of Fig. 2.24 with Fig. 2.5 shows that the signal recovery and rejection of correlated noise by filter *PR4 is not nearly so good as that of filter *PR1. Applying filter *PR4 once again to the filtered result of Fig. 2.24 gives the "double-filtered" result of Fig. 2.25. Comparison of Fig. 2.24 and Fig. 2.25 shows that the signal recovery and rejection of correlated noise for the latter case is considerably better than that of the former case.

In so far as the single application of a 12 trace filter is comparable to the double application of a 6 trace filter, one would expect that the filtered result of Fig. 2.5 should be similar to that of Fig. 2.25. Comparison of these results certainly show that they are similar, and that Fig. 2.25 is a much closer "match" to Fig. 2.5 than is Fig. 2.24. Such differences as exist between Fig. 2.5 and Fig. 2.25 are probably due to the differences in the correlated noise weighting factor σ.

It may be concluded from this section, therefore, that as many traces as possible should be included in the filter design as is practicable for the particular problem under analysis.

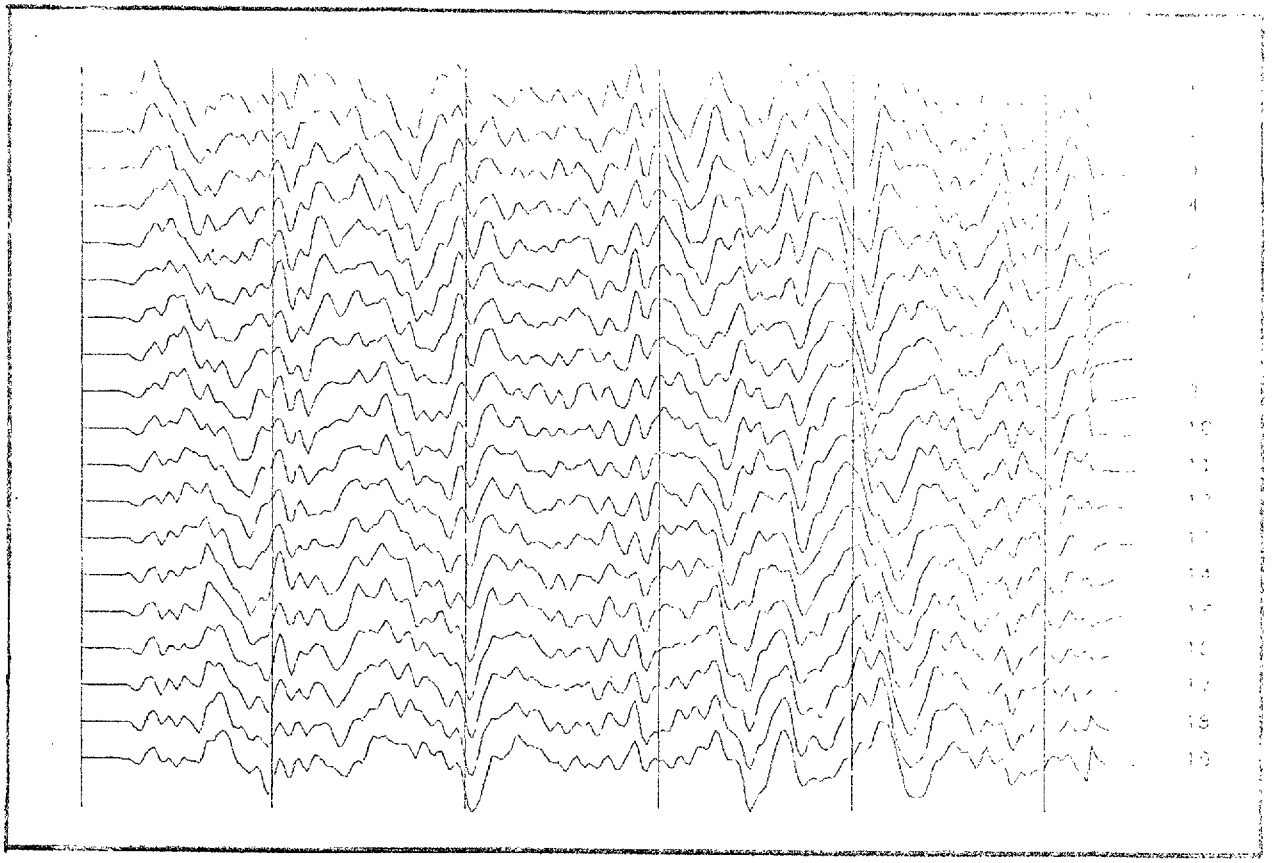


Fig. 2.24 result of filtering Fig. 2.4 with *PP4

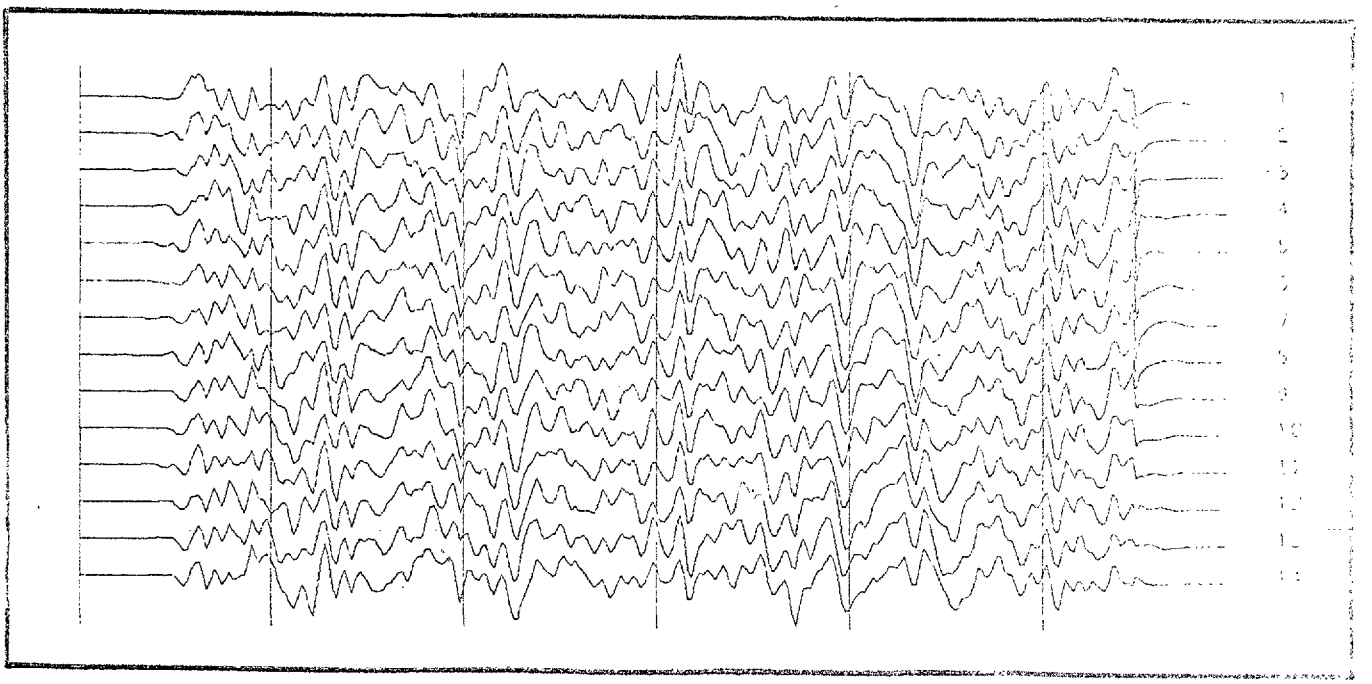


Fig. 2.25 result of filtering Fig. 2.4 with *PP4 (twice)

2.2.4 quadratic filtering

The analysis of all records so far have been concerned with correlated noise of linear moveout. The purpose of this section is to investigate records for which the correlated noise possesses a quadratic moveout, whilst retaining the linear moveout for the signal. In order to effect a more suitable comparison with the results of linear moveout filtering, three examples were chosen with signal to noise ratio conditions the same as for the linear case.

Three records of quadratic correlated noise moveout, for signal to noise conditions of (i) ρ = -15.0, ν = 6.0 db, (ii) ρ = 0.0, ν = 0.0 db and (iii) ρ = 0.0, ν = -6.0 db, are presented as Fig. 2.26, Fig. 2.28 and Fig. 2.30, respectively. The results of applying the set of quadratic filters Q1- Q13 (quadratic filter "Q") to these records are presented as Fig. 2.27, Fig. 2.29 and Fig. 2.31, respectively.

Comparison of Fig. 2.27 with Fig. 2.5, and Fig. 2.29 with Fig. 2.11, immediately shows that the general features of quadratic filtering are directly comparable to that of linear filtering. Both these results of quadratic filtering, in fact, are a little better than their linear counterparts. This is probably due to the extra cancellation of random noise caused by the higher weightings given to the random noise factor, ν , of the quadratic filters. Comparison of Fig. 2.31 with Fig. 2.13, for which the uncorrelated noise level was -6.0 db, would tend to confirm this view.

To conclude this section, the quadratic input record of Fig. 2.26 was filtered by the linear pass/reject filter *PR1. As might be expected, the result (Fig. 2.32) is very poor.

This section has shown that the results of multichannel quadratic filtering are in good agreement with those of linear filtering.

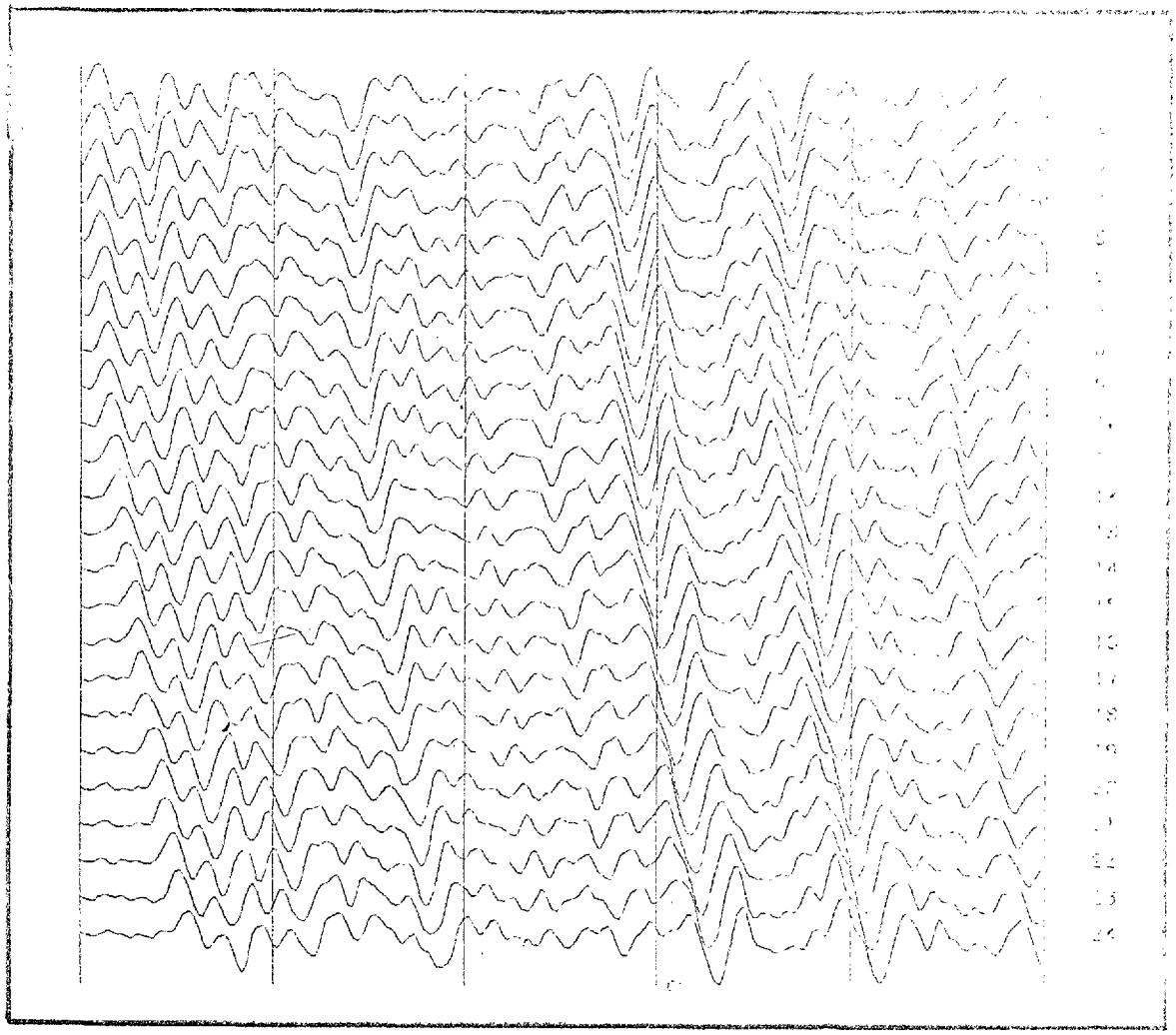


Fig. 2.26 input record, $\rho = -15.0$, $\nu = 6.0$

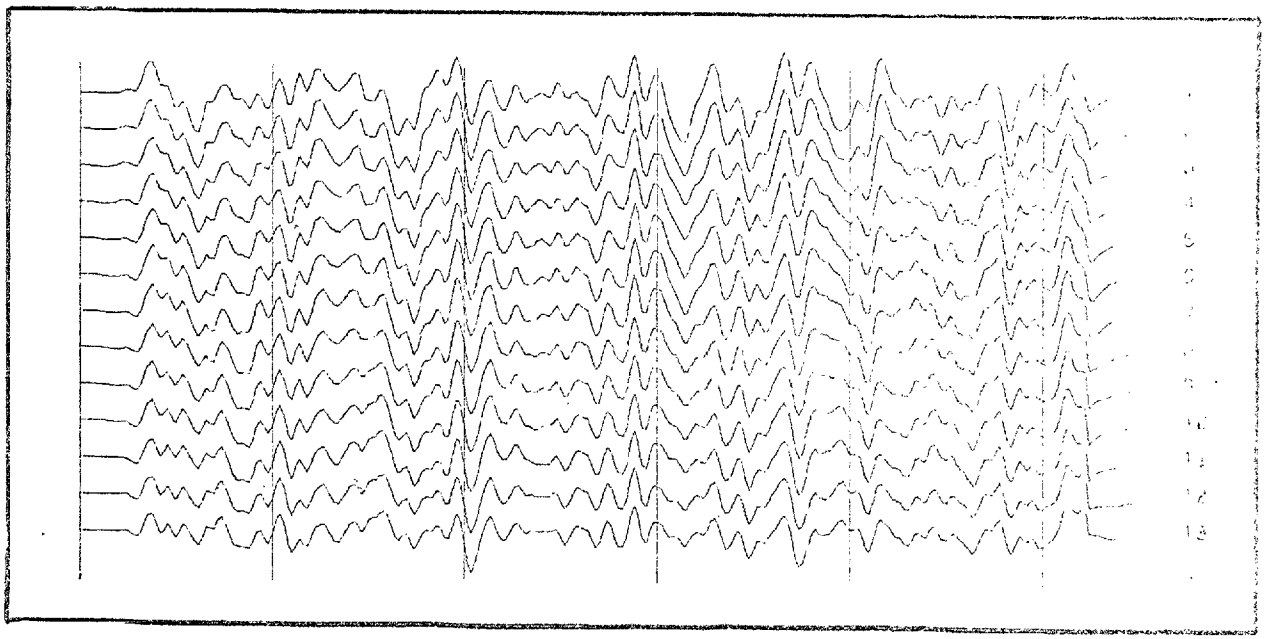


Fig. 2.27 result of filtering Fig 2.26 with filter Q

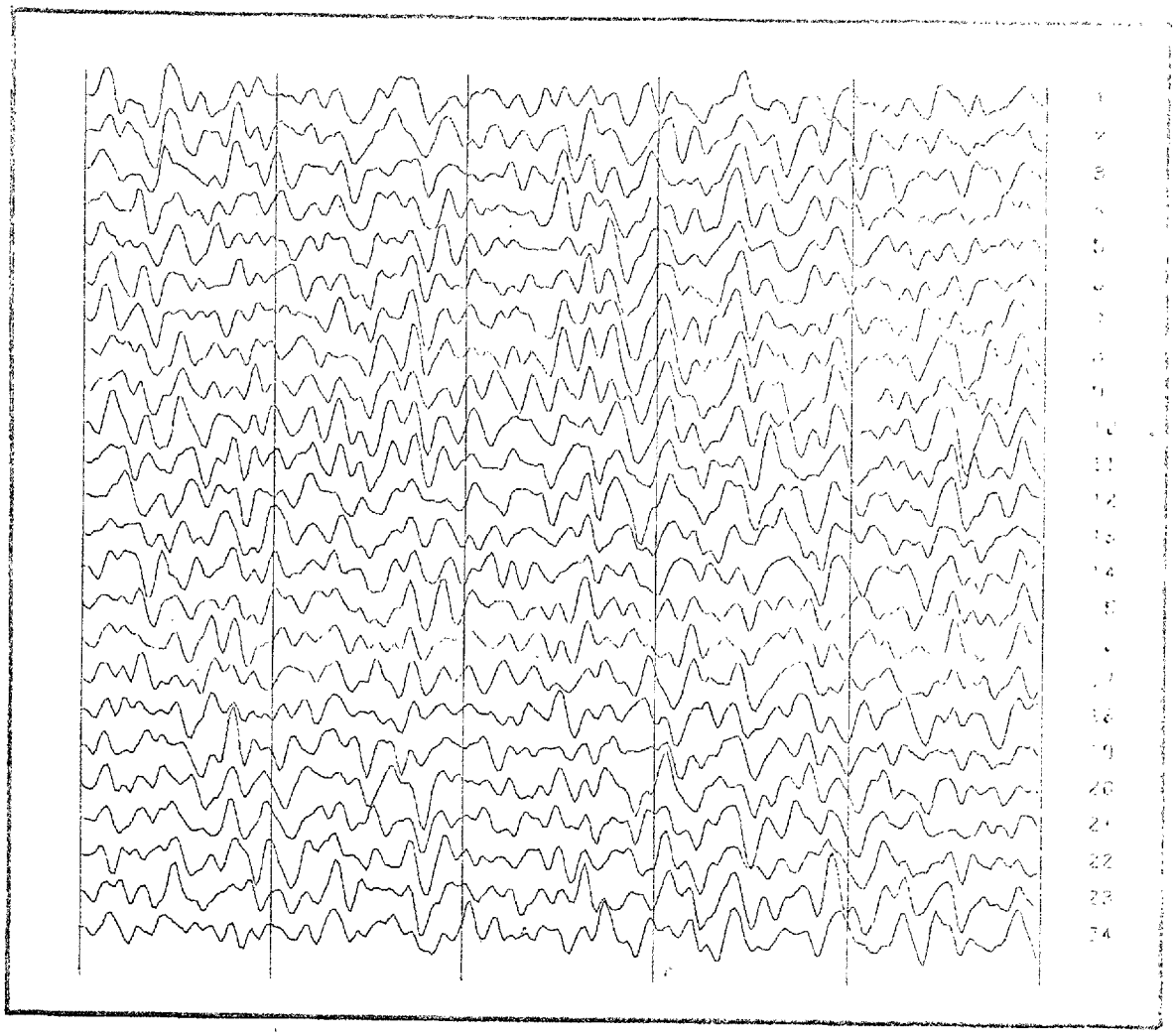


Fig. 2.28 input record, $\rho = 0.0$, $\nu = 0.0$

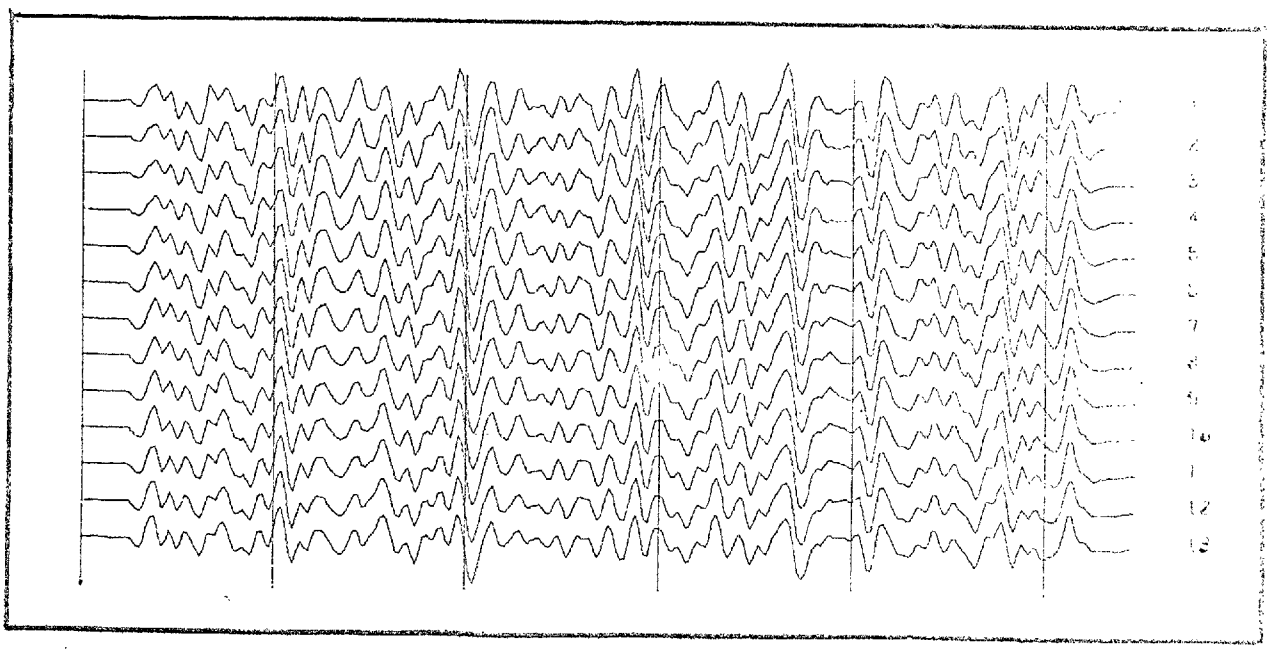


Fig. 2.29 result of filtering Fig. 2.28 with filter

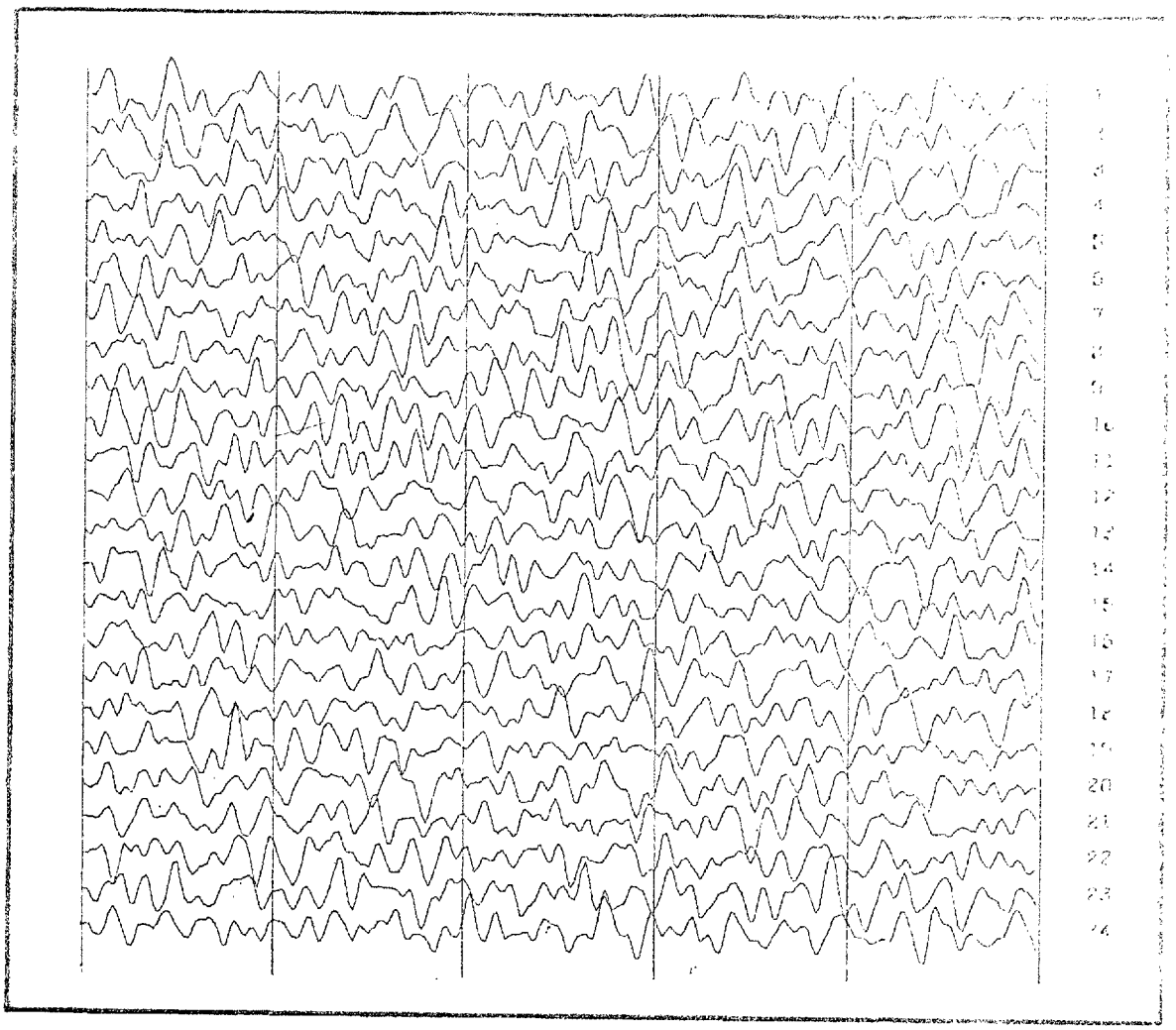


Fig. 2.30 input record, ρ = 0.0, ν = -6.0

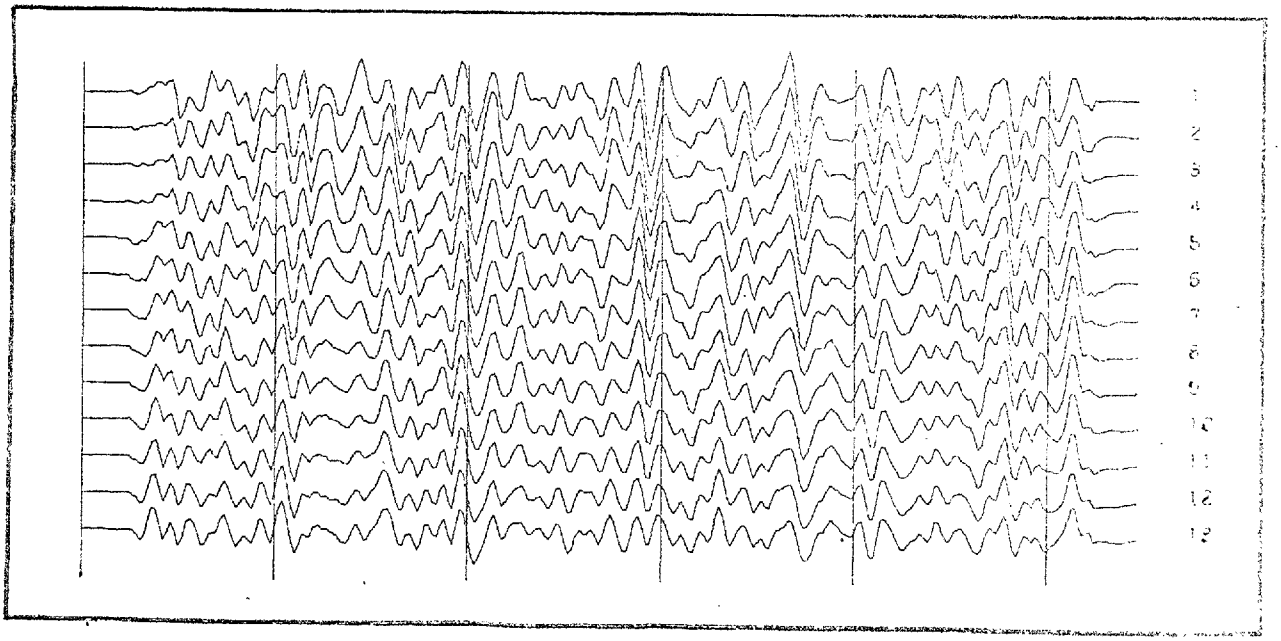


Fig. 2.31 result of filtering Fig. 2.30 with filter

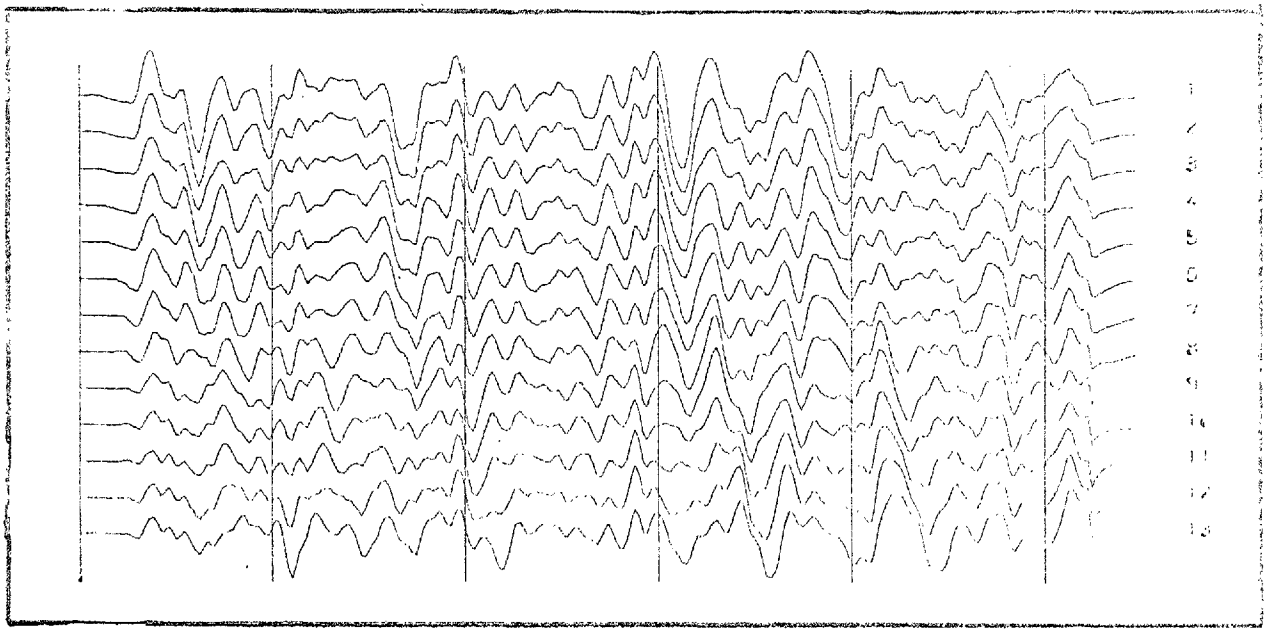


Fig. 2.32 result of filtering Fig. 2.26 with A1R1

2.3 Filter applications to real data

The purpose of this section is to apply multichannel filtering techniques to the real data of Chapter 1, and to assess to what extent the findings from the synthetic data results are applicable to the real case. Details of the records chosen and the filters applied may be found in Table 2.4. Labelling of axes and presentation of plots are the same as for synthetic data. It must be remembered, of course, that the concepts of signal to noise ratio are now somewhat different due to the "distribution" of these ratios along the length of the real traces.

Of particular interest in this section is the introduction of the "multichannel filter scan", i.e. the applying of a set of multichannel filters to the data in the hope that at least one of them will show something useful. This is important since, not only could a good result be otherwise missed, but a filter may actually produce a record that was worse than the original.

Fig. 2.33, Fig. 2.34 and Fig. 2.35 show the results of applying filters *PR8, *PR9 and *PR10 to shotpoint 3005 (Fig. 1.4), respectively. The first two of these results show very little in the way of signal recovery or in rejection of correlated noise. In some respects they are definitely worse than the original unfiltered record. Fig. 2.35, however, does show the recovery of signal, with some break up of correlated noise. For the sake of completeness, the filter *PR10 was also applied to the 24 trace version of Fig. 1.4, the result being presented as Fig. 2.36. Comparison of Fig. 2.35 and Fig. 2.36 shows that the latter picture contains less signal information and noise rejection is less good. Hence the necessity for choosing the 23 trace records for analysis.

In practice, one would seek to remove the presence of ground roll from a record by the suitable application of a band pass filter. Accordingly, therefore, a multichannel filter scan was performed on

shotpoint number	unfiltered Fig. No.	filtered Fig. No.	filter name
3005	1.4	2.33	*PR8
3005	1.4	2.34	*PR9
3005	1.4	2.35	*PR10
3005	1.4	2.36	*PR10
3005	1.8	2.37	*PR8
3005	1.8	2.38	*PR9
3005	1.8	2.39	*PR10
3005	1.8	2.40	Q
3002	1.2	2.41	*PR9
3002	1.2	2.42	*PR10
3002	1.7	2.43	*PR9
3002	1.7	2.44	*PR10
3003	1.3	2.45	*PR1
3003	1.3	2.46	Q
3003	1.3	2.47	*PR10
3007	1.6	2.48	Q

Table 2.4 Index of multichannel filtering for real data

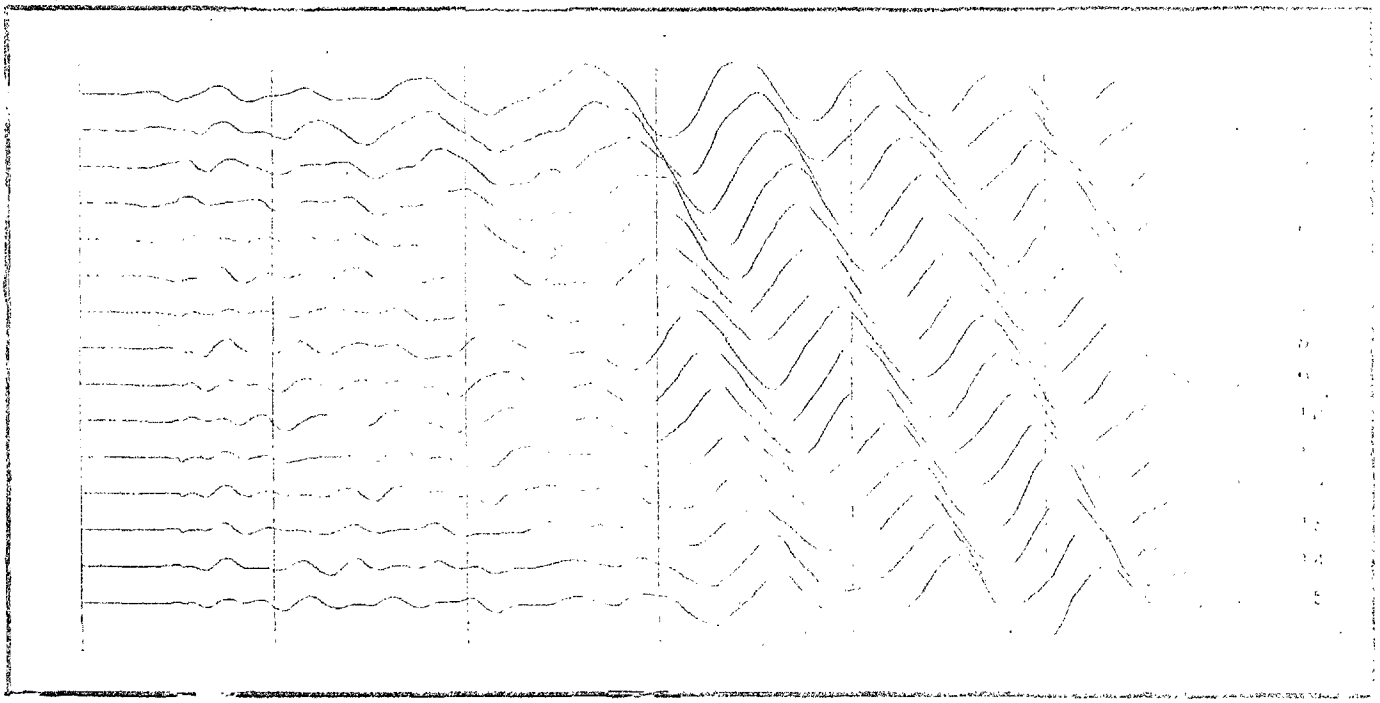


Fig. 2.33 result of filtering Fig. 1.4 with *FR8

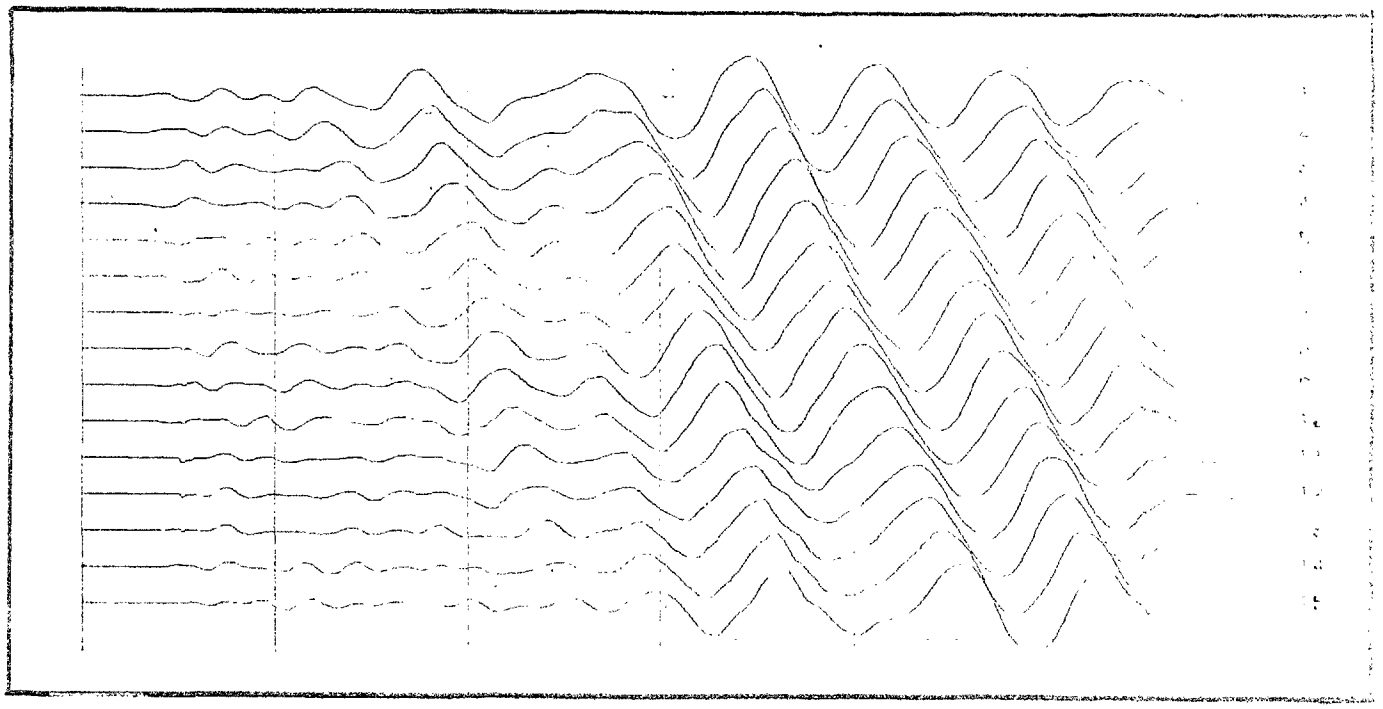


Fig. 2.34 result of filtering Fig. 1.4 with *FR9

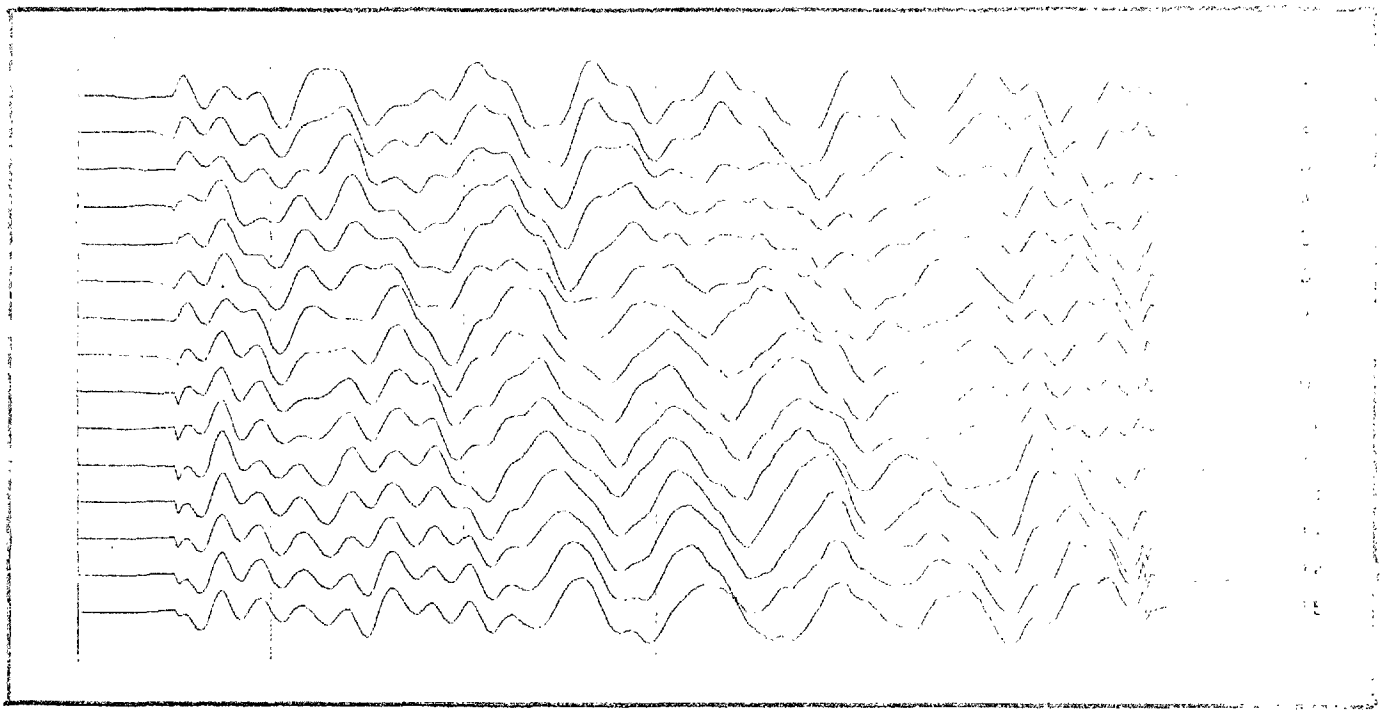


Fig. 2.35 result of filtering Fig. 1.4 with *ZR10

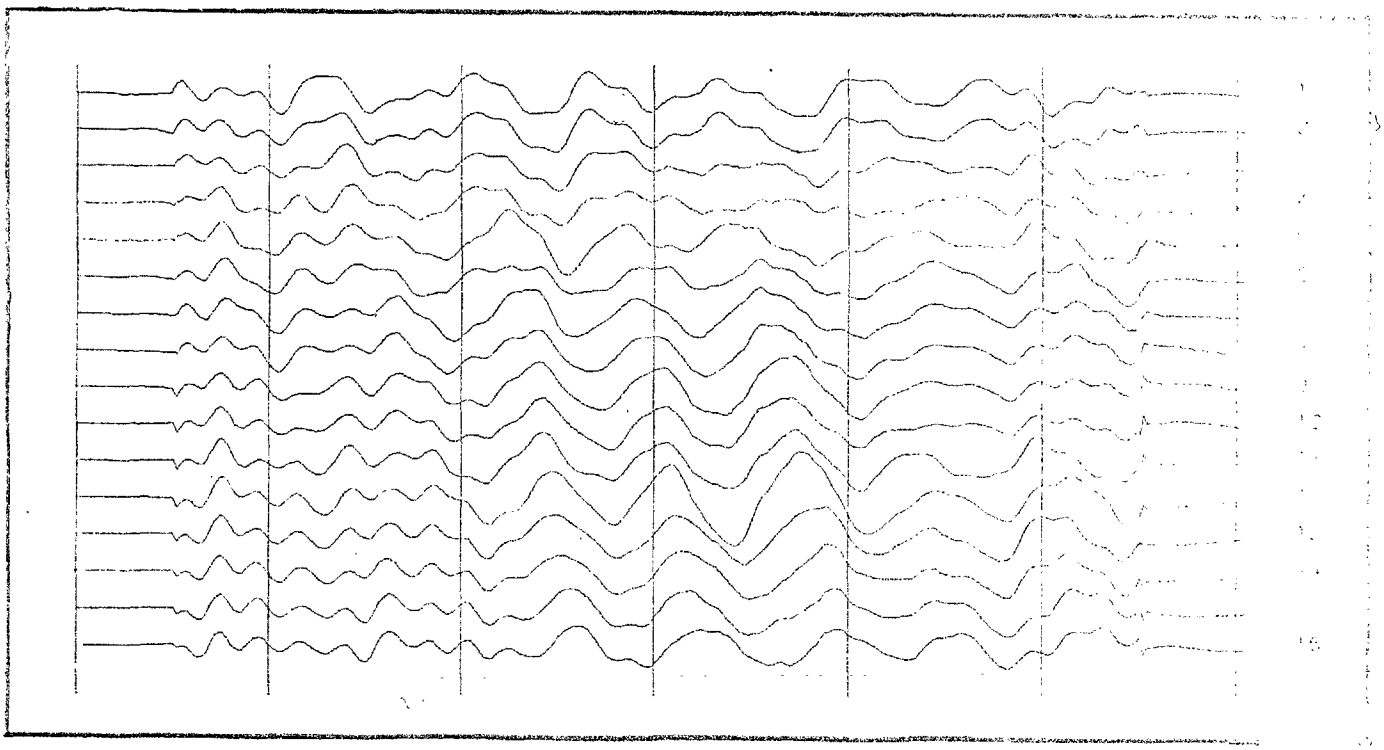


Fig. 2.36 result of filtering Fig. 1.4 (24 trace) with *ZR10

the band pass filtered version of shotpoint 3005 (Fig. 1.6). These filters were *PR8, *PR9, *PR10 and Q, with the filtered results being presented as Fig. 2.37, Fig. 2.38, Fig. 2.39 and Fig. 2.40, respectively. Once again, the first two of these results are not very good, but the third result (Fig. 2.39) clearly shows the presence of signal along the whole length of the record, with almost complete rejection of correlated noise. Comparison of Fig. 2.39 with Fig. 1.6 shows that multichannel filtering can produce very good results for real data. Fig. 2.40, the result of applying the quadratic filter, also shows good recovery of signal, but is less good in the rejection of correlated noise.

Better removal of ground roll by multichannel filtering is provided by shotpoint 3002 (Fig. 1.2). The result of applying filters *PR9 and *PR10 to this record are presented as Fig. 2.41 and Fig. 2.42, respectively. Comparison of these results shows that the second of these filters has succeeded in removing much of the ground roll. Both these filtered records show good signal recovery, and share the same general appearance, except for the roll. One would assume, therefore, that applying these filters to the band pass filtered version of shotpoint 3002 (Fig. 1.7) would produce quite similar results. These results are presented as Fig. 2.43 (filter *PR9) and Fig. 2.44 (filter *PR10), where it seen that they are very similar in appearance. It will be noticed that the absence of signal recovery in the region of the residual ground roll of Fig. 2.42 may well be attributed to the physical lack of such signal, as may be deduced from Fig. 2.43 and Fig. 2.44.

The next few results illustrate the use of a multichannel filter in simply "cleaning up" a given input record. Shotpoint 3003 (Fig. 1.3) was filtered by filters *PR1, Q, and *PR10, the results being presented as Fig. 2.45, Fig. 2.46 and Fig. 2.47, respectively. Fig 2.45 does not show any great improvement on the unfiltered record,

but Fig. 2.46 certainly does, particularly in the later stages of the record. A similar result to the quadratic filtering of Fig. 2.46 is given by the wide angle filtering of Fig. 2.47. These results are similar due to the moveout rejection range of the quadratic filter being largely encompassed by that of the wide angle filter.

The final result of this chapter, Fig. 2.48, shows the filtering of shotpoint 3007 (Fig. 1.6) by quadratic filter Q. As expected, the general appearance of the original record has been improved.

This section has shown that the general conclusions that were derived from the analysis of synthetic data are also valid for real data. Very good results can be obtained from real data by multichannel filters, provided that adequate notice is taken of the importance of matching the moveout of the filter to that of the data.

It is instructive to compare these findings to those of Davies and Mercado (1968). They obtained very poor results from real data, which they largely attributed to the computation of the filter coefficients from a correlation analysis of the input traces. These correlation estimates were generally not sufficiently accurate to give good filter coefficients. This problem has been avoided in this thesis by choosing pre-computed filters for specific time windows, but has introduced the problem of possibly selecting the wrong filter. The potential quality of the results that may be obtained, however, make this a problem worth accepting. A further difference between the work of Davies and Mercado and the present work is in the number of traces used for the design of the multichannel filter. The former work only used 2 or 3 traces, whereas 12 traces were used in the latter work. This difference could well be of prime importance.

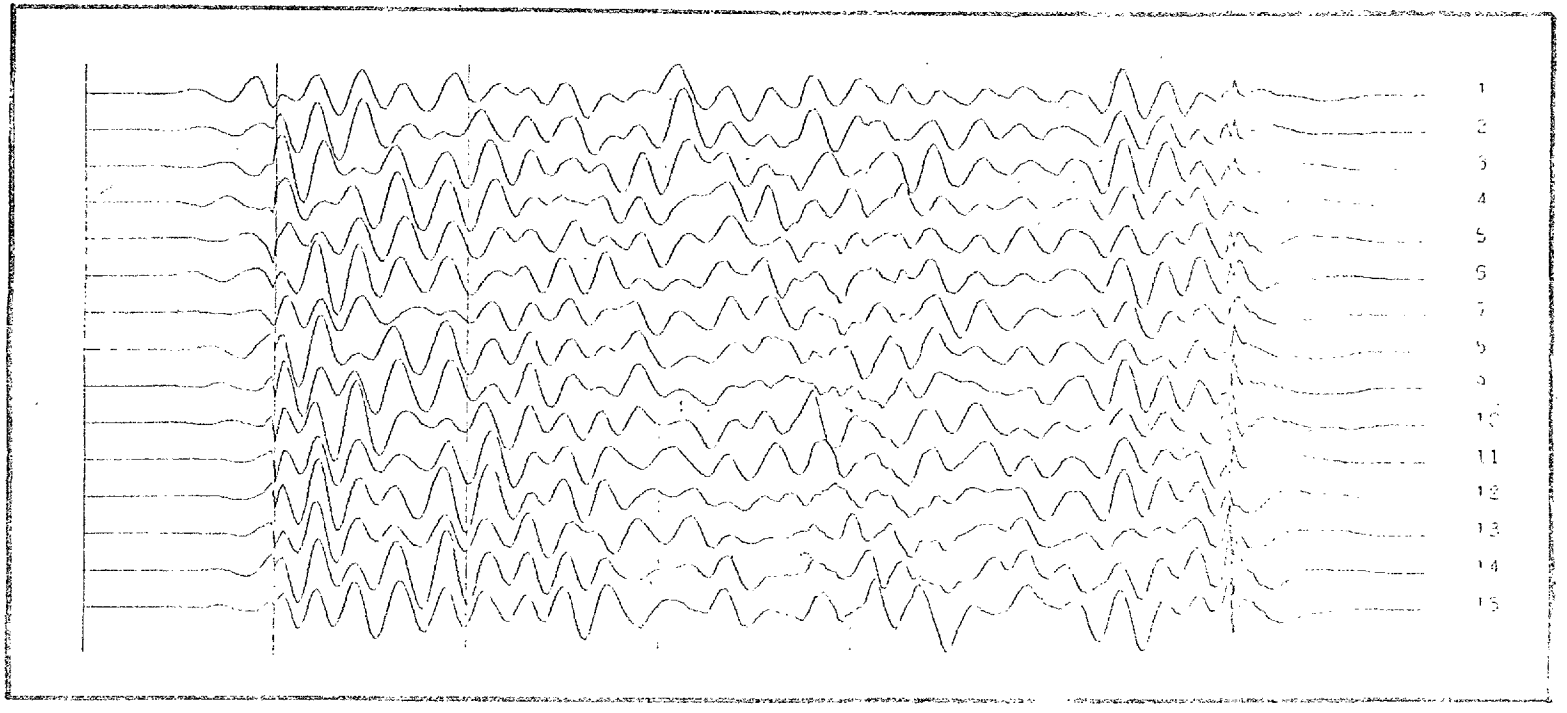


Fig. 2.37 result of filtering Fig. 1.8 with *PR8

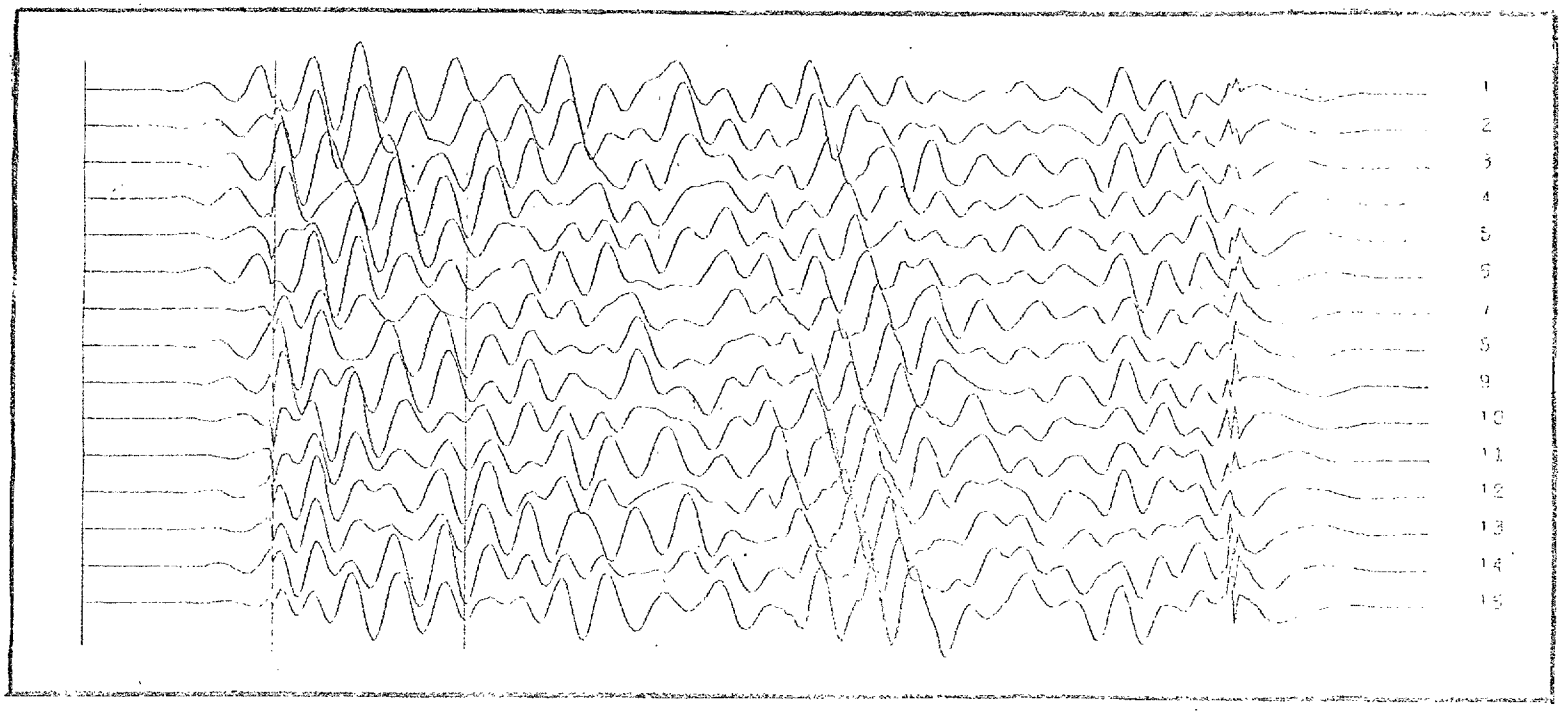


Fig. 2.38 result of filtering Fig. 1.8 with *PR9

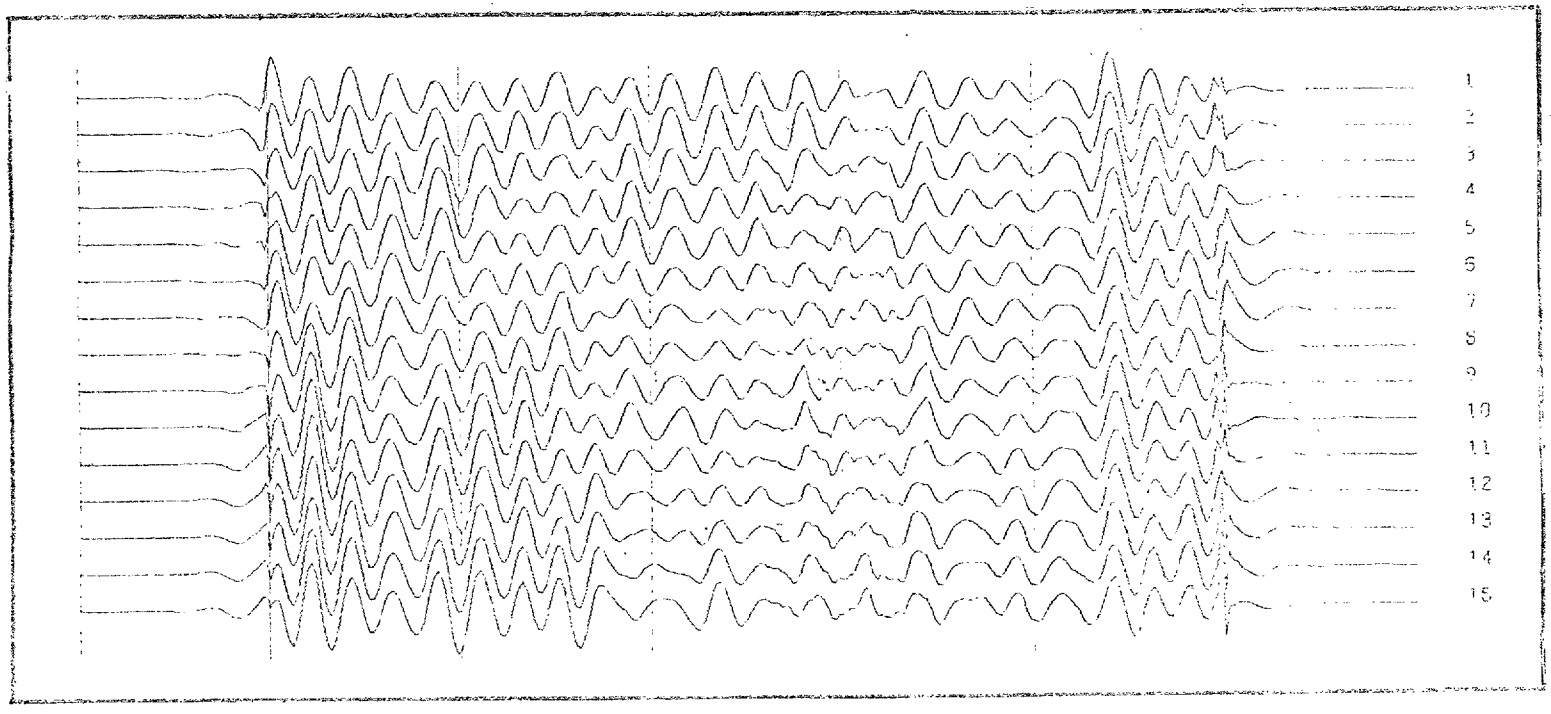


Fig. 2.39 result of filtering Fig. 1.8 with *PR10

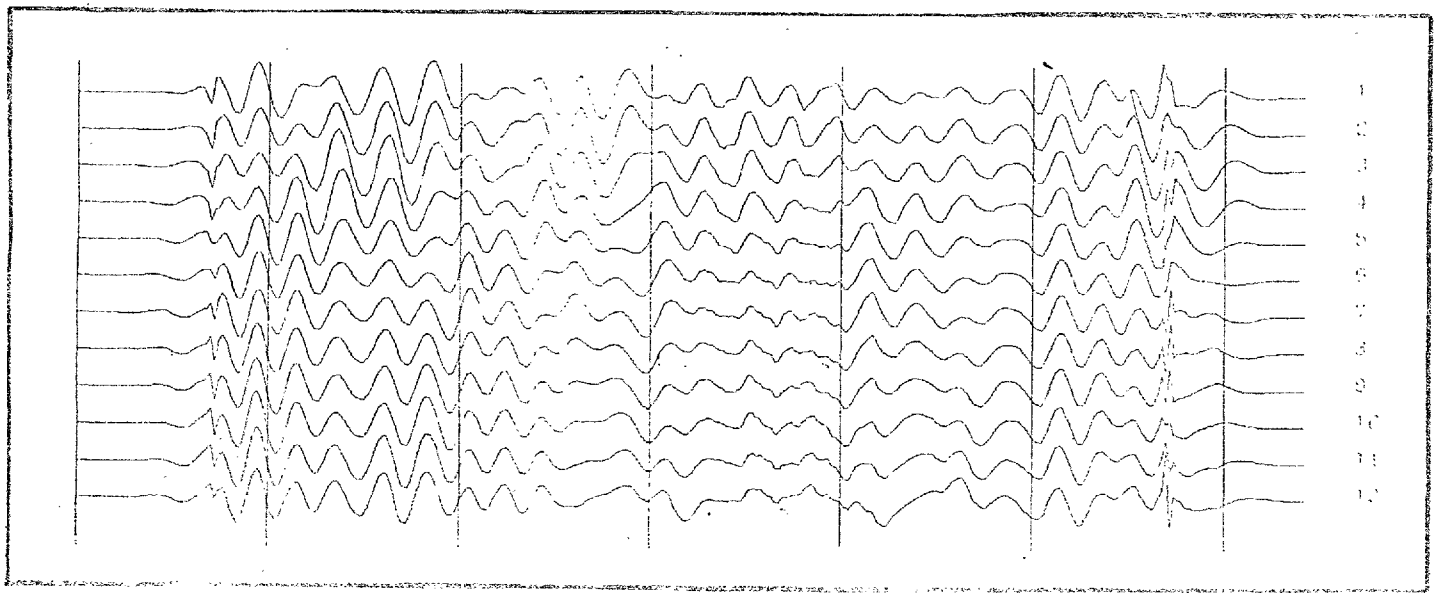


Fig. 2.40 result of filtering Fig. 1.8 with Q

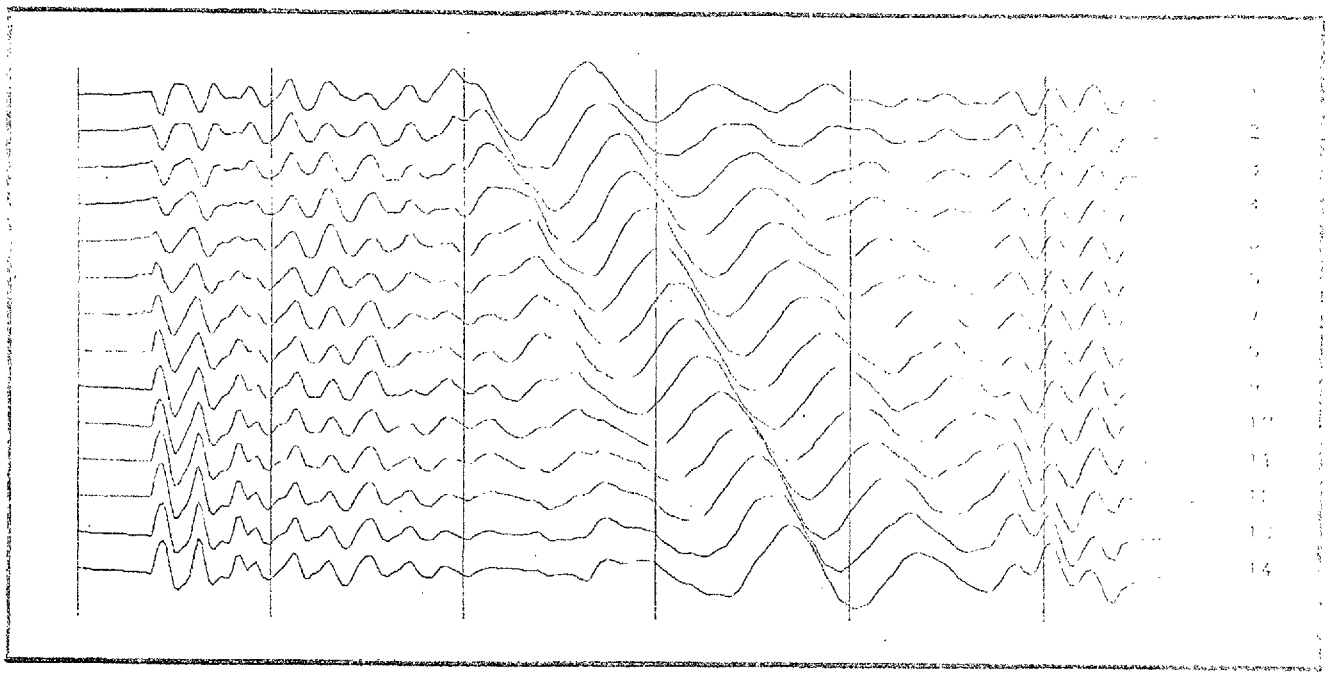


Fig. 2.41 result of filtering Fig. 1.2 with *FR9

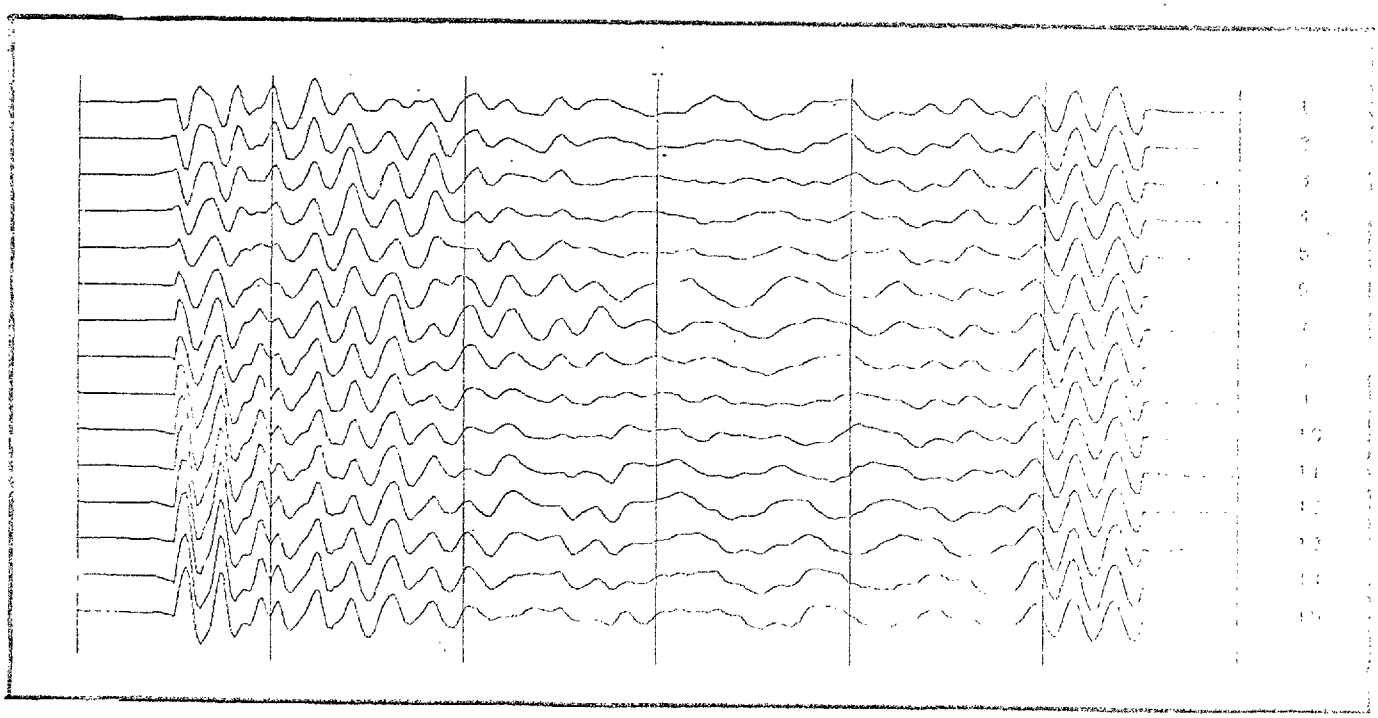


Fig. 2.42 result of filtering Fig. 1.2 with *FR10

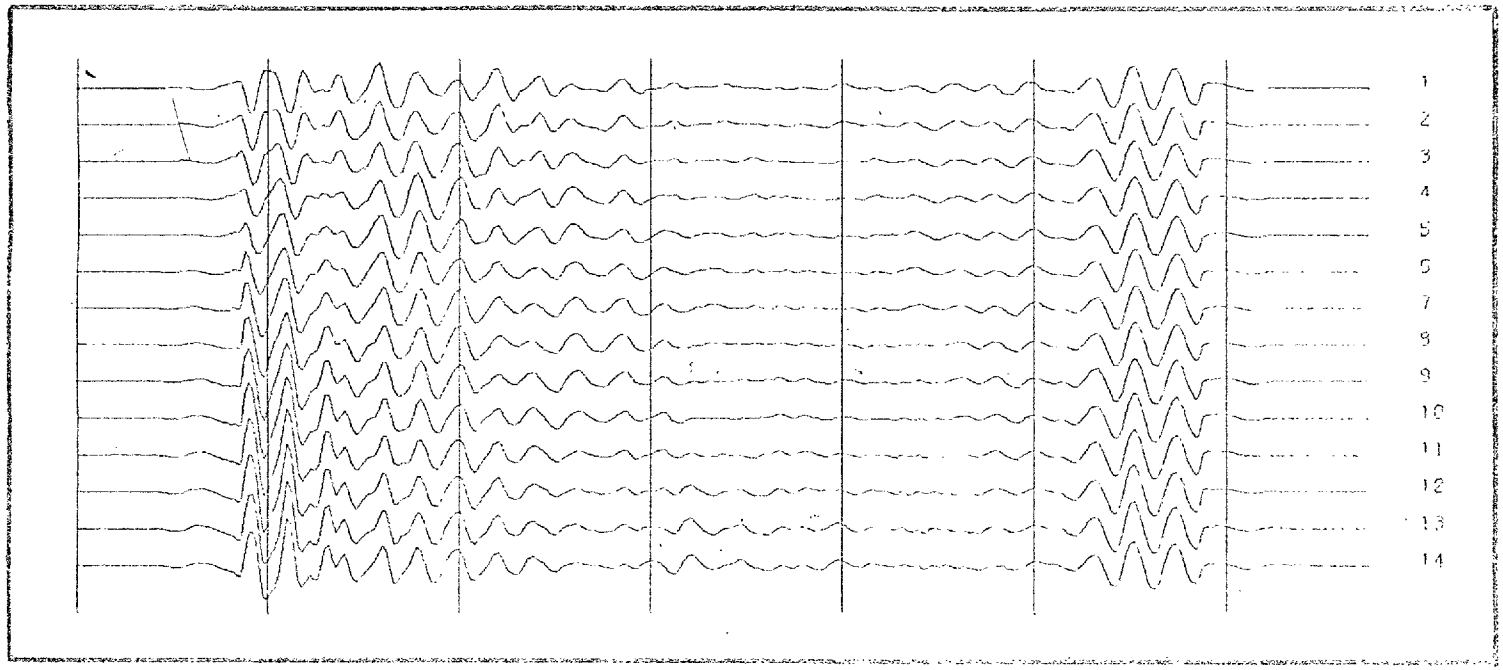


Fig. 2.43 result of filtering Fig. 1.7 with *PR9

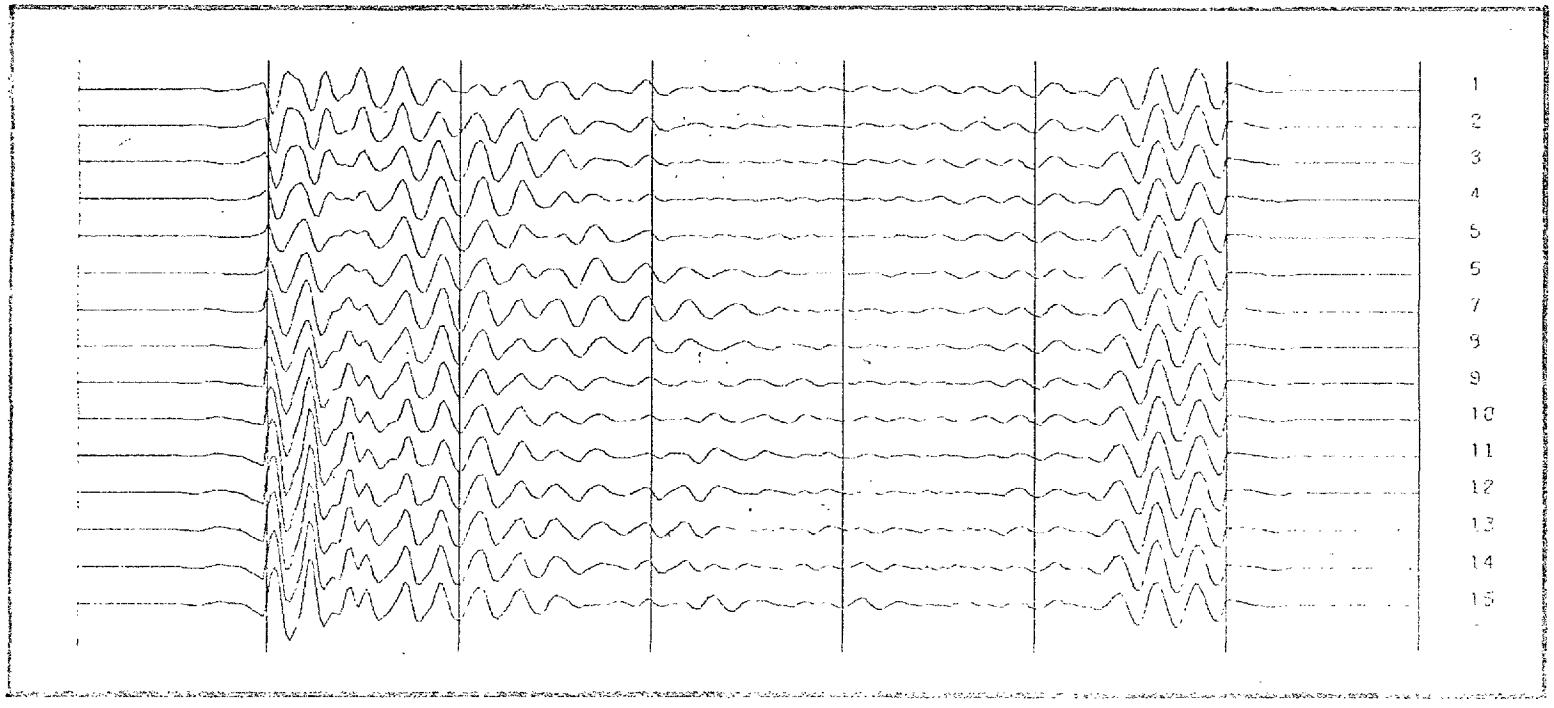


Fig. 2.44 result of filtering Fig. 1.7 with *PR10

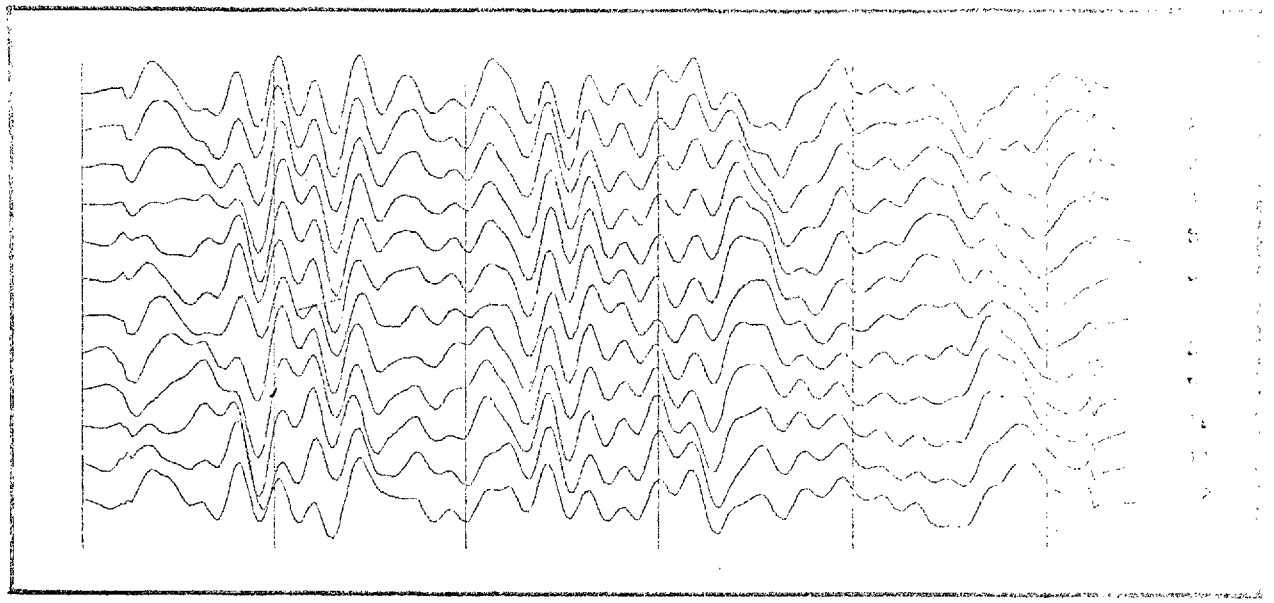


Fig. 2.45 result of filtering Fig. 1.3 with [illegible]R1

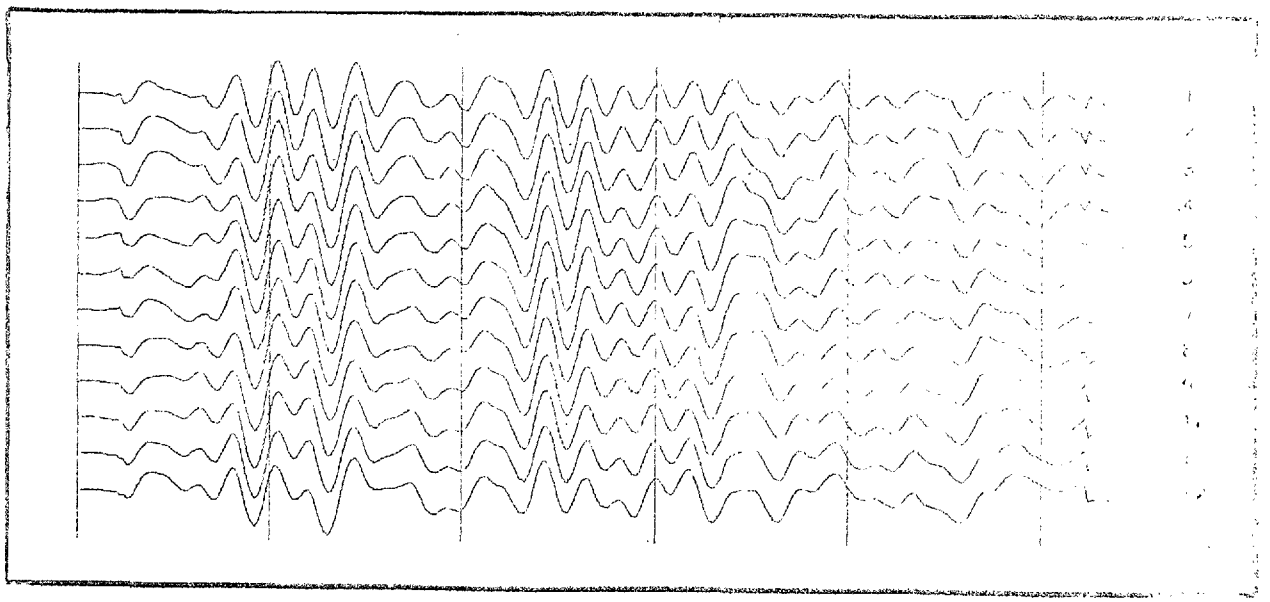


Fig. 2.46 result of filtering Fig. 1.3 with Q

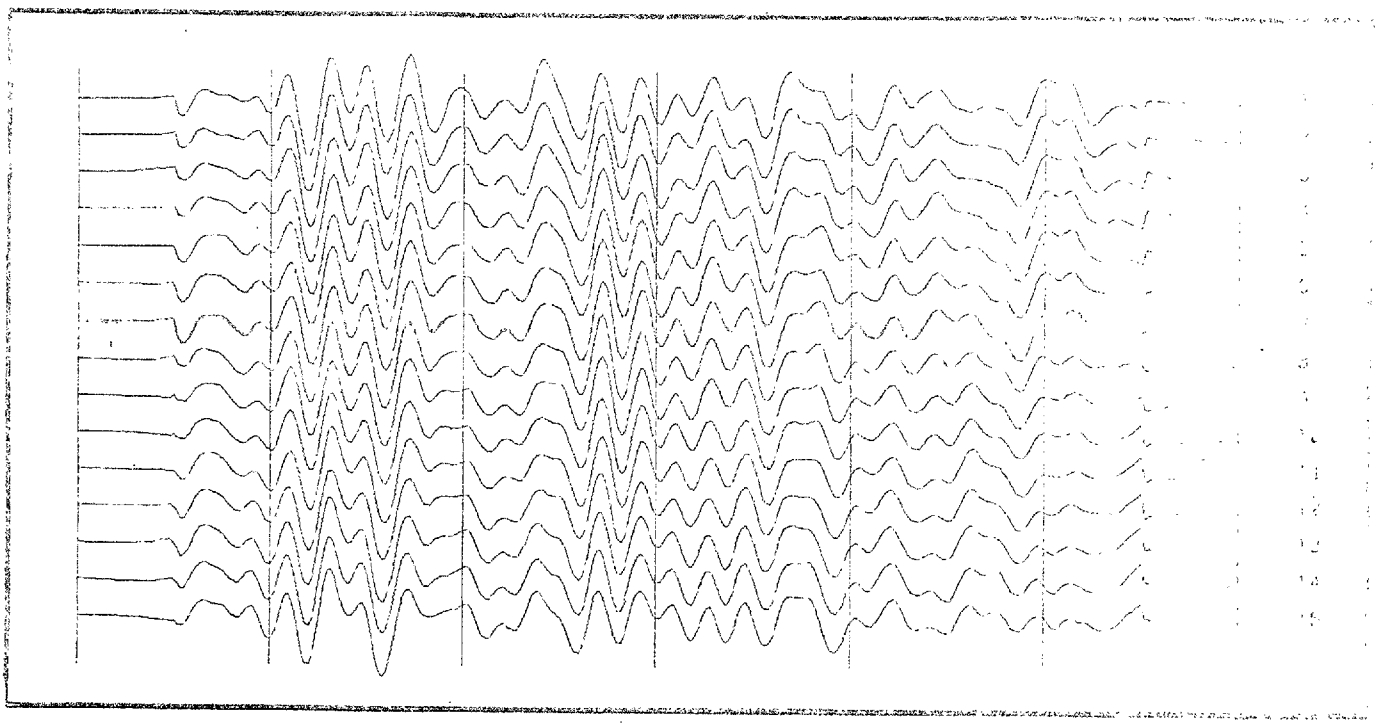


Fig. 2.47 result of filtering Fig. 1.3 with *1R10

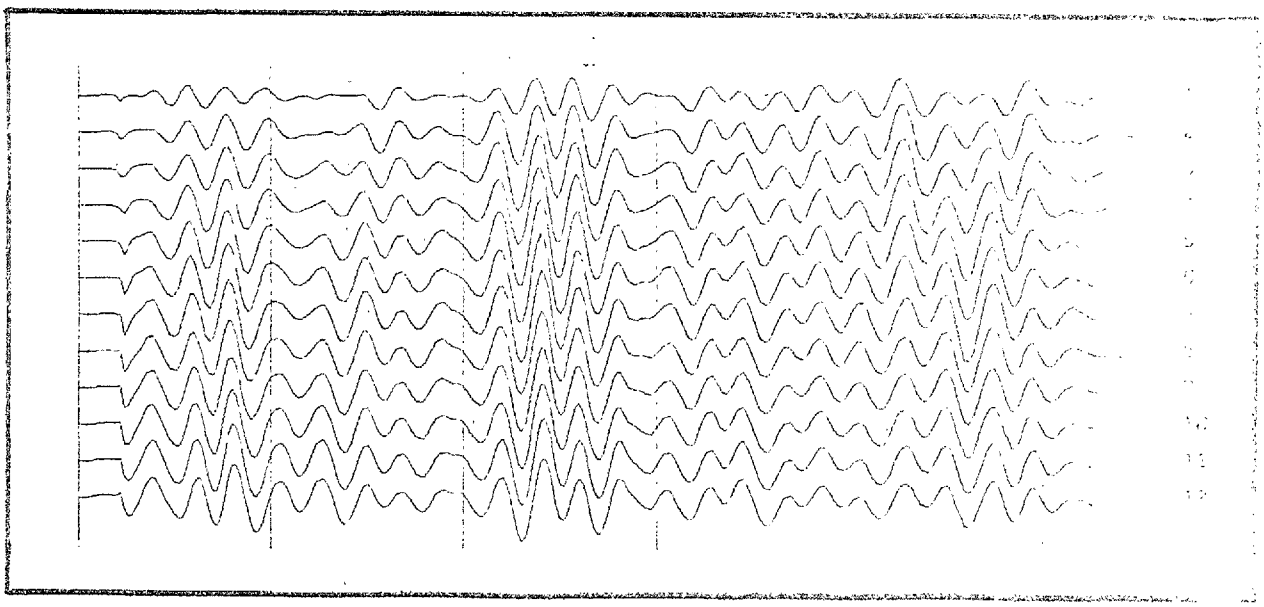


Fig. 2.48 result of filtering Fig. 1.6 with Q

2.4 Conclusions

The purpose of this chapter was to apply multichannel filters to a variety of real and synthetic data, in order to access how these filters may perform in a given situation. To this end the following results were obtained :

(a) experiments on synthetic data of linear moveout showed that signals as low in power as 20 db below that of the correlated noise could be successfully detected, provided that the background noise was not too severe. It was also shown that the filtering method was far more sensitive to the level of uncorrelated noise than it was to that of correlated noise. Filters of wide angle reject regions were shown to have particular application to the cancellation of random noise.

(b) the importance of the number of traces used in the filter design was discussed, and the sensitivity of the filtering process to the selection of a wrong filter was demonstrated. It was found that a very close match must exist between the movecuts of the data and those of the filter.

(c) experiments conducted on synthetic data of quadratic moveout gave results in good agreement with those of the linear case.

(d) a number of experiments were conducted on real data records that generally confirmed the findings of the synthetic case. The sensitivity of moveout rejection to the filter choice was again demonstrated, and good results were obtained from wide angle rejection filtering. The use of a multichannel filter to "clean up" a given record was shown, and the benefit in applying a simple band pass filter to remove the presence of ground roll was illustrated.

It may be concluded, therefore, that multichannel filtering is a very powerful, though somewhat sensitive, tool for the processing of seismic data.

Since one may not generally know, a priori, what filter to

apply, some additional approach is necessary. In some cases, of course, a straight forward application of a number of filters to the input data may suffice, or it may be advisable to apply a pre-filter to the data before performing such a filter scan. A second approach is to apply different analytical techniques to the data, that would specifically reveal the moveout information necessary to define which filter should be used. The methods of the autocorrelation matrix and Fourier Transform techniques are developed in the next two chapters with this aim in mind.

CHAPTER 3

THE AUTOCORRELATION MATRIX AND ITS APPLICATION TO THE ANALYSIS OF MOVEOUT

3.0 Introduction

In this chapter the autocorrelation matrix is defined and an averaging technique employed to improve the accuracy of the crosscorrelation estimates. The ability of the method to detect low power signals or correlated noise from synthetic data is investigated over a range of different noise levels, for both linear and quadratic moveout. It is shown that the use of multichannel filters can greatly assist this detection of low power events. Various pre-filtering experiments are discussed and the results reviewed with those of the previous chapter. Experiments are also conducted on the real data records of Chapter 1.

3.1 Autocorrelation theory

3.1.1 definition of autocorrelation matrix

Correlation is a concept by which the similarity between two seismic traces may be quantified. Essentially, the process is one by which the similarity in waveform shape between the two traces are measured for different relative displacements of the two traces.

Let $x_i(t)$ and $x_j(t)$ represent two seismic traces, sampled at intervals $\Delta t = 1$, and let the second trace be displaced by an amount τ relative to the first trace. The crosscorrelation function, $\phi_{ij}(\tau)$, for these two traces is defined by the relation

$$\phi_{ij}(\tau) = \frac{1}{n-\tau} \sum_{t=1}^{n-\tau} x_i(t)\, x_j(t-\tau) \; ; \quad (\tau = 0, \ldots, m)$$

where m = maximum relative displacement (i.e. the maximum lag or length of correlation)

n = length of each trace

When i = j the trace is correlated with itself to give the autocorrelation function $\phi_{ii}(\tau)$.

It should be noted that, strictly speaking, the function $\phi_{ij}(\tau)$ is an estimate of the covariance function for which the traces $x_i(t)$ and $x_j(t)$ each have a zero mean value. These mean values are assumed to be zero, in accord with the previous chapter, and the term "crosscorrelation function" will be used in place of "covariance function".

The sample function defined above gives an unbiased estimate of the crosscorrelation function. However, a small bias in this estimate would be desirable if the variance of the estimate could be reduced accordingly. Weighting these estimates with a Bartlett window achieves this result, reducing the amplitude of spurious peaks at large lag, and is obtained by using the following alternative definition for the crosscorrelation function :

$$\phi_{ij}(\tau) = \frac{1}{n} \sum_{t=1}^{n-\tau} x_i(t)\, x_j(t-\tau) \; ; \quad (\tau = 0,\ldots,m)$$

The bias becomes negligible, of course, for $n \gg m$.

Since all the traces of a given record used in this thesis are each of the same length, the division by the factor "n" is not necessary. Hence the form of the sample crosscorrelation function, used in this thesis, is given by

$$\phi_{ij}(\tau) = \sum_{t=1}^{n-\tau} x_i(t)\, x_j(t-\tau) \; ; \quad (\tau = 0,\ldots,m).$$

This is the same one-sided crosscorrelation function as is given in Robinson (1967a). It is shown in the next section, however, that it is advantageous to use the two-sided crosscorrelation function, so that $(\tau = -m,\ldots,m)$ giving 2m+1 samples in total.

If $\phi_{ij}(\tau)$ is determined for every pair of traces $x_i(t)$ and $x_j(t)$, then the complete set of these functions may be expressed by the matrix $\phi(\tau)$, where

$$\phi(\tau) = \left\{ \phi_{ij}(\tau) \right\}.$$

This matrix is defined as the "autocorrelation matrix" or as the

"first-order autocorrelation matrix". It will often be found convenient to refer to this by simply "auto-1". The leading diagonal of this matrix consists of the autocorrelation functions, and the off-diagonal elements the crosscorrelation functions.

Theorems and properties pertaining to crosscorrelation functions may be found in Lee (1960). Of particular interest to the later discussion are

(i) the symmetry property, $\phi_{ij}(\tau) = \phi_{ji}(-\tau)$.

(ii) that for random noise, $\phi_{ij}(\tau) = \delta_{ij}(\tau)$, where δ_{ij} is the familiar Kronecker delta.

3.1.2 detection of moveout

As was discussed in Chapter 1, the moveout of correlated noise at a given point in the seismic record is greater than that of signal at the same point. The purpose of autocorrelation matrix methods are to detect these moveouts and to present them in a form suitable for interpretation.

The crosscorrelation function will have a marked peak at a lag equal to the relative moveout of an event on the two traces in question. This may be deduced from the following simple analysis :

$$\text{let } x_i(t) = \delta(t-\alpha_i)$$

$$\text{then } \phi_{ij}(\tau) = \sum_{t=1}^{n-\tau} \delta(t-\alpha_i)\,\delta(t-\alpha_j-\tau)$$

$$\therefore \quad \phi_{ij}(\tau) = \delta[\tau-(\alpha_i-\alpha_j)]$$

i.e. peaks occur in the $\phi_{ij}(\tau)$ at $\tau = (\alpha_i - \alpha_j)$

A pictorial presentation of this example is given in Fig. 3.1.

Fig. 3.2 shows the two-sided autocorrelation matrix for traces of the form $x_i(t) = s(t) + r(t-\beta_i)$, where $\beta_i = 5i$. Note that by presenting the two-sided crosscorrelation functions in the autocorrelation matrix, all the necessary moveout information is contained in one column of the matrix. Hence, only one column of this matrix need be displayed. For synthetic data of linear moveout, this column was taken to be the "middle" column of the matrix, i.e.

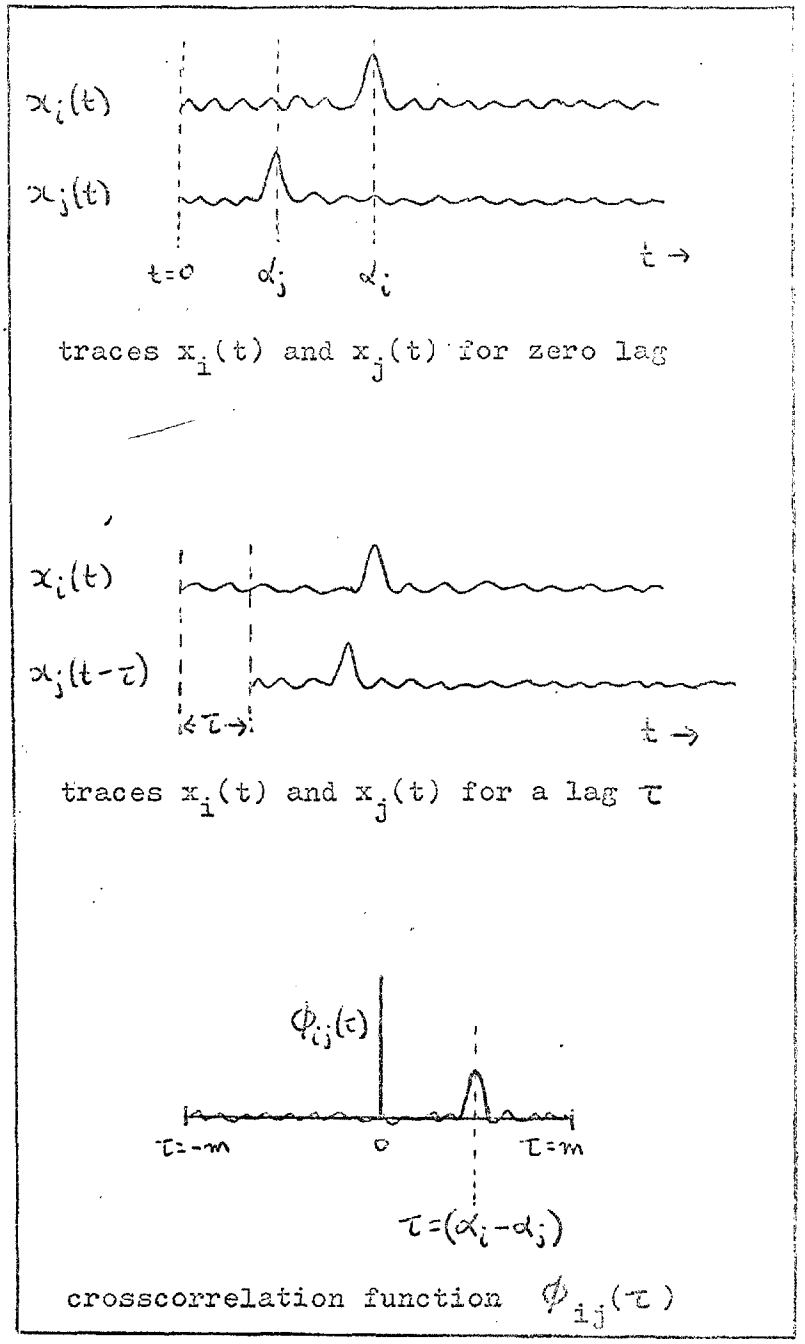
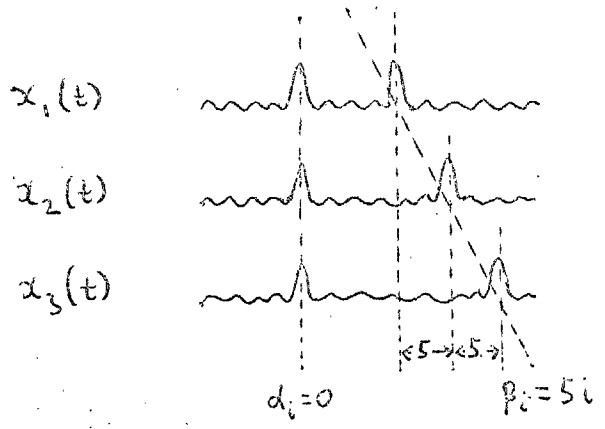
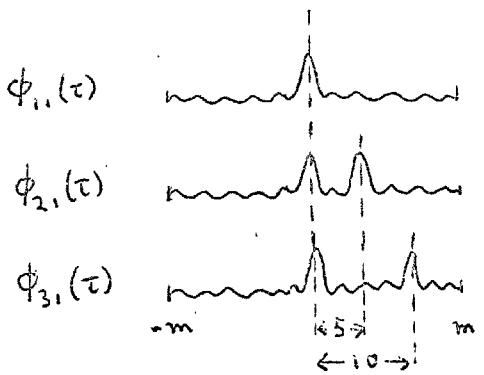


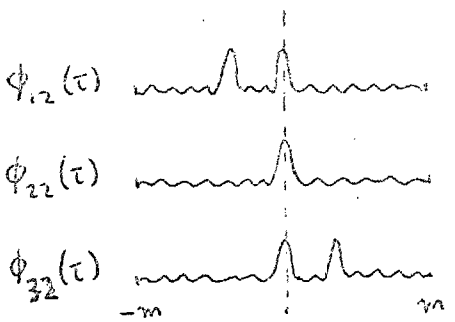
Fig. 3.1 Illustration of crosscorrelation moveout detection



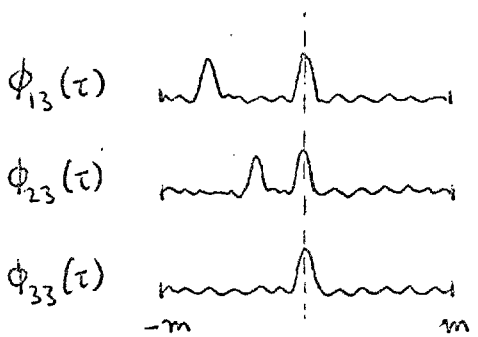
input traces



column one of autocorrelation matrix



column two of autocorrelation matrix



column three of autocorrelation matrix

Fig. 3.2 Example of an autocorrelation matrix

column 12 for a 24 trace record. For synthetic data of quadratic moveout, however, column 1 was chosen due to the design of the time window for the quadratic filter (filtering of this column is dicussed later).

In practice, of course, the degree to which correlation peaks are visible depend upon many factors, such as the constituent signal to noise power ratios, the number of moveouts in the section and the statistical accuracy of the estimates. These particular factors are studied in this chapter and are illustrated with appropriate examples. Mention must also be made of the presence of other peaks in the autocorrelation matrix. Some of these peaks will be due to the coincidence of random events adding together in phase, and may be identified as such since they appear irregularly across the matrix. Other peaks, however, can occur due to the correlation of signal and correlated noise. The presence of these "pseudo-correlation" peaks may be deduced from the following analysis :

$$\text{let } x_i(t) = s(t-\alpha_i) + r(t-\beta_i)$$

$$\therefore \phi_{ij}(\tau) = \sum_{t=1}^{n} \left[s(t-\alpha_i) + r(t-\beta_i) \right] . \left[s(t-\alpha_j-\tau) + r(t-\beta_j-\tau) \right]$$

$$\therefore \phi_{ij}(\tau) = \sum_{t=1}^{n} s(t-\alpha_i)\, s(t-\alpha_j-\tau) + \sum_{t=1}^{n} r(t-\beta_i)\, r(t-\beta_j-\tau)$$
$$+ \sum_{t=1}^{n} s(t-\alpha_i)\, r(t-\beta_j-\tau) + \sum_{t=1}^{n} r(t-\beta_i)\, s(t-\alpha_j-\tau)$$

The first two terms of this expression give the true correlation peaks, for signal and correlated noise, at $\tau = (\alpha_i - \alpha_j)$ and $\tau = (\beta_i - \beta_j)$ respectively; whereas the last two terms give the pseudo-correlation peaks at $\tau = (\alpha_i - \beta_j)$ and $\tau = (\beta_i - \alpha_j)$. In general, the signal and correlated noise waveforms will be sufficiently different so that these pseudo-correlated peaks will have a smaller amplitude than that of the true correlated peaks (ideally, one would have $\sum_{t=1}^{n} s(t)r(t) = 0$). However, it must be remembered that cases

can arise where the amplitude of random peaks and pseudo-correlation peaks are greater than the amplitude of the desired correlation peaks. It is for this reason that manual intervention, in the form of "quality control", in correlation analyses is preferable (in the opinion of the author) to automatic peak-picking devices. Significant line-ups across the autocorrelation matrix may not always involve those peaks of the highest amplitudes.

3.1.3 second-order autocorrelation matrix

From Fig. 3.2 it is clear that the autocorrelation matrix gives r estimates of the moveout information, where r is the number of input traces. The signal to noise ratio in the presentation of this moveout information can be improved by taking the average of these r estimates and presenting this average as a single result. This averaging process (Hubral, 1970) may be effected through the crosscorrelation of the columns of the autocorrelation matrix, in a manner described below :

A pseudo-trace, $\Psi_p(t)$, is constructed from the column p by the relation

$$\Psi_p(t) = \sum_{i=1}^{r} \phi_{ip}\left[t - (i-1)T\right] \quad , \quad \text{where } T = 3m.$$

The "average crosscorrelation function" is then defined by

$$\Psi_{pq}(\tau) = \sum_{t=1}^{rT-\tau} \Psi_p(t) \; \Psi_q(t-\tau)$$

The "average autocorrelation matrix" or "second-order autocorrelation matrix" is then defined by

$$\Psi(\tau) = \left\{\Psi_{pq}(\tau)\right\}$$

A pictorial presentation of this process for the example of Fig. 3.2 is given in Fig. 3.3. Note that the sense of the moveout peaks in the second-order autocorrelation matrix is the reverse of that in the autocorrelation matrix. This may also be demonstrated by the following analysis :

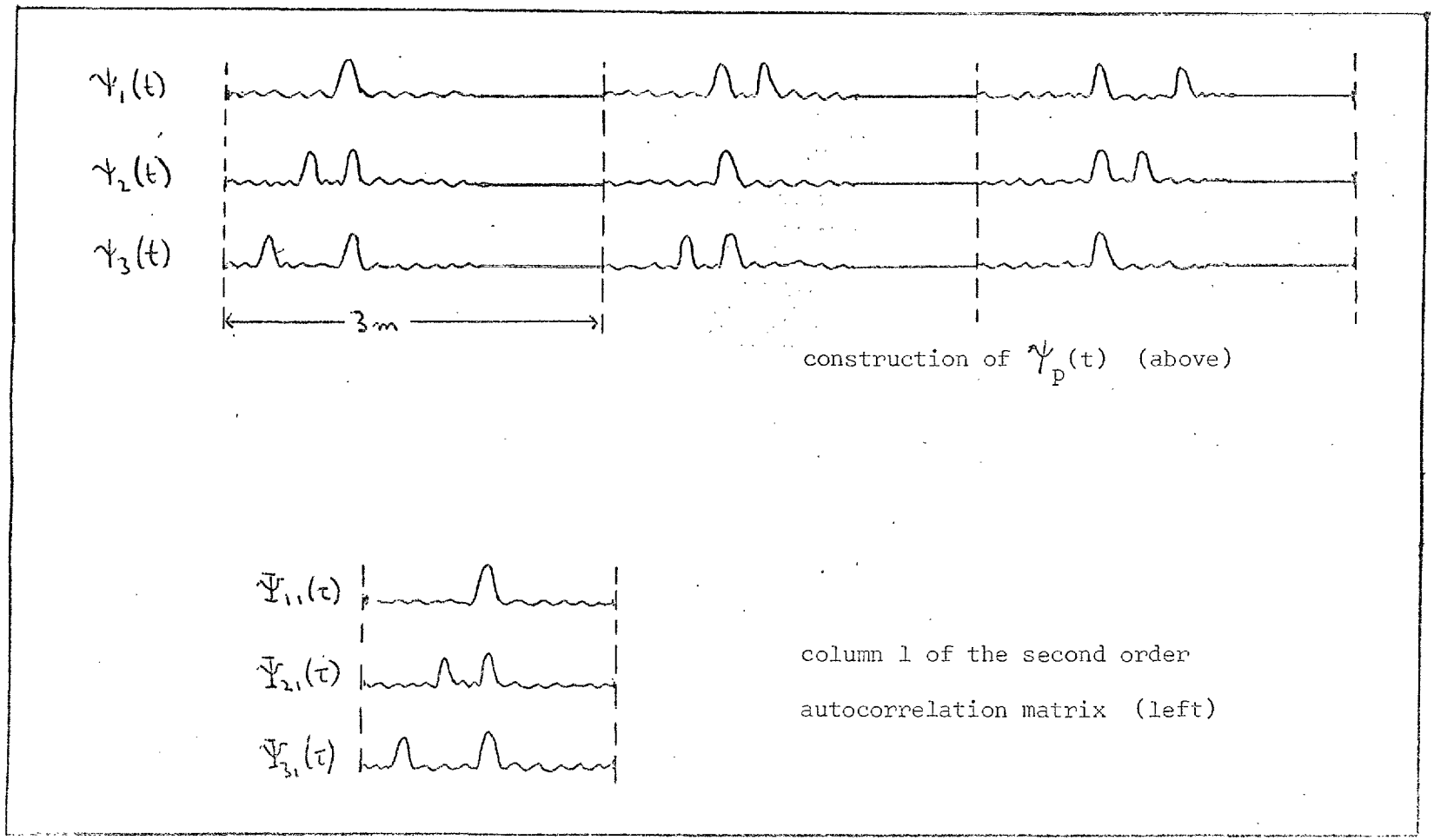


Fig. 3.3 Example of a second order autocorrelation matrix

let $\phi_{ij}(\tau) = \delta[\tau - (\alpha_i - \alpha_j)]$

Since $\tau \leq m$, and $T = 3m$, it follows that cross-terms involving factors of T will be zero, hence

$$\Psi_{pq}(\tau) = \sum_{t=1}^{T-\tau} \left(\sum_{i=1}^{r} \delta[t - (\alpha_i - \alpha_p)] \right) \cdot \left(\sum_{j=1}^{r} \delta[t - (\alpha_j - \alpha_q) - \tau] \right)$$

It also follows, from Fig. 3.3, that $\alpha_i = \alpha_j$, hence

$$\Psi_{pq}(\tau) = \delta[\tau - (\alpha_q - \alpha_p)]$$

i.e. $\phi_{ij}(\tau)$ has peaks at $\tau = (\alpha_i - \alpha_j)$

and $\Psi_{ij}(\tau)$ has peaks at $\tau = (\alpha_j - \alpha_i)$

It will often be found convenient to refer to the second-order auto-correlation matrix by simply "auto-2".

3.1.4 statistical considerations of the autocorrelation matrix technique

In the analysis of seismic records it is the aim to obtain clear and accurate estimates of particular seismic parameters, such as moveout or signal to noise ratios. Different scientific considerations very often place opposing constraints on the desired value of a given processing parameter, such as record length. In any case of practical interest a compromise in several different directions is generally necessary, and the validity of a particular compromise can only be judged by the quality of the results obtained. Some of the considerations necessary for the optimal choice of record length and maximum correlation lag are presented as follows :

(a) In many cases of physical interest the relative moveout of the signal is comparable to that of the correlated noise. These moveout differences are more clearly revealed by taking a large number of traces for analysis, and by restricting the record length to include only one or two moveouts of interest (where possible). Quite clearly, a large record length would include a large number of different moveouts that would all interfere with each other in the autocorrelation

matrix. The number of traces taken in this work was 24 for synthetic data and 23 for real data (ref. Chapter 1).

(b) Discussion of record length with regard to stationarity and cancellation of uncorrelated noise have been given in Chapter 2.

(c) The number of degrees of freedom in the correlation estimate is given by 2n/m (Bendat and Piersol, 1966), where n is the record length and m the maximum correlation lag. Hence, for statistical accuracy, it is necessary to have $n \gg m$. A sufficient practical consideration is given by $n > 5m$, a result derived from studies of band-limited white noise.

It is important, of course, that the maximum correlation lag should bear some relation to the moveout of the events it is desired to detect. Large moveout events would require a larger maximum lag then would low moveout events. The choice of the maximum correlation lag will, therefore, be the result of a compromise between the requirements of record length (ref. (b)), statistical accuracy (ref. (c)) and the moveouts present in the data.

Due to these considerations a maximum correlation lag of 50 samples was taken for the real data records, which were each of length 250 samples.

The synthetic data of linear moveout used in this chapter was computed for $\alpha_i = 0$ and $\beta_i = i$. Hence the correlated noise wavelets were displaced progressively across the record to a maximum of 24 samples. The length of the given Butterworth wavelets were typically 50 samples, hence a reasonable choice for the maximum correlation lag is given by m = 25 samples. In order to effect some sort of comparison between the results of synthetic and real data correlations, the synthetic record length was generally taken to be 125 samples.

3.2 Applications to synthetic data

Details of all synthetic data records may be found in Table 3.1, with corresponding details of correlation analyses performed on these records being given in Table 3.2 and Table 3.3.

The purpose of this section is to (i) investigate the ability of the autocorrelation matrix method to detect low power events for different conditions of signal to noise ratio, (ii) to show the effect of varying record length on the correlation estimates and (iii) to illustrate the advantages of applying a pre-filter to the input data before performing the correlation analysis.

Quite clearly, one may either pass the signal and reject the noise, or reject the signal and pass the noise. This latter appraoch was often used in this chapter in order to demonstrate the general applicability of the method. Timing lines were drawn across the autocorrelation columns at maximum, minimum and zero lag.

3.2.1 development of analytical approach

The first order autocorrelation matrix for the record of Fig. 3.4 was computed, of which column 12 is displayed as Fig. 3.5. Very little presence of the correlated noise can be seen here, though the signal, of course, is very much in evidence. This column was then filtered by reject/pass filter *RP1, and the result presented as fig. 3.6. It is seen that some evidence of correlated noise is given, though not a great deal. The previously discussed second order autocorrelation matrix technique was then applied, column 12 of the first order autocorrelation matrix being crosscorrelated with all the other columns of that matrix, in order to yield column 12 of the second order autocorrelation matrix (Fig. 3.7). The results at this stage, however, are still rather disappointing. When this second order column is filtered by reject/pass filter *RP1, however, the result of Fig. 3.8 is obtained, which clearly shows the presence of the required correlated noise. Similarity of waveform shape across this figure is

Figure number	ρ (db)	ν (db)	α_i	β_i	number of traces	length of traces (in samples)
3.4	6.0	6.0	0	i	24	125
3.11	0.0	3.0	0	i	24	125
3.16	3.0	3.0	0	i	24	125
3.20	3.0	0.0	0	i	24	60
3.24	3.0	0.0	0	i	24	125
3.28	3.0	0.0	0	i	24	200
3.33	3.0	3.0	0	i	24	125
3.37	9.0	3.0	0	i	24	125
3.41	15.0	3.0	0	i	24	125
3.45	3.0	-3.0	0	i	24	125
3.49	3.0	-6.0	0	i	24	125
3.53	-15.0	6.0	0	$i^2/24$	24	125
3.57	-9.0	0.0	0	$i^2/24$	24	125
3.61	0.0	-6.0	0	$i^2/24$	24	125

Table 3.1 Index of synthetic data records

Fig. No. of input record	Fig. No. of auto-1 (col 12)	Fig. No. of auto-2 (col 12)	Fig. No. of filtered auto-2	filter name
3.4	3.5	3.7	3.8	*RL1
3.4	3.5	3.7	3.9	*RM10
3.4	3.5	3.7	3.10	*RL7
3.11	3.12	3.13	3.14	*RL1
3.11	3.12	3.13	3.15	*RM1
3.16	3.17	3.18	3.19	*RL1
3.20	3.21	3.22	3.23	*RP1
3.24	3.25	3.26	3.27	*RL1
3.28	3.29	3.30	3.31	*RL1
3.33	3.34	3.35	3.36	*RH1
3.37	3.38	3.39	3.40	*RH1
3.41	3.42	3.43	3.44	*RH1
3.45	3.46	3.47	3.48	*RH1
3.49	3.50	3.51	3.52	*RH1
	(col 1)	(col 1)		
3.53	3.54	3.55	3.56	Q
3.57	3.58	3.59	3.60	Q
3.61	3.62	3.63	3.64	Q

Table 3.2 Index of correlation analyses for synthetic data

good, and the moveout can be accurately measured. Comparison of Fig. 3.8 with Fig. 3.6 shows the advantage of the double crosscorrelation technique.

A priori, of course, one does not know which filter to apply. Hence the required column of the second order matrix must be scanned by a number of different filters and the results displayed side by side. An example of such a filter scan is provided by Fig. 3.8 (*RP1), Fig. 3.9 (*RP10) and Fig. 3.10 (*RP7), for filters designed to reject moveouts in the range 1.0 ± 0.5, 2.0 ± 0.5 and 3.0 ± 0.5 samples per trace, respectively. As before, the recovery of the desired event is contingent upon the correct match of the moveout of the data and that of the filter. This sensitivity allows quite accurate moveout measurement to be performed.

From these results it would be concluded that the record of Fig. 3.4 should be filtered by reject/pass filter *RP1. The result of this filtering is presented in Fig. 3.65.

The poor quality of Fig. 3.7, with regard to detection of correlated noise, may be attributed to the interference between this noise and the signal. This may be demonstrated by taking the input record of Fig. 3.11, for which signal and correlated noise are of the same power, and the filtering the second order column by pass/reject filter *PR1 (Fig. 3.14) and by reject/pass filter *RP1 (Fig. 3.15). The former filtering has clearly revealed the presence of signal, and the latter that of correlated noise. Such information is not readily available from the second order column alone (Fig. 3.13). Hence the importance of filtering the second order column.

The next question to consider is how well the method will resolve signal and correlated noise solely on the basis of moveout alone, i.e. the signal and correlated noise wavelets are taken to be the same, $b_1(t) = b_2(t)$. These results are presented as Fig. 3.16 - Fig. 3.19, where it is seen that the recovery of the correlated noise

event, of moveout 1 sample per trace, has been entirely successful.

This section has shown that a suitable "modus operandi" for correlation analysis is to (i) compute the first order autocorrelation matrix, (ii) compute a column of the second order autocorrelation matrix and (iii) apply a multichannel filter scan to this second order column.

It is convenient, at this stage, to return to the question of removing the average amplitude of each trace from each trace before commencing any analysis. A study of the autocorrelation functions in this chapter show that there is little or no vertical shift in these functions, hence the removal of the average amplitudes is not necessary.

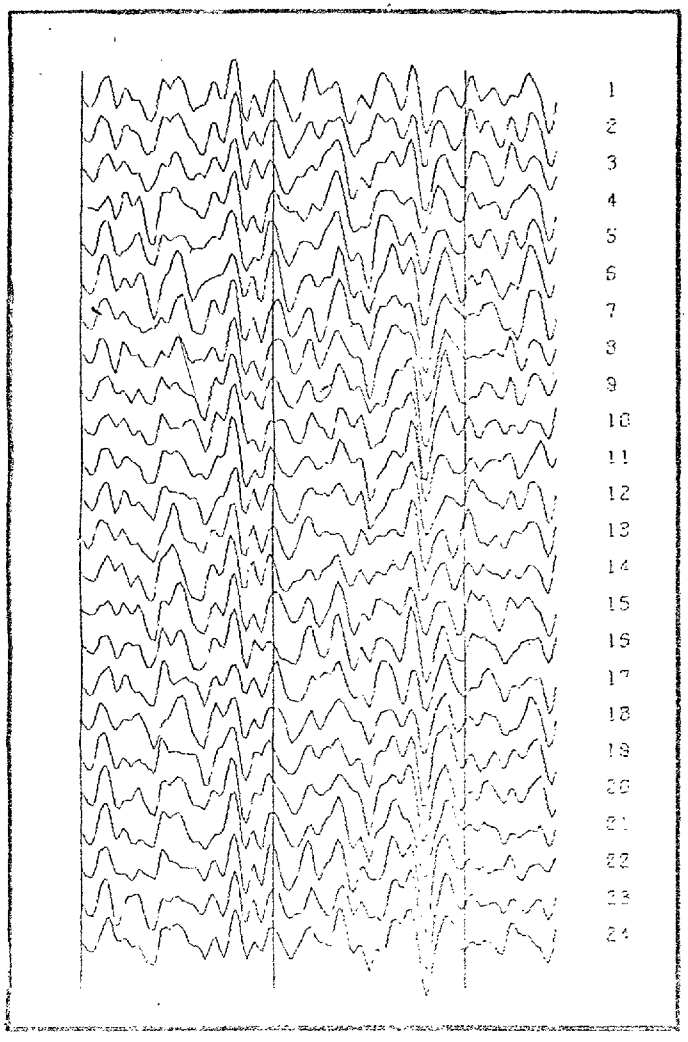


Fig. 3.4 input record,

$\rho = 6.0$, $\nu = 6.0$ db

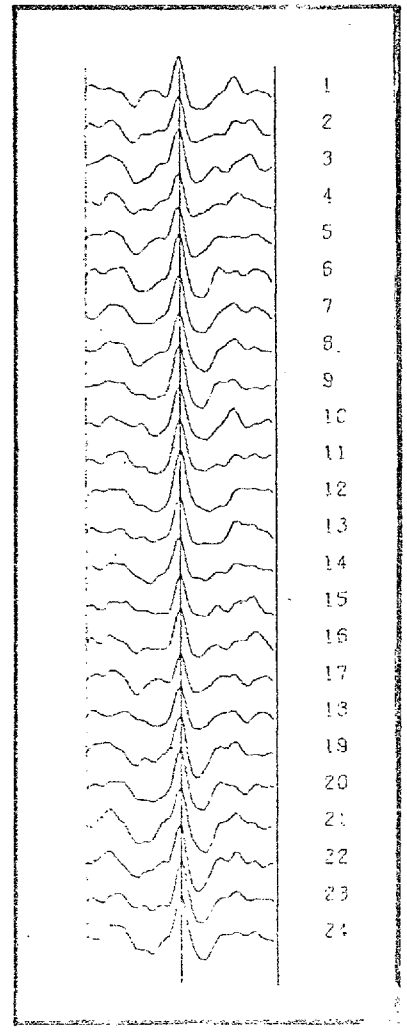


Fig. 3.5 auto-1

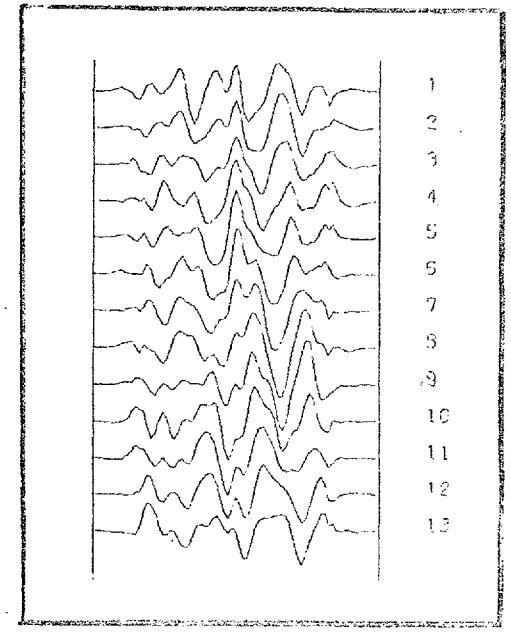


Fig. 3.6 auto-1

filtered by *RP1

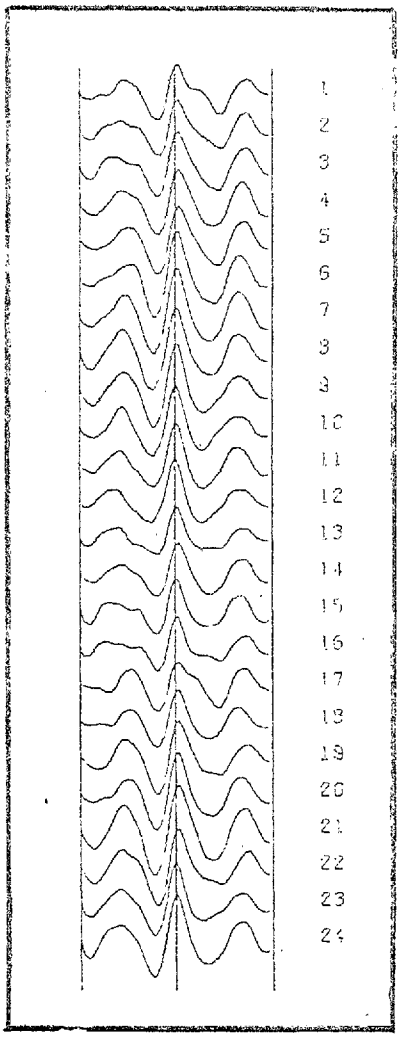


Fig. 3.7 auto-2

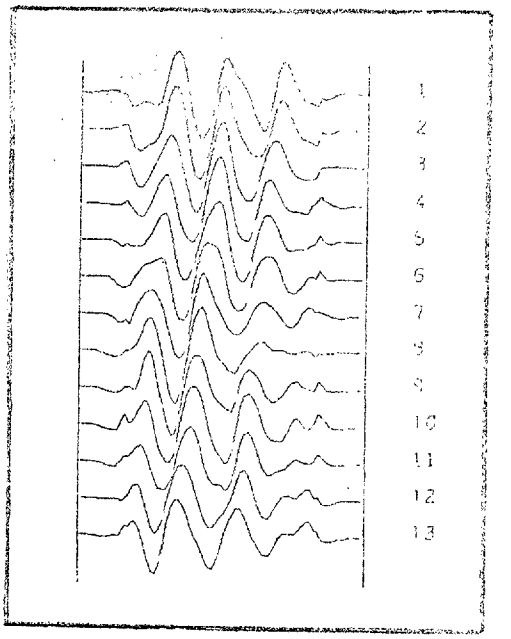


Fig. 3.8 auto-2

filtered by *RP1

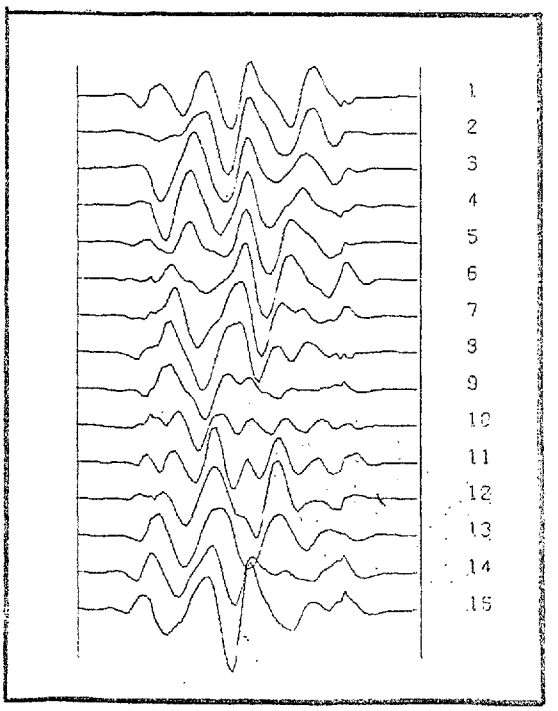


Fig. 3.9 auto-2

filtered by *RP10

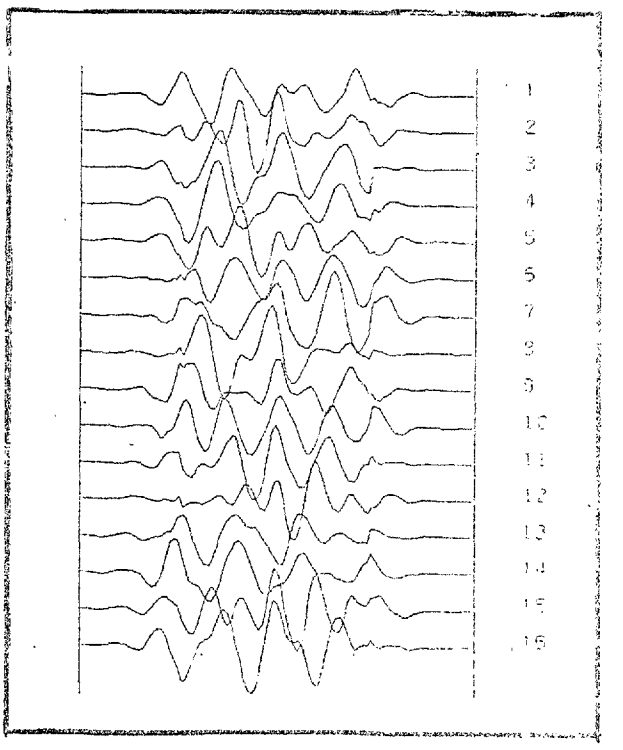


Fig. 3.10 auto-2

filtered by *RP7

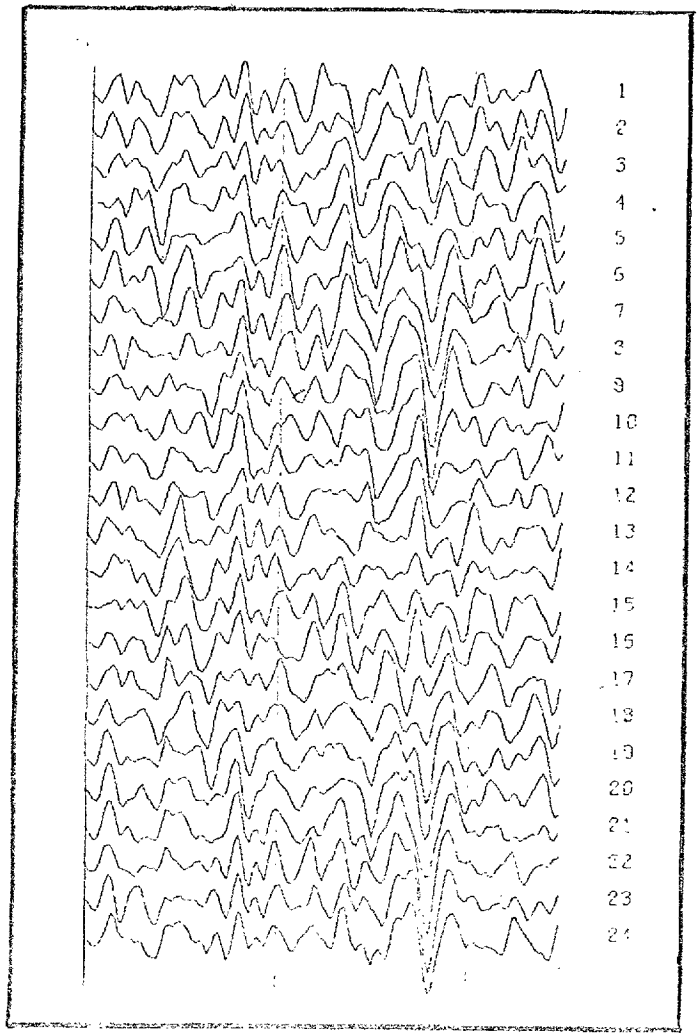


Fig. 3.11 input record,
P = 0.0, γ = 3.0 db

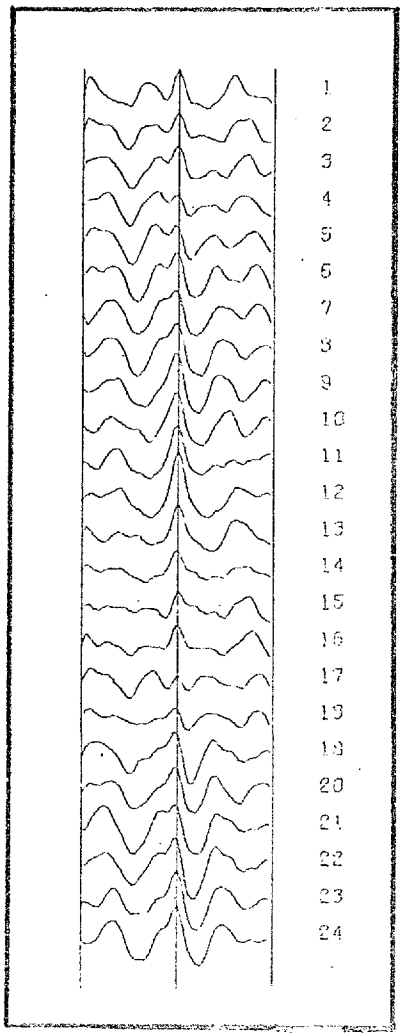


Fig. 3.12 auto-1

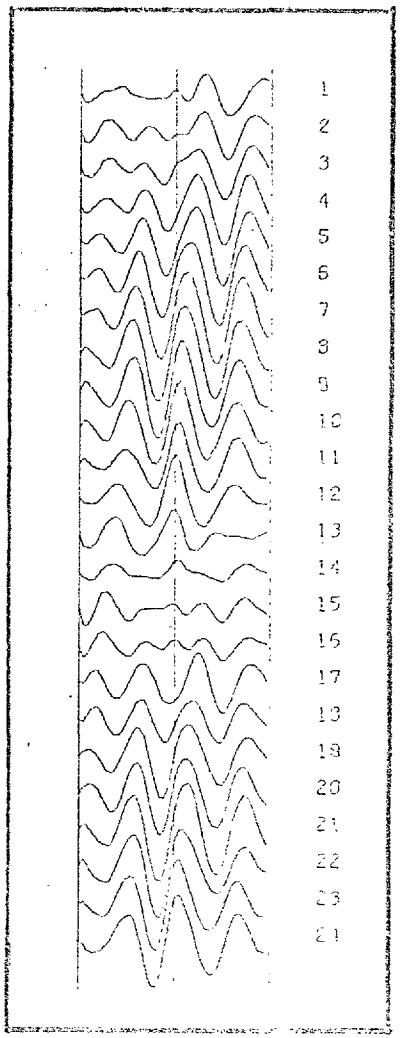


Fig. 3.13 auto-2

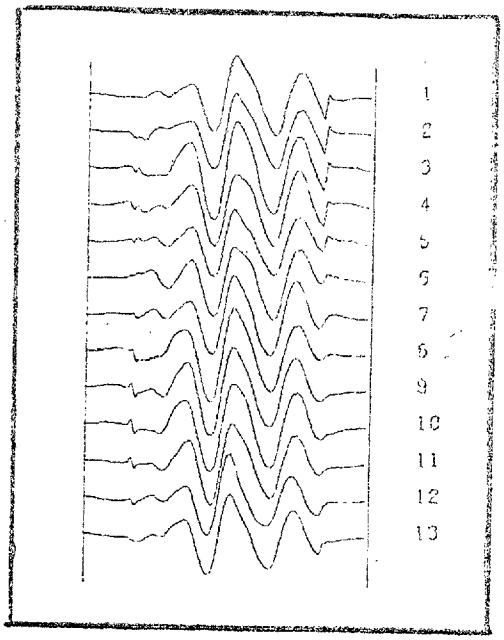


Fig. 3.14 auto-2

filtered by *PR1

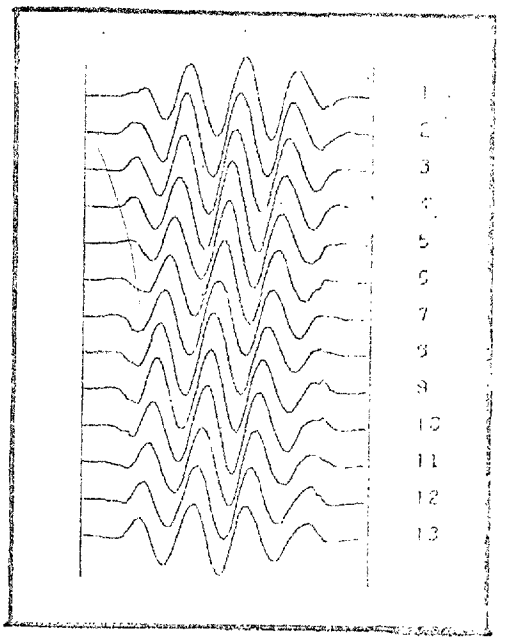


Fig. 3.15 auto-2

filtered by *RP1

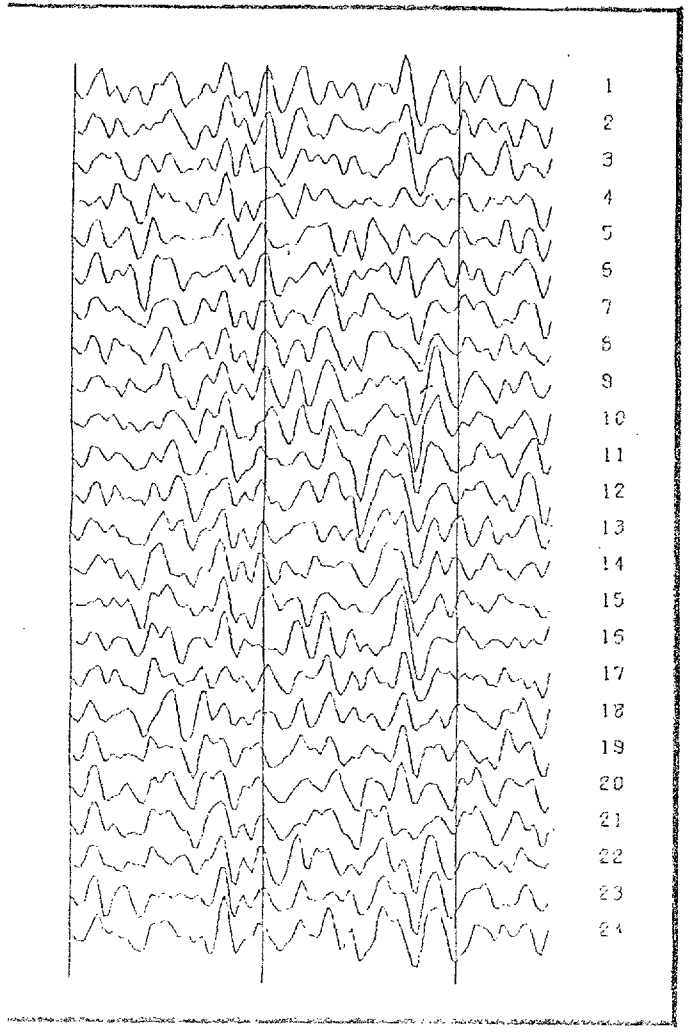


Fig. 3.16 input record,

ρ = 3.0, ν = 3.0 db

$b_1(t) = b_2(t)$

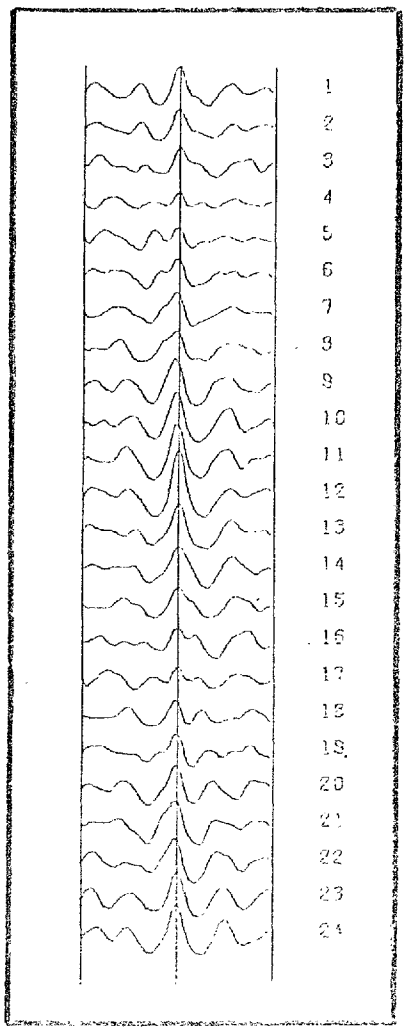


Fig. 3.17 auto-1

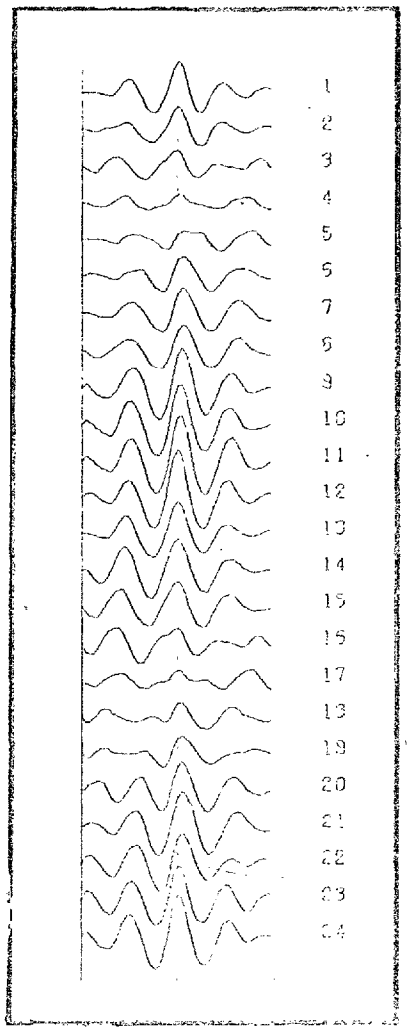


Fig. 3.18 auto-2

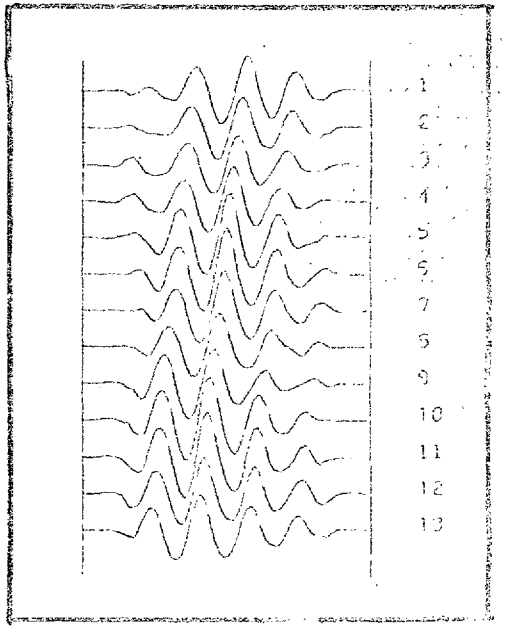


Fig. 3.19 auto-2

filtered by *RP1

3.2.2 importance of record length

Much has already been said on the considerations of record length in previous chapters. The purpose of this section is simply to show that correlation estimates improve with increasing record length, provided that all other things remain equal. This improvement is due to both better cancellation of random noise and to better statistical accuracy.

Fig. 3.20 - Fig. 3.23 show a correlation analysis for a record length of 60 samples, Fig. 3.24 - Fig. 3.27 that for a record length of 125 samples, and Fig. 3.28 - Fig. 3.31 that for a record length of 200 samples. Signal to noise ratios for each input record were 3.0 db for correlated noise and 0.0 db for uncorrelated noise. Reject/pass filter *RP1 was applied to each of the second order columns. Comparison of these filtered second order columns, Fig. 3.23, Fig. 3.27 and Fig. 3.31, show the expected improvement with increasing record length.

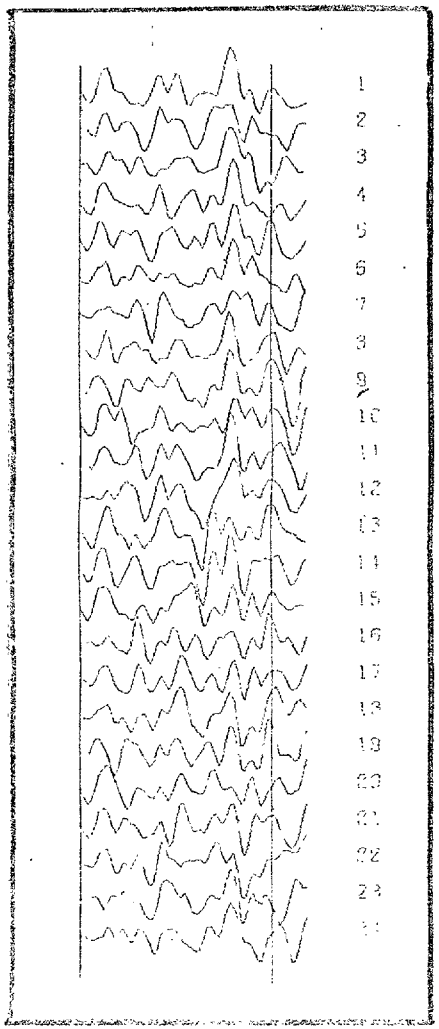


Fig. 3.20 input record,

ρ = 3.0, ν = 0.0 db

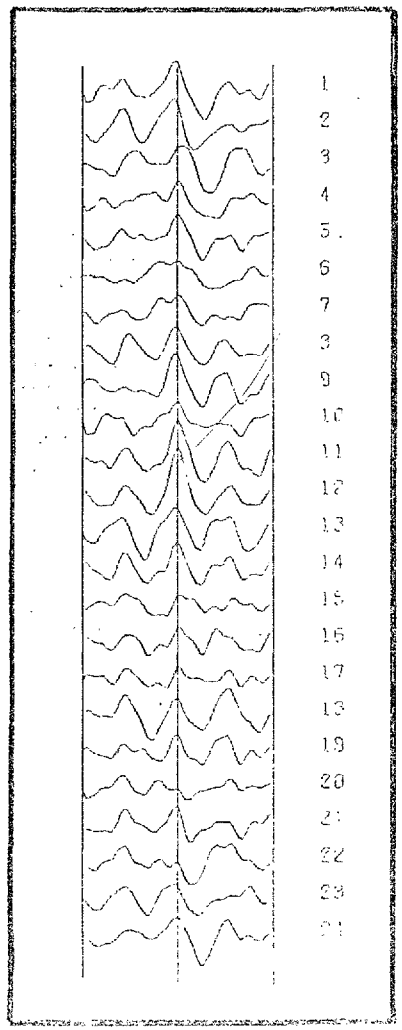


Fig. 3.21 auto-1

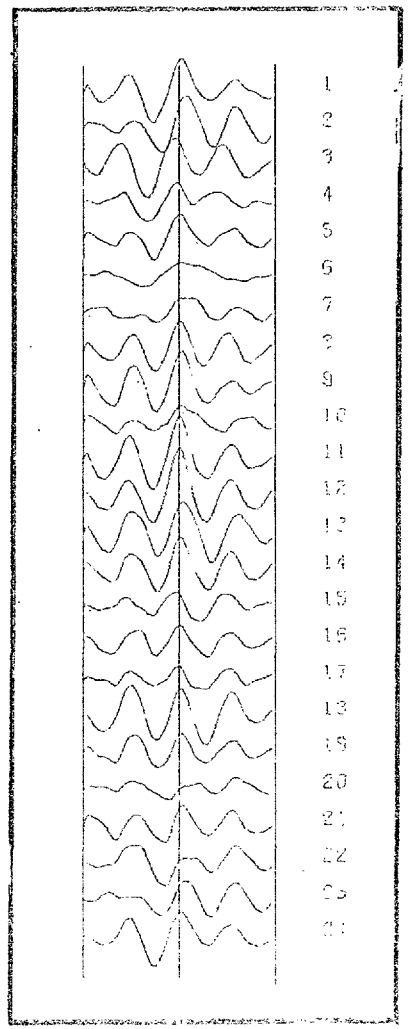


Fig. 3.22 auto-2

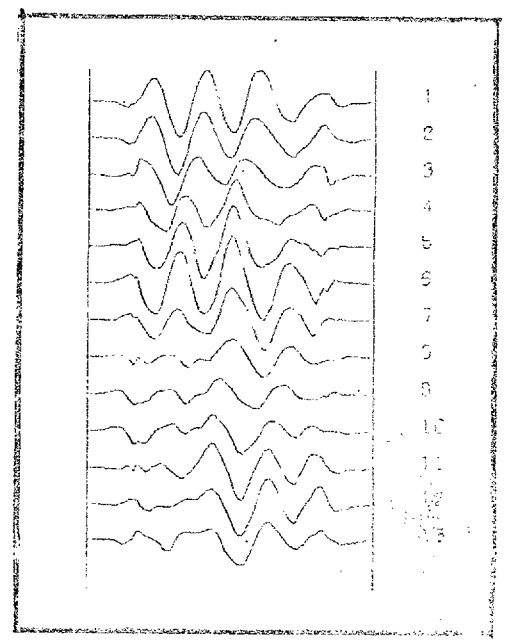


Fig. 3.23 auto-2

filtered by *RP1

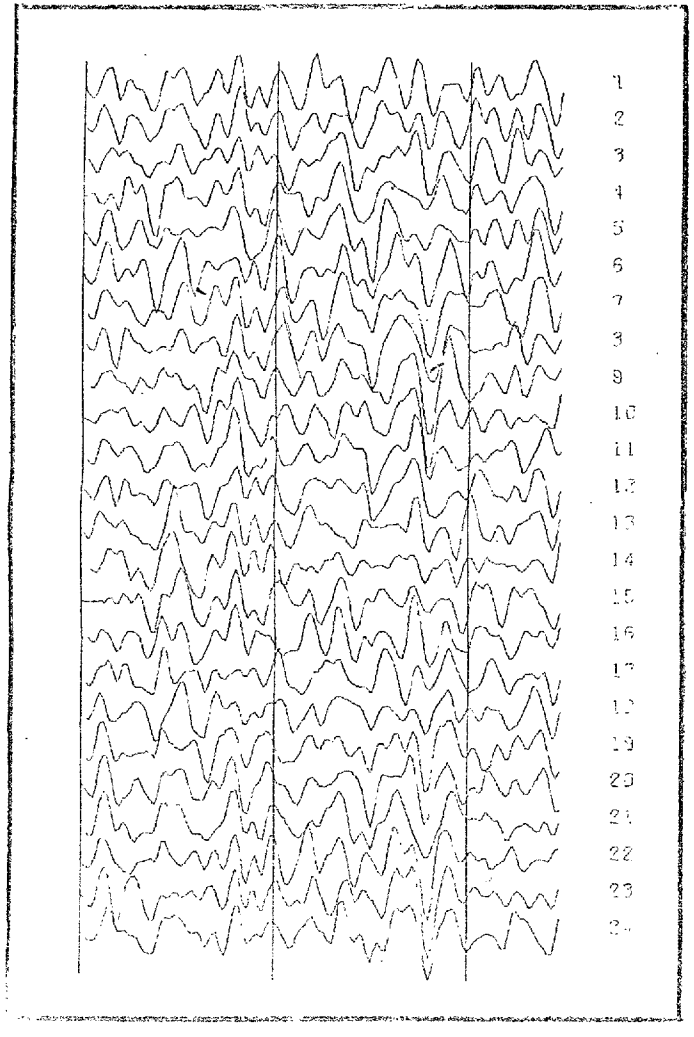


Fig. 3.24 input record,

p = 3.0, γ = 0.0 db

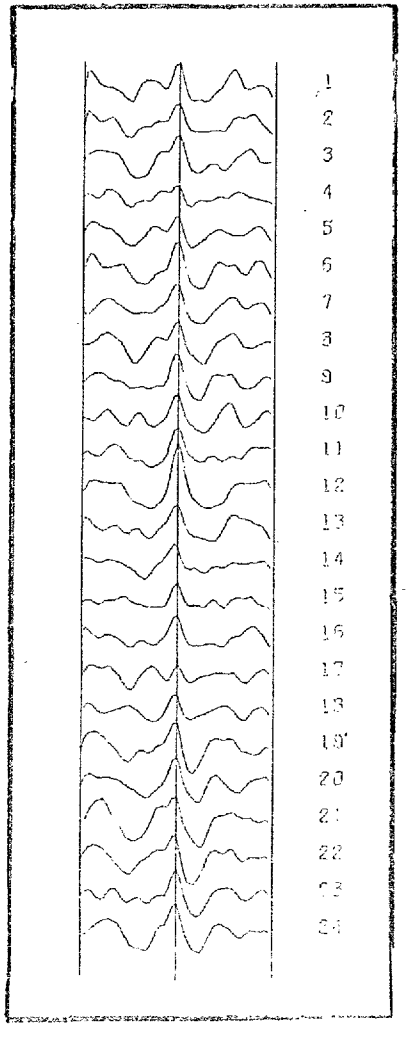


Fig. 3.25 auto-1

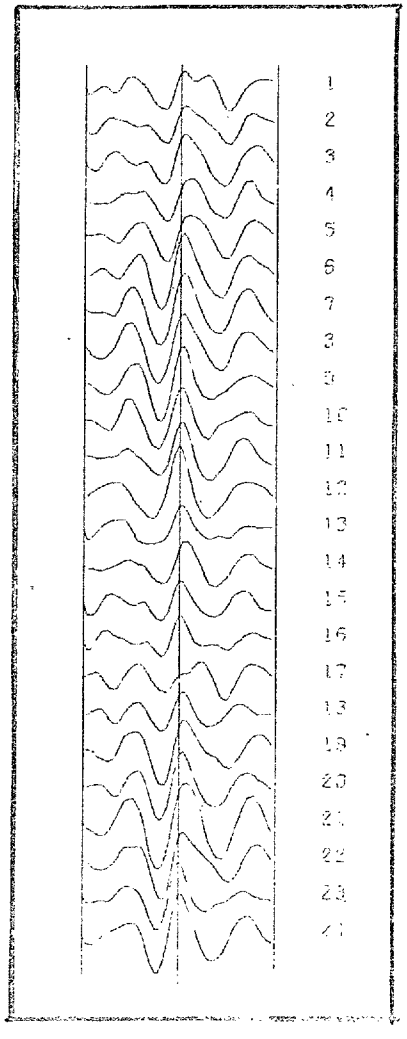


Fig. 3.26 auto-2

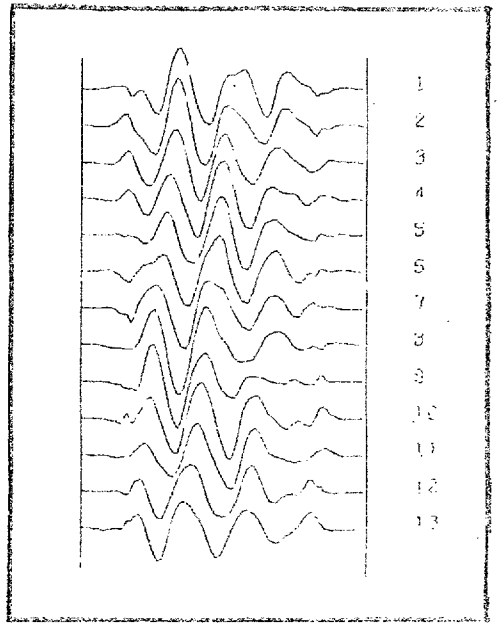


Fig. 3.27 auto-2

filtered by *RP1

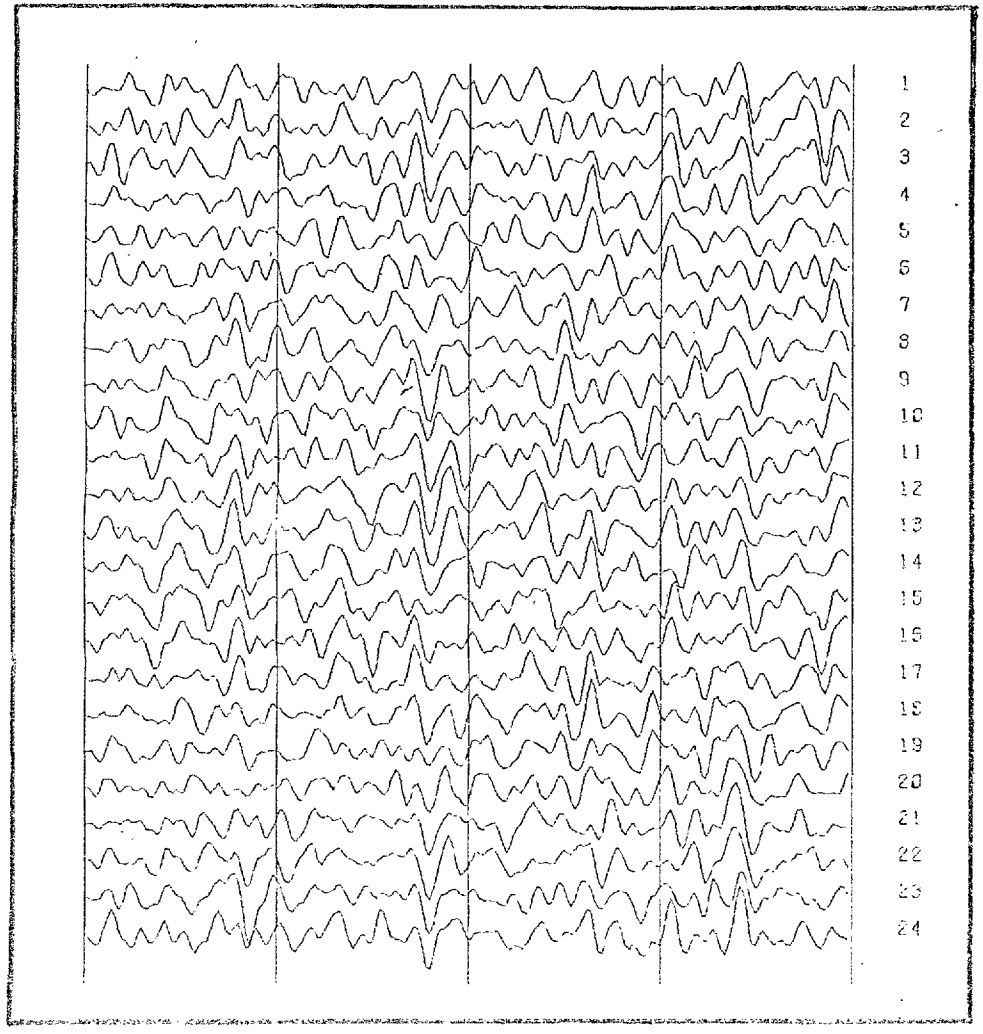


Fig. 3.28 input record, ρ = 3.0, ν = 0.0 db

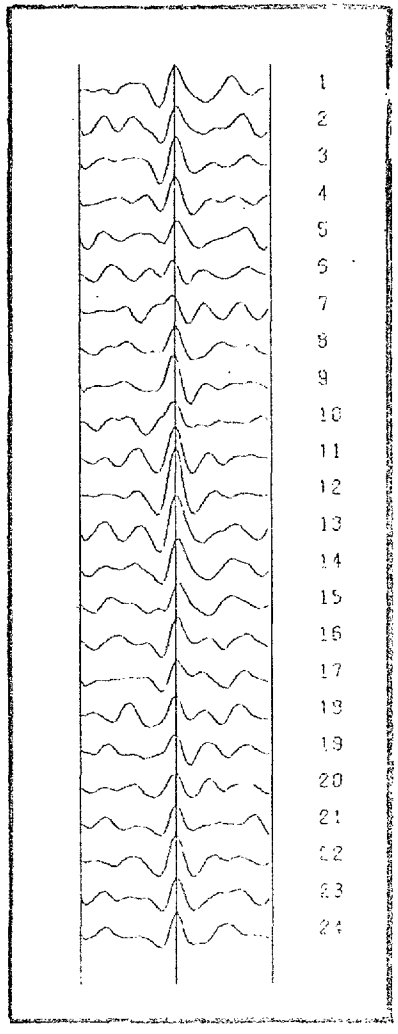


Fig. 3.29 auto-1

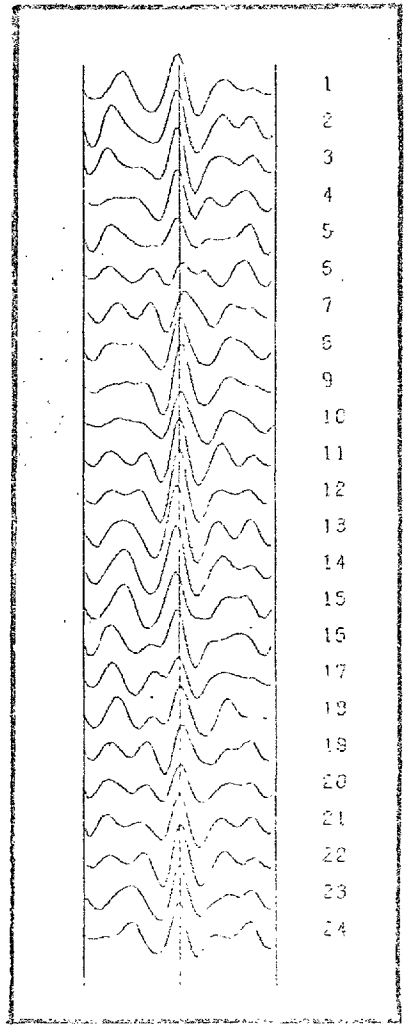


Fig. 3.30 auto-2

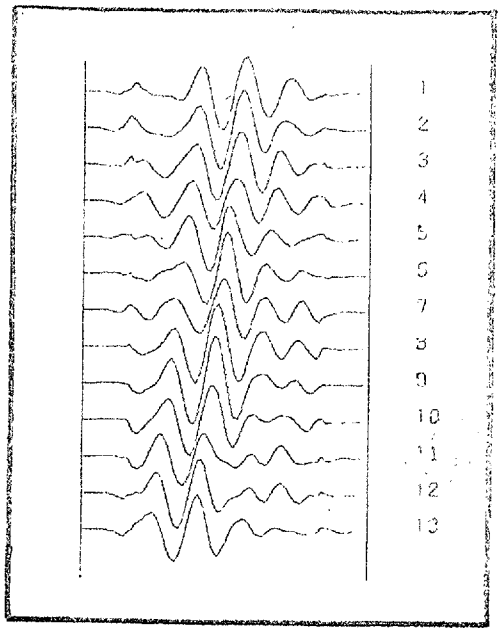


Fig. 3.31 auto-2

filtered by *RP1

3.2.3 effects of different noise levels

Various experiments were performed on records of different signal to noise ratios, but of similar record length and moveout specifications, in order to determine the limitations of the filtered second order autocorrelation matrix technique. These results are summarised in Fig. 3.32, where an asterisk * denotes a particular experiment and an encircled asterisk ⊛ denotes a result presented in this thesis. The dashed lines represent "readability contours" derived from a study of these results. The classification of very good, good, poor or bad refers to the relative recovery of the correlated noise event of moveout 1 sample per trace. Reject/pass filter "R1" was used throughout on all second order columns.

It is, of course, somewhat subjective as to which particular classification a given result should be assigned. Variations in record length, for example, can affect the quality of the filtered result, and so it may be seen that the exact position of these contours is rather arbitrary. They should be interpreted, therefore, as being a representative average of a number of possible contours that could have arisen from slightly different considerations.

The performance of the correlation method for decreasing levels of correlated noise, in a constant background of random noise, is given by the comparison of Fig. 3.15, Fig. 3.36, Fig. 3.40 and Fig. 3.44. The successive degradation of these results is immediately apparent.

Similarly, the performance of the correlation method for increasing levels of random noise and a constant level of correlated noise, is given by a comparison of Fig. 3.36, Fig. 3.27, Fig. 3.48 and Fig. 3.52. Once again, the successive degradation of these results is immediately apparent.

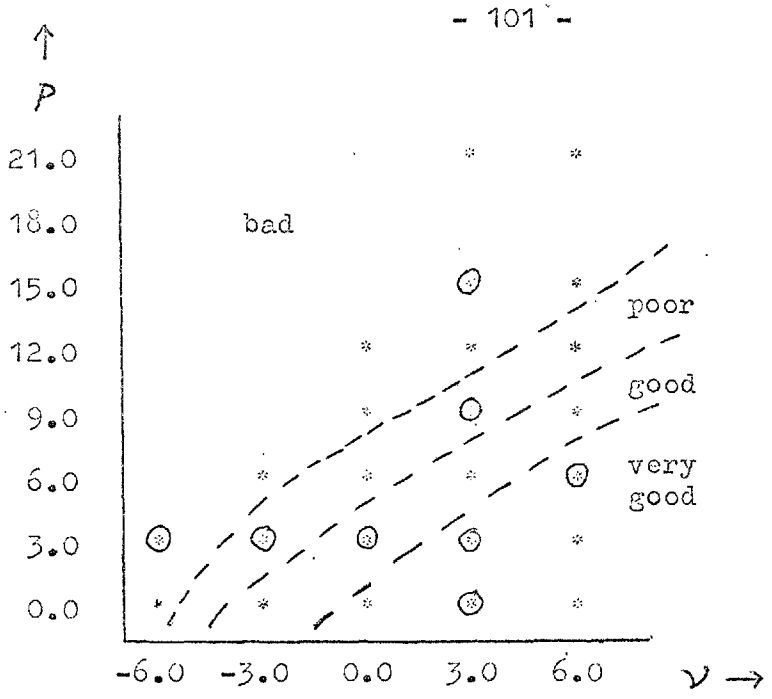


Fig. 3.32 Map of experiments conducted on synthetic data

An encircled asterisk ⊙ denotes a result presented in the thesis, a plain asterisk denotes a result not presented in the thesis.

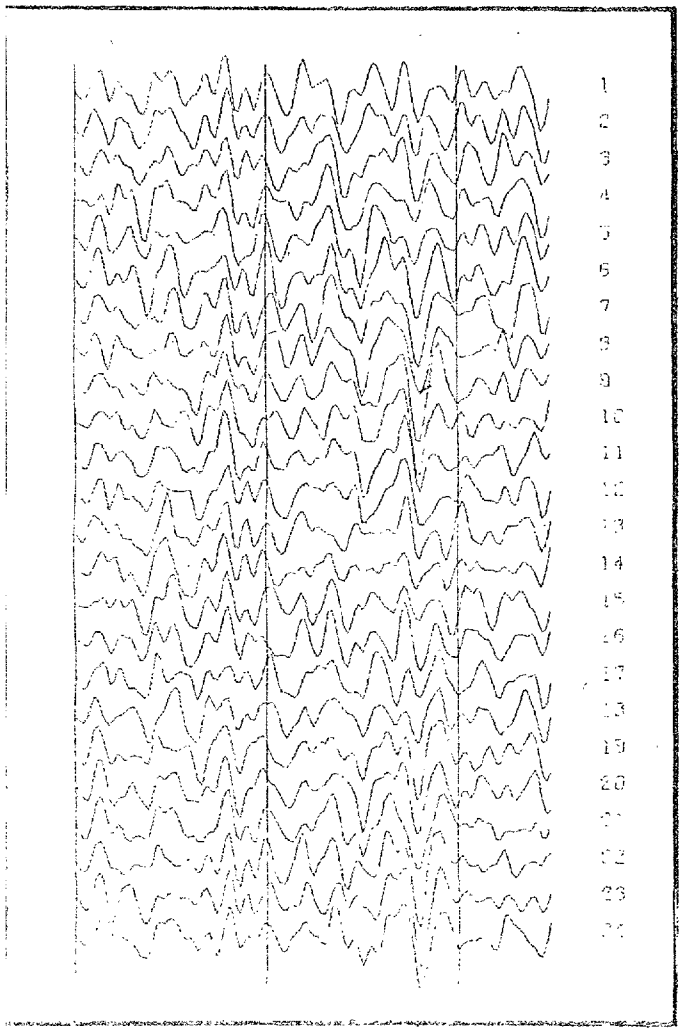


Fig. 3.33 input record,

ρ = 3.0, ν = 3.0 db

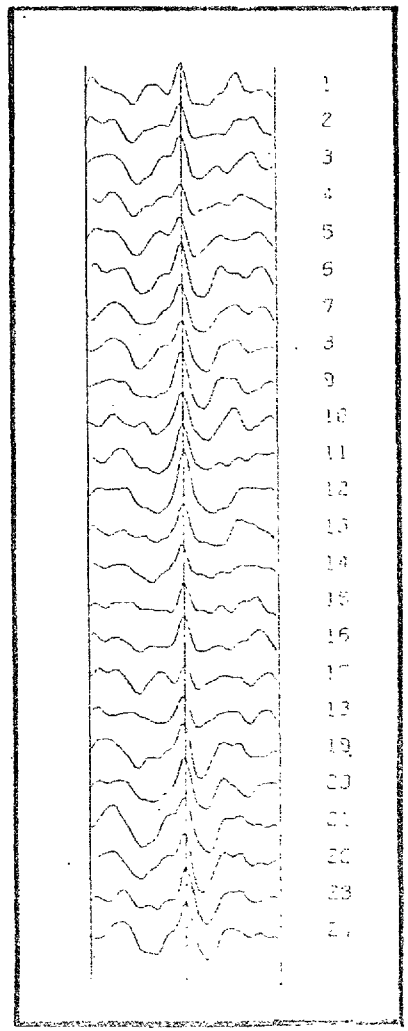


Fig. 3.34 auto-1

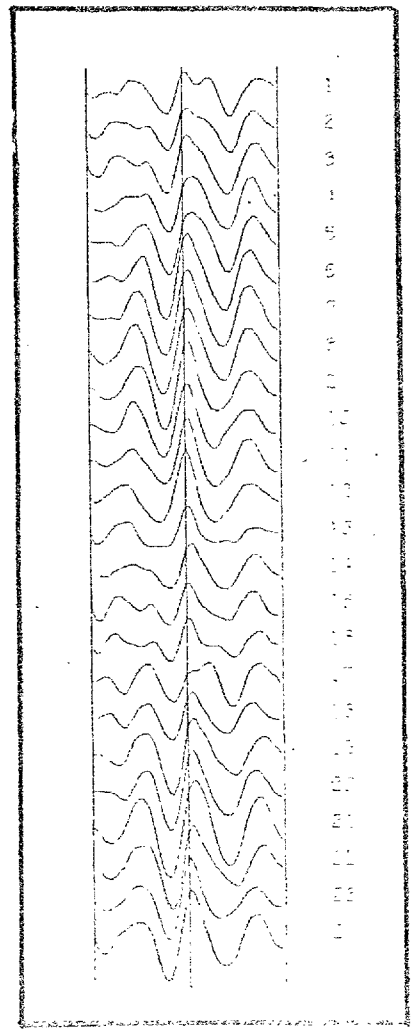


Fig. 3.35 auto-2

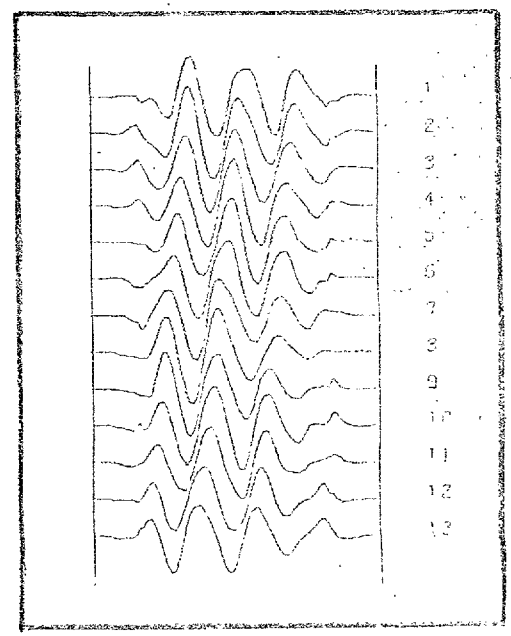


Fig. 3.36 auto-2

filtered by *RP1

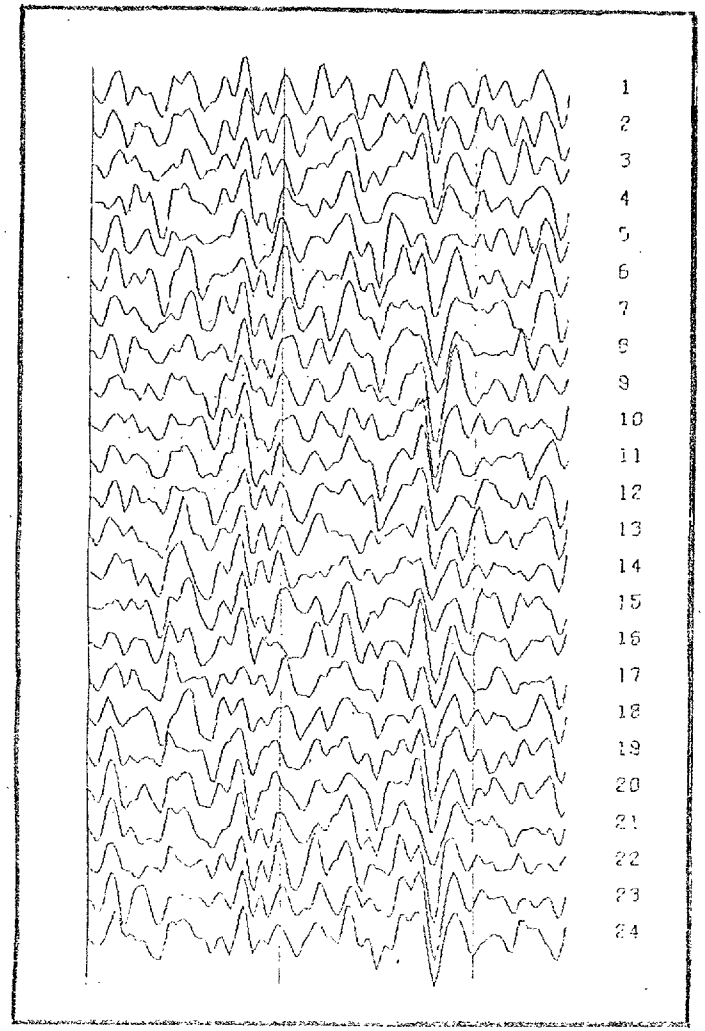


Fig. 3.37 input record,

ρ = 9.0, γ = 3.0 db

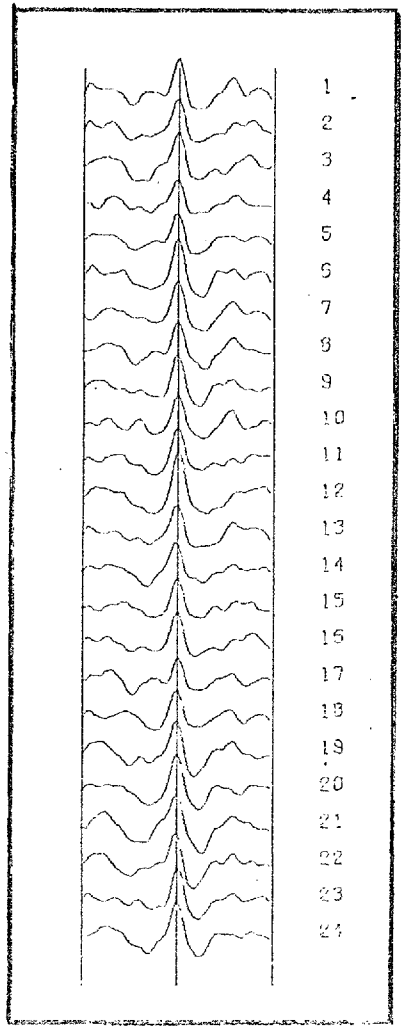


Fig. 3.38 auto-1

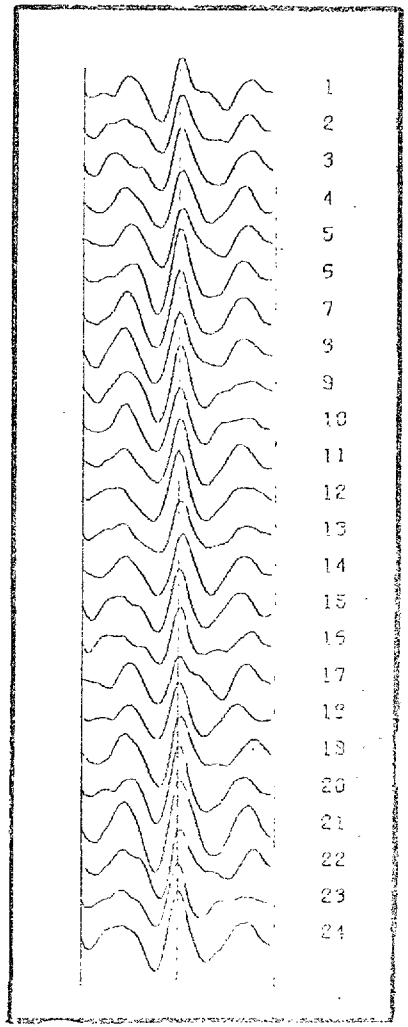


Fig. 3.39 auto-2

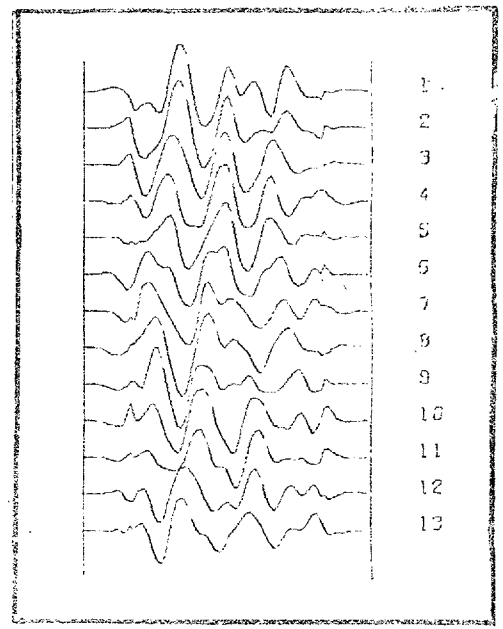


Fig. 3.40 auto-2

filtered by *RP1

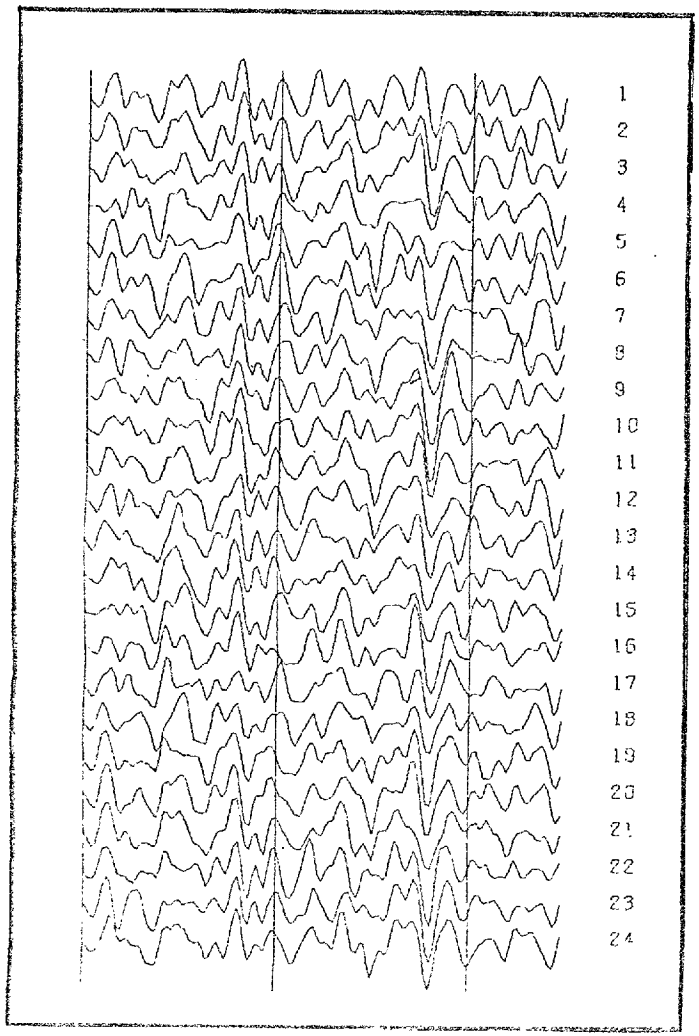


Fig. 3.41 input record,

ρ = 15.0, ν = 3.0 db

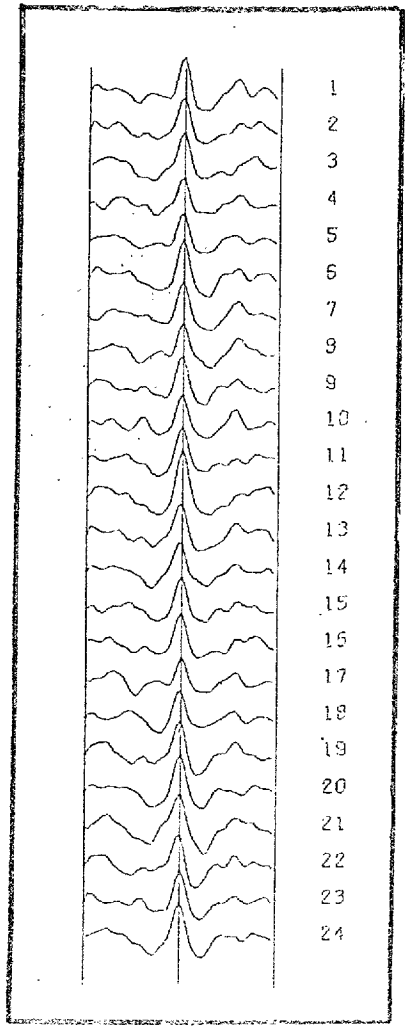


Fig. 3.42 auto-1

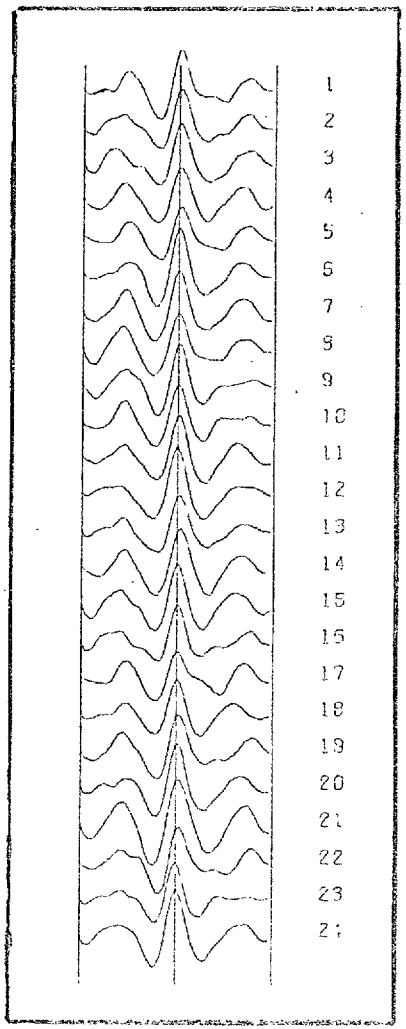


Fig. 3.43 auto-2

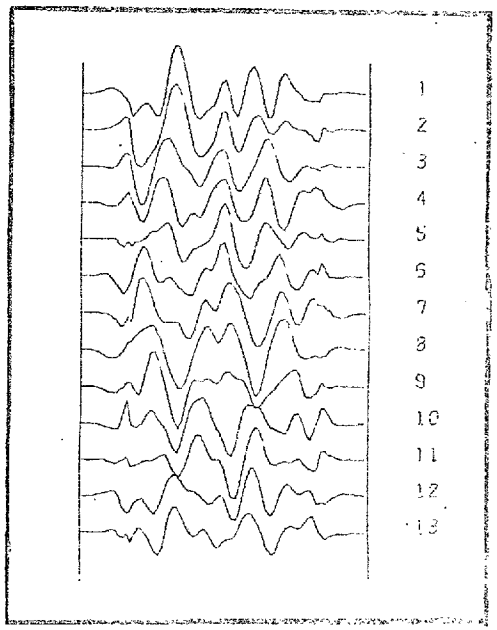


Fig. 3.44 auto-2

filtered by *RP1

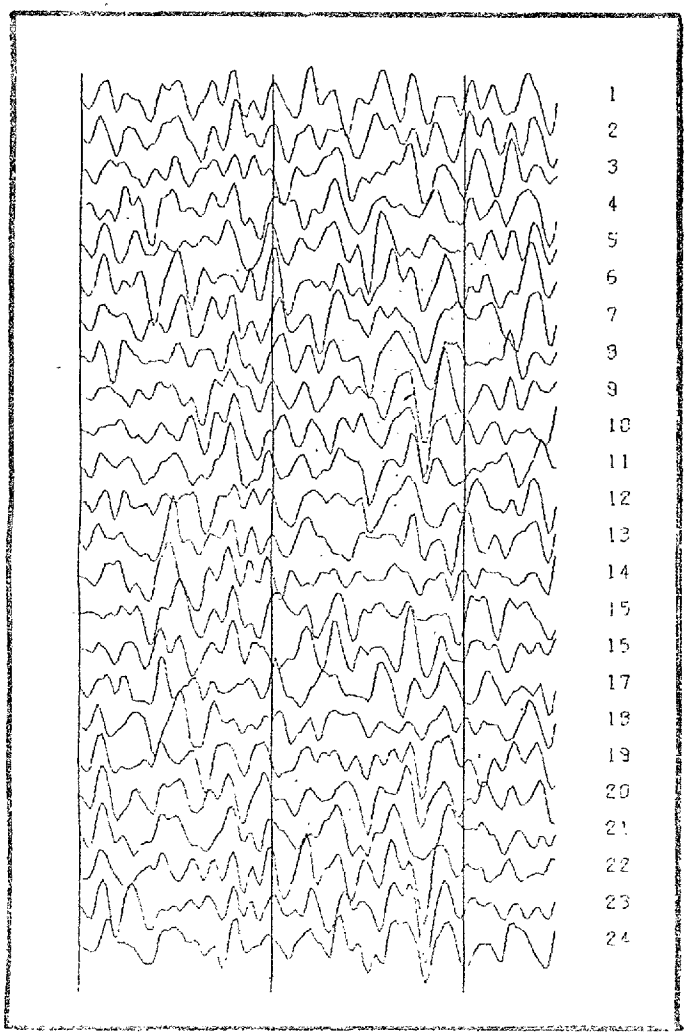


Fig. 3.45 input record,

ρ = 3.0, ν = -3.0 db

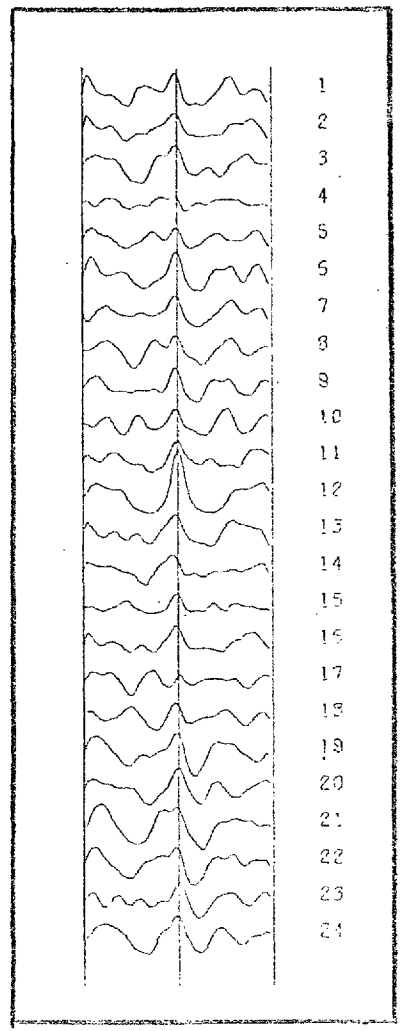


Fig. 3.46 auto-1

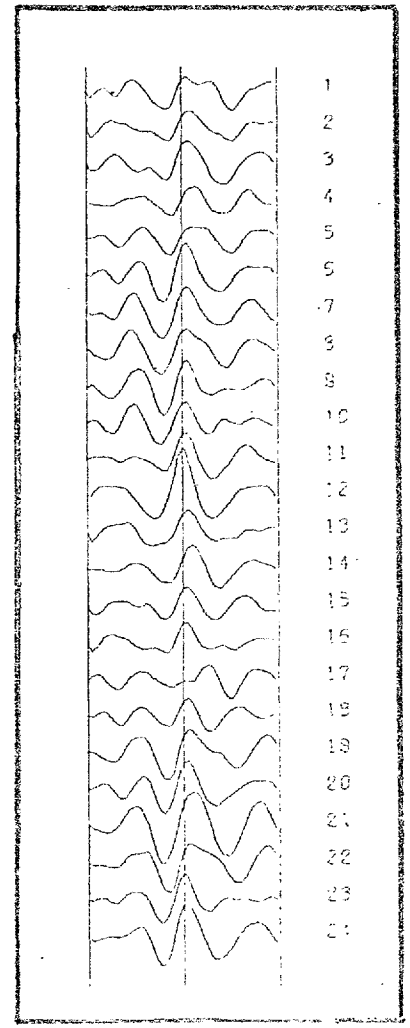


Fig. 3.47 auto-2

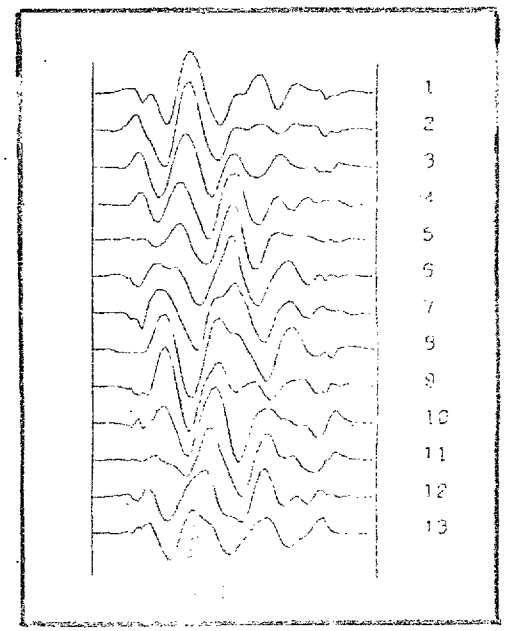


Fig. 3.48 auto-2

filtered by *RP1

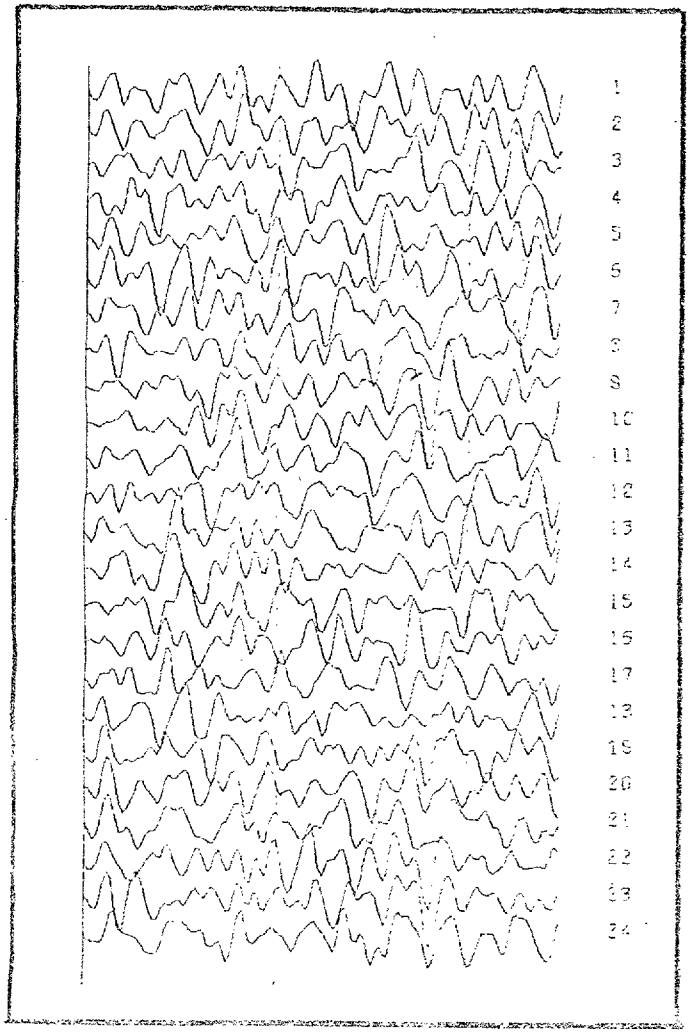


Fig. 3.49 input record,

ρ = 3.0, ν = -6.0 db

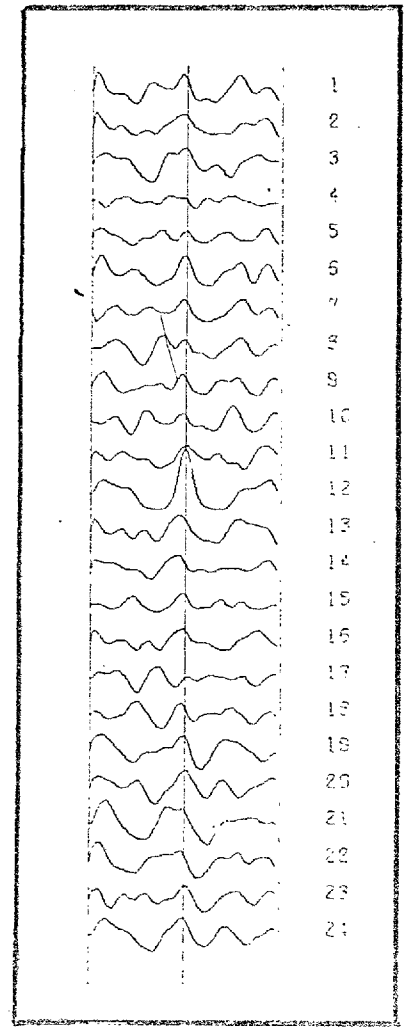


Fig. 3.50 auto-1

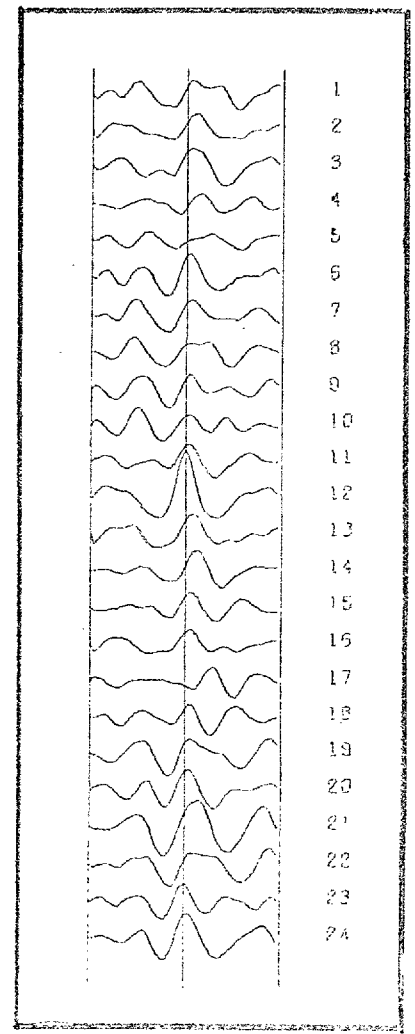


Fig. 3.51 auto-2

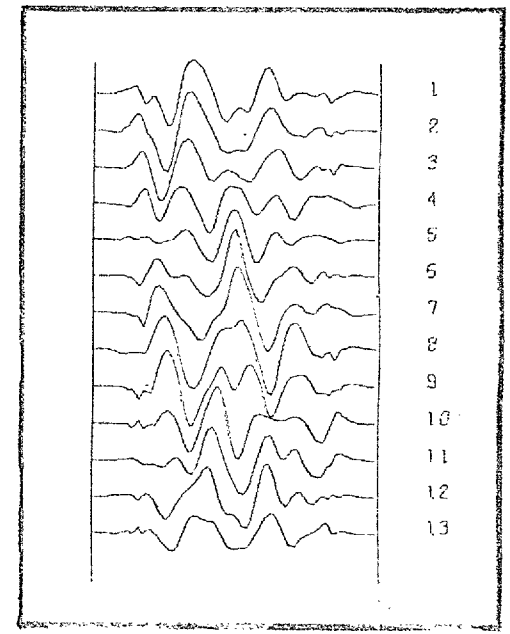


Fig. 3.52 auto-2

filtered by *RP1

3.2.3.1 analysis of synthetic records of quadratic moveout

Three records of quadratic correlated noise moveout, Fig. 3.53, Fig. 3.57 and Fig. 3.61, were subjected to a correlation analysis with pass/reject filter Q being used to filter the second order column. Note that column 1 was used in these analyses, and that the intention is now to recover the signal, of zero moveout, and to reject the correlated noise of quadratic moveout.

The first of these filtered results, Fig. 3.56, has not succeeded in revealing the presence of the signal. The next result, Fig. 3.60, is a little better though somewhat ambiguous. The last result, Fig. 3.64, is very good, clearly showing the presence of signal over the whole record.

Direct comparison of these results with those of section 3.2.3 is not possible due to the differences in experimental design. Rejection of correlated noise in the quadratic case was not as good as the rejection of signal in the linear case. This is probably due to the difference in the relative weights assigned to the pass and reject regions of filters Q and *RP1 (Ref. Table 2.1 and Table 2.2). None the less it may be said that, within this context, these quadratic results are in reasonable accord to what one would expect from a study of the linear results and the quadratic filtering results of Chapter 2.

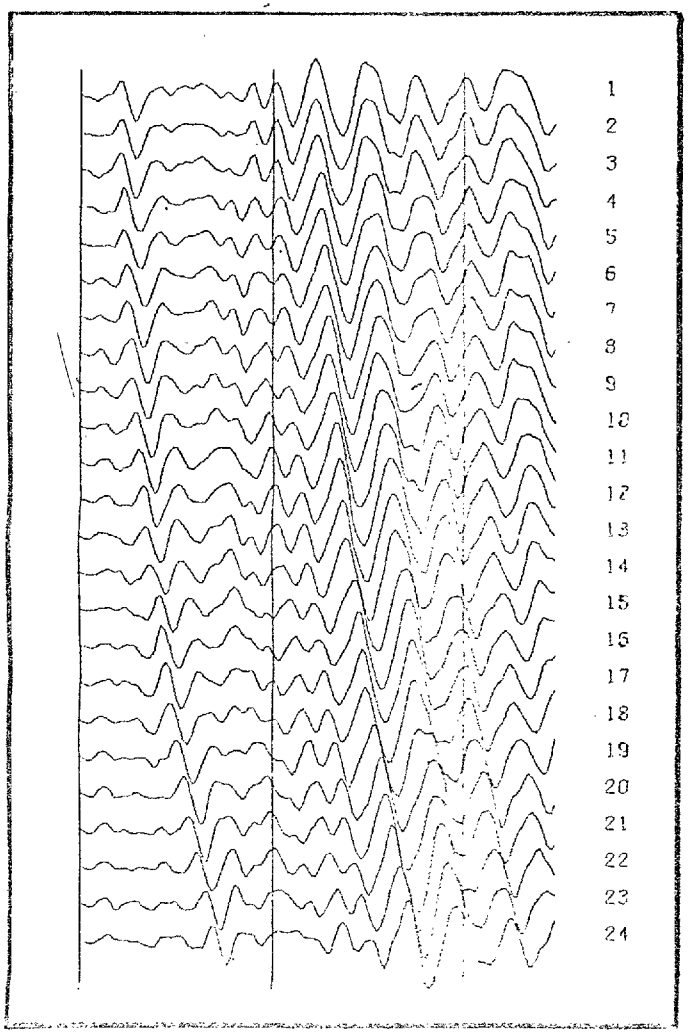


Fig. 3.53 input record,

ρ = -15.0, ν = 6.0 db

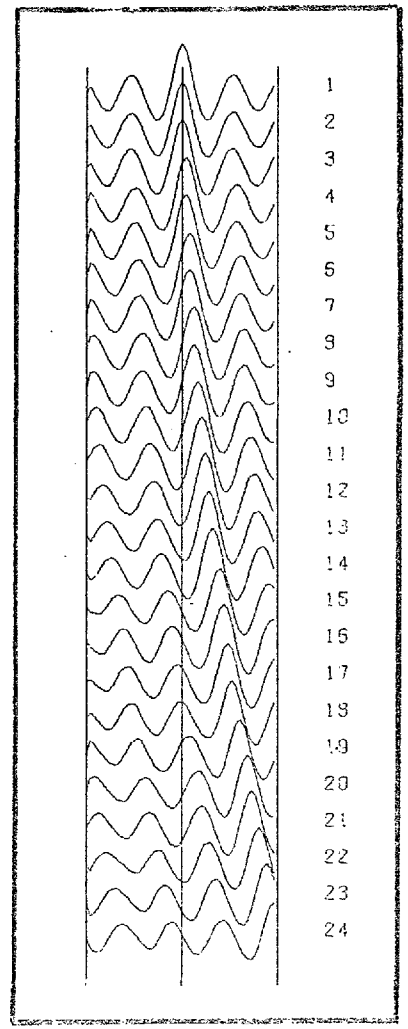


Fig. 3.54 auto-1

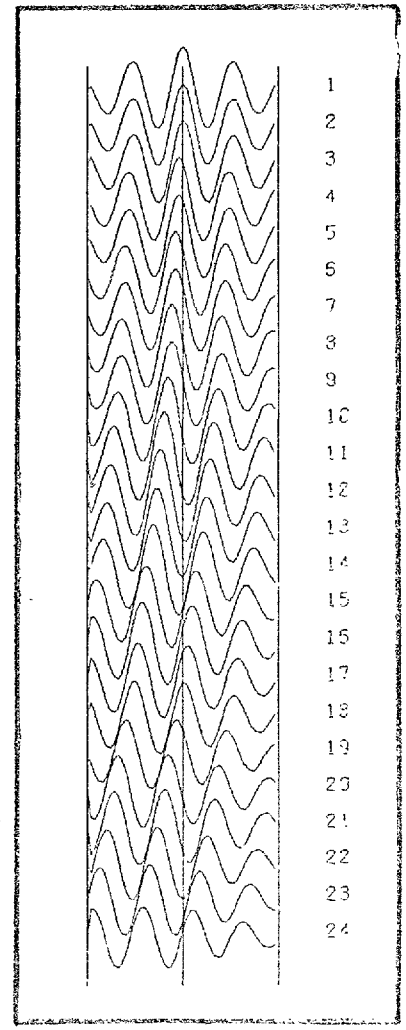


Fig. 3.55 auto-2

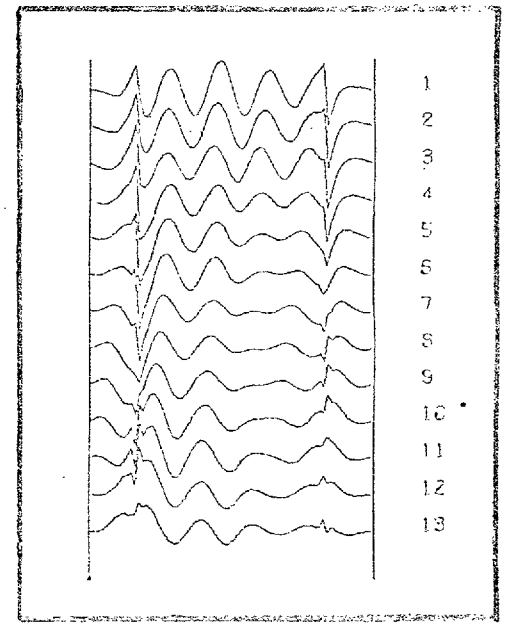


Fig. 3.56 auto-2

filtered by Q

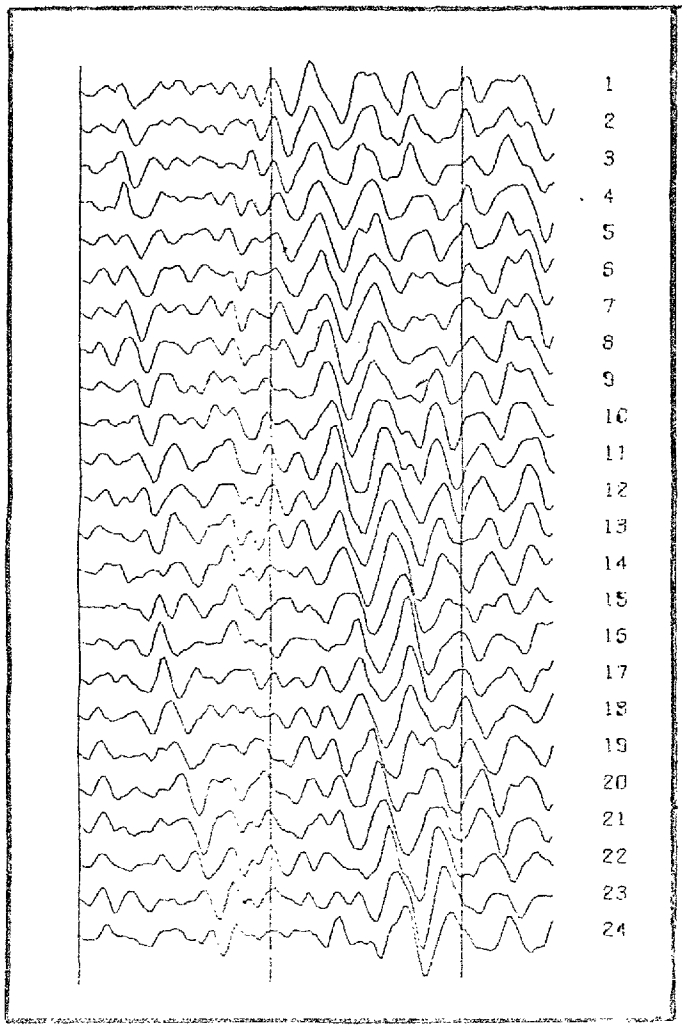


Fig. 3.57 input record,

ρ = -9.0, ν = 0.0 db

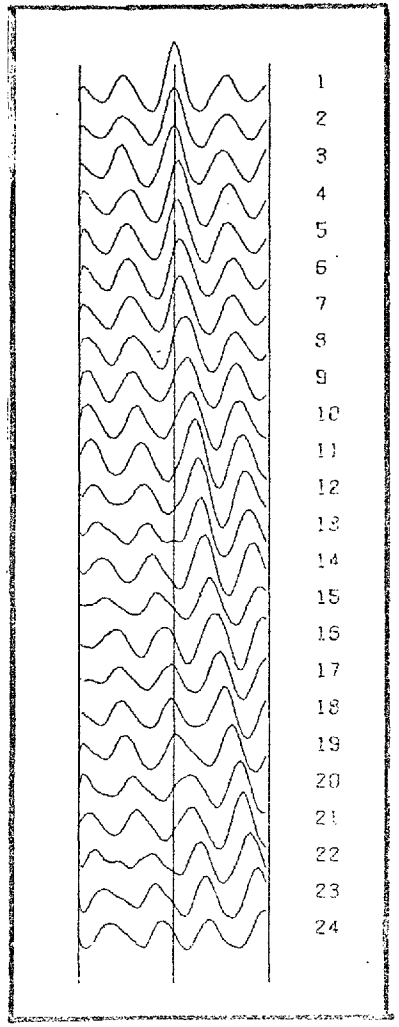


Fig. 3.58 auto-1

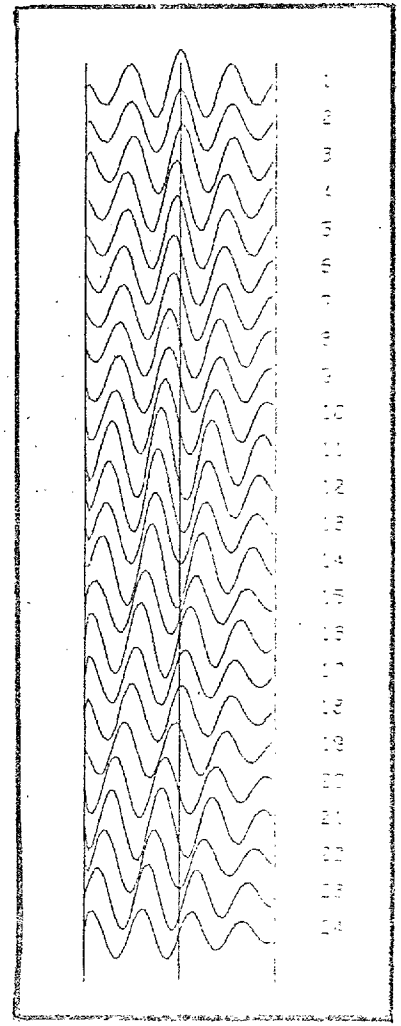


Fig. 3.59 auto-2

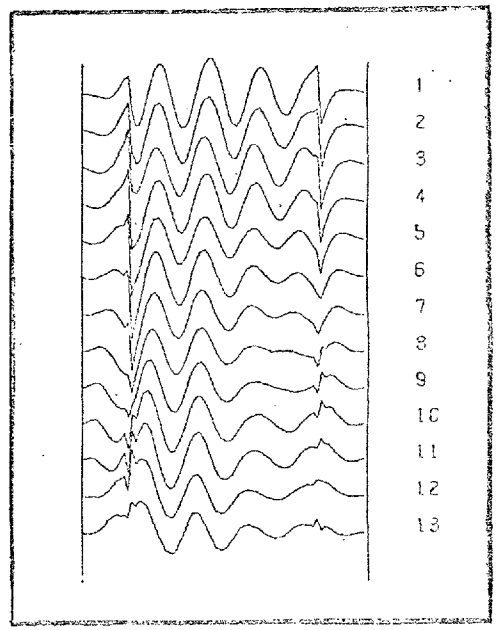


Fig. 3.60 auto-2

filtered by Q

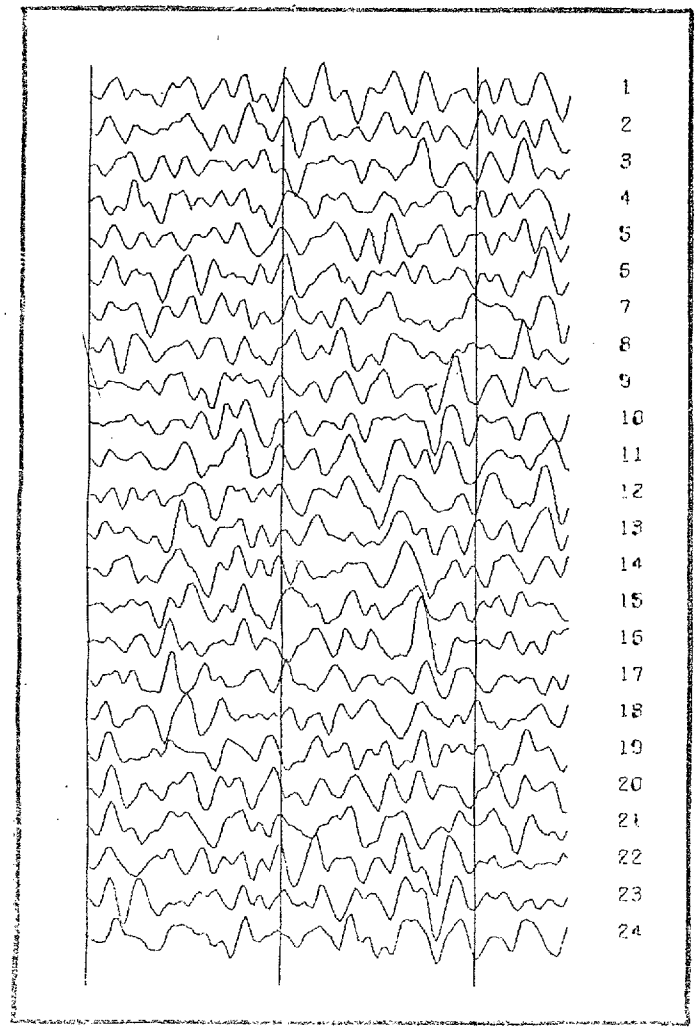


Fig. 3.61 input record,

ρ = 0.0, ν = -6.0 db

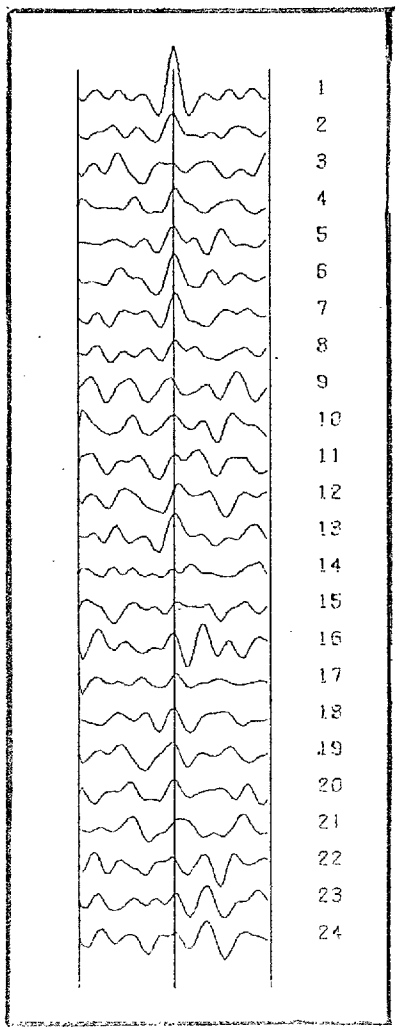


Fig. 3.62 auto-1

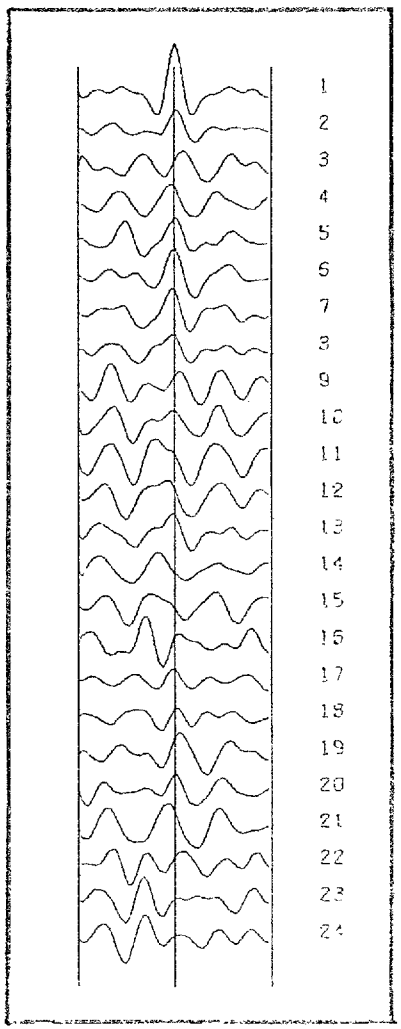


Fig. 3.63 auto-2

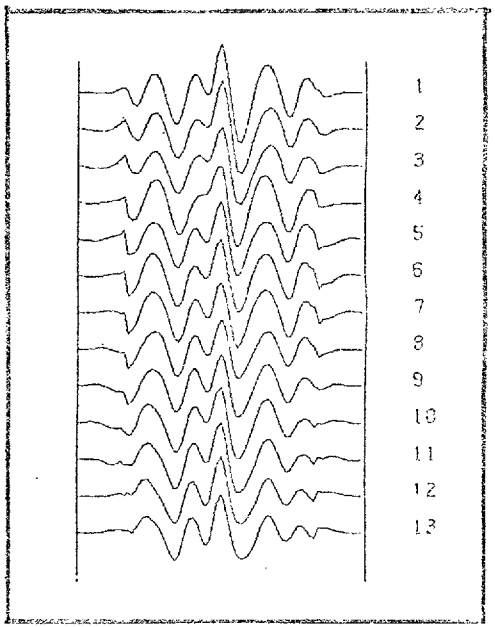


Fig. 3.64 auto-2

filtered by Q

3.2.4 pre-filtering experiments with correlation analyses

Fig. No. of input record	Fig. No. of auto-1	Fig. No. of auto-2	column number	Fig. No. of filtered auto-2	filter name
3.65	3.66	3.67	7		
2.27 *	3.68	3.69	1		
3.70	3.71	3.72	12	3.73	*RP5

Table 3.3 Index of further correlation analyses on synthetic data

N.B. a 125 sample trace version of Fig. 2.27 was used for this section.

Fig. 3.65 shows the result of applying reject/pass filter *RP1 to the input record of Fig. 3.4 (ρ = 6.0, ν = 6.0 db). Column 7 of the first and second order autocorrelation matrices, computed from Fig. 3.65, are presented as Fig. 3.66 and Fig. 3.67, respectively. Comparison of Fig. 3.67 with Fig. 3.8 shows that the filtering of the input record before the correlation analysis has produced a somewhat better result than the filtering of the second order column after the correlation analysis. This difference may be attributed to the fact that a correlation process will generally magnify the relative importance of any correlated event, be it signal or correlated noise. Hence the filtering in Fig. 3.8 has to contend with amplified signal and amplified correlated noise, whereas the correlation result of Fig. 3.67 has only to contend with the correlated noise itself, the presence of signal having been removed by the pre-filter.

Fig. 3.68 and Fig. 3.69 show column 1 of the first and second order autocorrelation matrices computed from the quadratic filtered record of Fig. 2.27 (a 125 sample version, thereof), (ρ = -15.0, ν = 6.0 db). Comparison of Fig. 3.69 with Fig. 3.56 clearly shows the

advantage of a pre-filter.

One would conclude from these results, therefore, that in order to make best use of the autocorrelation matrix method one should first remove any obvious moveouts from the data before commencing the analysis, since the filter may not be able to remove these obvious moveouts after analysis.

A further possibility exists, of course, in that a multichannel filter scan could be applied to the second order column computed from a pre-filtered input record. The result of such a study is presented as Fig. 3.70 - Fig. 3.73. Fig. 3.70 shows the input record of Fig. 3.41 (P = 15.0, ν = 3.0 db), after filtering by reject/pass filter *RP5. Column 12 of the first and second order autocorrelation matrices are given as Fig. 3.71 and Fig. 3.72, respectively, with Fig. 3.73 showing the result of applying reject/pass filter *RP5 to Fig. 3.72. This last result shows some evidence of the required correlated noise event (compare with Fig. 3.44), but is certainly not too good.

A better result could no doubt have been obtained if filter *RP1 had been used rather than filter *RP5. However, the reduction in the number of output traces caused by using filter *RP1 would have left a final result of only two traces. Further work on this topic, therefore, must await the development of a multichannel filter that will give the same number of output traces as there are input traces. None the less, some encouragement may be taken from Fig. 3.73 in that some indication of the required event was found, whereas no such indication could be found elsewhere.

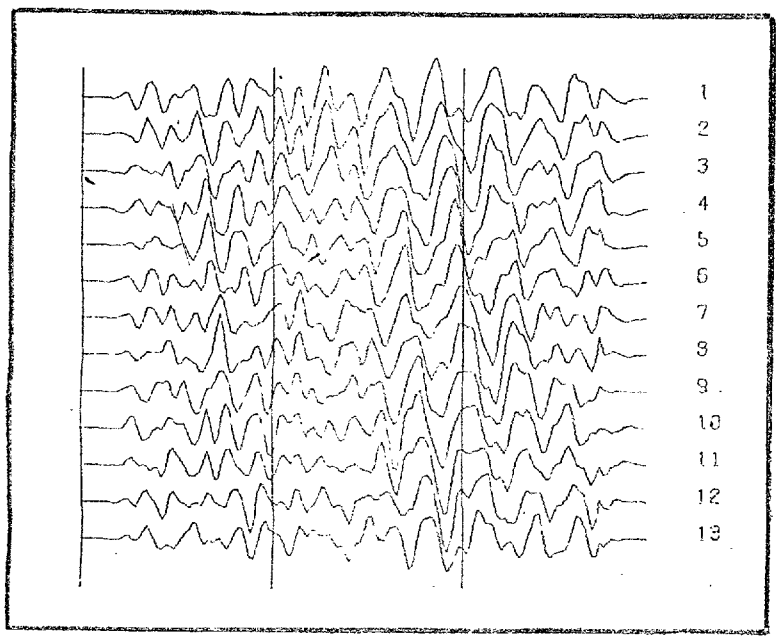


Fig. 3.65 result of filtering Fig. 3.4 with *RP1

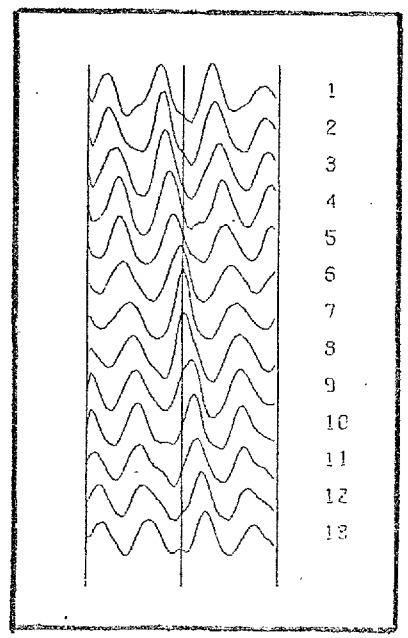


Fig. 3.66 auto-1 col.7

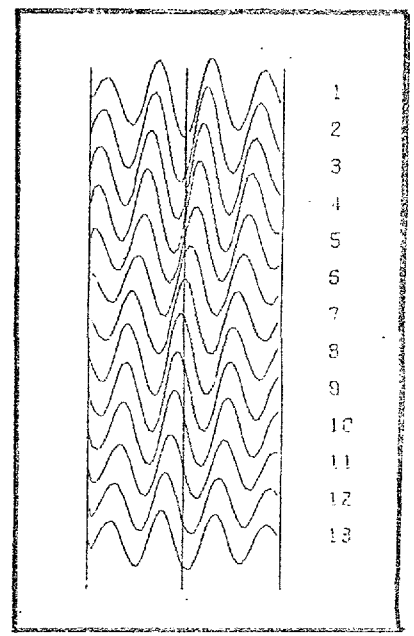


Fig. 3.67 auto-2 col.7

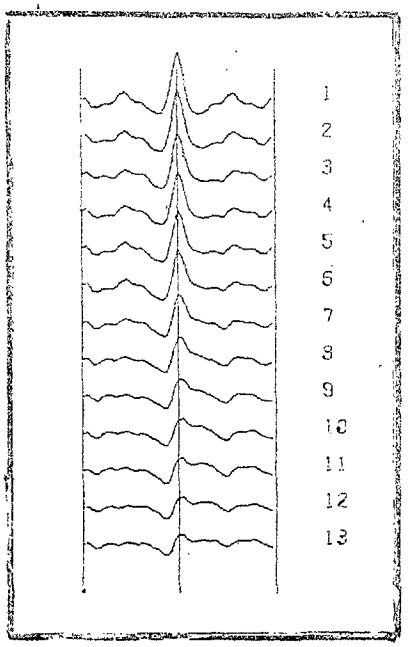


Fig. 3.68

auto-1, col.1

(from Fig. 2.27,

see text)

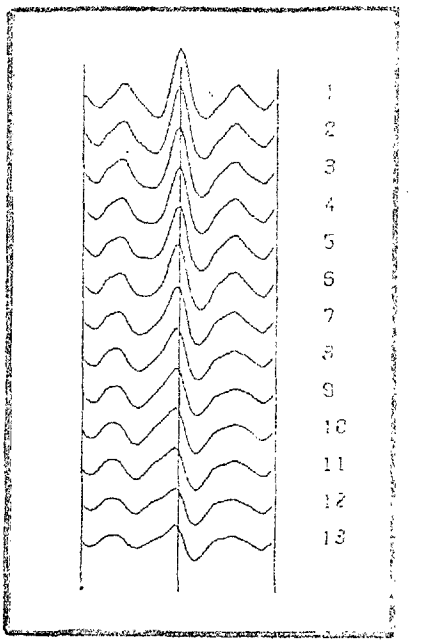


Fig. 3.69

auto-2, col.1

(from Fig. 2.27,

see text)

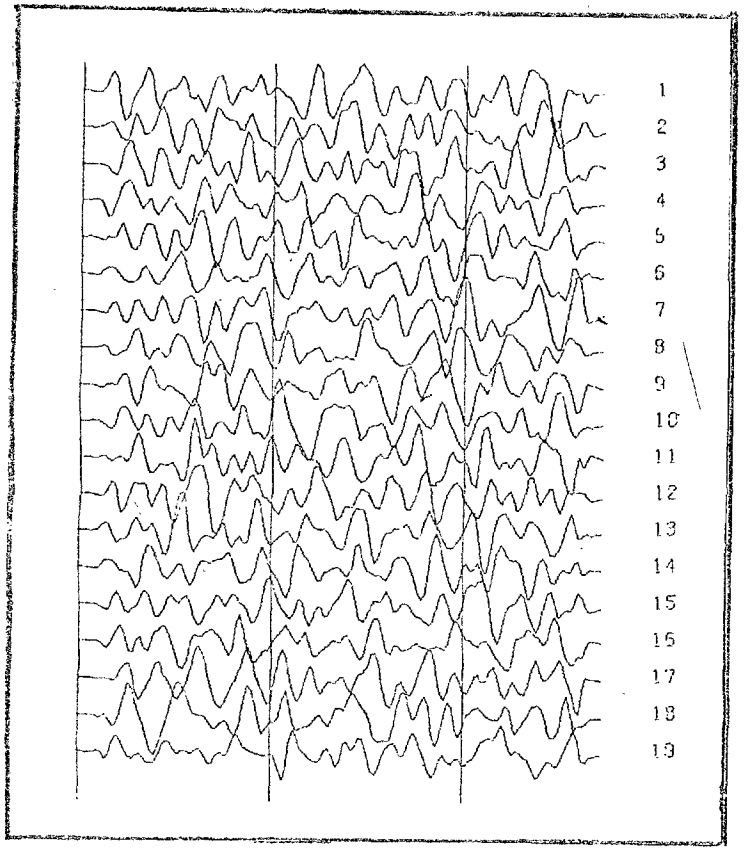


Fig. 3.70 result of filtering Fig. 3.41 with *RP5

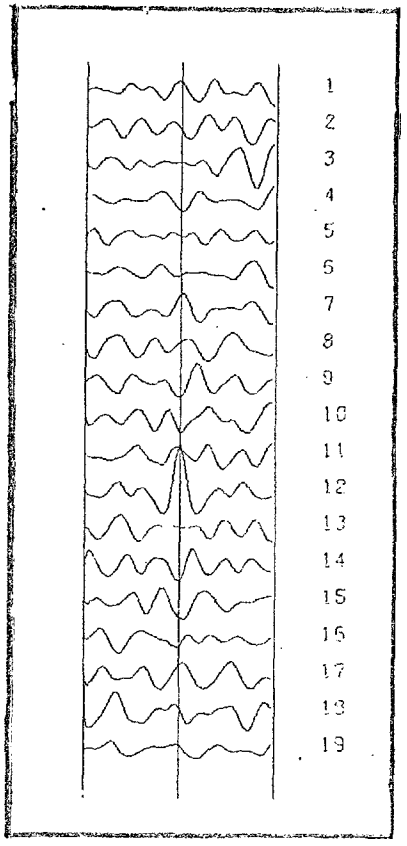


Fig. 3.71 auto-1

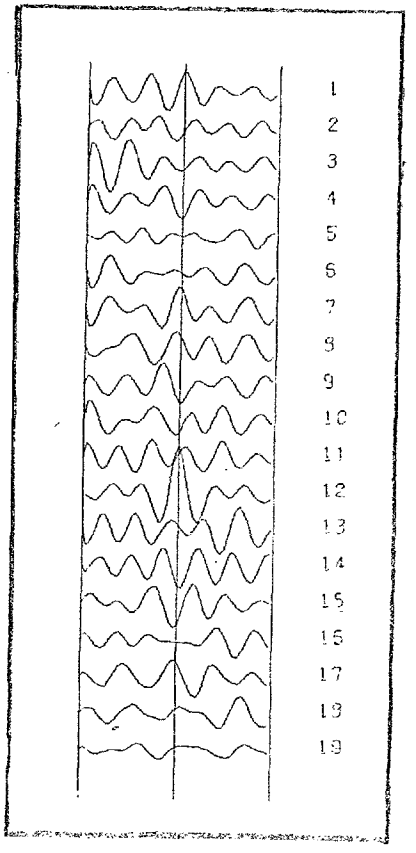


Fig. 3.72 auto-2

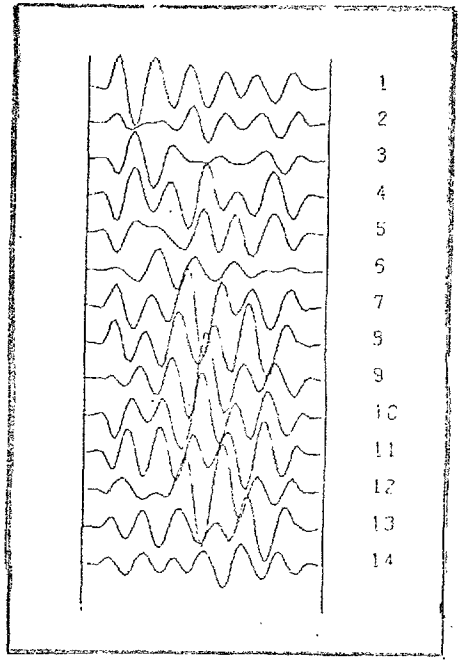


Fig. 3.73 auto-2 filtered by *RP5

3.3 Applications to real data

Various experiments were performed on the real data of Chapter 1, and on the filtered results of Chapter 2, as are specified in Table 3.4. One extra filtered result, namely that of applying a pass/reject filter, *PR10, to the band pass filtered version of shotpoint 3006 (Fig. 1.9) is presented as Fig. 3.74. Due to the considerations of record length and the presence of high moveout events in the data, a maximum correlation lag of 50 samples was taken throughout this section. As for the synthetic case, timing lines were drawn across the autocorrelation columns at maximum, minimum and zero lag.

It is the purpose of this section to assess to what extent the findings from the analyses of synthetic data are applicable to the real case, bearing in mind the earlier discussion on comparisons between the results of real and synthetic data. In general, the real data records were rather better than the earlier synthetic data records, in that some signal could be seen on some of these real records. The correlation analyses should, therefore, further improve the appearance of such signal.

A correlation analysis, together with a multichannel filter scan of the second order column, was conducted on the band pass filtered version of shotpoint 3002 (Fig. 1.7). Fig. 3.75 and Fig. 3.76 show column 12 of the first and second order autocorrelation matrices respectively, with Fig. 3.77 (*PR1), Fig. 3.78 (*PR2) and Fig. 3.79 (*PR8) presenting the filtered second order column for the respective filters. Fig. 3.78 clearly shows the presence of a zero moveout signal better than that of the second order column (Fig. 3.76, though this result does show some evidence of such signal). Comparison of the three filtered results, together with Fig. 1.7, once again show the importance of "moveout matching" between filter and data, not only with respect to the moveout that is to be passed, but also to that

which is to be rejected.

An example of a pre-filtering experiment is given by Fig. 3.80 - Fig. 3.83. Fig. 3.80 and Fig. 3.81 are column 8 of the first and second order autocorrelation matrices of shotpoint 3002 (Fig. 1.2), whereas Fig. 3.82 and Fig. 3.83 are those of the pre-filtered version of the record (Fig. 2.42, filter *PR10). Comparison of these results immediately show the benefit of a prefilter for correlation analysis.

An example of comparing the results of filtering before or after correlation analysis is provided by Fig. 3.84 - Fig. 3.88. Fig. 3.84 and Fig. 3.85 are column 12 of the first and second order autocorrelation matrices for the band pass filtered version of shotpoint 3006 (Fig. 1.9). The result of filtering Fig. 3.85 by pass/reject filter *PR2 is given in Fig. 3.86. Fig. 3.87 and Fig. 3.88 are column 8 of the first and second order autocorrelation matrices for the pre-filtered version of Fig. 1.9 (namely Fig. 3.74). Comparison of Fig. 3.86 with Fig. 3.88 reveals very little difference. This is probably due to the lack of appreciable correlated noise in the original record.

Another example of filtering before or after correlation analysis is given by Fig. 3.89 to Fig. 3.95. Fig. 3.89 and Fig. 3.90 show column 8 of the first and second order autocorrelation matrices for shotpoint 3003 (Fig. 1.3), whereas as Fig. 3.91 and Fig. 3.92 show that for the pre-filtered version of the record (Fig. 2.47, filter *PR10). The result of applying filter *PR10 to Fig. 3.94 is presented as Fig. 3.95. Comparison of Fig. 3.92 with Fig. 3.95 shows that the former picture is somewhat better than the latter picture. This result is consistent with the earlier discussion on the removal of correlated noise by a filter before correlation analysis being somewhat easier than the removal of the noise after correlation analysis.

The last results of this chapter show column 12 of the first and second order autocorrelation matrices for the band pass filtered version of shotpoint 3005 (Fig. 1.8), presented as Fig. 3.96 and Fig.

3.97, respectively. The result of applying pass/reject filter PR10 to the second order column (Fig. 3.97) is given as Fig. 3.98. Comparison of these results show that the presence of signal is revealed in Fig. 3.98, whereas no such evidence was forthcoming from Fig. 3.96 or Fig. 3.97. It is of interest to compare Fig. 3.98 with both Fig. 1.8 and with the version of this record filtered by pass/reject filter PR10 (Fig. 2.39). The evidence of signal is more prominent in Fig. 3.98 than it is in Fig. 1.8, though clearly it is not as strong as it is in Fig. 2.39. This is again an illustration of the difficulty in rejecting "amplified" correlated noise.

This section has shown that the results of correlation analyses on real data are consistent with those of synthetic data. The general features of the multichannel filter scan on the second order column, and the benefit of pre-filtering the data before commencing analysis, were both well illustrated.

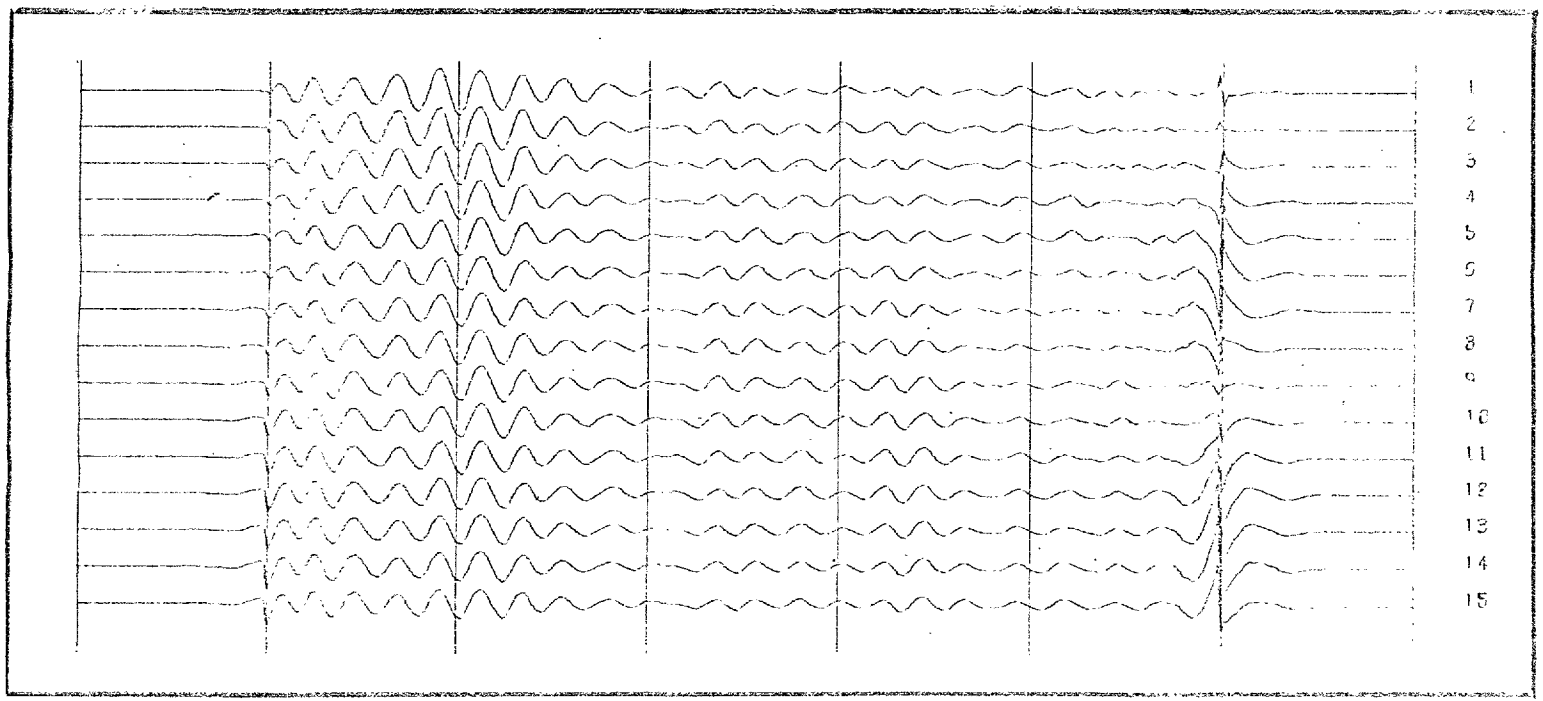
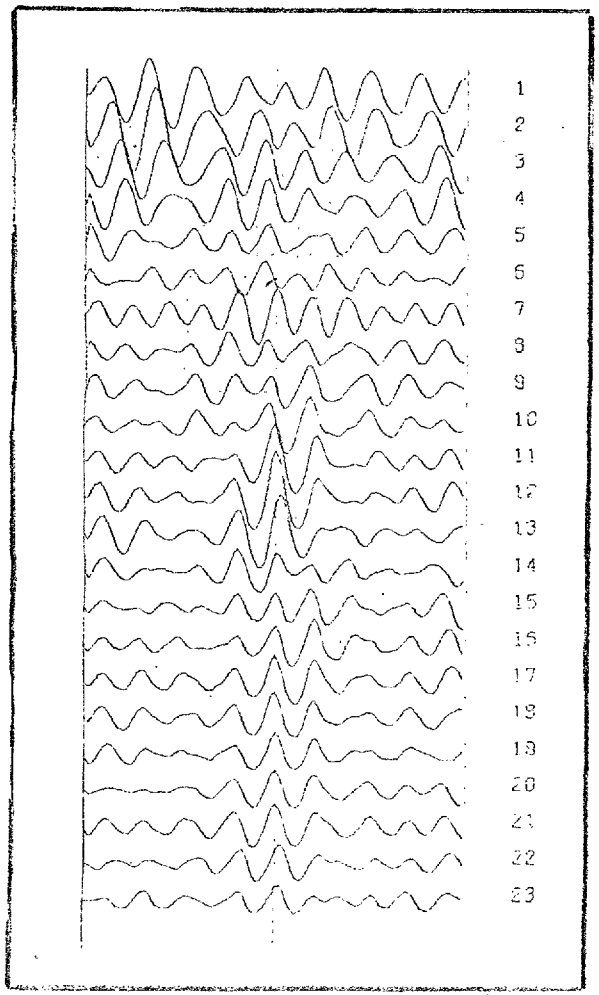


Fig. 3.74 result of filtering Fig. 1.9 with *PR10

shot-point number	Fig. No. of input record	Fig. No. of auto-1	Fig. No. of auto-2	column number	Fig. No. of filtered auto-2	filter name
3002	1.7	3.75	3.76	12	3.77	*PR1
3002	1.7	3.75	3.76	12	3.78	*PR2
3002	1.7	3.75	3.76	12	3.79	*PR8
3002	1.2	3.80	3.81	8		
3002	2.42	3.82	3.83	8		
3006	1.9	3.84	3.85	12	3.86	*PR2
3006	3.74	3.87	3.88	8		
3003	1.3	3.89	3.90	8		
3003	2.47	3.91	3.92	8		
3003	1.3	3.93	3.94	12	3.95	*PR10
3005	1.8	3.96	3.97	12	3.98	*PR10

Table 3.4 Index of correlation analyses for real data



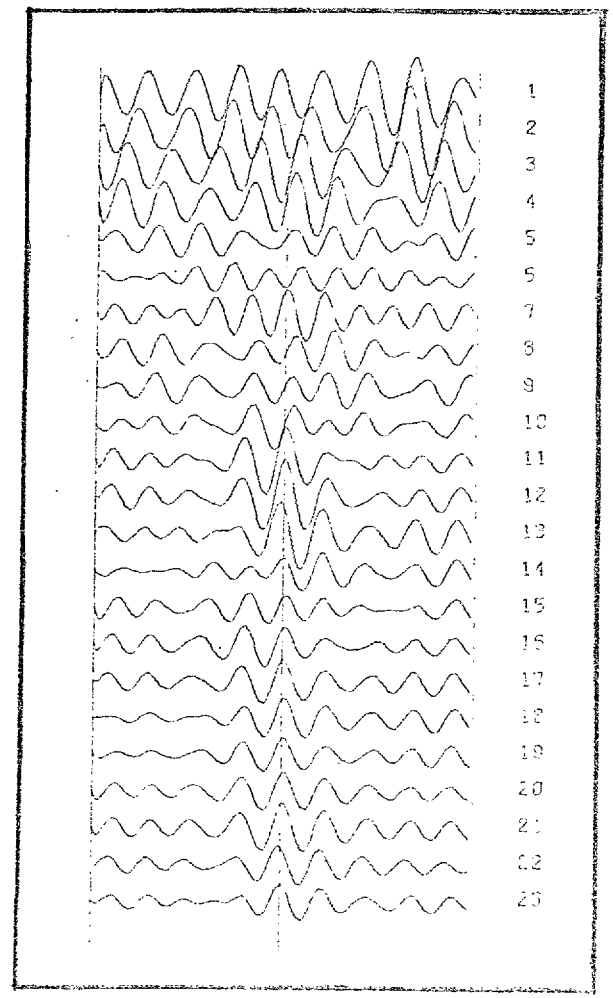


Fig. 3.75 (left) auto-1, col.12,
for Fig. 1.7
(shotpoint 3002)

Fig. 3.76 (right) auto-2, col.12,
for Fig. 1.7
(shotpoint 3002)

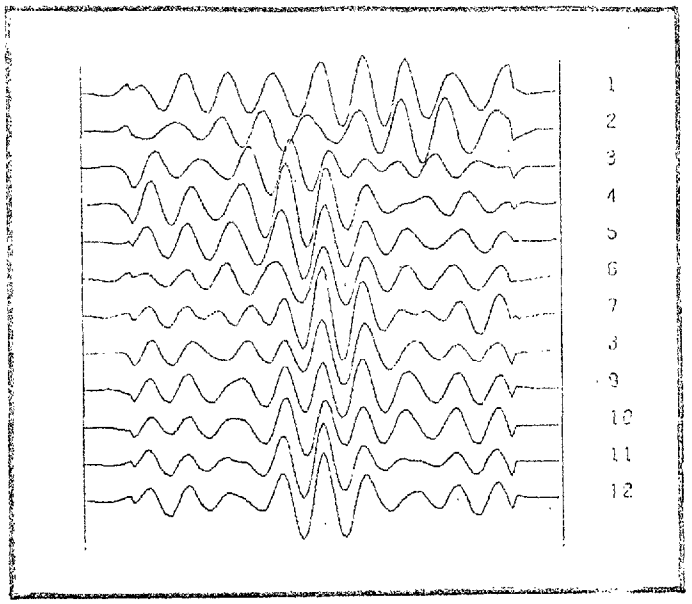


Fig. 3.77
auto-2 filtered
by *PR1

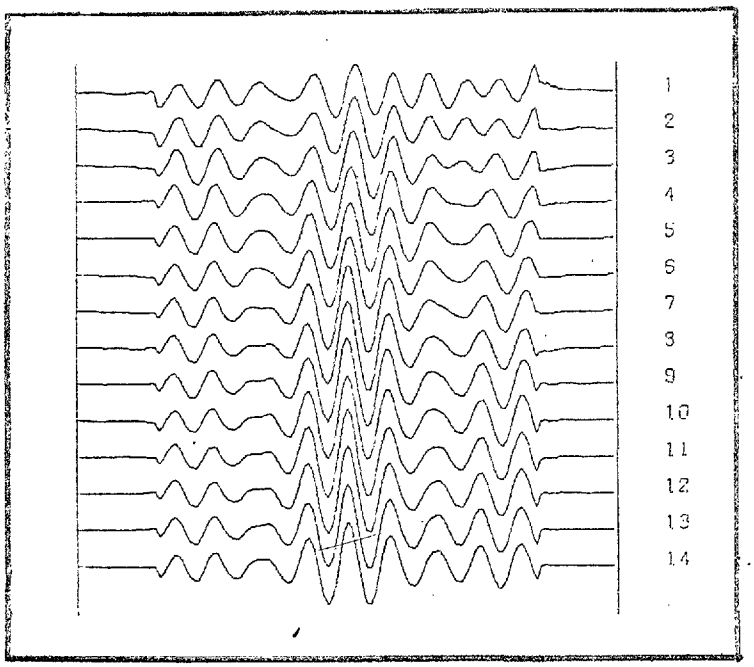


Fig. 3.78
auto-2 filtered
by *PR2

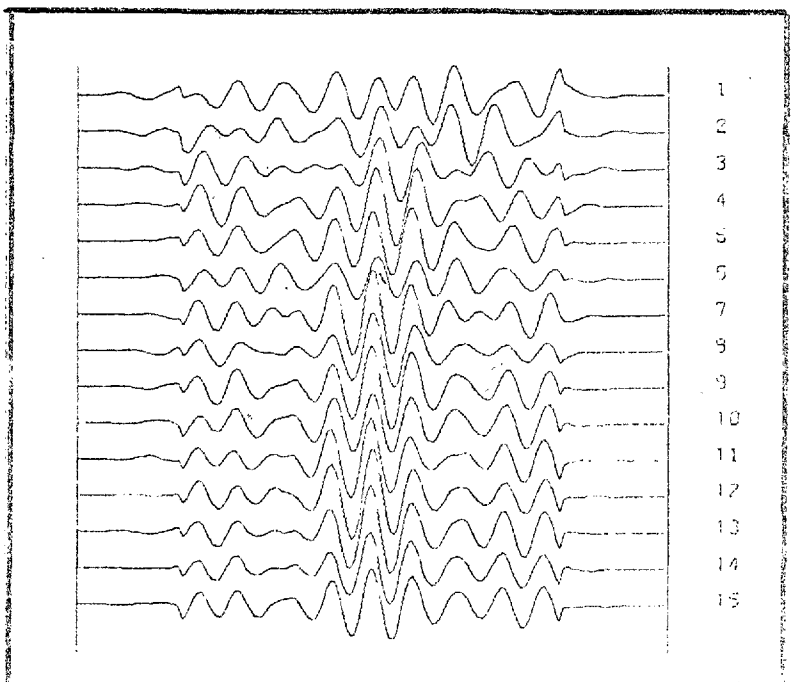
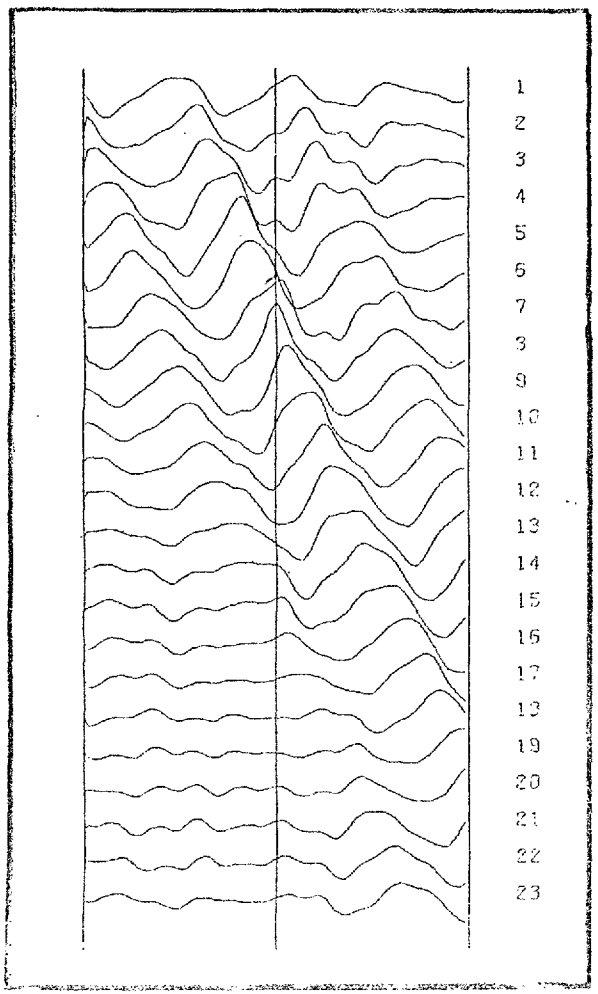


Fig. 3.79
auto-2 filtered
by *PR8



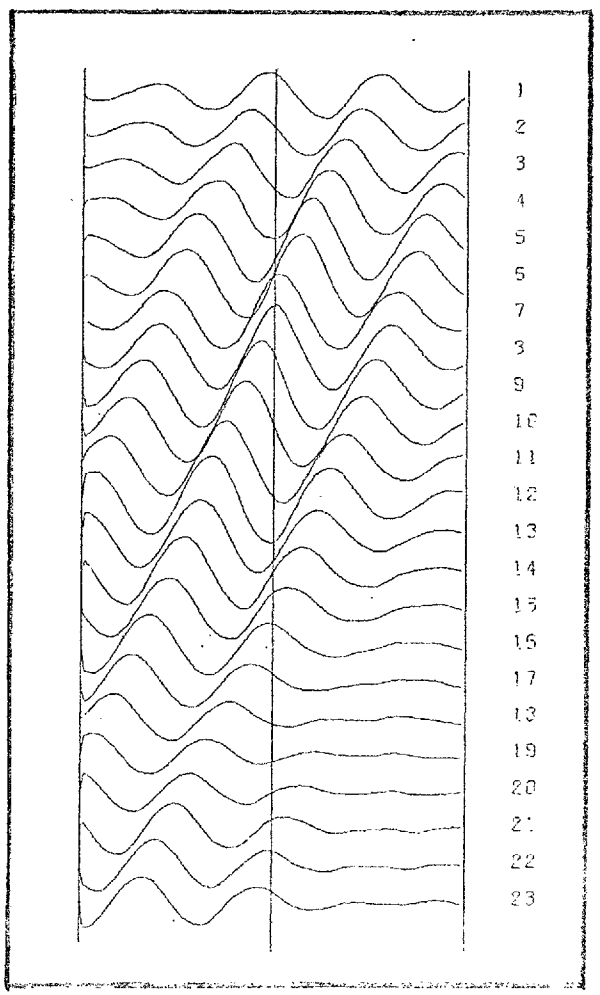
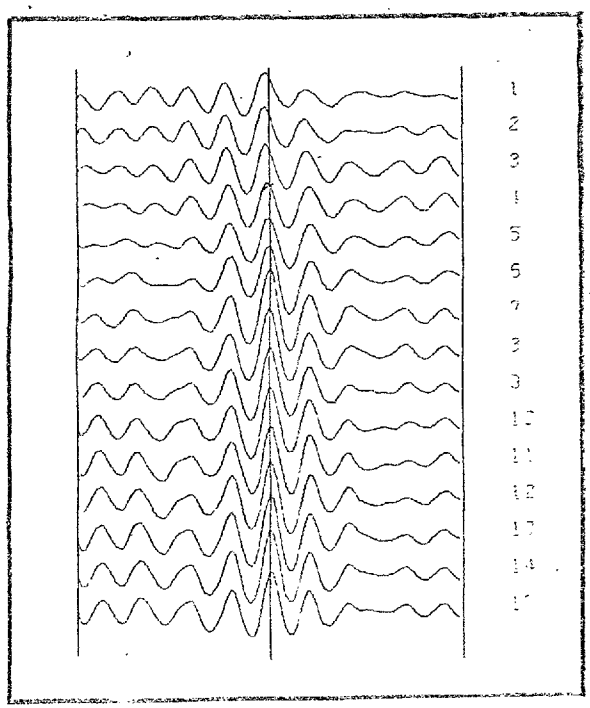


Fig. 3.80 (left) auto-1, col.8,
for Fig. 1.2
(shotpoint 3002)

Fig. 3.81 (right) auto-2, col.8,
for Fig. 1.2
(shotpoint 3002)



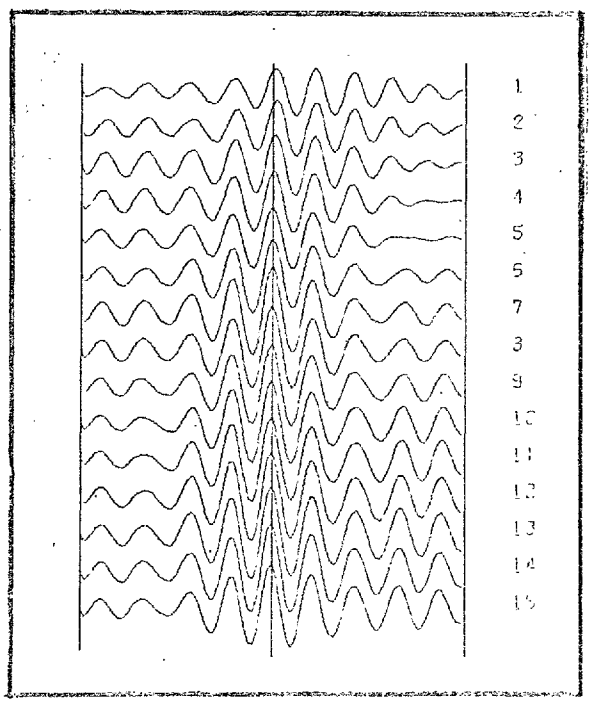
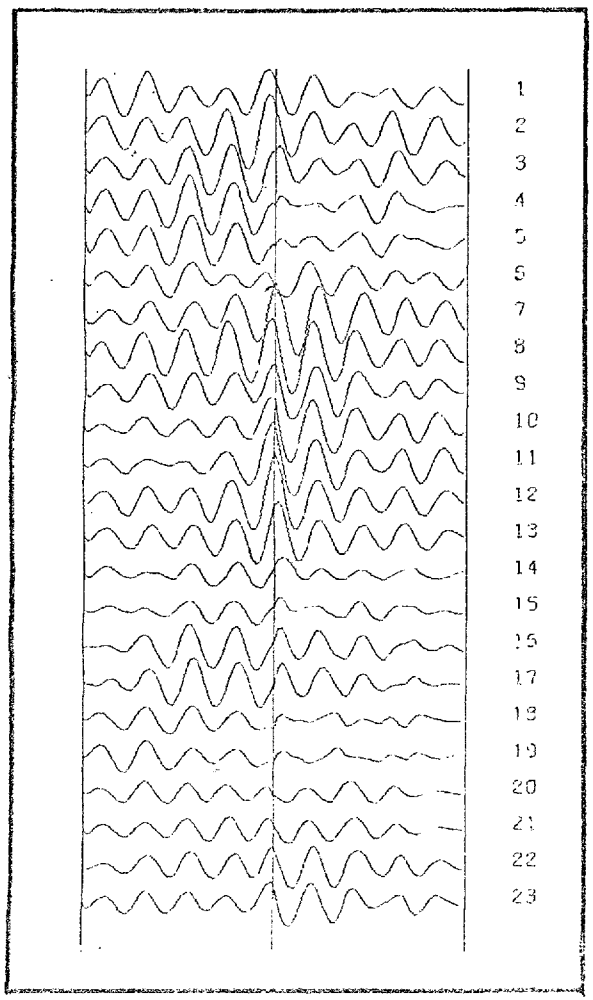


Fig. 3.82 (left) auto-1, col.8, for Fig. 2.42 (Fig. 1.2 filtered by *PR10)

Fig. 3.83 (right) auto-2, col.8, For Fig. 2.42 (Fig. 1.2 filtered by *PR10)



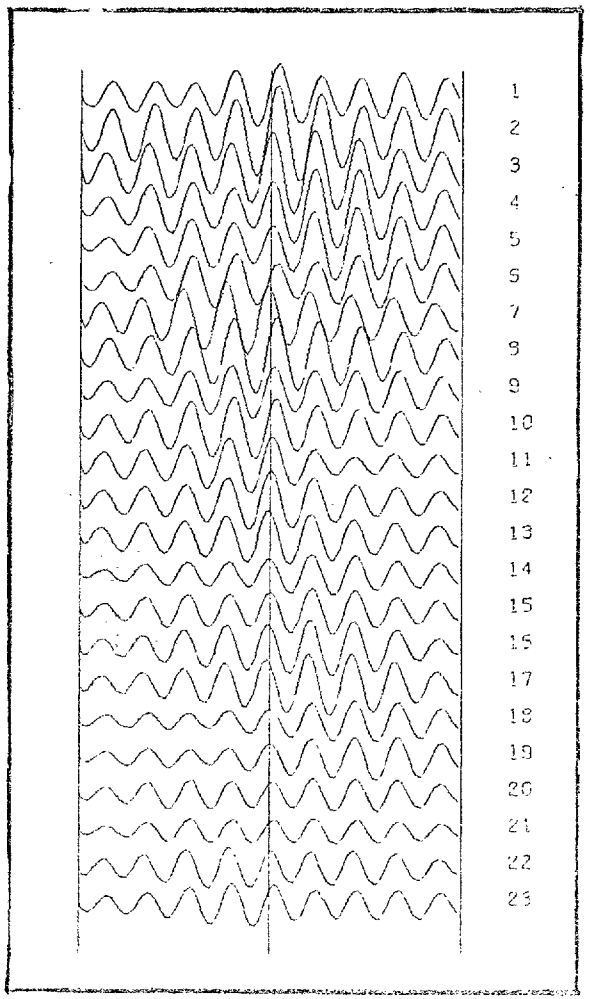


Fig. 3.84 (left) auto-1, col.12, for Fig. 1.9 (band pass filtered version of shotpoint 3006)

Fig. 3.85 (right) auto-2, col.12, for Fig. 1.9 (band pass filtered version of shotpoint 3006)

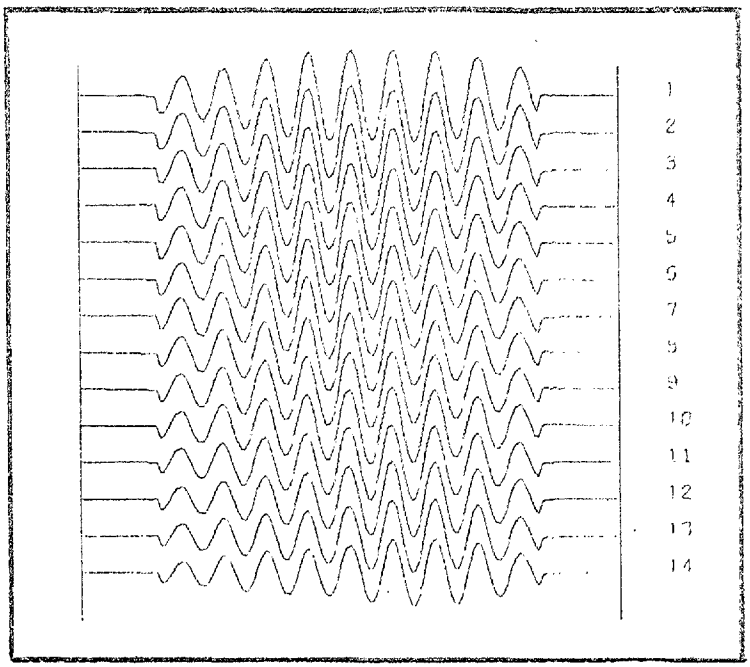
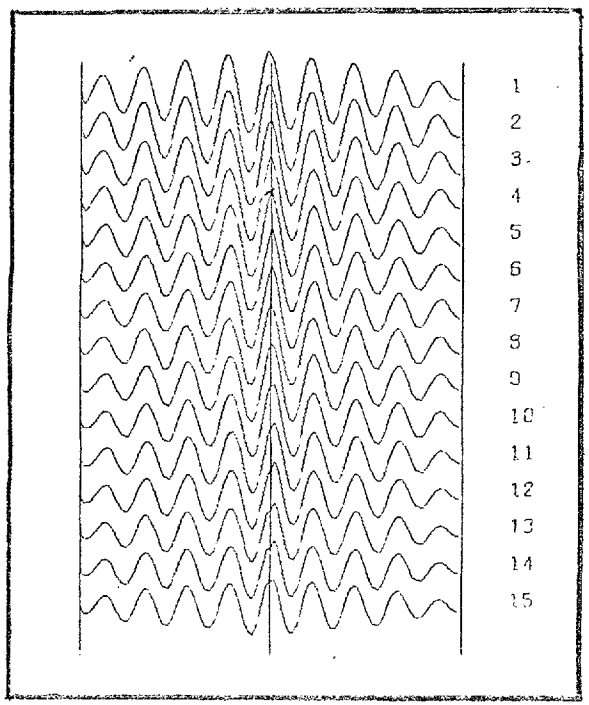


Fig. 3.86 auto-2

filtered by *PR2

(from Fig. 1.9)



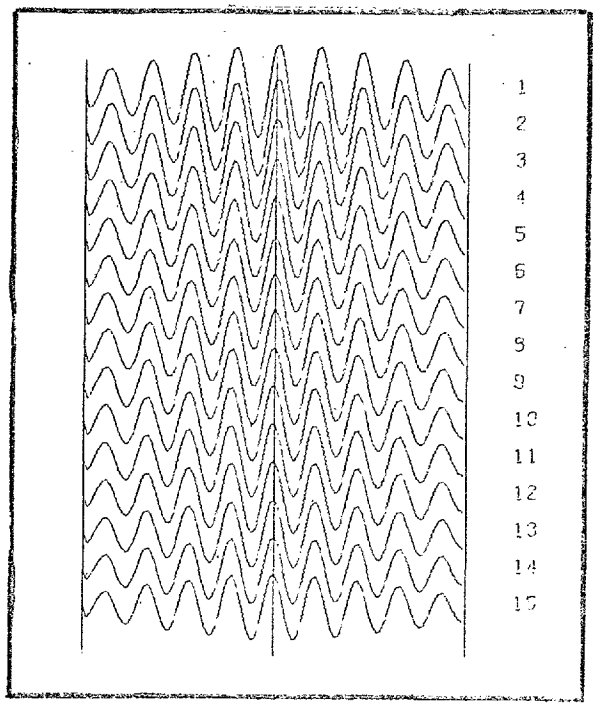
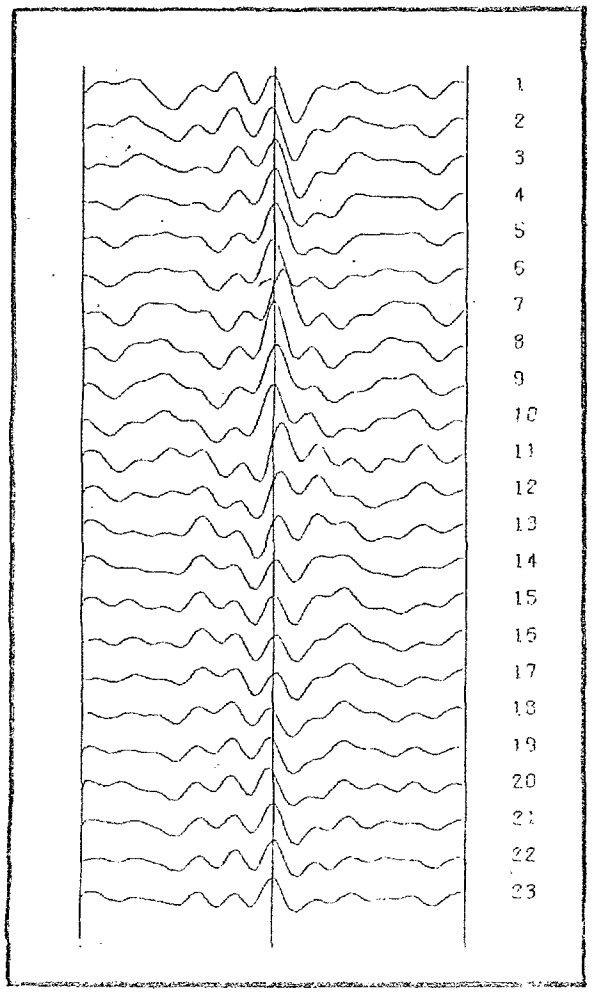


Fig. 3.87 (left) auto-1, col.8, for Fig. 3.74 (Fig. 1.9 filtered by *PR10)

Fig. 3.88 (right) auto-2, col.8, for Fig. 3.74 (Fig. 1.9 filtered by *PR10)



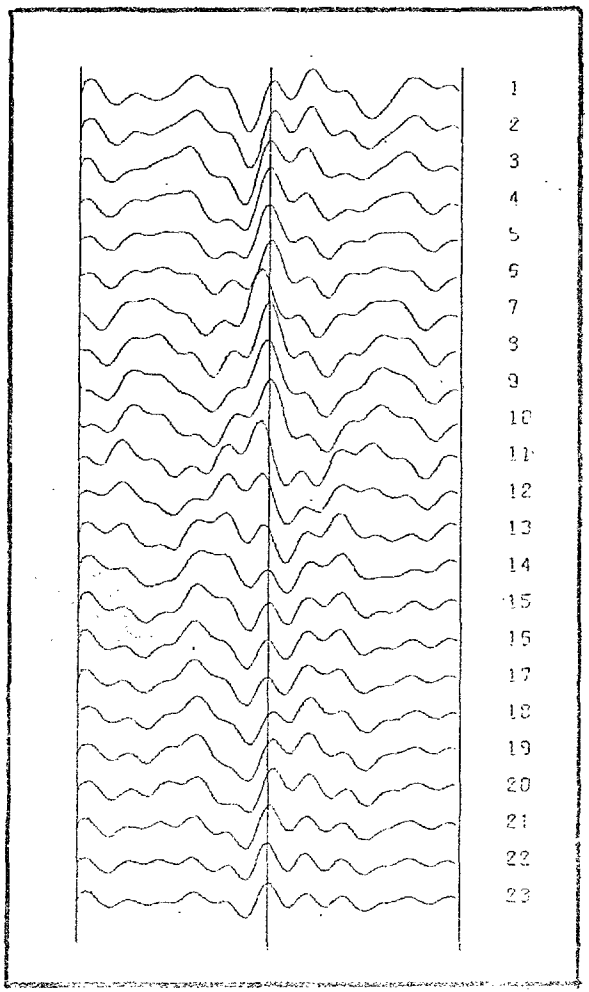
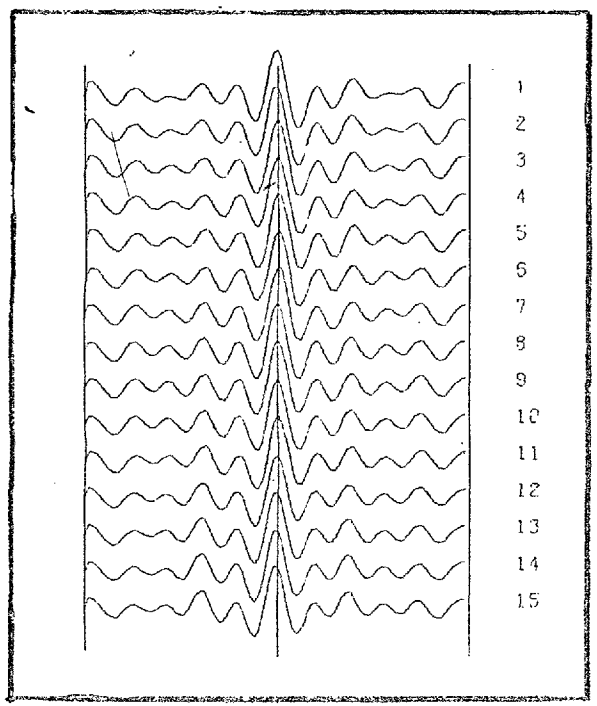


Fig. 3.89 (left) auto-1, col.8, for Fig. 1.3 (shotpoint 3003)

Fig. 3.90 (right) auto-2, col.8, for Fig. 1.3, (shotpoint 3003)



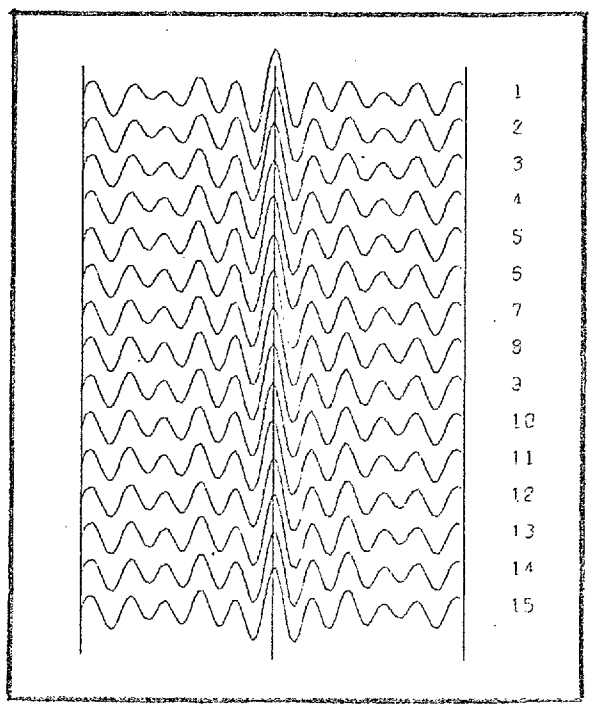
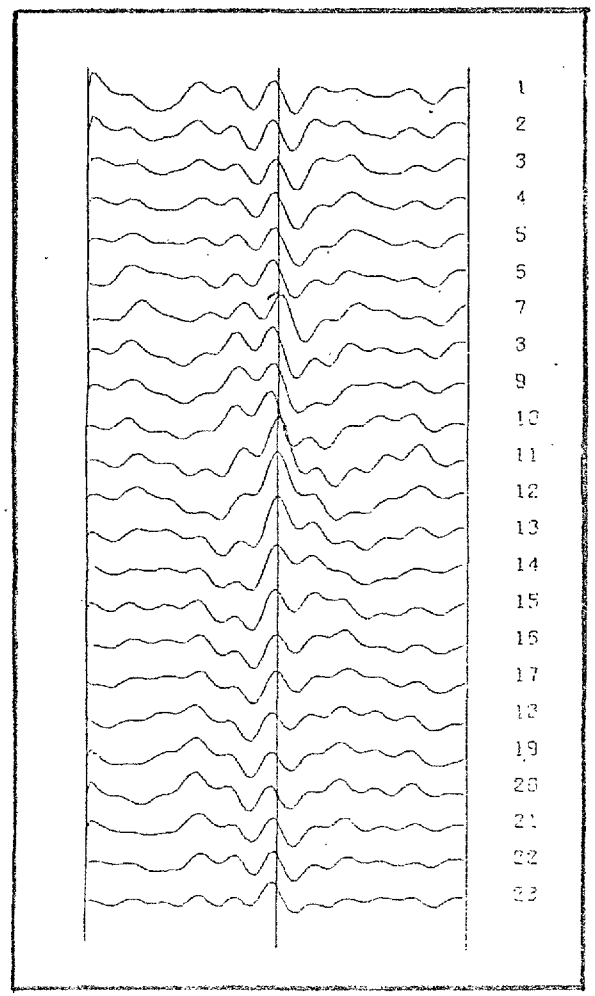


Fig. 3.91 (left) auto-1, col.8, for Fig. 2.47 (Fig. 1.3 filtered by *PR10)

Fig. 3.92 (right) auto-2, col.8, for Fig. 2.47 (Fig. 1.3 filtered by *PR10)



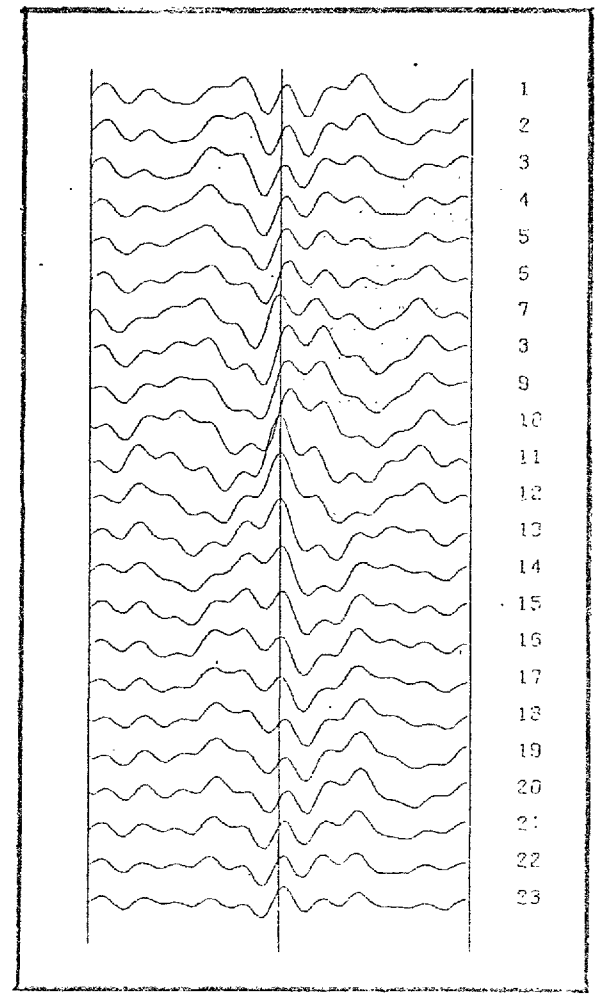


Fig. 3.93 (left) auto-1, col.12,
for Fig. 1.3
(shotpoint 3003)

Fig. 3.94 (right) auto-2, col.12,
for Fig. 1.3
(shotpoint 3003)

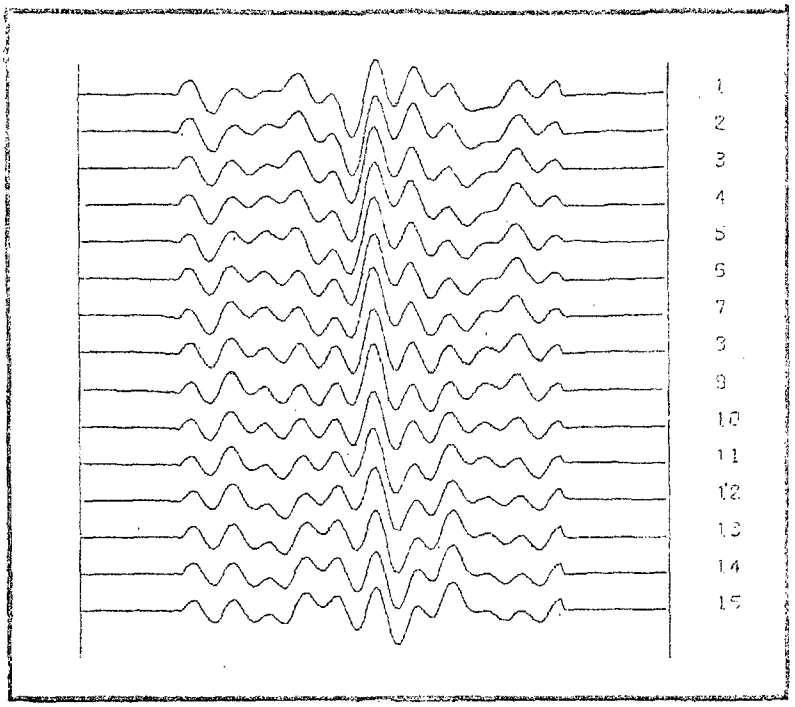
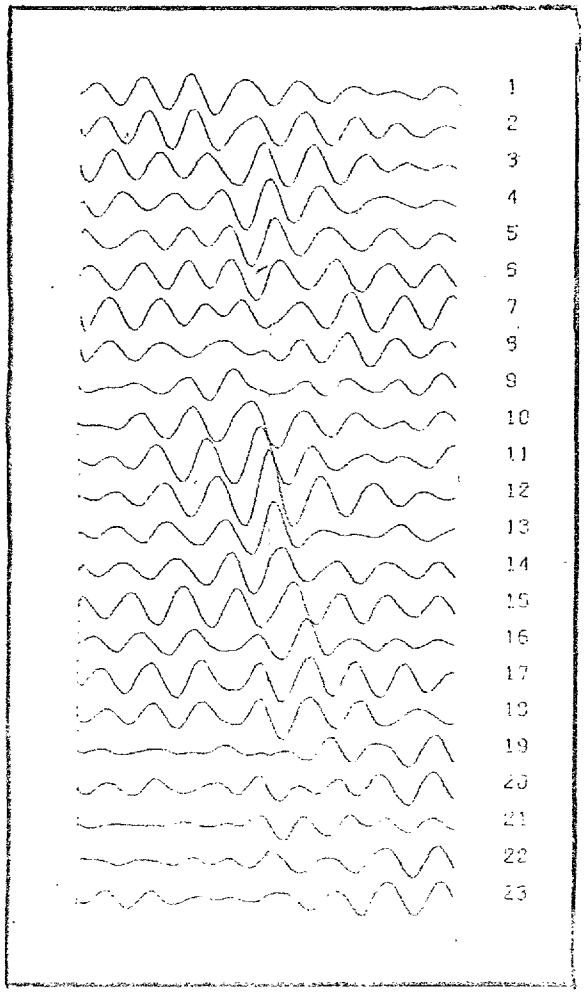


Fig. 3.95 auto-2

filtered by *PR10

(from Fig. 1.3)



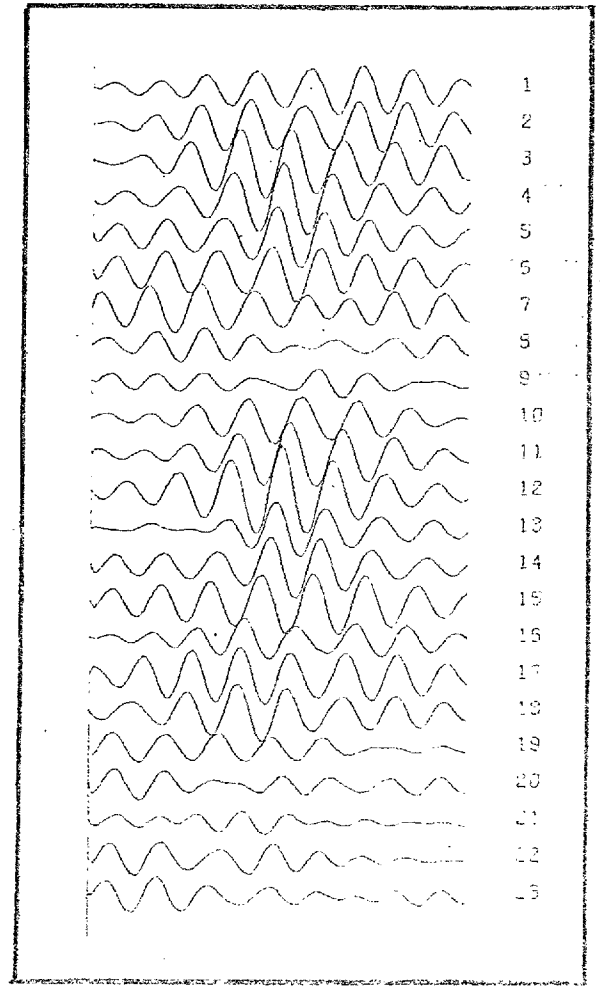


Fig. 3.96 (left) auto-1, col.12, for Fig. 1.8 (band pass filtered version of shotpoint 3005)

Fig. 3.97 (right) auto-2, col.12, for Fig. 1.8 (band pass filtered version of shotpoint 3005)

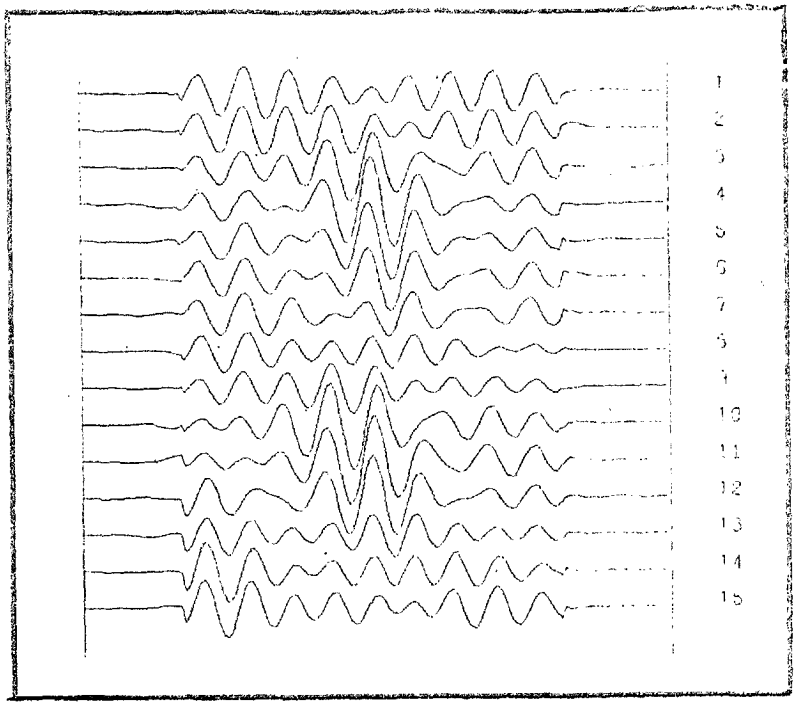


Fig. 3.98 auto-2
filtered by *PR10
(from Fig. 1.8)

3.4 Conclusions

The purpose of this chapter was to investigate the application of the autocorelation matrix method to the analysis of moveout. To this end, the following results were obtained :

(a) experiments on synthetic data of linear moveout showed a positive improvement in moveout detection brought about by the multichannel filtering of the column computed from the second order autocorrelation matrix. This detection was better than that obtained from filtering the comparable column of the first order autocorrelation matrix. The interference of signal and correlated noise in the second order column was demonstrated, and it was shown that variation in record length affected the quality of the final result (i.e. the filtered second order column). The multichannel filter scan of the second order column was introduced, where the sensitivity of matching moveouts in the data to that of the filter was once again shown.

(b) the limitations of the method with regard to different signal to noise ratios were investigated, and it was found that low power correlated events could be detected, provided that the background random noise was not too severe. It was found (Fig. 3.32) that the method was approximately equally sensitive to variations in random noise as it was to variations in correlated noise (unlike the filtered results of the previous chapter). Experiments on synthetic data of quadratic moveout gave results consistent with the linear case, bearing in mind the different weights assigned to the pass/reject regions of the different filters.

(c) the benefit of applying a multichannel pre-filter to the data, before commencing the correlation analysis, was demonstrated. The multichannel filter scan of a second order column computed from such pre-filtered data was introduced, but could not be adequately developed due to the "trace reduction" inherent in the present set of filters. It is thought that this approach should be of considerable interest

if filters are developed that have the same number of output traces as there are input traces. Quite clearly, it would not be possible to use the centre trace estimate for each of these output traces, hence the quality of the filtered result would be less for the outer traces than for the inner traces - none the less, the use of such filters would probably be of some interest.

(d) a correlation process will amplify the realtive importance of any correlated event. Consequently, both signal and correlated noise are amplified by the correlation process, the stronger of the two gaining more in magnitude than the weaker. Whether or not a filter will be able to reject, say, the amplified correlated noise will depend very much upon the filter. The pass/reject filters used in this study were generally unsuccessful in this respect, with a value of σ equal to about 0.9. The reject/pass filters, however, were very successful in rejecting the amplified signal, with a value of σ equal to 20.0. The conclusion, therefore, is that a multichannel pre-filter should be applied to remove the presence of any obvious moveout in the input record if the filter to be used has a low value of σ. This pre-filter is not so important for filters with a high value of σ, but the application of the pre-filter may still be quite useful.

(e) in the second order autocorrelation matrix method, two actual correlation processes are performed. One would assume, therefore, that the method should find particular application for records of high random noise and moderate correlated noise. To some extent the results from synthetic data confirm this view, particularly the last result from quadratic filtering ($\rho = 0.0$, $\nu = -6.0$ db).

(f) a number of experiments were conducted on real data, the results of which were consistent with that of the synthetic data. The following features were demonstrated - (i) the importance of matching not only the moveout to be passed, but also the moveout to be rejected, between the data and the filter, (ii) the benefits of applying a multichannel

pre-filter to the data before commencing analysis, and (iii) the generally improved appearance of signal in the filtered second order column over that visible in the original record.

Comparison of the results from this chapter with those of the previous chapter have been largely dealt with above. Principal comparison may be made between (i) the "moveout matching" of filter and data, and (ii) the difficult filtering problem caused by the correlation process worsening the signal to correlated noise power ratio in the column of the second order autocorrelation matrix, for filters with a low value of σ.

CHAPTER 4

THE TWO-DIMENSIONAL FOURIER TRANSFORM AND ITS APPLICATION TO THE ANALYSIS OF MOVEOUT

4.0 Introduction

The discrete two-dimensional Fourier Transform is defined and discussed in this chapter, and the effects of (i) pre-whitening the data before taking the transform, and (ii) smoothing the spectral values before plotting the transform, are illustrated. The ability of the method to detect low power events from synthetic data is investigated over a range of different noise levels for linear moveout, and the benefit of applying a multichannel pre-filter to the data is shown. Experiments are also conducted on both synthetic data of quadratic moveout and the real data records of Chapter 1. The results are reviewed with reference to the previous chapters.

4.1 Fourier Transform theory

A useful introduction to Fourier Transform theory may be found in any one of the standard works on the subject, such as Lee (1960), Bracewell (1965), Bendat and Piersol (1966). A number of theorems exist relating various concepts in the time and frequency domains, (for example, the convolution theorem mentioned in Chapter 1), for which ample coverage is provided by these works. It should be noted, of course, that the frequency representation does not introduce more information into the problem, rather it re-orders the information into a form which may be more suitable for the analysis of a particular problem. The formal equivalence of the time and frequency domains is provided by the Fourier Transform; for example, the autocorrelation function $\phi_{ii}(\tau)$ and the power spectral density function $\Phi(f)$ form a Fourier Transform pair, with a similar relationship holding for the crosscorrelation function $\phi_{ij}(\tau)$ and the cross-power spectral

density function $\Phi_{ij}(f)$:

$$\phi_{ii}(\tau) = \int_{-\infty}^{\infty} \Phi(f)\, e^{2\pi i f\tau}\, df$$

$$\phi_{ij}(\tau) = \int_{-\infty}^{\infty} \Phi_{ij}(f)\, e^{2\pi i f\tau}\, df$$

4.1.1 definition of the discrete two-dimensional Fourier Transform

The two-dimensional Fourier Transform of the continuous functions a(t,x) and A(f,k), where x is distance and k is wavenumber, is given by

$$a(t,x) = \int_{-\infty}^{\infty}\int_{-\infty}^{\infty} A(f,k)\, e^{2\pi i(ft+kx)}\, df\, dk$$

$$A(f,k) = \int_{-\infty}^{\infty}\int_{-\infty}^{\infty} a(t,x)\, e^{-2\pi i(ft+kx)}\, dt\, dx$$

Let us assume that a(t,x) is sampled at N discrete points, ΔT units apart in the time direction, and at M discrete points ΔX units apart in the spatial direction. (Within the seismic context, the spatial sampling is effected by the array of seismic detectors). Without loss of generality one may take $\Delta T = \Delta X = 1$, so that the discrete two-dimensional Fourier Transform pair is given by

$$a_{nm} = \sum_{p=0}^{N-1}\sum_{q=0}^{M-1} A_{pq}\, e^{2\pi i(np/N + mq/M)}, \quad \begin{matrix}(n=0,\ldots,N-1),\\ (m=0,\ldots,M-1).\end{matrix}$$

$$Apq = \frac{1}{NM}\sum_{n=0}^{N-1}\sum_{m=0}^{M-1} a_{nm}\, e^{-2\pi i(np/N + mq/M)}, \quad \begin{matrix}(p=0,\ldots,N-1)\\ (q=0,\ldots,M-1)\end{matrix}$$

The discrete frequencies are given by $f = np/N$, and the discrete wavenumbers by $k = mq/M$. It has been assumed, in this formulation, that $|f| \leq \frac{1}{2}$ and $|k| \leq \frac{1}{2}$ in order to avoid the problems of aliasing.

The resolution bandwidth for the discrete two-dimensional Fourier Transform is given by $\Delta f = 1/N$ for the frequency axis and $\Delta k = 1/M$ for the wavenumber axis. Due to the periodicity of the "f-k" plane (Bracewell, 1965) it is sufficient to describe the

$A(f,k)$ in the region $0 \leq f \leq \frac{1}{2}, -\frac{1}{2} \leq k \leq \frac{1}{2}$.

The definition of the Fourier Transform given above is derived from that of Cooley and Tukey (1965), and leads to the subroutine algorithm provided by the IBM Scientific Subroutine Package library. This subroutine performs the transformation in $N \log_e N$ steps, where N is the number of data samples per channel, as opposed to the earlier N^2 algorithms. It should be noted that this definition of the Fourier Transform is different to that used by Hinich and Clay (1968), for example, in that the sign of the wavenumber exponent is reversed. The result of this is that a reflection of the Fourier Transform plot occurs about the line $k = 0$, so that a line of constant moveout appears in the left hand quadrant rather than in the right hand quadrant (see below).

4.1.2 interpretation of the f-k plane

From the previous section it is clear that the function $a(t,x)$ may be thought of as representing a plane wave of velocity $v = -f/k$. This velocity is related to the moveout, τ, by $v = \Delta x/\tau$. Hence, for $\Delta x = 1$, $v = 1/\tau$. It follows, therefore, $f = -k/\tau$, i.e. events of linear moveout appear as straight lines in the f-k plane. Due to the periodicity of the f-k plane, any moveout greater than 1 sample per trace will exhibit a "fold-over" at the Nyquist wavenumber. Fig. 4.1 shows the appearance of an event of moveout $\tau = 1$ sample per trace, and Fig. 4.2 that for $\tau = 2$ samples per trace.

It will be recalled that the moveout of correlated noise is greater than that of signal at the same point in the seismic record. Hence, provided that these moveouts are linear, the taking of the Fourier Transform of the seismic data effects a separation of signal and correlated noise on this basis.

The square of the modulus of the two-dimensional Fourier

Transform gives the power spectral density function (or power spectrum), as a function of frequency and wavenumber, i.e.

$$\underline{\bar{\Phi}}(f,k) = |A(f,k)|^2$$

The normalised power spectrum $\underline{\tilde{\Phi}}(f,k)$ is used exclusively for the f-k plots presented in this thesis, and is derived from the power spectrum by

$$\underline{\tilde{\Phi}}(f,k) = 10 \log_{10} \left(\frac{\underline{\bar{\Phi}}(f,k)}{\underline{\bar{\Phi}}_{max}(f,k)} \right) \text{ decibels}$$

where $\underline{\bar{\Phi}}_{max}(f,k)$ is the maximum value of $\underline{\bar{\Phi}}(f,k)$.

Experiments conducted on both real and synthetic data generally involved the presence of an event of zero moveout. It is for this reason that the spectra are plotted in the range $-\frac{1}{2} \leq k \leq \frac{1}{2}$, rather than in the range $0 \leq k \leq 1$.

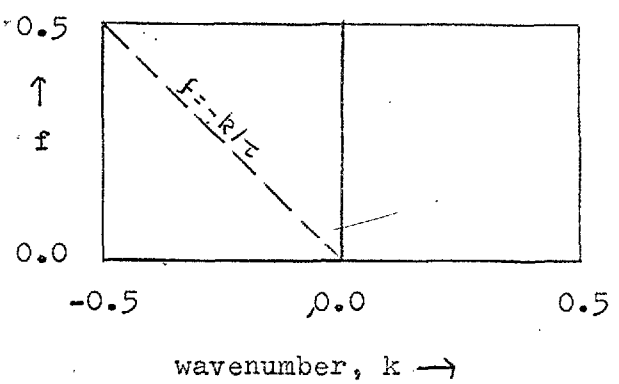


Fig. 4.1 example in the f-k plane for $\tau = 1$.

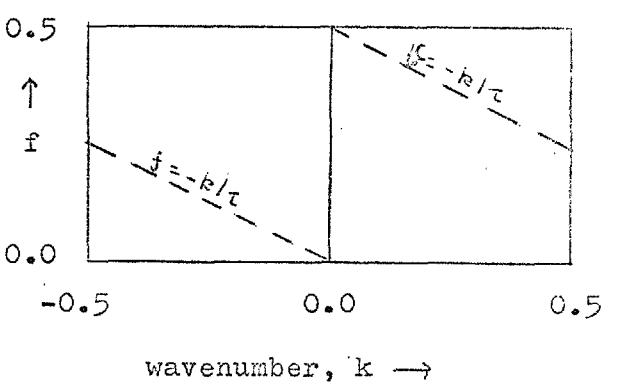


Fig. 4.2 example in the f-k plane for $\tau = 2$.

4.1.3 statistical considerations of the Fourier Transform

A very poorly defined power spectrum is obtained whenever the Fourier Transform is directly applied to seismic data. Even for very good data, the f-k plane only shows long narrow streaks parallel to the wavenumber axis. This is principally due to the following reasons :

(a) there is a great disparity between the number of samples in the frequency axis and the number of samples in the wavenumber axis.

(b) correlated noise is primarily of low frequency, hence the maxima due to signal and correlated noise tend to overlap.

(c) severe bias can occur due to "leakage" from the side lobes of the Fourier Transform.

(d) the large variance associated with each estimate of the power spectrum.

Each of these difficulties, together with their respective remedies, are now discussed.

4.1.3.1 bias and leakage

The taking of a Fourier Transform of a seismic record may be regarded as scanning the large input bandwidth of the data by a small analysing filter, of bandwidth $B_f = 1/N$ for the frequency axis and $B_k = 1/M$ for the wavenumber axis. (From this it may be immediately observed that increased resolution is obtained by increasing the number of samples). Fig. 4.3 shows the estimation of a power spectrum by an "ideal" filter, and Fig. 4.4 that for a "real" filter - (for the sake of simplicity only frequency need be considered here). It is seen that the ideal filter will only pass frequencies within its bandwidth, whereas the real filter possesses side lobes that will also contribute to the estimated power at the frequency f_e. This contribution from the side lobes is termed "leakage" or "bias", and is particularly important in the estimation of a non-uniform power spectrum such as

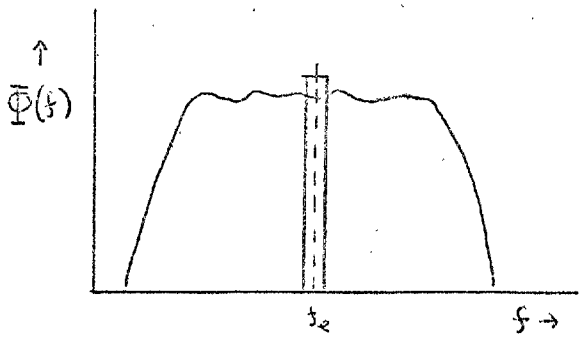


Fig. 4.3 spectral estimation by an ideal filter

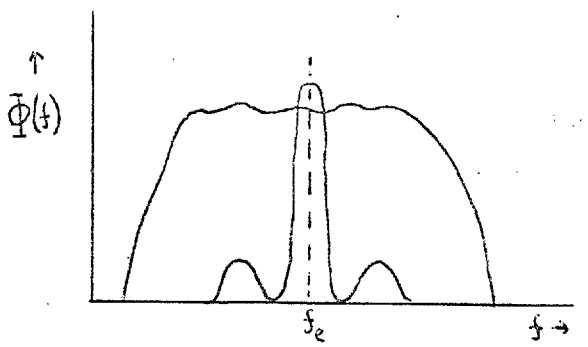


Fig. 4.4 spectral estimation by a real filter

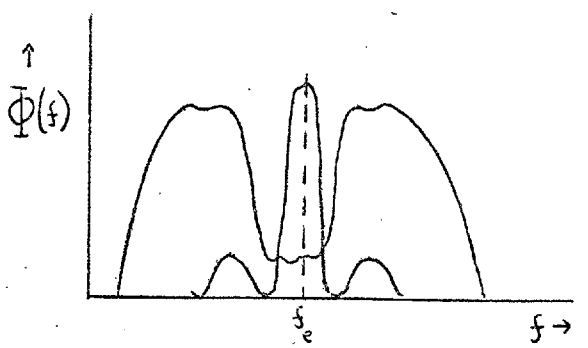


Fig. 4.5 illustration of error due to leakage

Fig. 4.5. A totally erroneous estimate for the power at frequency f_e would be obtained from Fig. 4.5. This problem may be remedied, to some extent, by "pre-whitening" the power spectrum before its estimation.

Pre-whitening is a process by which the power spectrum of the signal to be estimated is "flattened", so that at every frequency f the central lobe of the analysing filter will contribute the major portion to the power spectrum at that frequency, i.e. the power spectrum of Fig. 4.5 is made to approximate that of Fig. 4.4. The inherent disadvantage of pre-whitening is that, in order for it to be fully effective, the shape of the input spectrum should be known. In practice, the adopted procedure used was as follows :

In principle, the application of an inverse filter to a seismic trace should result in the recovery of the original spike series (Robinson, 1967c). It has been shown (Dash and Obaidullah, 1970), that the autocorrelation function of a seismic trace is very similar to that of the signal wavelet alone, provided that the length of the function does not exceed that of the wavelet. To this end the auto-correlation function (single channel) was computed for each trace and used to design a set of inverse single channel filters, each with a unit spike at zero lag as the desired output, by means of subroutine "EUREKA" (Robinson, 1967a- this has been corrected). Each filter was ← then convolved with the appropriate input trace to yield a record of "whitened" traces. The presence of correlated noise on the input traces, of course, results in the computed autocorrelation function being a "composite" of that due to the signal and correlated noise wavelets alone. None the less, this attempt to contract the signal and correlated noise wavelets to spikes, whilst preserving the relative moveout information, was quite successful and is illustrated later in this chapter.

4.1.3.2 distinction between signal and correlated noise

In order to accentuate the difference in relative moveout between the signal and correlated noise, it is desirable that the lines of constant moveout in the f-k plane should be as long as possible. This may be effected by boosting the power of the signal and correlated noise at high frequency, a process which occurs in the pre-whitening of the spectrum discussed in the previous section.

4.1.3.3 variance of the spectral estimate

If it can be assumed that the bias in the spectral estimate is negligible, then the estimated value of the power spectrum at a frequency f, $\hat{\Phi}(f)$, is equal to the actual value of the power spectrum, $\Phi(f)$, at that frequency, i.e. $E\left[\hat{\Phi}(f)\right] \approx \Phi(f)$. In point of fact, of course, every spectrum contains bias due to the taking of a finite length of data, since this is equivalent to multiplying the infinite seismic trace with a box function, i.e. convolving the true spectrum with a sinc function. As the data length increases, so does this sinc function approximate towards a delta function, thereby approaching an unbiassed spectrum. This bias should not be confused with that of section 4.1.3.1.

It can be shown (Hinich and Clay, 1968), that the large sample variance of the spectral estimate, $\text{var}\left[\hat{\Phi}(f)\right]$, is given by

$$\text{var}\left[\hat{\Phi}(f)\right] \approx \Phi^2(f) \quad \text{for } k > 0$$
$$\text{var}\left[\hat{\Phi}(f)\right] \approx 2\Phi^2(f) \quad \text{for } k = 0$$

Since the variance of the estimate does not approach zero for increasing sample size, it follows that the Fourier Transform is not a consistent estimator of the true power spectrum. Taking the standard deviation as an indication of the error associated with each spectral estimate, it can be seen that each estimate has a possible error of 100%, i.e. $\hat{\Phi}(f) = \Phi(f) \pm \Phi(f)$.

It is also known (Hinich and Clay, 1968), that a small bandwidth, desirable for large resolution, leads to a large variance. In practice, therefore, a compromise has to be made between the resolution of the spectral estimates and the variance of those estimates. A simple method to reduce the variance of the power spectrum is to use the following spectral smoothing procedure (Hinich and Clay, 1968) :

The N spectral values are divided up into r equal blocks of length K samples. The K samples within each block are then averaged together to give one smoothed estimate for each block. The variance of the smoothed spectral estimates, $\hat{\Phi}_{av}(f)$, is given by

$$\text{var}\left[\hat{\Phi}_{av}(f)\right] \approx \frac{1}{r}\Phi^2(f)$$

and the bandwidth resolution is given by $\Delta f = r/N$. For the work in this thesis, a value of $K = 8$ was generally taken. In order for this procedure to be successful, it is desirable that the spectrum to be smoothed should be reasonably flat. This is another reason for the application of the pre-whitening process described earlier.

4.1.3.4 sampling disparity between frequency and wavenumber axes

The great disparity between the sampling of the frequency axis and that of the wavenumber axis, leads to a rather poor visual display. For "squareness" of plot it is desirable to have $\Delta f \approx \Delta k$, hence the number of samples on the frequency axis should be reduced in relation to that on the wavenumber axis. This reduction is amply satisfied by the spectral smoothing process described earlier.

4.2 Applications to synthetic data

The purpose of this section is to investigate (i) the ability of the Fourier Transform method to detect low power correlated events, for different conditions of signal to noise ratio, and (ii) the benefit in applying a multichannel filter to the input data before commencing the Fourier analysis.

An index of the synthetic data records, that have not been encountered earlier in this thesis, is presented in Table 4.1. A complete index for the Fourier Transform analyses on synthetic data is presented in Table 4.2. It should be noted that in all of the Fourier Transform plots (also referred to as "f-k" plots, for brevity), the vertical scale corresponds to frequency (in c.p.s.) and the horizontal scale to wavenumber (in fractions of the Nyquist wavenumber). In order to assist the interpretation of these plots, each contour was assigned a specific colour (Ref. "Geodat", Chapter 1). All spectral values in the two-dimensional array were normalised by the maximum amplitude present in that array, and the contours were plotted on a scale ranging from 0.0 db to -30.0 db.

4.2.1 development of analytical approach

Section 4.1 discussed the importance of pre-whitening the input data before the taking of the Fourier Transform, and also of smoothing the spectral values before the plotting of this Transform. A demonstration of this importance is given by the comparison of Fig. 4.14, Fig. 4.15 and Fig. 4.16. Fig. 4.14 shows the Fourier Transform of the input data of Fig. 4.6, with spectral smoothing but without pre-whitening; Fig. 4.15 that with spectral smoothing and with pre-whitening; and Fig. 4.16 that without spectral smoothing but with pre-whitening. The necessity for both pre-whitening and spectral smoothing is immediately apparent.

It will be noticed from Fig. 4.15 that although signal and

Figure number	ρ (db)	ν (db)	α_i	β_i	number of traces	length of traces (in samples)
4.6	0.0	6.0	0	i	24	250
4.7	0.0	6.0	0	i	24	250
	-9.0			2i		
4.8	6.0	6.0	0	i	24	250
4.9	3.0	0.0	0	i	24	250
4.10	0.0	6.0	0	i	24	250
4.11	6.0	0.0	0	i	24	250
4.12	9.0	6.0	0	2i	24	250

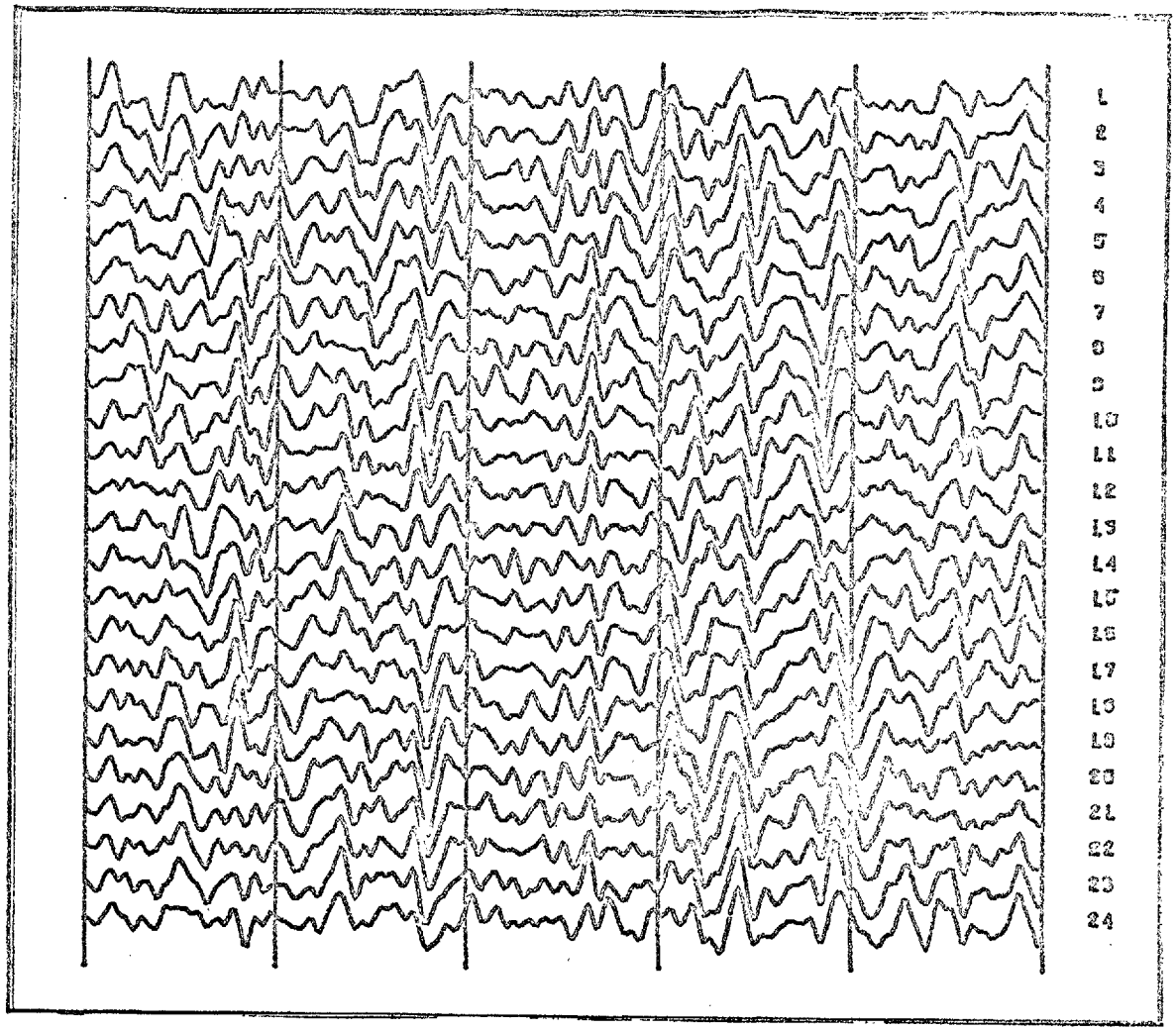
Table 4.1 Index of synthetic data records

The result of applying reject/pass filter *R110 to the data of Fig. 4.12 is presented as Fig. 4.13. Note that the data of Fig. 4.7 contains two correlated noise events.

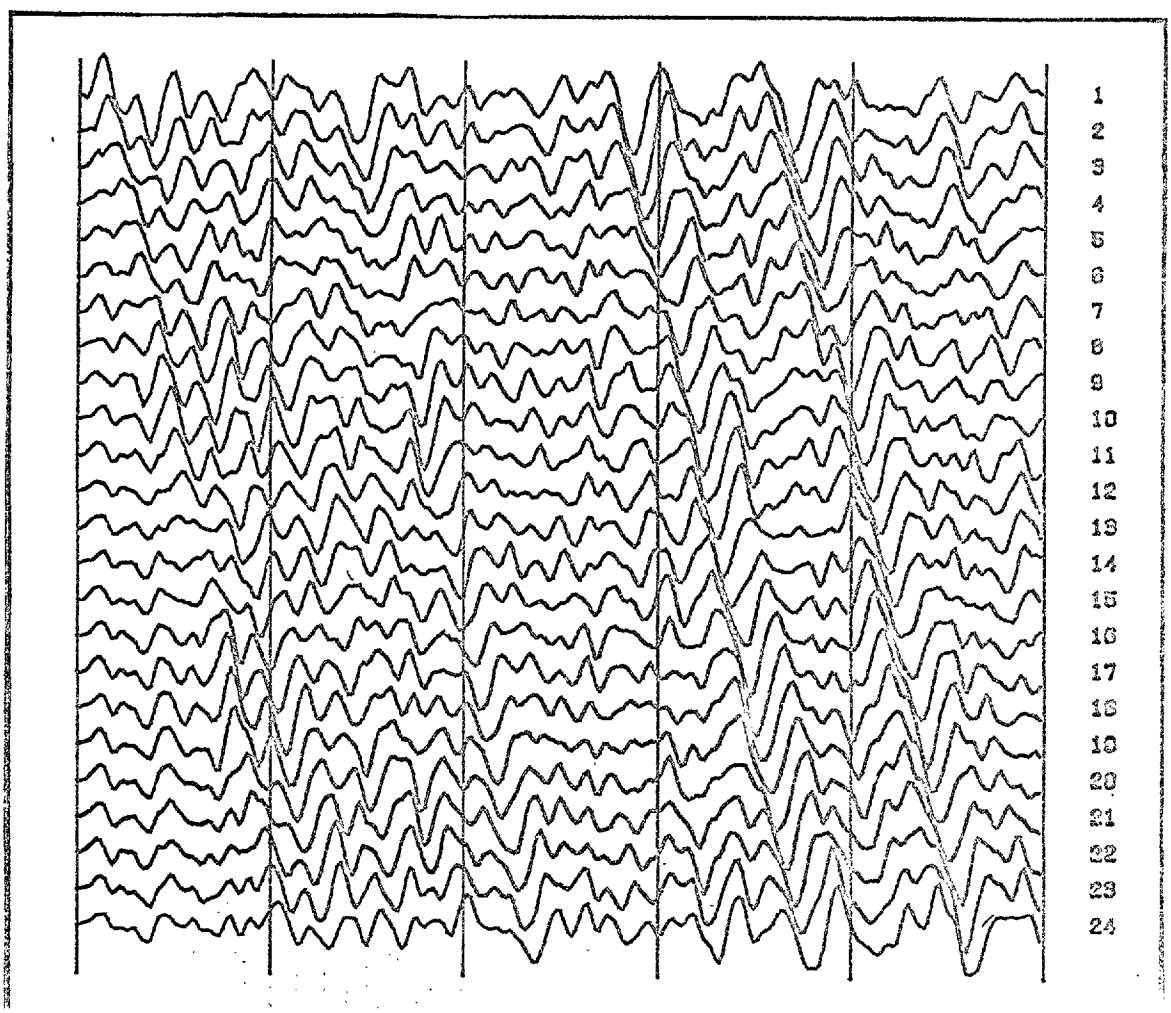
Fig. No. of input record	Fig. No. of (f-k) plot	Fig. No. of input record	Fig. No. of (f-k) plot
4.6	4.14	4.8	4.26
4.6	4.15	2.4	4.27
4.6	4.16	2.26	4.28
4.10	4.17	2.28	4.29
4.7	4.18	2.5	4.30
2.10	4.19	2.22	4.31
-	4.20	2.23	4.32
2.12	4.22	2.27	4.33
2.14	4.23	2.29	4.34
4.9	4.24	4.12	4.35
4.11	4.25	4.13	4.36

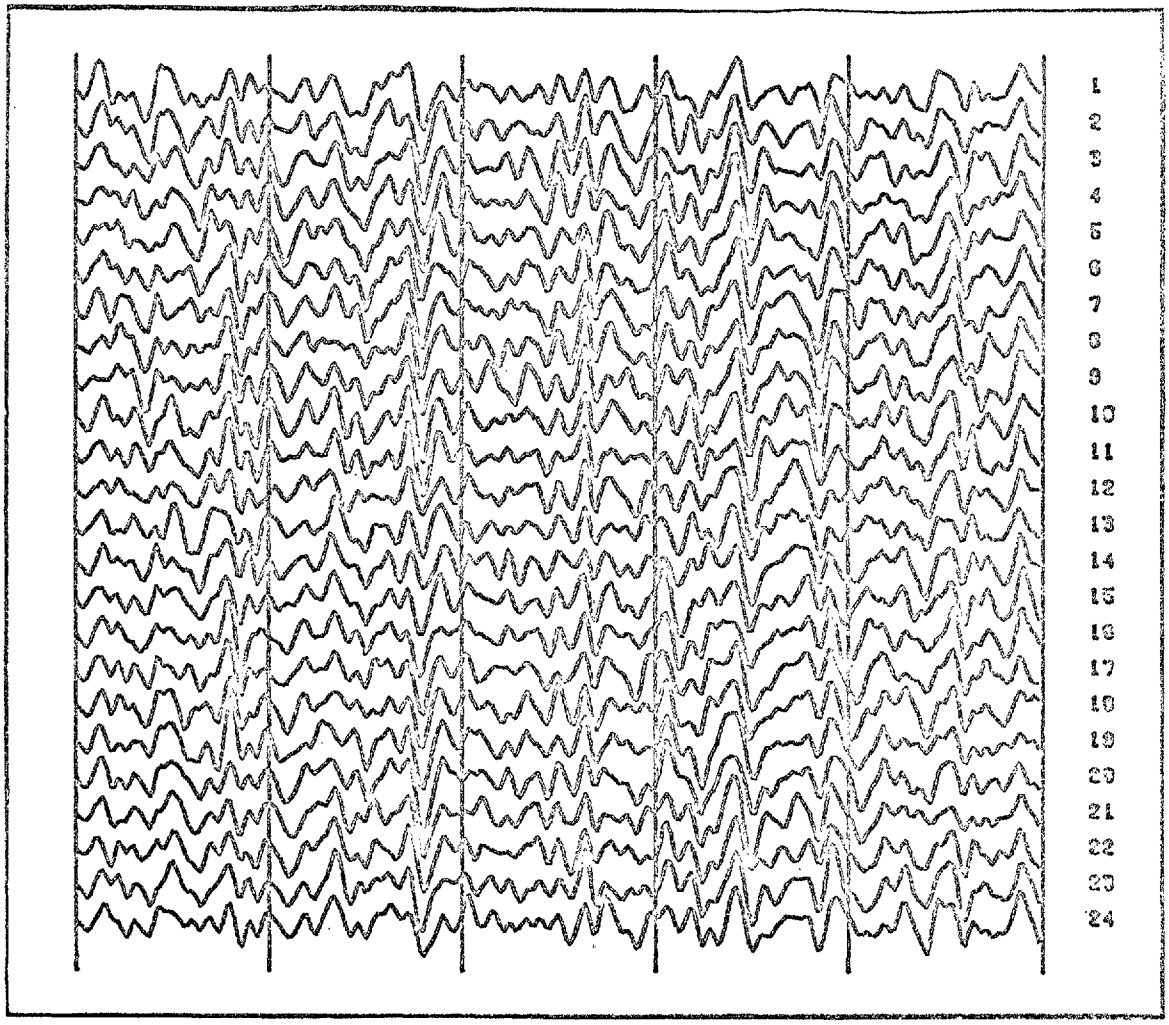
Table 4.2 Index of Fourier Transform analyses on synthetic data

N.B. the input record for the (f-k) plot of Fig. 4.20 was a 450 sample version of Fig. 4.6.



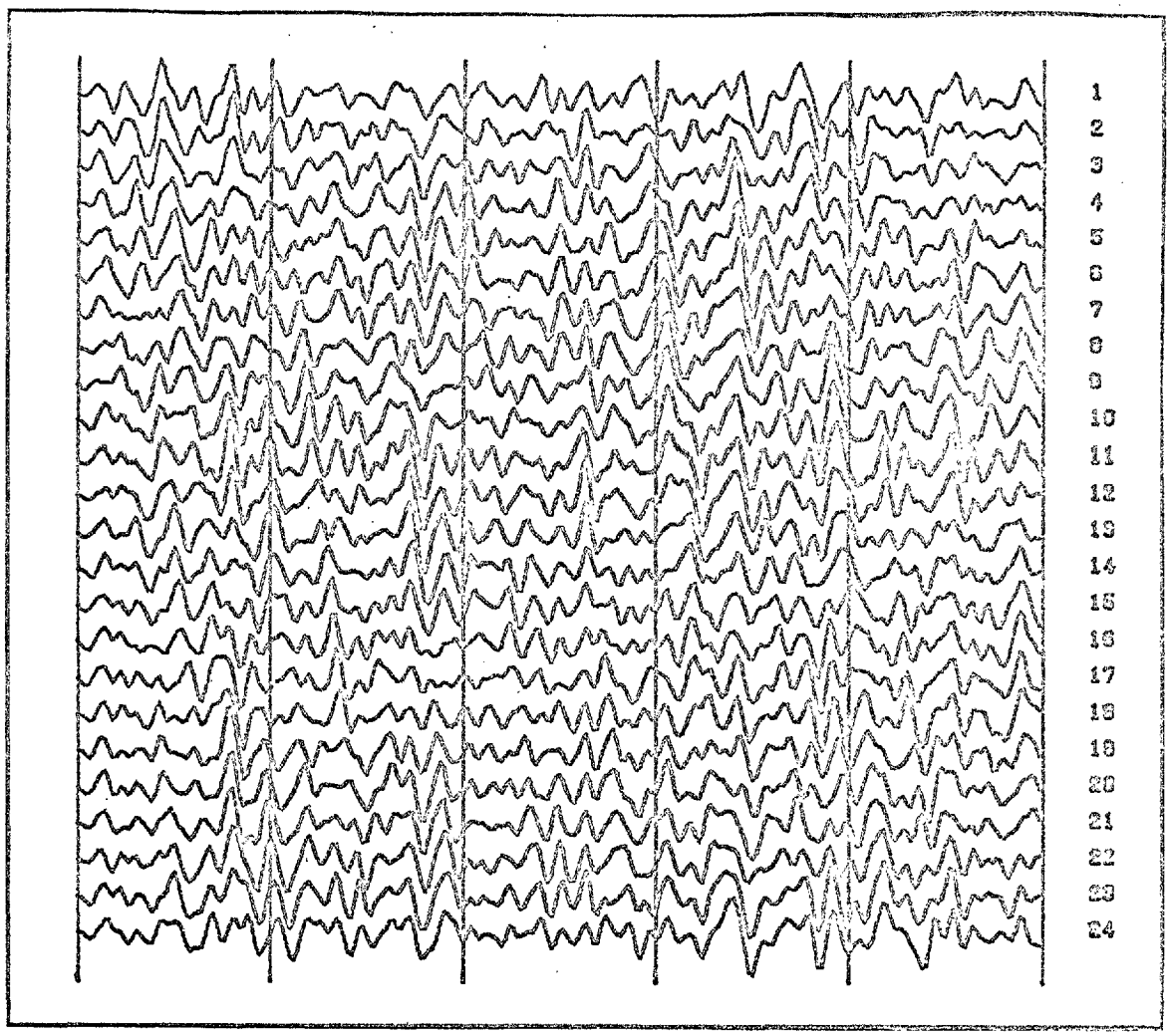
Input records, Fig. 4.6 (above) and Fig. 4.7 (below)





Input records, Fig. 4.8 (above) and Fig. 4.9 (below)





Input records, Fig. 4.10 (above) and Fig. 4.11 (below)



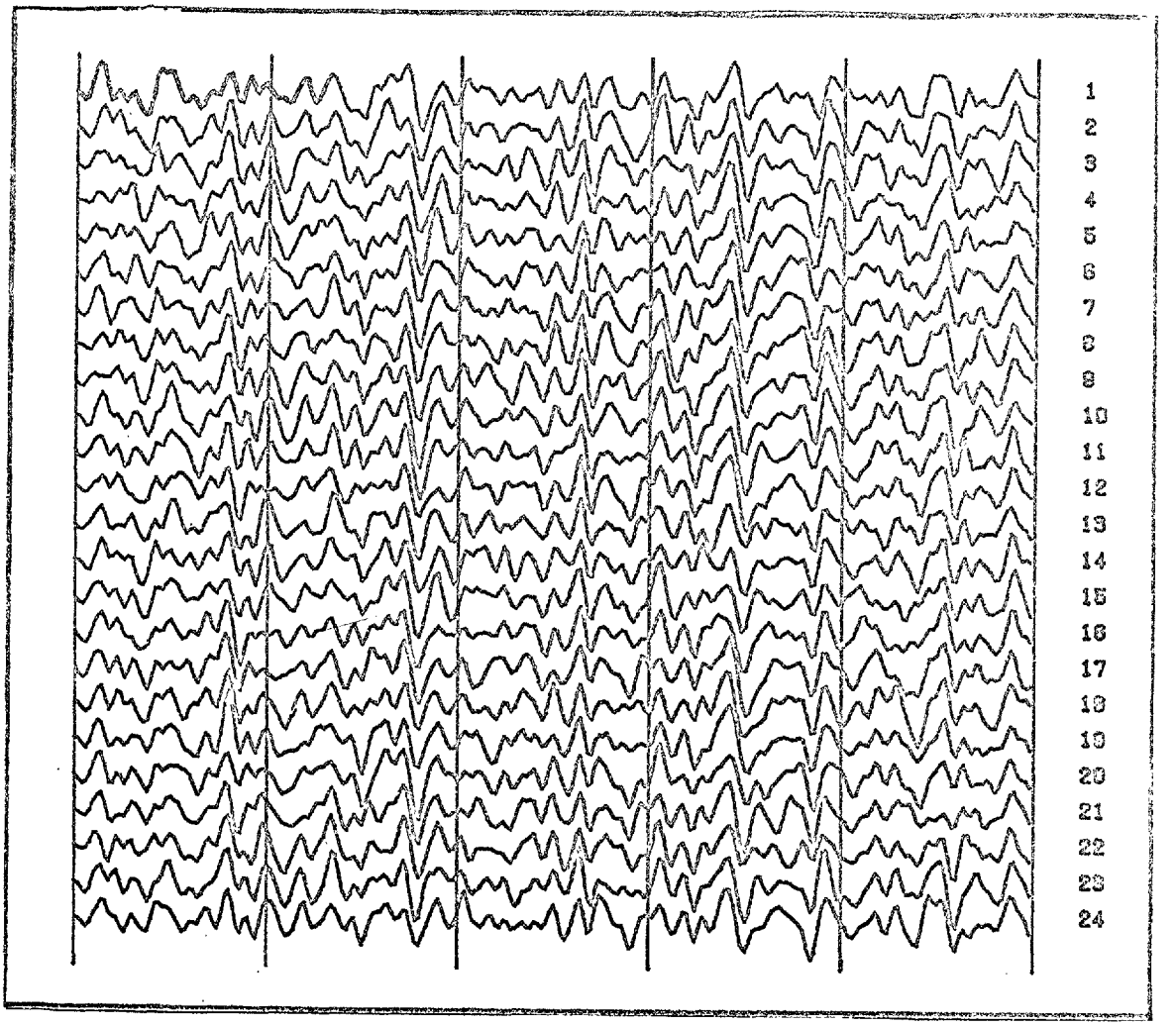
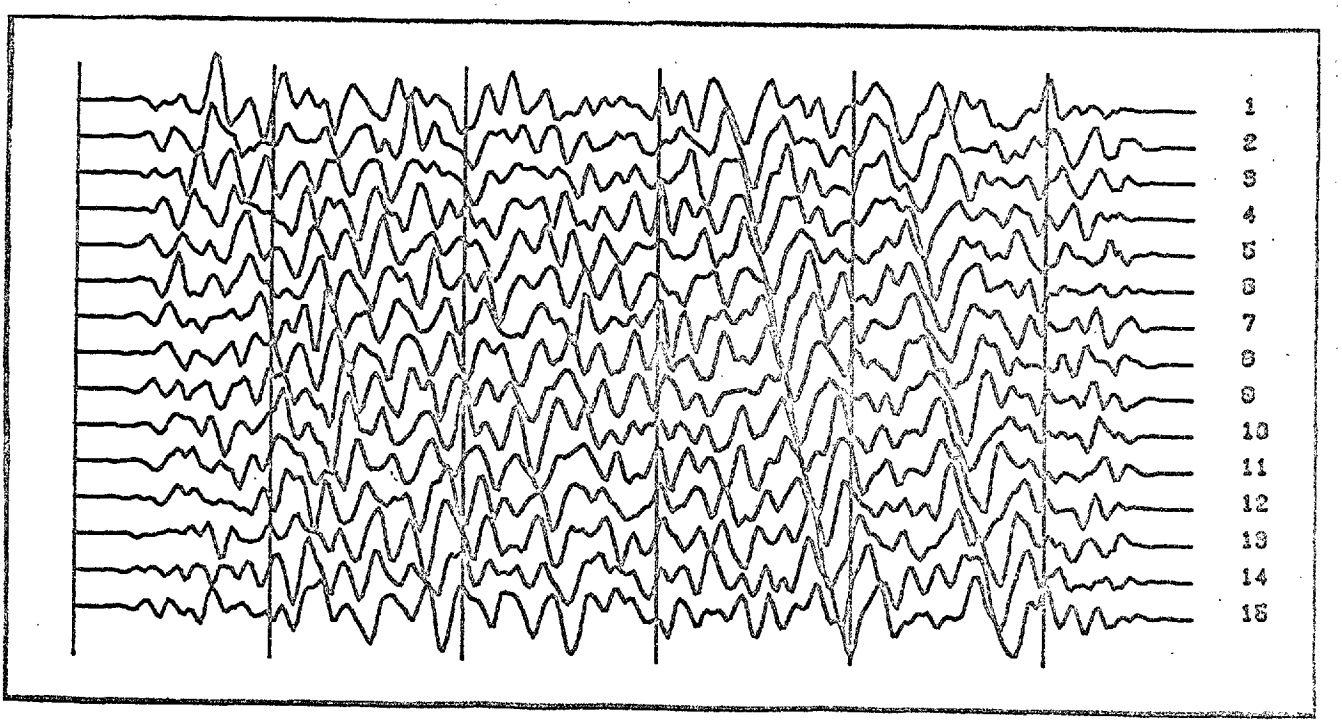


Fig. 4.12 (above) input record, Fig. 4.13 (below) result of filtering Fig. 4.12 with *RP10



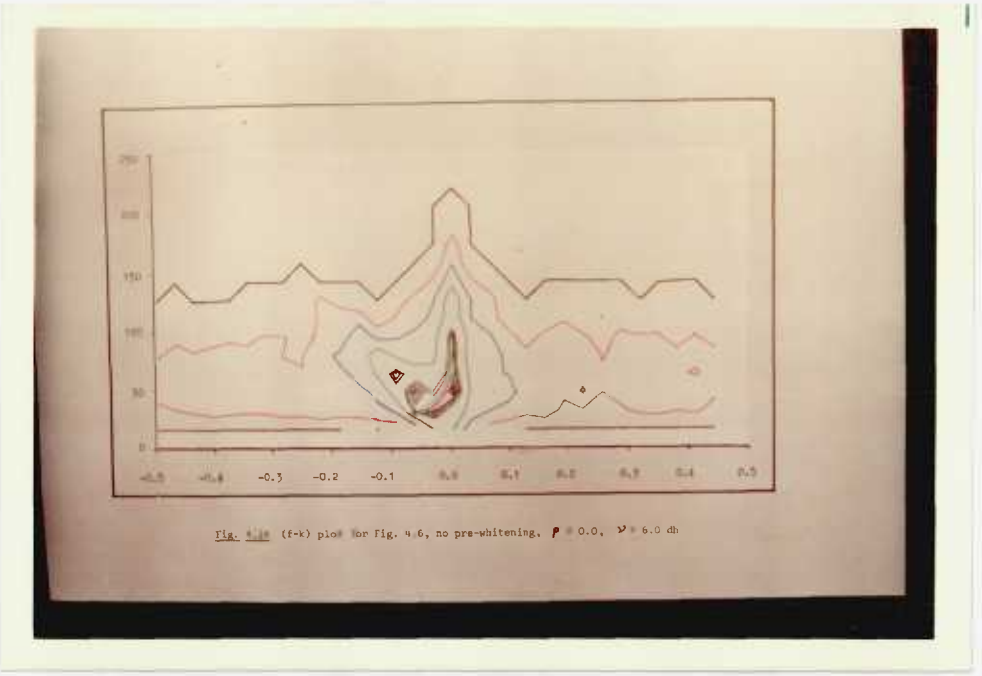


Fig. 4.14 (f-k) plot for Fig. 4.6, no pre-whitening, $P = 0.0$, $\nu = 6.0$ db

Fig. 4.14 (f-k) plot for Fig. 4.6, no pre-whitening, $P = 0.0$, $\nu = 6.0$ db

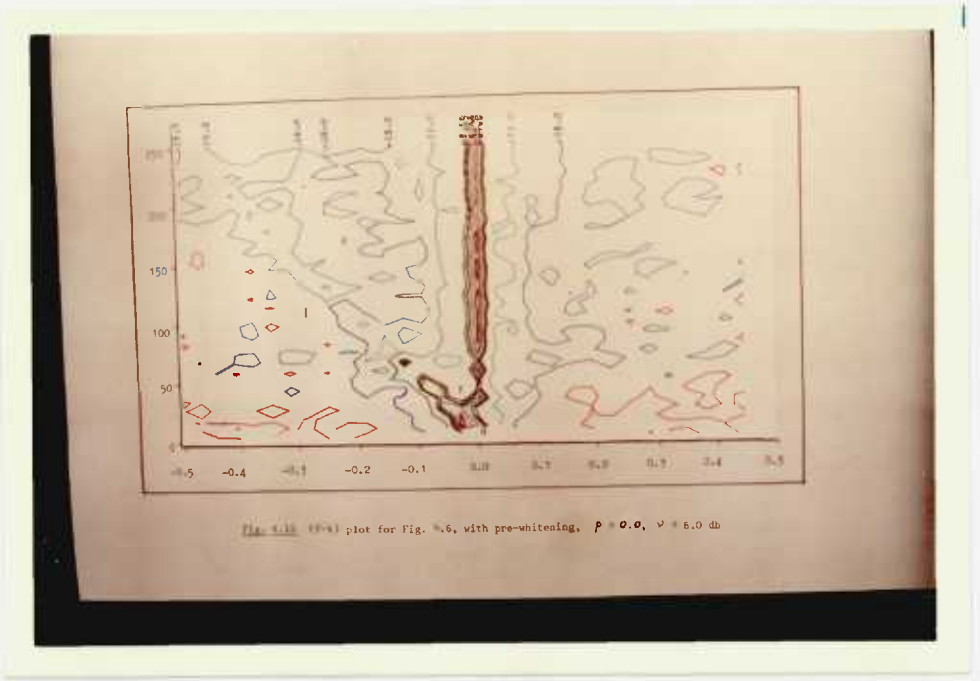


Fig. 4.15 (f-k) plot for Fig. 4.6, with pre-whitening, $P = 0.0$, $\nu = 6.0$ db

Fig. 4.15 (f-k) plot for Fig. 4.6, with pre-whitening, $P = 0.0$, $\nu = 6.0$ db

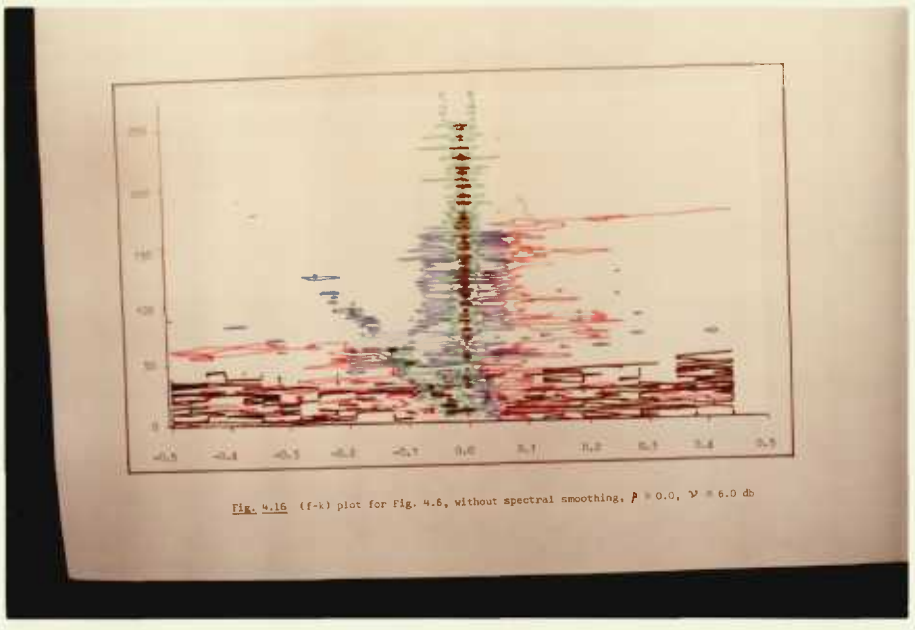


Fig. 4.16 (f-k) plot for Fig. 4.6, without spectral smoothing, ρ = 0.0, ν = 6.0 db

correlated noise are of the same power, the signal shows up rather more clearly. The reason for this is two-fold - (i) there is more signal than correlated noise at high frequency, in the synthetic data, to benefit from the pre-whitening boost, and (ii) the spectral smoothing takes place parallel to the frequency axis, hence the average of spectral values parallel to the frequency axis and within the smoothing "window" will be greater than that for values oblique to this window. The Fourier Transform for the input data of Fig. 4.10, data for which the Butterworth wavelets for signal and correlated noise were the same, is presented as Fig. 4.17. As expected, the relative difference between signal and correlated noise (on the basis of pre-whitening) is now less, evidence of this noise being found as high as the Nyquist frequency. The fragmentary appearance of the correlated noise lobe, due to the spectral smoothing process, is also well in evidence.

From now on, all Fourier Transform plots are shown with pre-whitening and spectral smoothing having been applied.

An example of "fold-over" at the Nyquist wavenumber is given by Fig. 4.18, the Fourier Transform of the input data of Fig. 4.7. This data contains two correlated noise events, the one of signal to correlated noise power ratio of 0.0 db and moveout 1 sample per trace, and the other that of -9.0 db and moveout 2 samples per trace. The observed fold-over is produced by the latter event, a result that may be compared to Fig. 4.2. More on this plot will be said later on in this chapter.

From earlier discussion, one would expect a lower contribution from random noise as the record length was increased. Fig. 4.19 shows the Fourier Transform for the input data of Fig. 2.10 (record length of 250 samples), and Fig. 4.20 that for the same noise conditions ($P = 0.0$, $\nu = 0.0$ db) but a record length of 450 samples. Comparison of these results show that a general lowering of the background random

noise has taken place in Fig. 4.20, as expected, leading to a better moveout determination for the correlated noise.

This section has demonstrated several of the points raised in earlier discussion, namely (i) the importance of pre-whitening the input data before taking the Fourier Transform, (ii) the importance of smoothing the spectral values before plotting the Transform, (iii) the occurrence of fold-over at the wavenumber boundary for events of moveout greater than 1 sample per trace, and (iv) the better cancellation of random noise due to increasing record length.

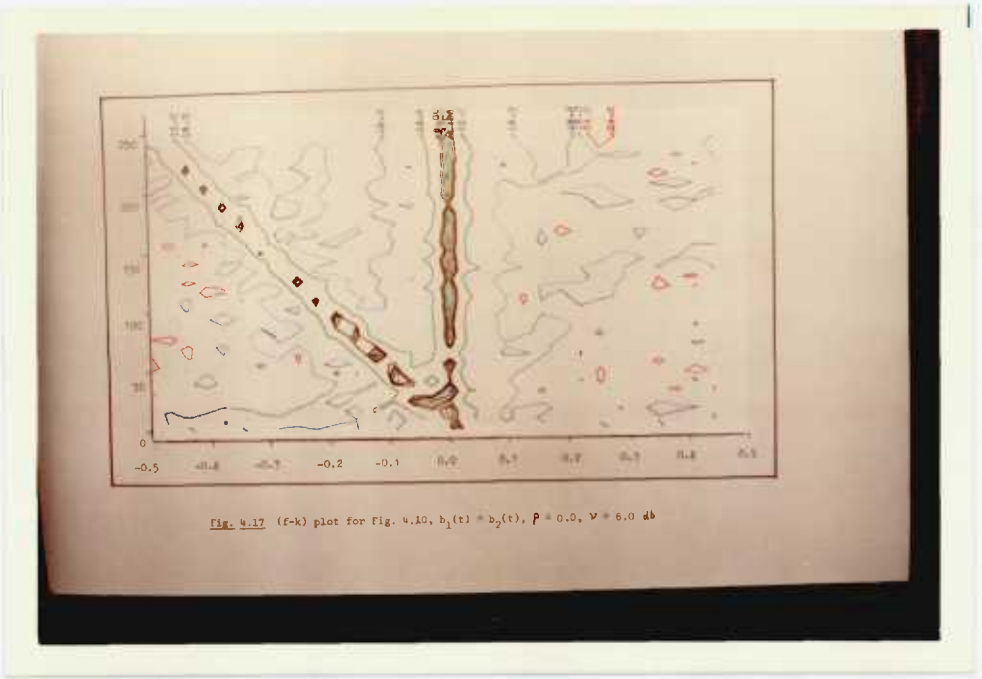


Fig. 4.17 (f-k) plot for Fig. 4.10, $b_1(t) = b_2(t)$, $\rho = 0.0$, $\nu = 6.0$ db

Fig. 4.17 (f-k) plot for Fig. 4.10, $b_1(t) = b_2(t)$, $\rho = 0.0$, $\nu = 6.0$ db

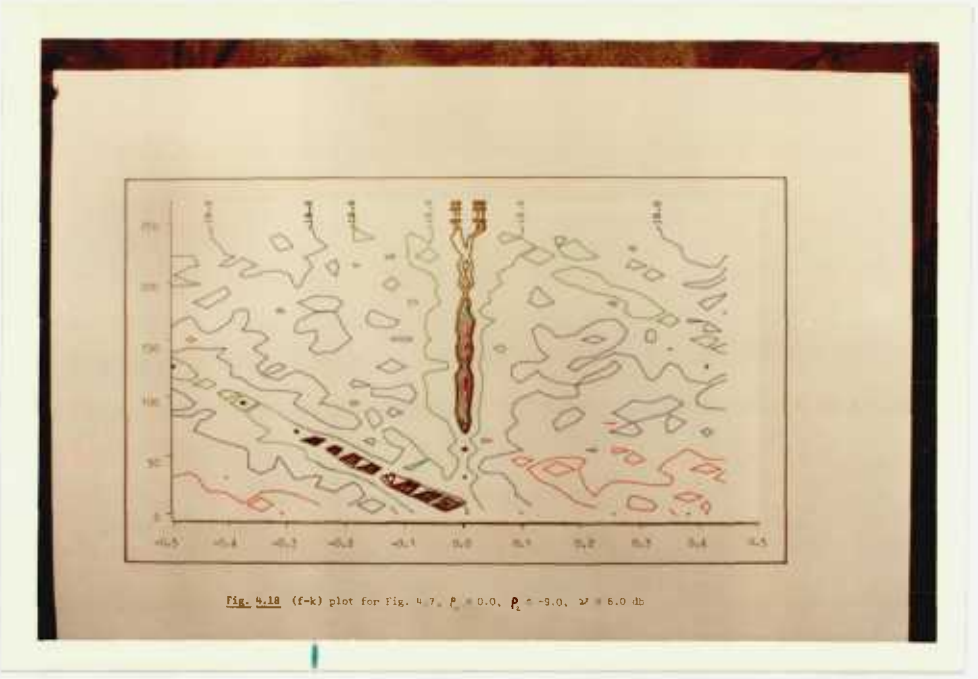


Fig. 4.18 (f-k) plot for Fig. 4.7, P_1 = 0.0, P_2 = -9.0, ν = 6.0 db

Fig. 4.18 (f-k) plot for Fig. 4.7, P_1 = 0.0, P_2 = -9.0, ν = 6.0 db

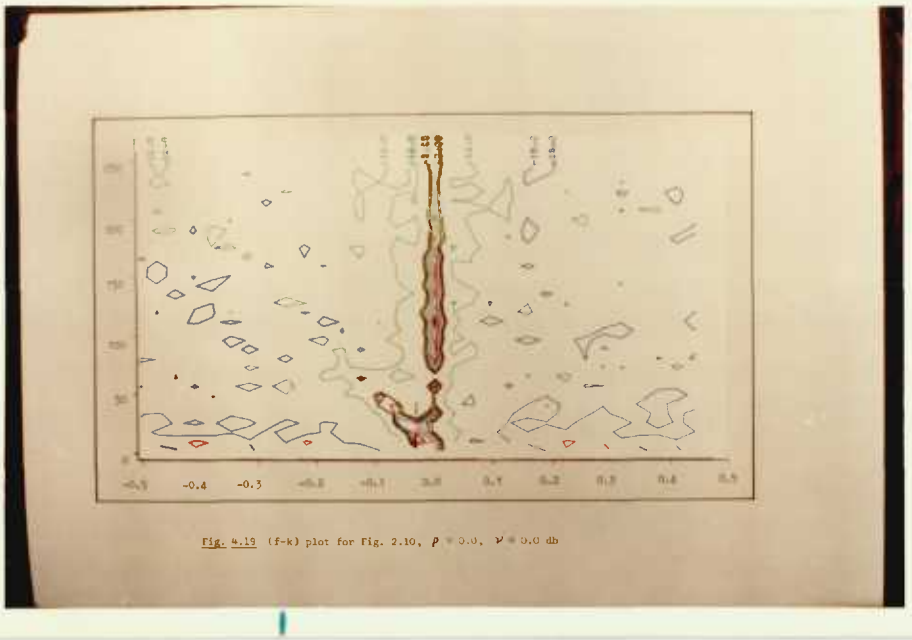


Fig. 4.19 (f-k) plot for Fig. 2.10, ρ = 0.0, ν = 0.0 db

Fig. 4.19 (f-k) plot for Fig. 2.10, ρ = 0.0, ν = 0.0 db

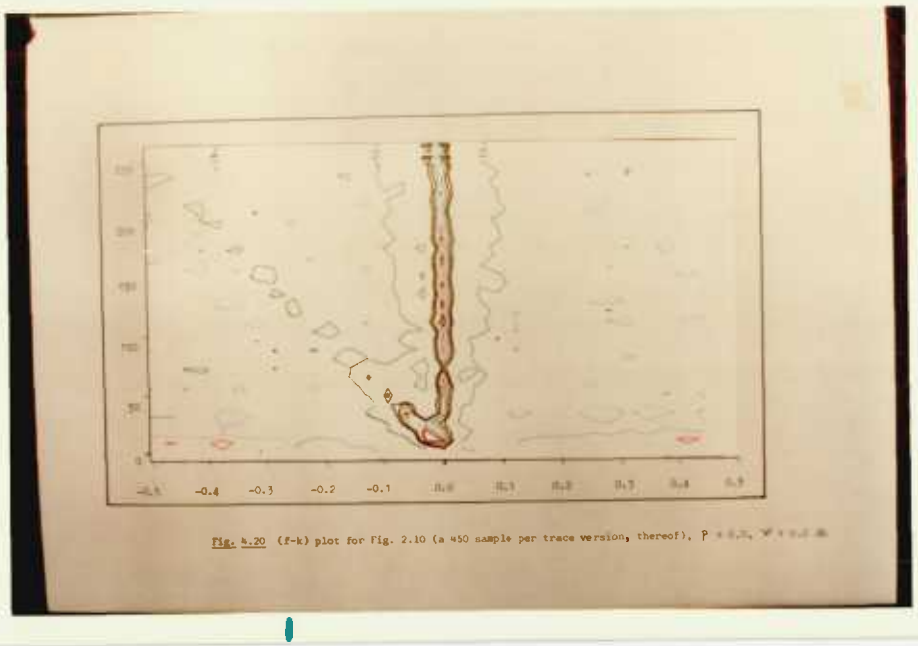


Fig. 4.20 (f-k) plot for Fig. 2.10 (a 450 sample per trace version, thereof),

Fig. 4.20 (f-k) plot for Fig. 2.10 (a 450 sample per trace version, thereof), ρ = 0.0, ν = 0.0 db

4.2.2 effects of different noise levels

Various experiments were performed on records of different signal to noise ratios, but of similar record length and moveout specifications, in order to determine the limitations of the Fourier Transform technique. These results are summarised in Fig. 4.21, where an asterisk * denotes a particular experiment and an encircled asterisk ⊛ denotes a result presented in this thesis. As in the previous chapter, the dashed lines represent "readability contours" derived from a study of the results. The classification of very good, good, poor or bad refers to the relative recovery of the correlated noise event of moveout 1 sample per trace. Discussion on the position of these contours may be found in section 3.2.3.

The performance of the Fourier Transform method for detecting a constant level of correlated noise, in a background of increasing random noise, is given by the comparison of Fig. 4.15, Fig. 4.19, Fig. 4.22 and Fig. 4.23. It is seen that the relative difference between the main amplitudes of the correlated noise and the general background noise decreases for increasing random noise level, as expected. The -12.0 db contour of Fig. 4.15, for example, reveals the presence of correlated noise at very high frequency. Differentiation between this contour and the general background is quite good. The next result (Fig. 4.19), however, shows that this differentiation for the -12.0 db contour has now been lost, the required moveout being revealed by the -6.0 db contour at a much lower frequency. The result of Fig. 4.22 shows that the method is now beginning to fail. Although the correlated noise moveout may be seen at 70 c.p.s., it is very doubtful whether one would assign, a priori, a great importance to these peaks. The last result, Fig. 4.23, is quite bad.

The next results, Fig. 4.19, Fig. 4.24 and Fig. 4.25, show the effect of decreasing the correlated noise level in a constant level of random noise. One would expect that the general features of these plots would be the same, except that the amplitudes of the correlated noise

peaks should become smaller. Comparison of these results confirms this view. Comparison of Fig. 4.15 with Fig. 4.26 also shows this expected deterioration.

These results show that the Fourier Transform method works in quite a predictable manner. Lowering the power of correlated noise, for example, leads to a direct reduction in the amplitude of such peaks in the f-k plane. This gives the Fourier Transform method a degree of "feel" that was not so apparent in the autocorrelation matrix method. A more meaningful relationship, therefore, can be established between the experimental design and the final result.

A general comparison of the f-k plots with their respective input records, for example, comparing Fig. 4.19 with Fig. 2.10, shows an overall improvement in the detection of the correlated noise event, without the necessary application of a multichannel filter to the input data. The Fourier Transform method has also shown to be of particular relevance to the detection of signal in a high background of random noise. Fig. 4.22, for example, clearly shows the presence of signal, whereas no such indication could be evinced from the input record of Fig. 2.12. A similar comparison may also be made between Fig. 4.27 and Fig. 2.4.

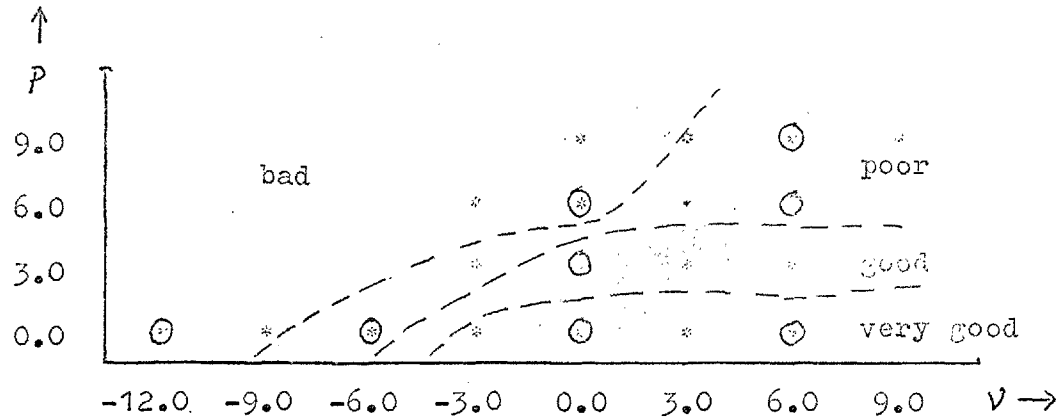


Fig. 4.21 Map of experiments conducted on synthetic data

An encircled asterisk ⊛ denotes a result presented in the thesis, a plain asterisk denotes a result not presented in the thesis.

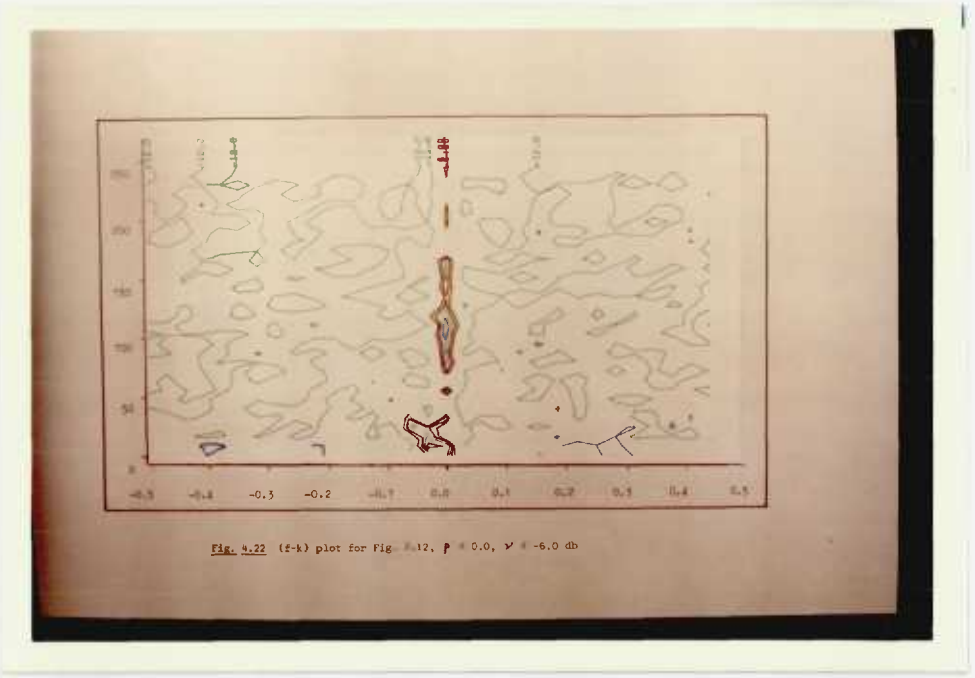


Fig. 4.22 (f-k) plot for Fig. 2.12, ρ = 0.0, ν = -6.0 db

Fig. 4.22 (f-k) plot for Fig. 2.12, ρ = 0.0, ν = -6.0 db

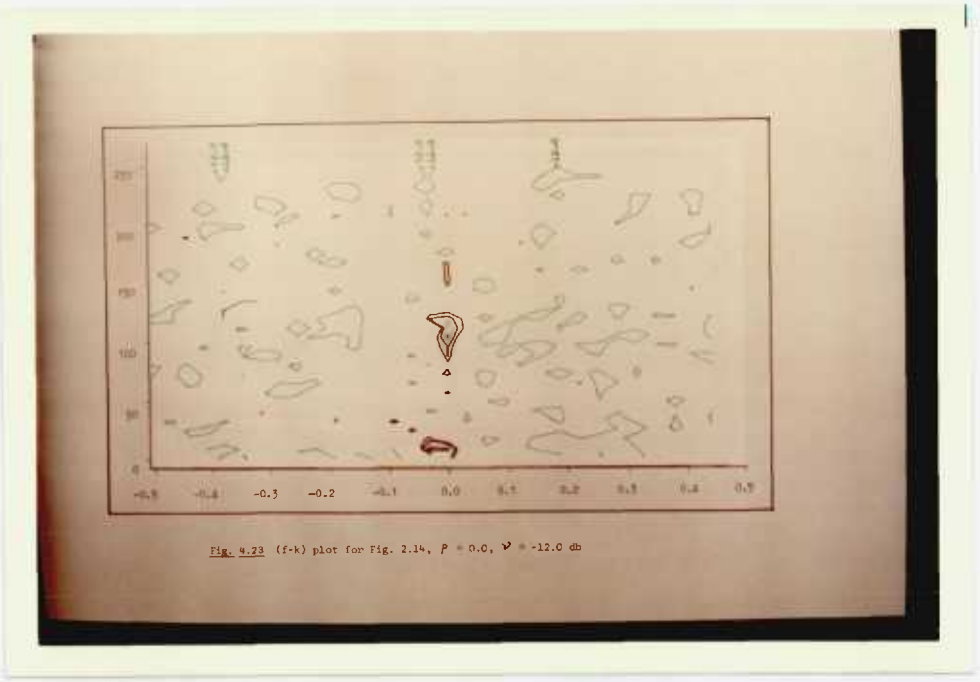


Fig. 4.23 (f-k) plot for Fig. 2.14, ρ = 0.0, ν = -12.0 db

Fig. 4.23 (f-k) plot for Fig. 2.14, ρ = 0.0, ν = -12.0 db

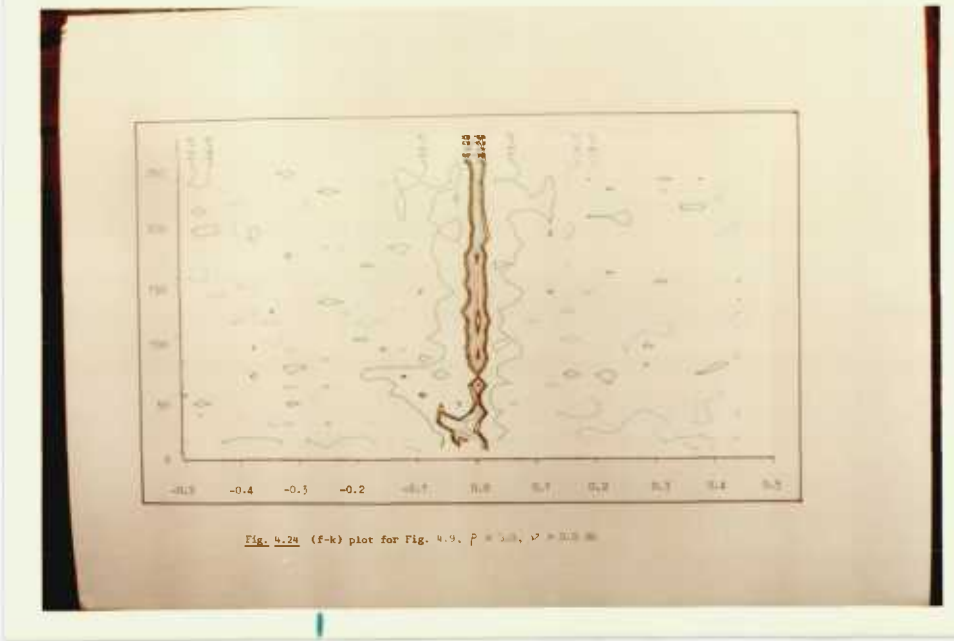


Fig. 4.24 (f-k) plot for Fig. 4.9, ρ = 3.0, γ = 0.0 db

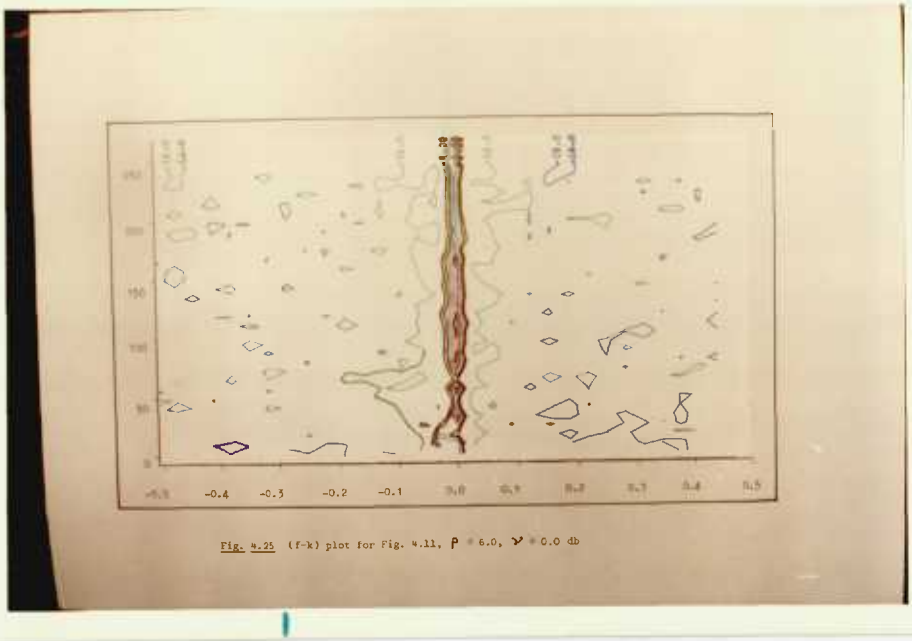


Fig. 4.25 (f-k) plot for Fig. 4.11, ρ = 6.0, ν = 0.0 db

Fig. 4.25 (f-k) plot for Fig. 4.11, ρ = 6.0, ν = 0.0 db

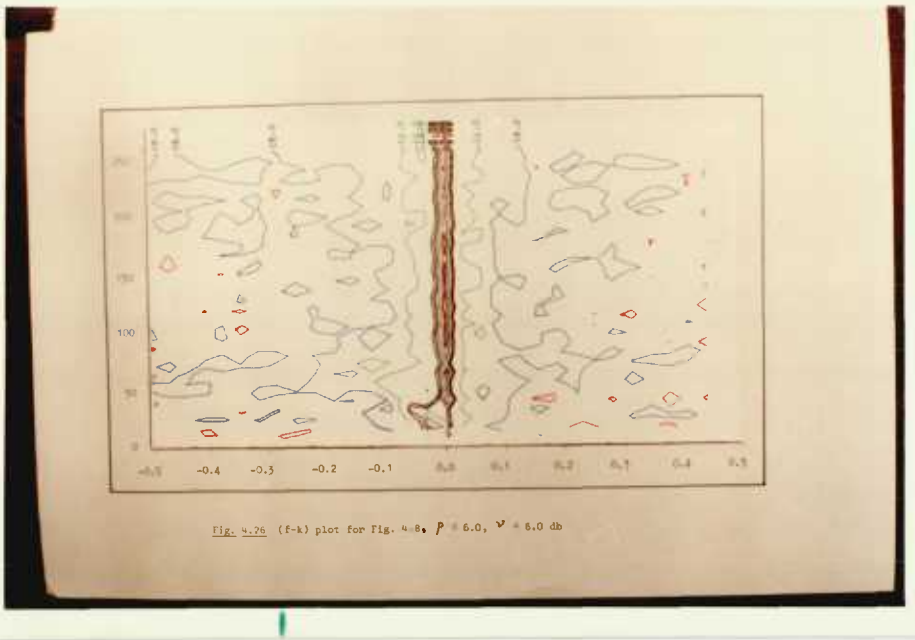


Fig. 4.26 (f-k) plot for Fig. 4.8, ρ = 6.0, ν = 6.0 db

Fig. 4.26 (f-k) plot for Fig. 4.8, ρ = 6.0, ν = 6.0 db

4.2.2.1 analysis of synthetic records of quadratic moveout

An inherent limitation of the Fourier Transform method is that it is only strictly applicable to the analysis of events of linear moveout. Since real data records contain a number of events of non-linear moveout, it will be instructive to investigate the appearance of the f-k plane for events of quadratic moveout.

A comparison of two results, for input data of the same signal to noise ratios but the one with linear moveout and the other with quadratic moveout, is given by Fig. 4.27 and Fig. 4.28, respectively. The latter result reveals several interesting features. The general appearance of this plot would suggest, at first sight, the presence of a linear correlated noise event of moveout 1.3 samples per trace. However, a closer study of this result, together with the earlier results for linear moveout, show that the degree of resolution and line up of coherent energy is not as good as one would expect for linear moveout. The appearance of the -12.0 db contour, for example, shows three distinct lobes - a feature that was not observed in the earlier plots for one correlated noise event. One may conclude, therefore, that the Fourier Transform has "tried" to approximate the quadratic moveout by a succession of linear moveouts, and has presented the final result as a conglomeration of these linear moveouts.

This leads to a certain ambiguity in the interpretation of a Fourier Transform result. Fig. 4.18 shows the Fourier Transform for data that possesses two correlated noise events, both of which are visible in the Transform. On this basis, therefore, it is difficult to determine whether the result of Fig. 4.28 was derived from data of quadratic moveout, or from data that genuinely contained more than one event of correlated noise. However, this is a somewhat artificial example in that a study of the respective input records would clearly reveal whether the data for Fig. 4.28 was linear or quadratic. This merely illustrates the necessity for considering each plot in relation to the data that created it.

Fig. 4.29 shows the Fourier Transform for the input data of Fig. 2.28. Comparison of this result with Fig. 4.19 once again shows the possibility of an ambiguous interpretation. Further comparison of these results, however, show that the marked separation between signal and correlated noise is far more pronounced for the linear case than for the quadratic case.

This section has shown that the interpretation of Fourier Transform plots must be effected with great care. One must not only consider the absolute position of major peaks (0.0 - -6.0 db) in the f-k plane, but also the relative position of these peaks both in relation to each other and to the -12.0 db contour. The shape of the -12.0 db contour itself may also be of considerable importance. With these points in mind, the possibility of an ambiguous interpretation is very much reduced.

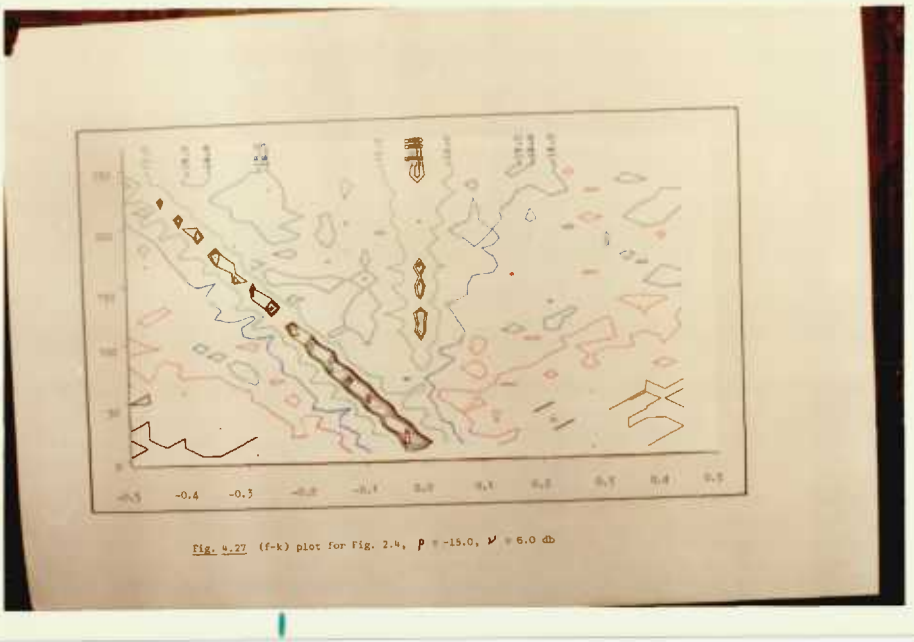


Fig. 4.27 (f-k) plot for Fig. 2.4, ρ = -15.0, ν = 6.0 db



Fig. 4.28 (f-k) plot for Fig. 2.26, P = -15.0, ν = 6.0 db, quadratic moveout

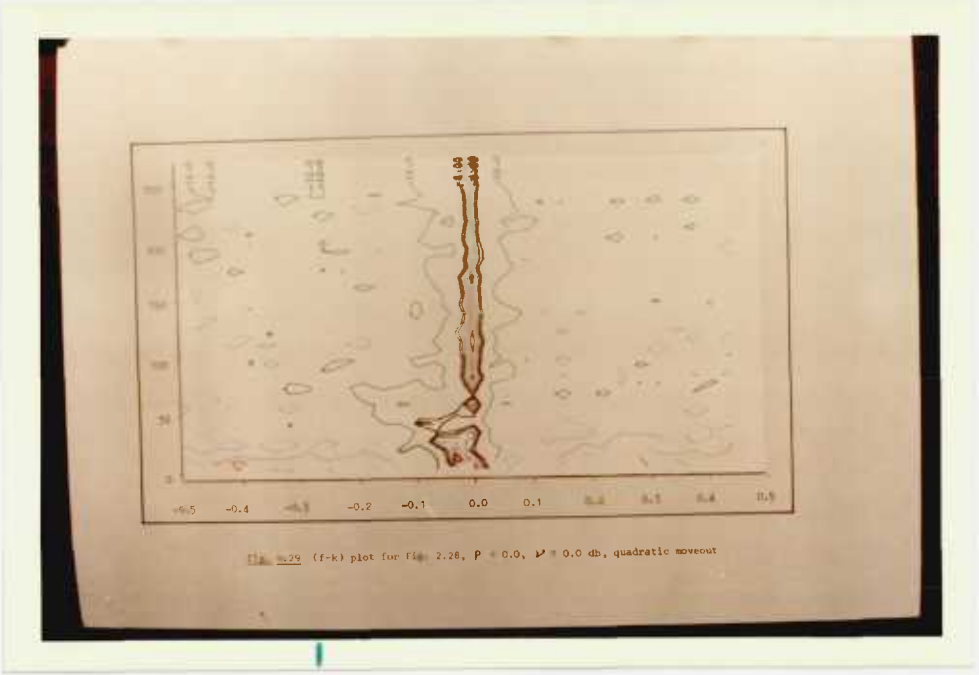


Fig. 4.29 (f-k) plot for Fig. 2.28, ρ = 0.0, ν = 0.0 db, quadratic moveout

4.3 pre-filtering experiments in Fourier analysis

The applicability of the Fourier Transform method is greatly extended by removing the obvious moveouts, from the input record, by a multichannel filter. Fig. 4.30 shows the result of taking the Fourier Transform of the input record of Fig. 2.5, i.e. the input data of Fig. 2.4 filtered by pass/reject filter *PR1. Comparison of this result with that of Fig. 4.27 clearly shows the benefit of the pre-filter.

As before, the possibility of choosing the wrong filter will now be investigated. Fig. 4.31 shows the Fourier Transform for the input record of Fig. 2.22 (Fig. 2.4 filtered by pass/reject filter *PR7), and Fig. 4.32 that for the input record of Fig. 2.23 (Fig. 2.4 filtered by pass/reject filter *PR2). Comparison of these results with Fig. 4.30 clearly show the presence of the correlated noise "missed" by the wrong filter.

One would expect that the general appearance of Fig. 4.30 would be shared by the f-k plots for the input records of Fig. 2.27 and Fig. 2.29, i.e. the quadratic data having been filtered by filter Q. These results are presented as Fig. 4.33 and Fig. 4.34, respectively, where it is seen that the expected similarity is well shown.

The use of a multichannel pre-filter, of course, can help to reduce the ambiguity associated with the interpretation of f-k plots for quadratic data. Even if one had not seen the input record of Fig. 2.26, one would conclude from a comparison of Fig. 4.33 with Fig. 4.28 that the dominant moveout in the input record was quadratic. Comparison of Fig. 4.34 with Fig. 4.29 would also verify the correct choice of a quadratic pre-filter, for this case.

Finally, one may consider the inverse problem of rejecting the signal and passing the correlated noise. Fig. 4.35 shows the Fourier Transform for the input data of Fig. 4.12. The evidence for the correlated noise event, of movecut 2 samples per trace, is given by the -12.0 db contours. Filtering the data of Fig. 4.12 by reject/pass

filter *RP10 gives the input record of Fig. 4.13, of which the Fourier Transform is presented as Fig. 4.36. It is immediately apparent that the level of correlated noise has been greatly amplified by this process, and that considerable rejection of signal has also taken place. The fact that some signal is still present at high frequency is probably due to a property of the filter.

This section has shown that the application of a multichannel filter to the input data, before commencing the Fourier analysis, can not only extend the power of the method for detecting weak events, but is also useful for the clarification of an otherwise somewhat ambiguous interpretation.

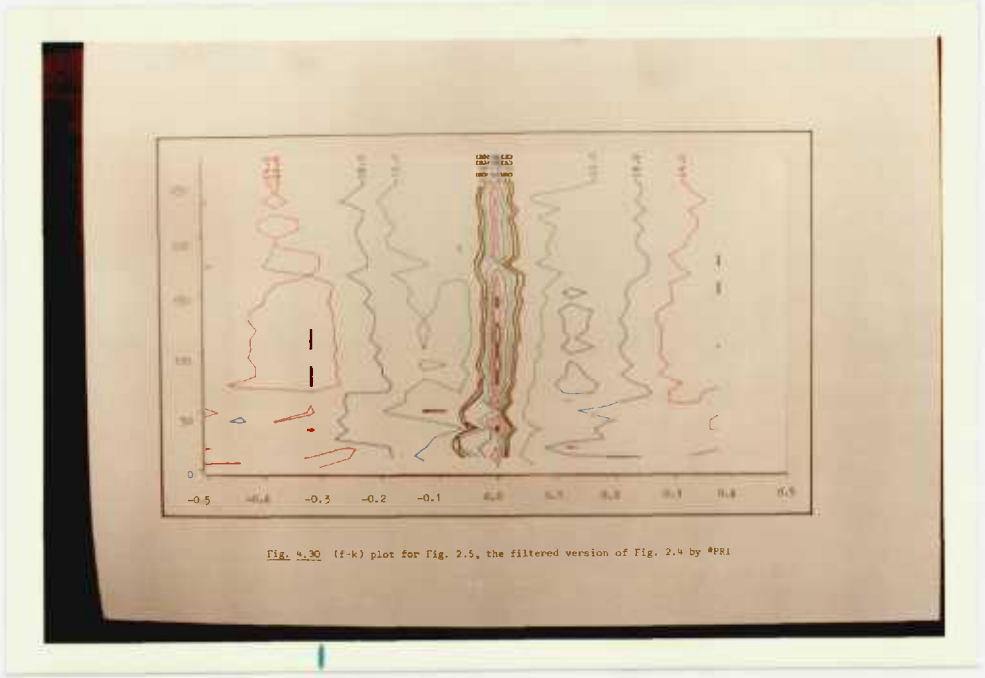


Fig. 4.30 (f-k) plot for Fig. 2.5, the filtered version of Fig. 2.4 by *PR1

Fig. 4.30 (f-k) plot for Fig. 2.5, the filtered version of Fig. 2.4 by *PR1

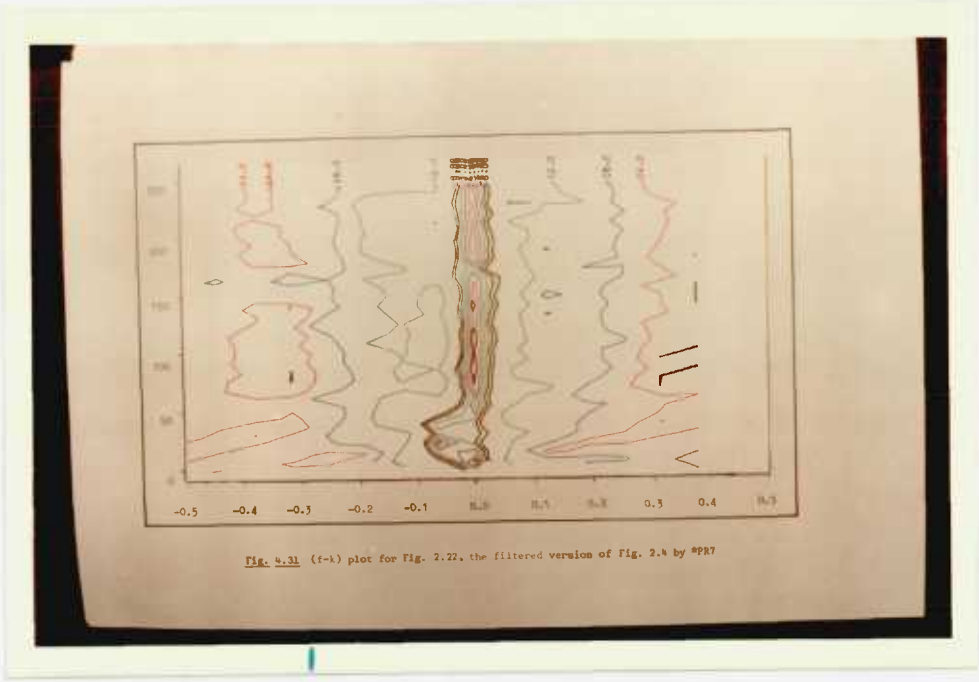


Fig. 4.31 (f-k) plot for Fig. 2.22, the filtered version of Fig. 2.4 by *PR7

Fig. 4.31 (f-k) plot for Fig. 2.22, the filtered version of Fig. 2.4 by *PR7

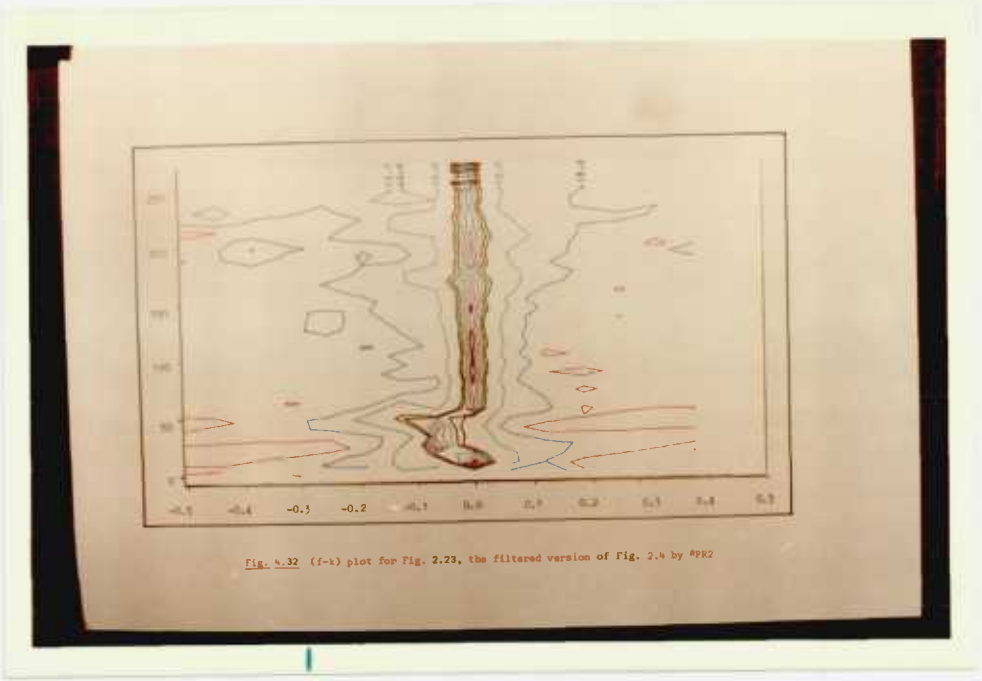


Fig. 4.32 (f-k) plot for Fig. 2.23, the filtered version of Fig. 2.4 by *PR2

Fig. 4.32 (f-k) plot for Fig. 2.23, the filtered version of Fig. 2.4 by *PR2

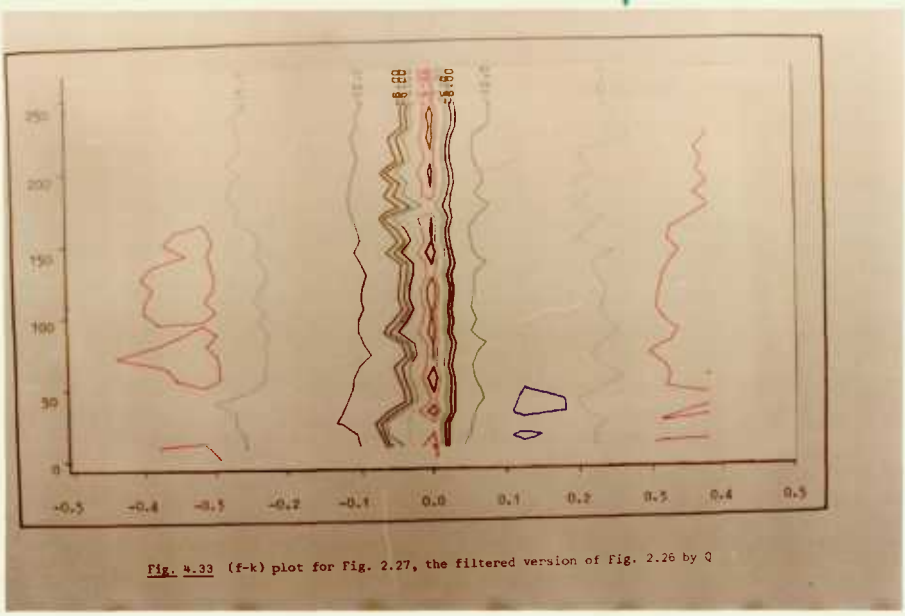


Fig. 4.33 (f-k) plot for Fig. 2.27, the filtered version of Fig. 2.26 by Q

Fig. 4.33 (f-k) plot for Fig. 2.27, the filtered version of Fig. 2.26 by Q

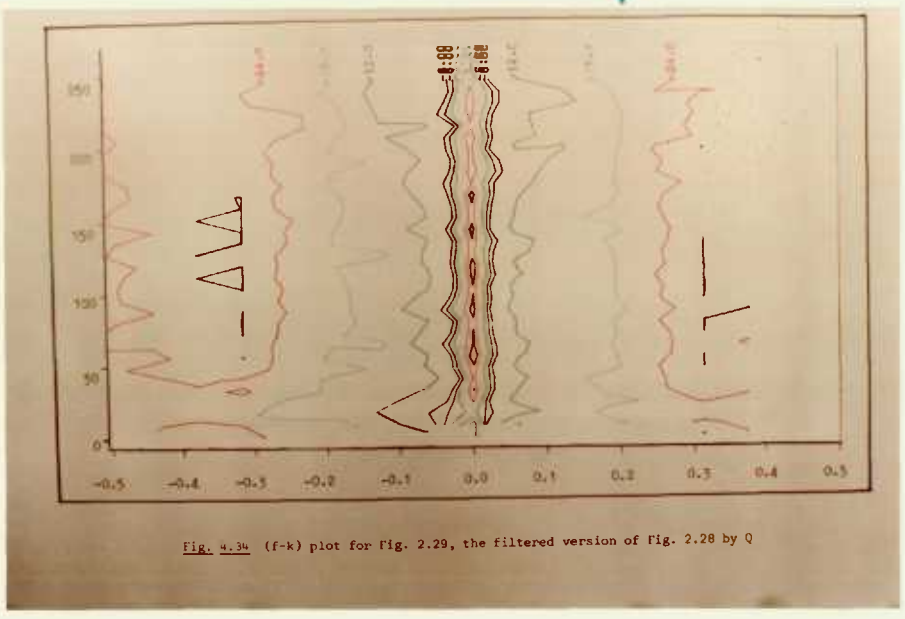


Fig. 4.34 (f-k) plot for Fig. 2.29, the filtered version of Fig. 2.28 by Q

Fig. 4.34 (f-k) plot for Fig. 2.29, the filtered version of Fig. 2.28 by Q

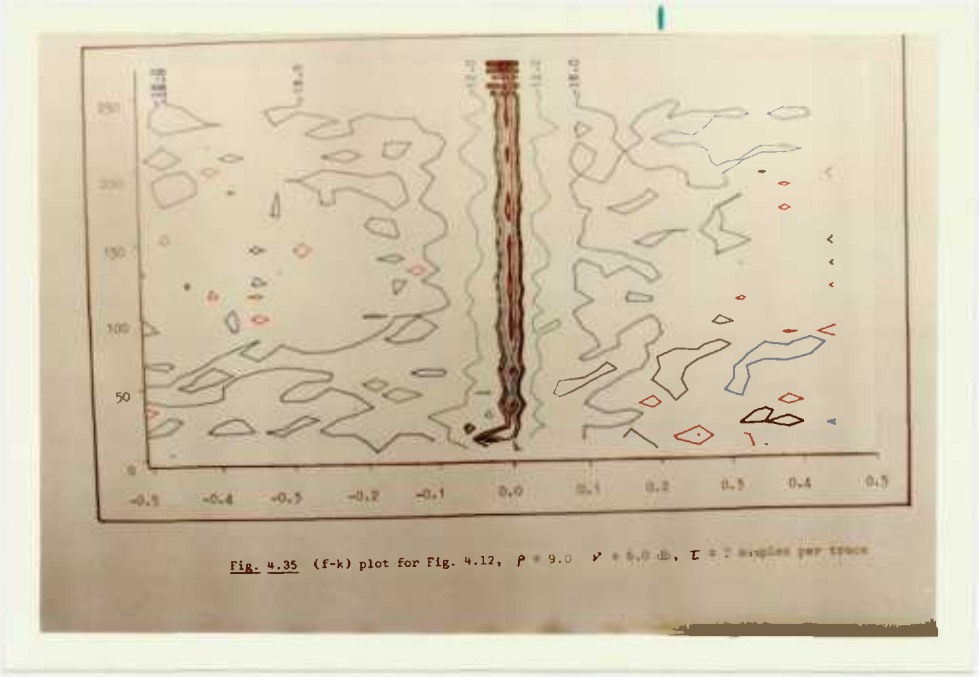


Fig. 4.35 (f-k) plot for Fig. 4.12, ρ = 9.0 ν = 6.0 db, τ = 2 samples per trace

Fig. 4.35 (f-k) plot for Fig. 4.12, ρ = 9.0, ν = 6.0 db, τ = 2 samples per trace

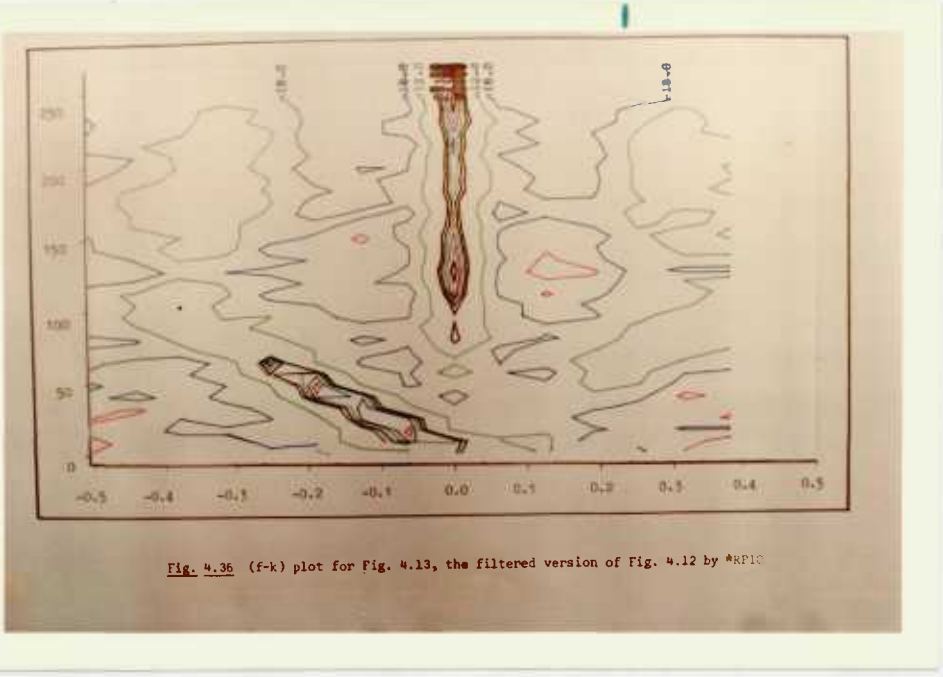


Fig. 4.36 (f-k) plot for Fig. 4.13, the filtered version of Fig. 4.12 by *RP10

Fig. 4.36 (f-k) plot for Fig. 4.13, the filtered version of Fig. 4.12 by *RP10

4.4 Applications to real data

A number of experiments were performed on real data in order to ascertain to what extent the findings from the analyses of synthetic data are applicable to the real case. Two more real data records were necessary for this study, namely Fig. 4.37 (the band pass filtered version of shotpoint 3005, filtered by pass/reject filter Q), and Fig. 4.38 (shotpoint 3001, filtered by reject/pass filter *RP1). An index of the real data experiments is given by Table 4.3. Several difficulties in the comparison of real and synthetic results have been discussed in ealier chapters, and need not be repeated here. The general suitability of the Fourier Transform method for real data is complicated, of course, by the presence of non-linear moveouts.

Fig. 4.39 shows the Fourier Transform of shotpoint 3001 (Fig. 1.1). As expected from a study of the input record, there is strong evidence for a signal of zero moveout and a suggestion of correlated noise. Fig. 4.40 shows the Fourier Transform of the filtered data from Fig. 4.38. This result shows considerable rejection of the signal, with some indication for a correlated noise event of moveout 1 sample per trace.

Fig. 4.41 and Fig. 4.42 show the effect, in the f-k plane, of applying the band pass filter to shotpoint 3002. As expected, the Fourier Transform of the band pass filtered data (Fig. 4.42) shows less evidence of the ground roll. The appearance of the signal on both these plots is rather interesting. This signal possesses a general fragmented and "offset" character, probably due to the presence of events of either quadratic/hyperbolic moveout and/or events of very low linear moveout per trace. Both of these results show the "many-lobed" -12.0 db contour previously encountered in the quadratic moveout case of Fig. 4.28. The final result for this shotpoint, Fig. 4.43, shows the Fourier Transform of the filtered data of Fig. 2.44. This result clearly shows the presence of zero moveout signal, as well as revealing the presence

of high moveout correlated noise missed by the filter. The width of the central lobe of this f-k plane would suggest the presence of very low moveout signal (about a moveout of 0.25 samples per trace).

The presence of very low moveout signals is again demonstrated by a comparison of Fig. 4.44, the Fourier Transform for the data of shotpoint 3003 (Fig. 1.3), with Fig. 4.45, the Fourier Transform of the filtered data of Fig. 2.47. The residual presence of these low moveout events is due to their moveout range being encompassed by that of the "pass" region of the filter. Quite clearly, a narrower pass region would be necessary for their suppression.

The next result, Fig. 4.46, shows the Fourier Transform of shotpoint 3005 (Fig. 1.4). The presence of correlated noise is well established, as is that of some non-linear signal. The Fourier Transform for the filtered version of shotpoint 3005 (Fig. 2.39), is given by Fig. 4.47. Here it is seen that some residual correlated noise is still remaining, with the moveout character of the signal being more faithfully presented. The suspicion that this correlated noise is non-linear may be tested by applying pass/reject filter Q to the input data and computing the Fourier Transform. The result of this presented as Fig. 4.48, where it may be seen that some of the character of this event has been reduced. A more appropriate non-linear filter would propbably achieve a better result.

The last two results, Fig. 4.49 and Fig. 4.50, show the Fourier Transform of shotpoint 3006 (Fig. 1.9, the band pass filtered version), and the filtered version of Fig. 3.74, respectively. The general benefit of this pre-filtering process is immediately apparent.

This section has shown that the results from the analyses of real data are consistent with those of synthetic data. The detection of signal, and the benefit of pre-filtering the data before commencing analysis, were both well demonstrated.

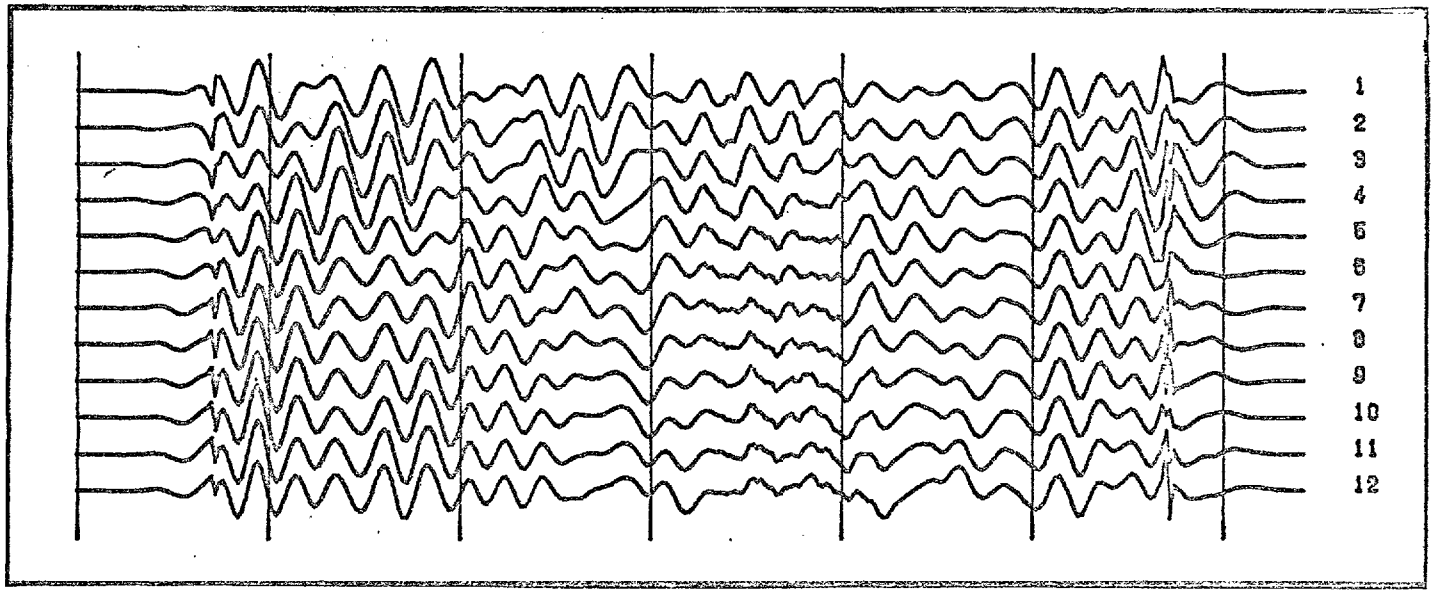


Fig. 4.37 result of filtering Fig. 1.8 with Q

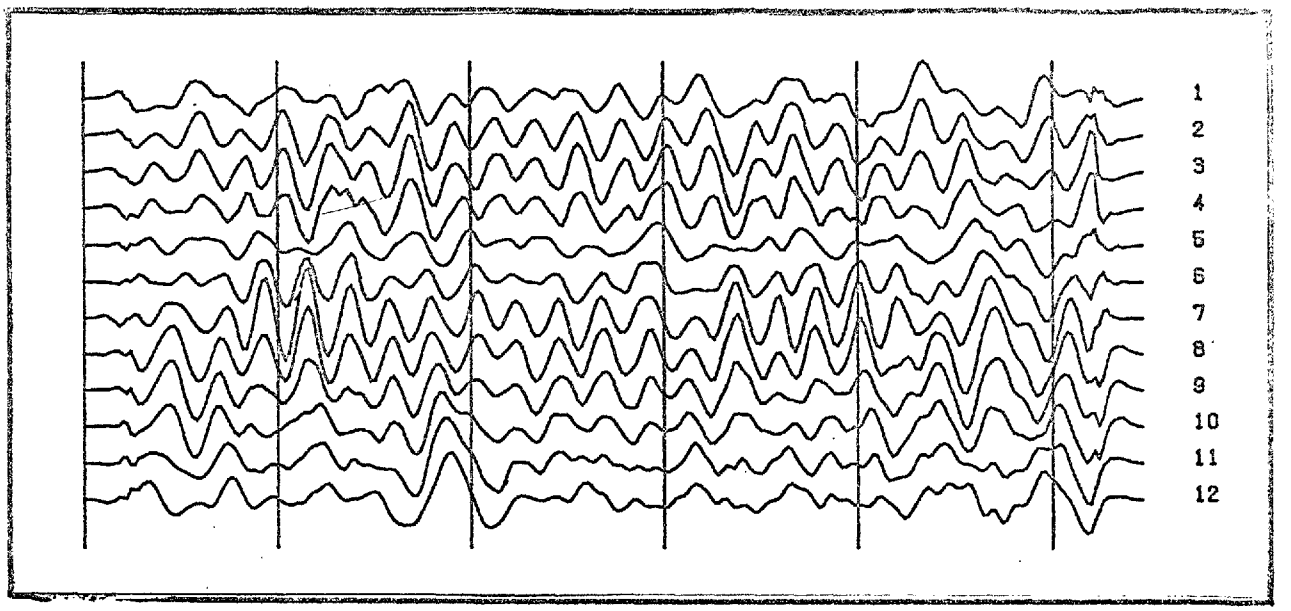


Fig. 4.38 result of filtering Fig. 1.1 with *RP1

shotpoint number	Fig. No. of input record	Fig. No. of (f-k) plot
3001	1.1	4.39
3001	4.38	4.40
3002	1.2	4.41
3002	1.7	4.42
3002	2.44	4.43
3003	1.3	4.44
3003	2.47	4.45
3005	1.4	4.46
3005	2.39	4.47
3005	4.37	4.48
3006	1.9	4.49
3006	3.74	4.50

Table 4.3 Index of Fourier Transform analyses for real data

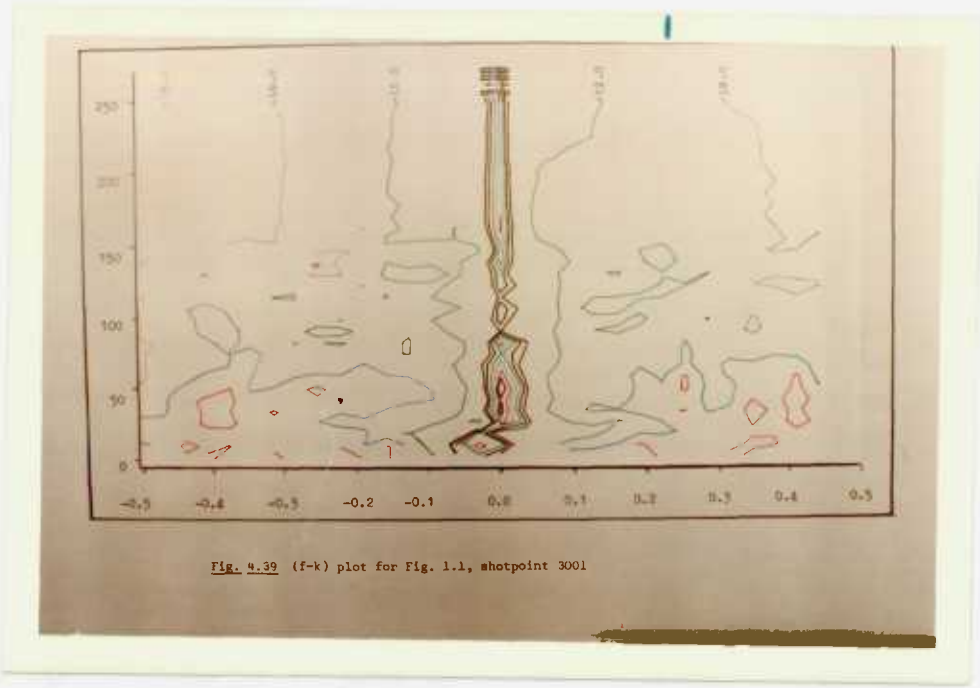


Fig. 4.39 (f-k) plot for Fig. 1.1, shotpoint 3001

Fig. 4.39 (f-k) plot for Fig. 1.1, shotpoint 3001

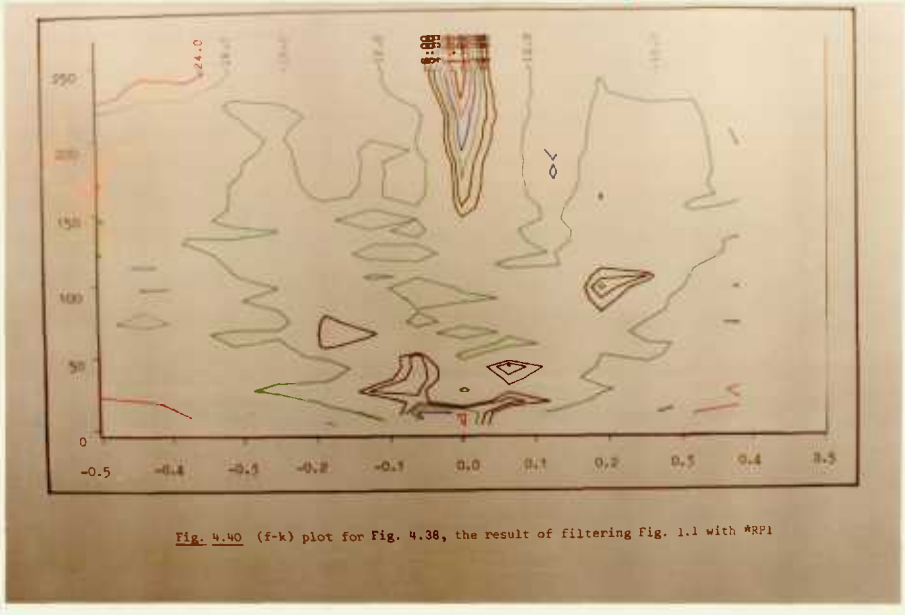


Fig. 4.40 (f-k) plot for Fig. 4.38, the result of filtering Fig. 1.1 with *RP1

Fig. 4.40 (f-k) plot for Fig. 4.38, the result of filtering Fig. 1.1 with *RP1

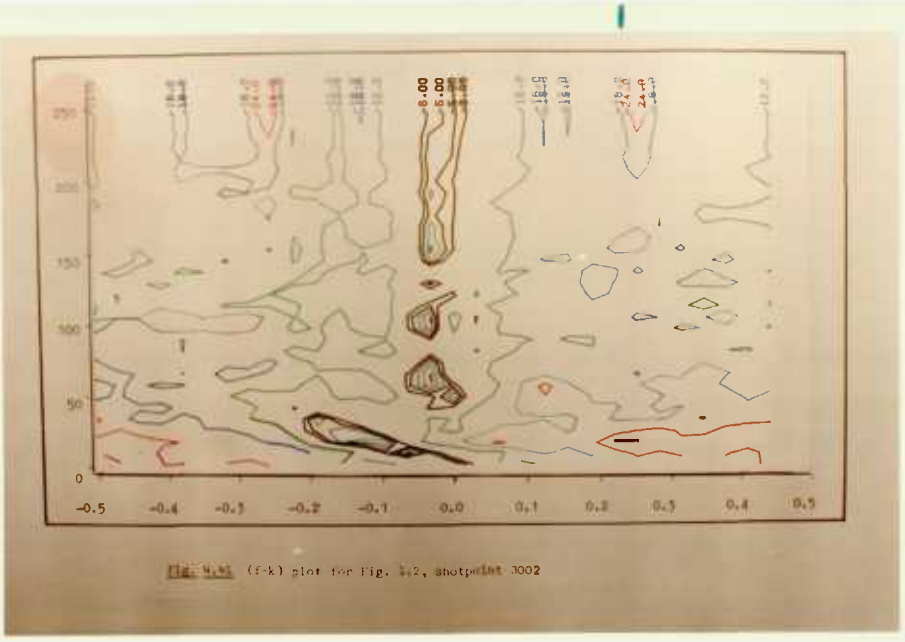


Fig. 4.41 (f-k) plot for Fig. 1.2, shotpoint 3002

Fig. 4.41 (f-k) plot for Fig. 1.2, shotpoint 3002

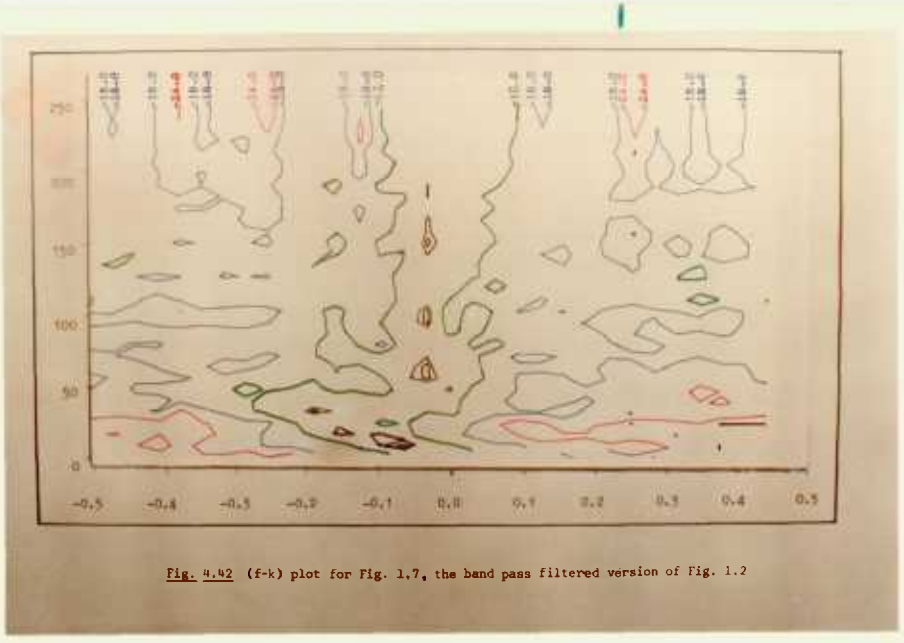


Fig. 4.42 (f-k) plot for Fig. 1.7, the band pass filtered version of Fig. 1.2

Fig. 4.42 (f-k) plot for Fig. 1.7, the band pass filtered version of Fig. 1.2

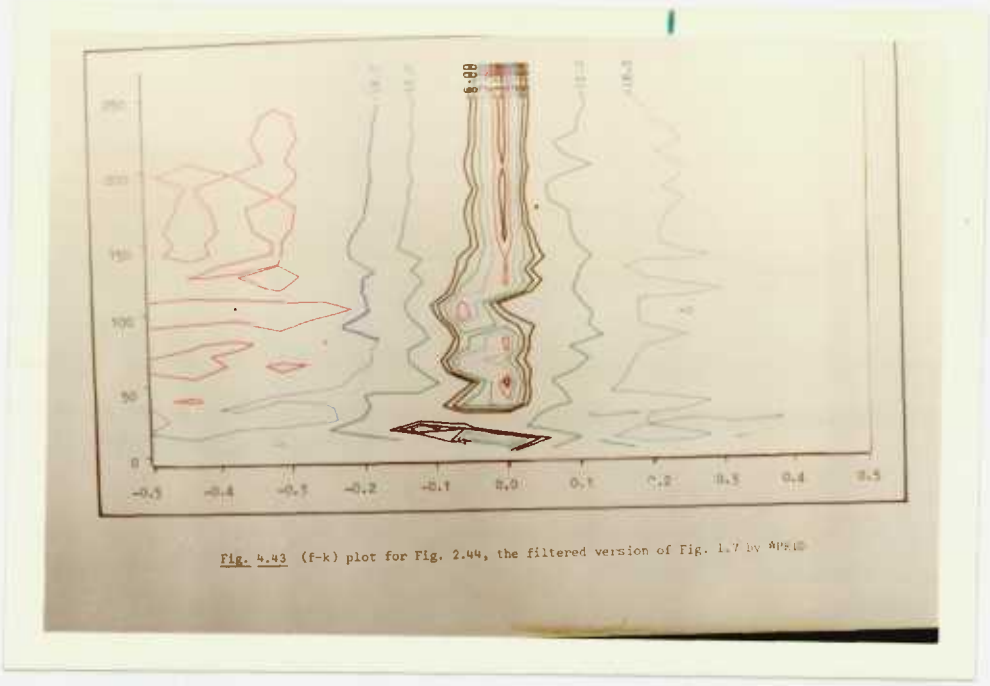


Fig. 4.43 (f-k) plot for Fig. 2.44, the filtered version of Fig. 1.7 by *PR10

Fig. 4.43 (f-k) plot for Fig. 2.44, the filtered version of Fig. 1.7 by *PR10

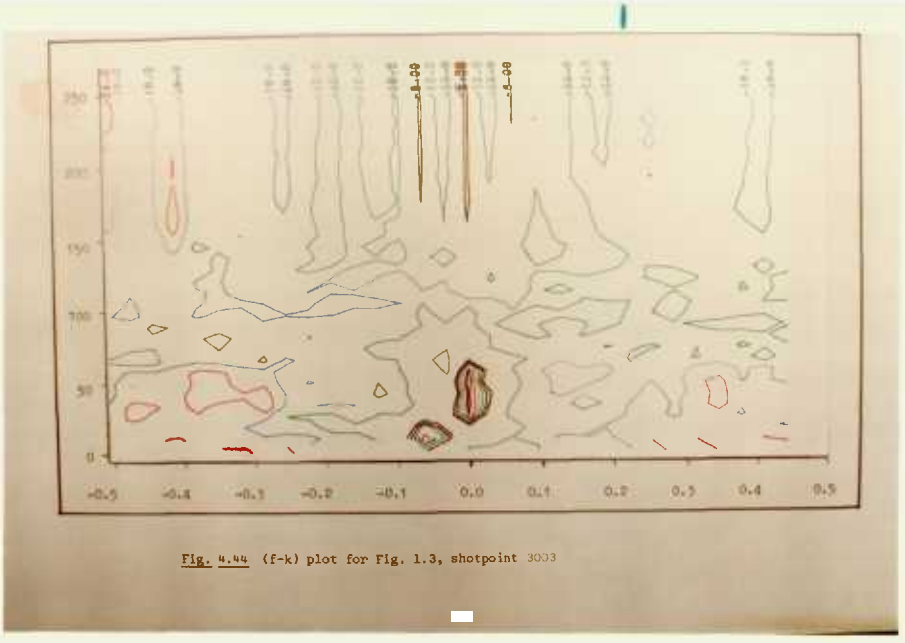


Fig. 4.44 (f-k) plot for Fig. 1.3, shotpoint 3003

Fig. 4.44 (f-k) plot for Fig. 1.3, shotpoint 3003

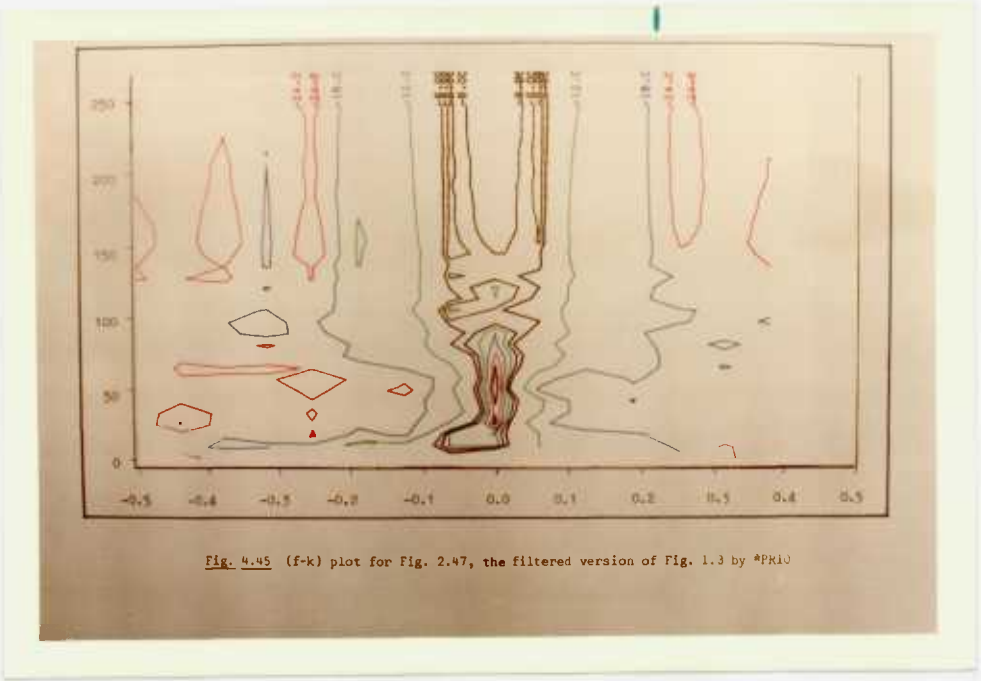


Fig. 4.45 (f-k) plot for Fig. 2.47, the filtered version of Fig. 1.3 by *PR10

Fig. 4.45 (f-k) plot for Fig. 2.47, the filtered version of Fig. 1.3 by *PR10

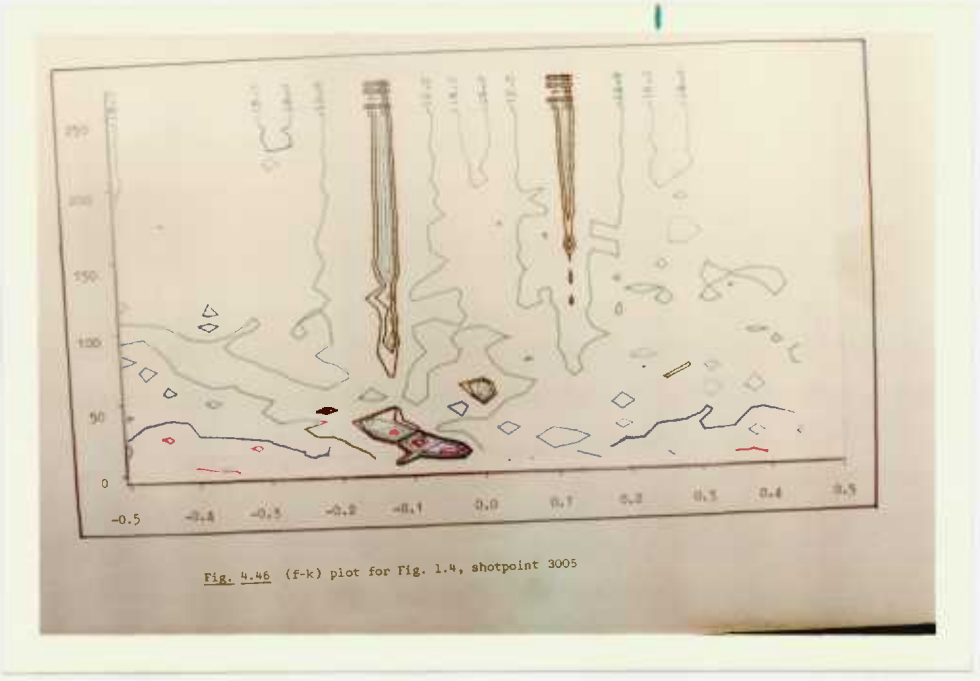


Fig. 4.46 (f-k) plot for Fig. 1.4, shotpoint 3005

Fig. 4.46 (f-k) plot for Fig. 1.4, shotpoint 3005

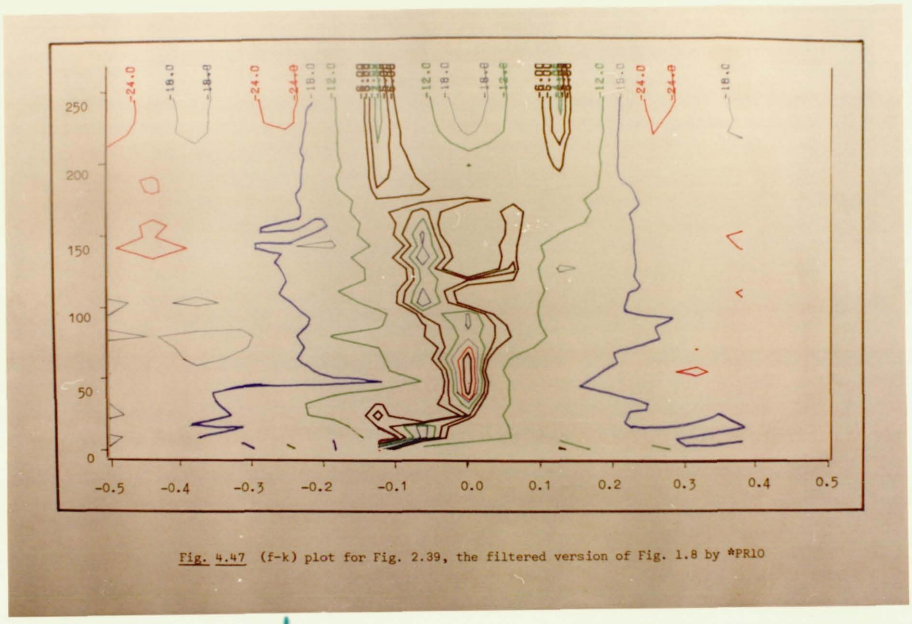


Fig. 4.47 (f-k) plot for Fig. 2.39, the filtered version of Fig. 1.8 by *PR10

Fig. 4.47 (f-k) plot for Fig. 2.39, the filtered version of Fig. 1.8 by *PR10

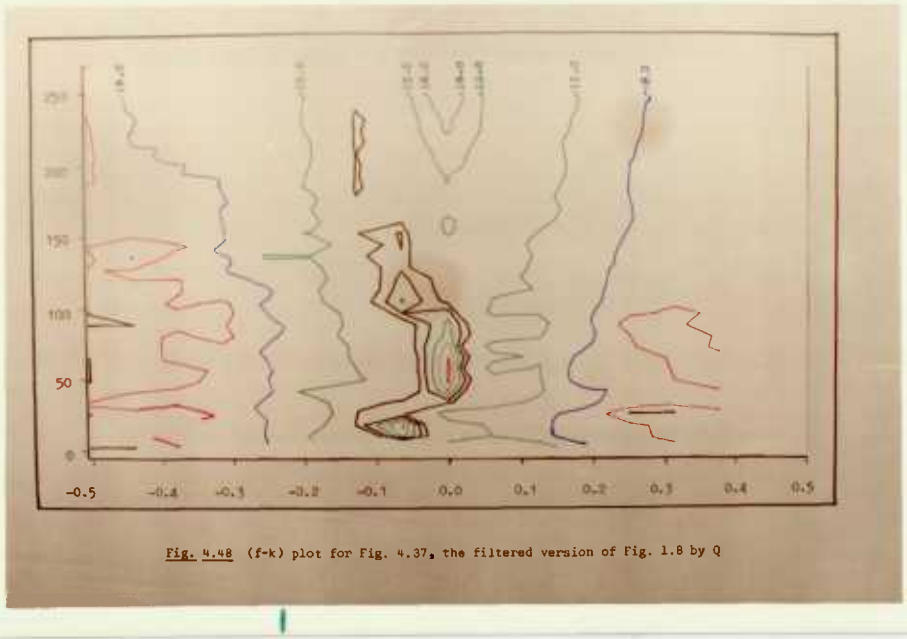


Fig. 4.48 (f-k) plot for Fig. 4.37, the filtered version of Fig. 1.8 by Q

Fig. 4.48 (f-k) plot for Fig. 4.37, the filtered version of Fig. 1.8 by Q

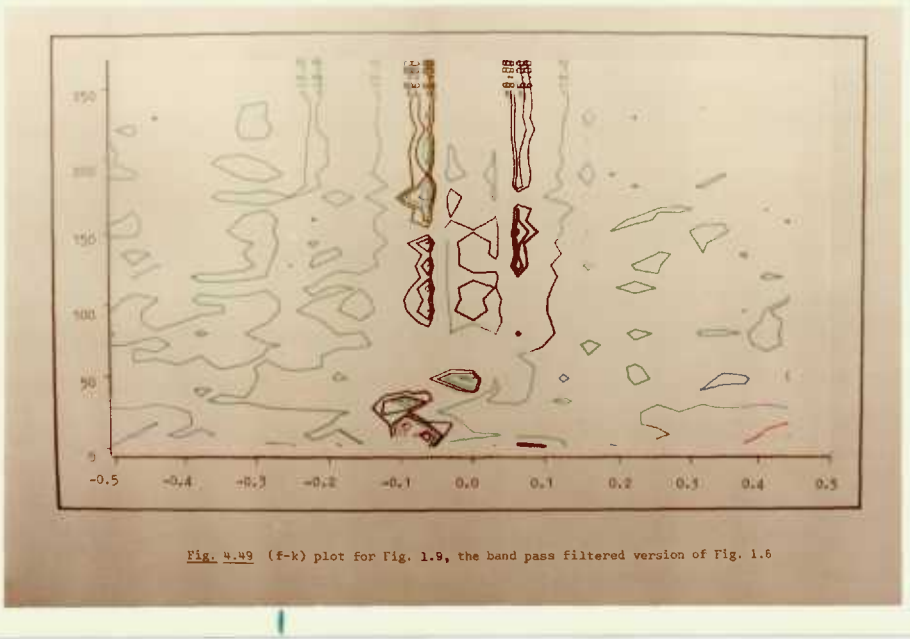


Fig. 4.49 (f-k) plot for Fig. 1.9, the band pass filtered version of Fig. 1.6

Fig. 4.49 (f-k) plot for Fig. 1.9, the band pass filtered version of Fig. 1.6

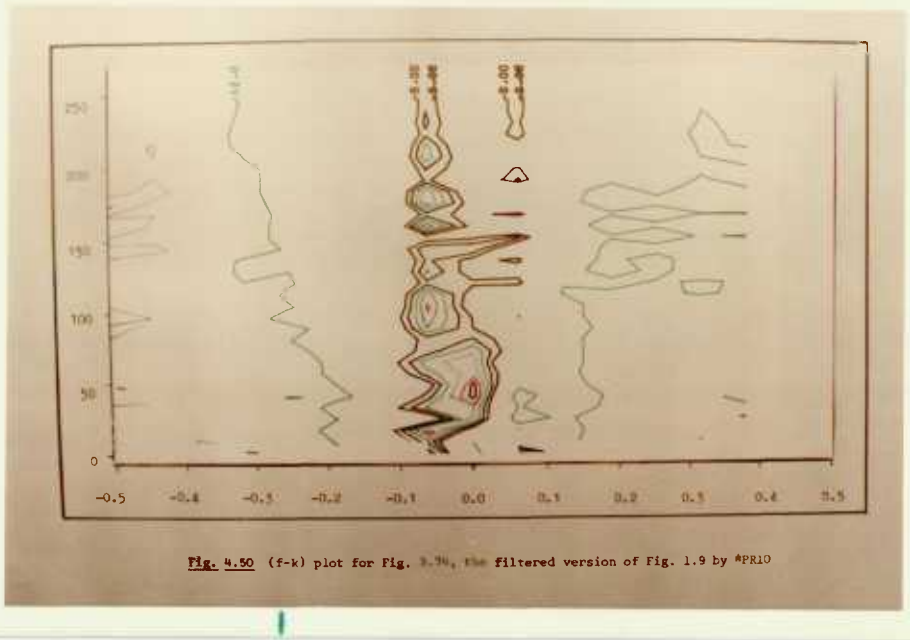


Fig. 4.50 (f-k) plot for Fig. 3.74, the filtered version of Fig. 1.9 by *PR10

Fig. 4.50 (f-k) plot for Fig. 3.74, the filtered version of Fig. 1.9 by *PR10

4.5 Conclusions

The purpose of this chapter was to investigate the application of the discrete two-dimensional Fourier Transform to the analysis of moveout, to this end the following results were obtained :

(a) the benefits of pre-whitening the input data before the taking of the Fourier Transform, and of smoothing the spectral values before the plotting of this Transform, were demonstrated. The appearance of the plots were discussed, and the effect of increasing the record length of one particular example was examined. Due to the direction of the spectral smoothing (parallel to the frequency axis), it is possible that the introduction of a true two-dimensional smoothing "scan" would produce better results for events of non-zero moveout. It would be desirable to rotate the smoothing window about the origin of the f-k plane for a number of different angles, whereupon those correlated events that were fully encompassed by such a window would be suitably "amplified".

(b) the limitations of the Fourier Transform method with regard to the detection of low power correlated events, for different conditions of signal to noise ratio, were investigated for synthetic data records of linear moveout and the results summarised by Fig. 4.21. It was shown that moderate levels of correlated noise could be identified, provided that the background random noise was not too severe. Analysis of synthetic records of quadratic correlated noise moveout showed that an ambiguous interpretation of the f-k plane could result if one were only expecting linear moveouts to be present. To some extent, the Fourier Transform "approximated" a large quadratic curve by a succession of small linear curves, and gave the final result as a conglomeration of these minor curves. Further comparison of quadratic and linear results for records of similar noise conditions, however, revealed some differences that may well be characteristic, namely (i) the separation at low frequency of signal and correlated noise, (ii) the general

appearance of the high contours (0.0 - -6.0 db) and the -12.0 db contour, both with respect to themselves and in relation to each other.

(c) various pre-filtering experiments were conducted, where it was found, as expected, that the application of the method was greatly extended by the removal of obvious moveouts, by a multichannel filter, from the input data. Filtering out the quadratic correlated noise, for example, gave very good results in the f-k plane, thereby affording a technique for reducing the possibility of an ambiguous interpretation. The effects of applying the wrong filter were studied, and the results found to be in general agreement with those of previous chapters.

(d) a number of experiments were conducted on the real data records of earlier chapters. These results were generally consistent with that expected from a study of the synthetic results. The presence of non-linear moveouts caused some difficulty, as did that of very low moveout quasi-linear events. The Fourier Transform of records, before and after band pass filtering, showed very little difference except at low frequency, as expected. The benefit of applying a multichannel pre-filter to the data was again demonstrated, as was the importance of matching the moveouts to be rejected in the data to that of the filter.

A comparison between the Fourier Transform and autocorrelation matrix methods, for synthetic data of different signal to noise ratios, may be effected by comparing Fig. 4.21 with Fig. 3.32. It must be remembered, of course, that the former results do not involve the use of a multichannel filter, whereas the latter results use the multi-channel filter scan of the second order column. Within this context it can be seen that the autocorrelation matrix method is generally more applicable than the Fourier Transform method. If no filtering is allowed, however, the latter method is the more useful.

The presence of non-linear moveouts may favour the use of the autocorrelation matrix method, over the Fourier Transform method, for some cases. None the less it is felt that these two methods should be

seen as analytical tools that can usefully complement each other, rather than being in direct competition. In conclusion, therefore, the Fourier Transform has shown to be a useful addition to the number of tools available for seismic data processing.

CHAPTER 5

CONCLUSIONS AND SUGGESTIONS FOR FURTHER RESEARCH

The basic discussion of results and detailed conclusions have, of course, been given where appropriate in the thesis. It is the purpose of this section to draw together the various themes of this work into one coherent whole.

The purpose of this study was to investigate the auto-correlation matrix and Fourier Transform techniques in relation to the estimation of moveout. From such moveout information it was hoped to establish which multichannel moveout filter, out of a number of possible filters, should be chosen to filter the given input data. To this end the following results were obtained :

(a) The correlation process will generally amplify the presence of any correlated event, be it signal or correlated noise. Consequently, therefore, these events will interfere with one another in the column of the second order autocorrelation matrix, unless a suitable multi-channel filter is applied. It was shown, for synthetic data records, that the use of a multichannel filter scan on this column of the second order autocorrelation matrix could give quite accurate estimates of the required moveout for events of considerably low power. The benefit of applying a multichannel pre-filter to the input data, before commencing the correlation analysis, was also demonstrated on synthetic data. A number of experiments were conducted on real data, the results of which were consistent with that from synthetic data.

(b) The Fourier Transform was shown to be capable of detecting low power correlated events, from synthetic data of linear moveout, particularly if these moveouts were very small. Detection of large moveout correlated energy suffered from the non-alignment of the spectral smoothing window, though good accuracy could still be obtained. No multichannel filter was used in those studies, though the results

were generally not quite so good as those of the autocorrelation matrix method. The later incorporation of a multichannel pre-filter, as in (a), greatly improved the applicability of the method. Results from the analyses of real data records were generally consistent with those of synthetic data.

(c) Much attention was given to a study of the multichannel filters used in the above analyses. It was generally found that good filtered results could only be obtained if the moveouts present in the data were directly comparable to those specified in the filter design. The filtering process was shown to be extremely sensitive to this "moveout-matching", and the application of the wrong filter gave completely poor results. It is important to not only match the moveouts to be passed, but also those to be rejected. Some discussion was given on the number of traces used in the filter design, and to the values assigned to the weighting factors for correlated and uncorrelated noise. The application of a multichannel filter scan to the input record alone, gave good results for both real and synthetic data. For some of these cases, in fact, no further analysis may be necessary.

In conclusion, it has been shown that in order to ascertain which filter shall be used on a given input record, an autocorrelation matrix analysis and/or a Fourier Transform analysis may well yield the required information. Considerable sensitivity in moveout selection can be obtained by the use of these methods, and it is to be hoped that they will find suitable application in seismic data processing.

To finally conclude this work, some areas in which further research may be pursued are given below :

(i) A study of the problems in multichannel filter design. To some extent this was covered by Hubral (1970), but more work should be done on the problems of filter stability and filter performance. A comprehensive comparative study of different filters, in both the time and frequency domains, could well be of interest. Of particular

importance is the development of multichannel filters that give the same number of output traces as there are input traces.

(ii) A variable angle spectral smoothing scheme, for use in the f-k plane, should be developed in order to fully recover correlated energy of non-zero moveout.

(iii) The development of the multichannel filter scan of the second order autocorrelation matrix column computed from pre-filtered input data. As mentioned in Chapter 3, this depends upon the successful design of the many output trace multichannel filter of part (i) above.

(iv) For the analysis of large volumes of data it would be useful to produce output tapes that could be played back on, say, a drum plotter, so that "variable area" displays could be obtained in addition to the existing "wiggle trace" presentation.

ACKNOWLEDGEMENTS

The author would like to take this opportunity to thank his colleagues in the Geophysics Data Processing Group of the Imperial College, for many helpful ideas and discussions. In particular, the author would like to thank his supervisor, Dr. B. P. Dash, and his colleague, Dr. J. W. Curtis, for reading the manuscript and making general helpful comments.

A great debt of thanks is due to Mr. J. W. J. Hosken, of British Petroleum (Sunbury), for the provision of the real data, some of the subroutines and for much technical advice.

The author would also like to extend a vote of thanks to the Imperial College Computer Centre for the use of their facilities, and in particular to Mr. S. Budd, of the Programme Advice Unit, for helping to smooth out some of the computing difficulties.

Last, but not least, the author would like to acknowledge the support given by the Natural Environment Research Council, who provided the finance for this project.

REFERENCES

(GP = Geophysical Prospecting, G = Geophysics)

J. Bendat, A. Piersol (1966), Measurement and analysis of random data (Wiley).

R. Blackman, J. Tukey (1958), The measurement of power spectra from the point of view of communications engineering (Dover).

R. Bracewell (1965), The Fourier transform and its applications (McGraw-Hill).

J. Cooley, J. Tukey (1965), An algorithm for the machine calculation of complex Fourier series (Math. Computation, Vol 19, pp 297-301).

J. Cooley et al. (1967)

(a) What is the Fast Fourier Transform?

(b) Modern techniques of power spectrum estimation.

(c) The use of the Fast Fourier Transform for the estimation of power spectra.

(d) Historical notes on the Fast Fourier Transform.

(IEEE Transactions on Audio and Electronics, Vol 15, No.2)

B. P. Dash, K. Obaidullah (1970), Determination of signal and noise statistics using correlation theory (G, Vol 35, pp 24-32).

E. Davies, E. Mercado (1968), Multichannel filtering of field recorded seismic data (G, Vol 33, pp 711-722).

S. Deregowski (1971), Optimum digital filtering and inverse filtering in the frequency domain (GP, Vol 19, pp 729-768).

J. Galbraith, R. Wiggins (1968), Characteristics of optimum multichannel stacking filters (G, Vol 33, pp 36-48).

I. Finetti, R. Nicolich, S. Sancin (1971), Review on the basic theoretical assumptions in seismic digital filtering (GP, Vol 19, pp 292-320).

M. Hinich, C. Clay (1968), Application of the discrete Fourier transform in the estimation of power spectra, coherence, and bispectra of geophysical data (Reviews of Geophysics, Vol 6, pp 347-363).

P. Hubral (1970), Ph.D. thesis, London University.

Y. Lee (1960), Statistical theory of communication (Wiley).

N. Levinson (1947), The Wiener RMS error criterion in filter design and prediction (J. Math. Physics, Vol 25, pp 261-278).

J. Lindsey (1970), The potential of digital seismic recordings for multichannel processing (G, Vol 35, pp 461-470).

A. Papoulis (1965), Probability, random variables and stochastic processes (McGraw-Hill).

E. Robinson (1957), Predictive decomposition of seismic traces (G, Vol 22).

E. Robinson, S. Treitel (1964), The stability of digital filters (IEEE Transactions of Geoscience Electronics, GE-2, No.1).

E. Robinson (1967a), Multichannel time series with digital computer programs (Holden-Day).

E. Robinson (1967b), Statistical communication and detection, with special reference to digital data processing of radar and seismic signals (Griffin).

E. Robinson (1967c), Predictive decomposition of time series with application to seismic exploration (G, Vol 32, pp 418-484).

E. Robinson, S. Treitel (1967), Principles of digital Wiener filtering (GP, Vol 15, pp 311-333).

J. Robinson (1968), Noise attenuation on common-depth-point seismic records by a semideterministic approach (G, Vol 33, pp 723-733).

J. Robinson (1969), HRVA - a velocity analysis technique applied to seismic data (G, Vol 34, pp 330-356).

J. Robinson (1970a), Statistically optimal stacking of seismic data (G, Vol 35, pp 436-446).

J. Robinson (1970b), An investigation of the relative accuracy of the most common normal-moveout expressions in velocity analyses (GP, Vol 18, pp 352-363).

J. Robinson (1972), Computer designed Wiener filters for seismic data (G, Vol 37, pp 235-259).

J. Robinson, C. Aldrich (1972), A novel high-speed algorithm for summational type seismic velocity analyses (GP, Vol 20, pp 814-827).

W. Schneider, M. Backus (1968), Dynamic correlation analysis (G, Vol 33, pp 105-126).

W. Schneider (1971), Developments in seismic data processing and analysis (1968-1970) (G, Vol 36, pp 1043-1073).

R. Sengbush, M. Foster (1968), Optimum multichannel velocity filters (G, Vol 33, pp 11-35).

S. Treitel, E. Robinson (1966), The design of high resolution digital filters (IEEE Transactions of Geoscience Electronics, GE-4, No.1).

S. Treitel, E. Robinson (1969), Optimum digital filters for signal to noise ratio enhancement (GP, Vol 17, pp 249-293).

S. Treitel (1970), Principles of digital multichannel filtering (G, Vol 35, pp 785-811).

G. Wadsworth, E. Robinson, P. Hurley, J. Bryan (1953), Detection of reflections on seismic records by linear operators (G, Vol 18, pp 539-586).

N. Wiener (1949) The extrapolation, interpolation and smoothing of stationary time series with engineering applications (Wiley).

R. Wiggins, E. Robinson (1965), Recursive solution to the multichannel filtering problem (Journal of Geophysical Research, Vol 70, pp 1885-1891).

H. Wold (1938), A study in the analysis of stationary time series (Uppsala, Almquist and Wiskells).

APPENDIX

"Geodat" - a moveout analysis data processing package

This package is designed to perform Fourier Transforms, correlation analyses and multichannel filtering, together with the plotting of the results on either a "Kingmatic" or "Calcomp" plotter. The whole program is written in FORTRAN IV, with a modular structure, for use on the Imperial College CDC 6400. Communication between the modules is effected through the use of appropriate disc files.

The package may operate in any one of eight different modes, each mode being defined by the parameter "IDJOB" as follows :

IDJOB = 1, Fourier Transform of a seismic record.

IDJOB = 2, Fourier Transforms of both a seismic record and a pre-filtered version of the record.

IDJOB = 3, Fourier Transform of a pre-filtered seismic record.

IDJOB = 4, second-order autocorrelation of a seismic record, together with a post-filter scan of this autocorrelation.

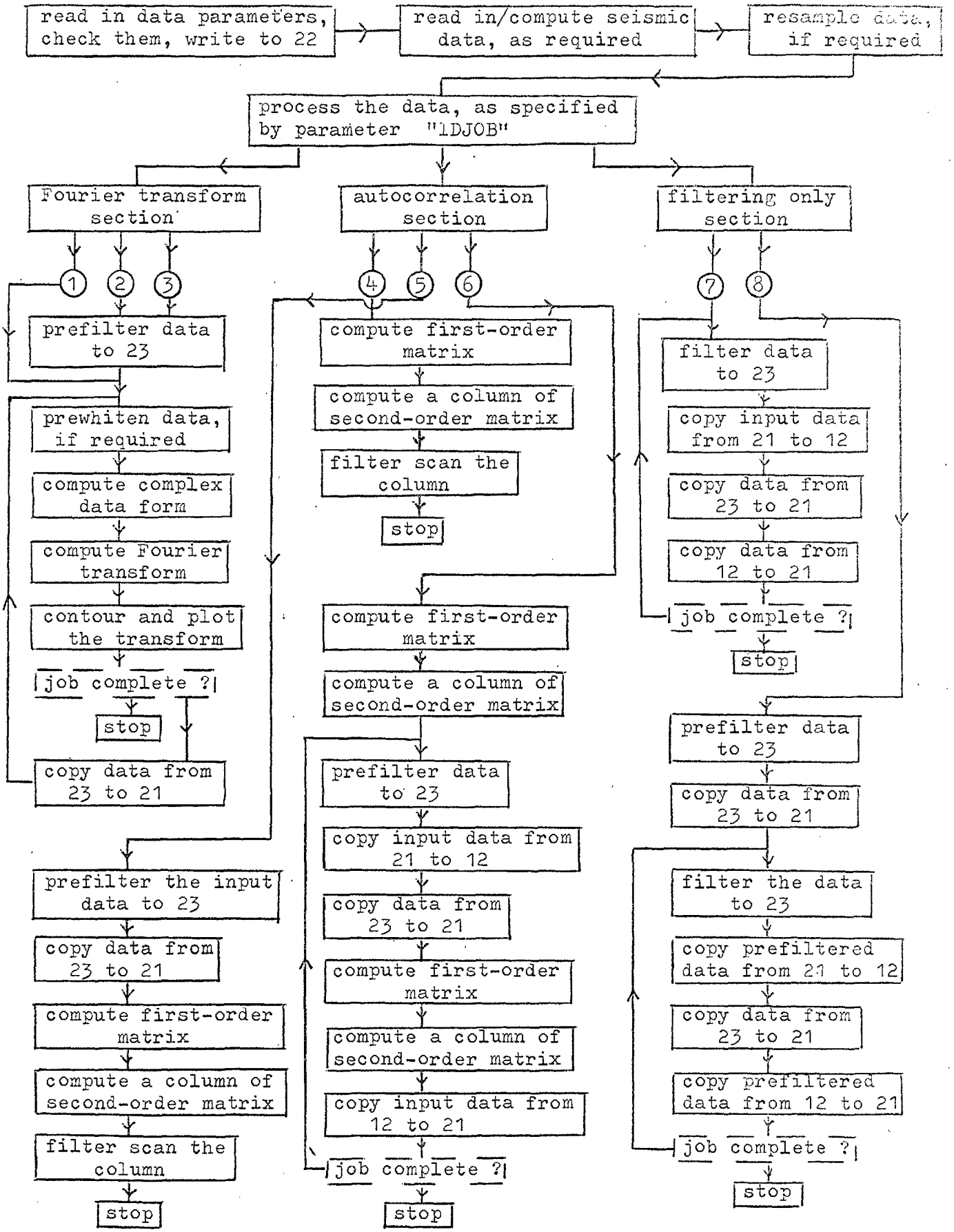
IDJOB = 5, second-order autocorrelation of a pre-filtered seismic record, together with a post-filter scan of this autocorrelation.

IDJOB = 6, filter scan of the input record, together with the second-order autocorrelation, for each filtered record.

IDJOB = 7, filter scan of a seismic record.

IDJOB = 8, filter scan of a pre-filtered seismic record.

The operation of the "Geodat" package may be deduced from the given flowchart. The encircled numbers refer to the particular "IDJOB" option mentioned above, and the other numbers to the name of a particular disc file.



FLOWCHART FOR GEODAT PACKAGE

The colour code for the contours of the Fourier Transform plots (Chapter 4) is given as follows :

0.0 db (red)	-4.0 db (green)	-18.0 db (blue)
-1.0 db (black)	-5.0 db (black)	-24.0 db (red)
-2.0 db (red)	-6.0 db (black)	-30.0 db (black)
-3.0 db (blue)	-12.0 db (green)	